CHALMERS
UNIVERSITY OF TECHNOLOGY

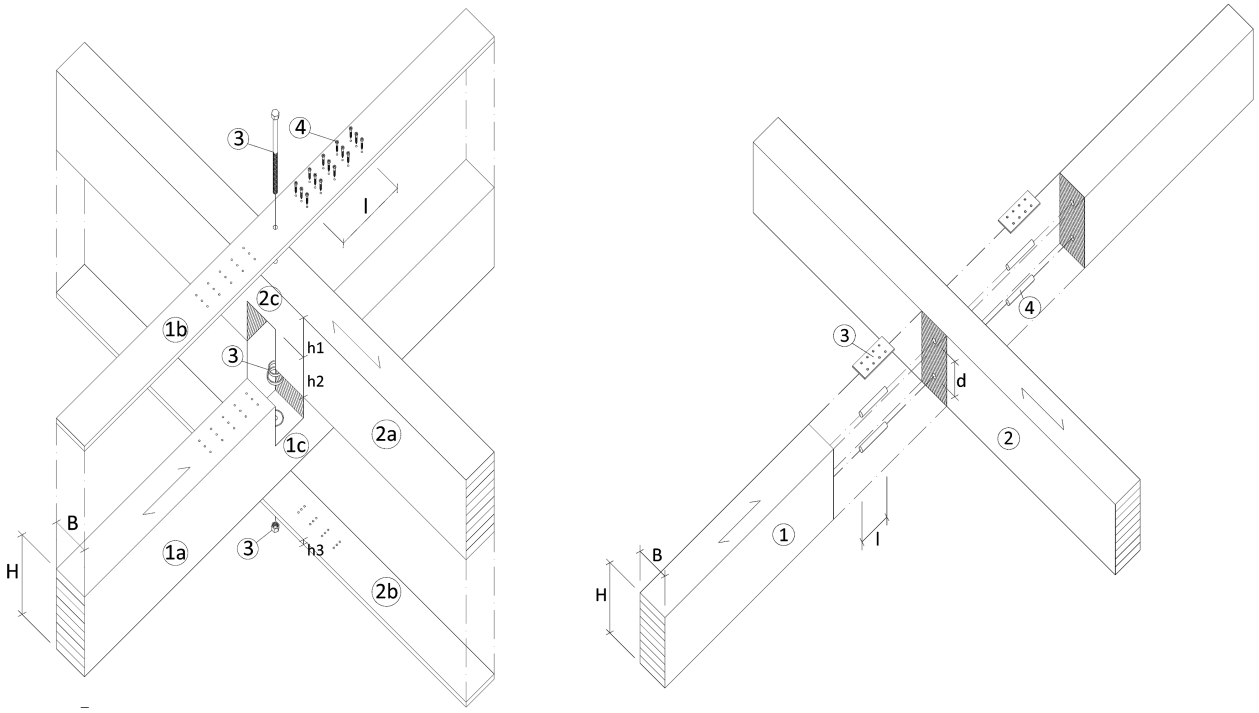

Design Implications of Rigid Timber Gridshells

A Method for the Planning and Manufacture of Load-carrying, Rigid, Freeform Structures of Timber

Master's thesis in Structural Engineering and Building Technology

SIMON LARSSON

Architecture and Civil Engineering
Division of Architectural Theory and Methods
Architecture and Engineering Research Group
CHALMERS UNIVERSITY OF TECHNOLOGY

Master's thesis ACEX30-19-5
Gothenburg, Sweden 2018

MASTER'S THESIS ACEX30-19-5

Design Implications of Rigid Timber Gridshells

A Method for the Planning and Manufacture of Load-carrying, Rigid, Freeform Structures of Timber

Master's thesis in Structural Engineering and Building Technology

SIMON LARSSON

Architecture and Civil Engineering
Division of Architectural Theory and Methods
Architecture and Engineering Research Group
CHALMERS UNIVERSITY OF TECHNOLOGY

Gothenburg, Sweden 2018

Design Implications of Rigid Timber Gridshells
A Method for the Planning and Manufacture of Load-carrying, Rigid, Freeform Structures of Timber
SIMON LARSSON
Email: larsson.simon.m@gmail.com

© SIMON LARSSON, 2018

Master's thesis ACEX30-19-5
Architecture and Civil Engineering
Division of Architectural Theory and Methods
Architecture and Engineering Research Group
Chalmers University of Technology
SE-412 96 Gothenburg
Sweden
Telephone: +46 (0)31-772 1000

Colophon:
The thesis was typeset in LaTeX.
All pictures made by the author.

Cover:
Exploded axonometry of proposed joint typologies, the *Half lap joint* and the *Basic contact joint* with the weak points in respective typology.

Chalmers Reproservice
Gothenburg, Sweden 2018

Design Implications of Rigid Timber Gridshells
A Method for the Planning and Manufacture of Load-carrying, Rigid, Freeform Structures of Timber
Master's thesis in Structural Engineering and Building Technology
SIMON LARSSON
Architecture and Civil Engineering
Division of Architectural Theory and Methods
Architecture and Engineering Research Group
Chalmers University of Technology

Abstract

With its high specific strength and workability timber is a suitable material for long span freeform structures, such as gridshells. Gridshells as structural typology are often divided into two sub-typologies; *elastic gridshells* and *rigid gridshells*. Where *elastic gridshells* are made of thin continuous members placed in a planar grid then bent to form. Whereas *rigid gridshells* is joined together of discrete, pre-shaped members.

The biggest difference between *elastic gridshells* (notable examples: *Mannheim Multihalle*, 1975; *Saville Building*, 2006) and *rigid gridshells* (notable examples: *Toskana Therme Bad Sulza*, 1999; *Centre Pompidou Metz*, 2010), is that *elastic gridshells* by design, have less out-of-plane resistance. *Rigid gridshells* on the other hand, which is the focus of this thesis, can provide higher out-of-plane resistance and is thus more forgiving for longer spans and less optimized shell geometries, with the expense of the simple construction method. Losing the simplified construction process creates high requirements on the design process for *rigid gridshells*, on aspects such as assembly methods, member manufacturing and joinery.

Timber is a material that can not be shaped into an arbitrary form, nor joined without loss of strength and stiffness. This thesis project will therefore study the geometrical implications and limitations of freeform timber structures, and possible assemblies thereof. Through a study of geometrical queries that are common in the design process a suggestion of how to avoid overly expensive solutions is presented. The thesis also presents a study of the semi-rigid behaviour of different joints and the consequences of this reduced global stiffness. Thus evaluating the potential of long-span freeform structures.

The study shows high potential in the use of timber for these types of structure, both structurally and economically, although both aspects are highly dependent on a number of choices throughout the process. Amongst them the type of joint and the global curvature as well as chosen manufacturing methods of members in the grid.

Keywords: Freeform structures, Timber, Gridshells, Timber Manufacturing, Curved timber, Timber joints, Semi-rigidity, Design for manufacturability, Design for assembly

Contents

Preface

This Master's Thesis was written as part of the Master's programme *Structural Engineering and Building Technology* at Chalmers University of Technology, Gothenburg, Sweden in collaboration with Knippers Helbig Advanced Engineering GmbH, Stuttgart, Germany.

I want to express my gratitude to my supervisor Dr. Laurent Giampellegrini for his support, ideas and constructive criticism through this process. I would also like to thank the rest of the team at Knippers Helbig for their support as well as providing me with an inspiring environment.

Gratitude also goes to Dr. Mats Ander, Chalmers University of Technology who served as examiner for this thesis and to his important input and comments.

I would also like to take the opportunity to thank my opponent Joel Hilmersson for our discussions and his comments.

Gothenburg, January 2019
Simon Larsson

1 Introduction

1.1 Background

With its relatively low embodied energy, timber has regained a lot of interest as a construction material during the last decades. It is a sustainable alternative to the common materials of contemporary construction, e.g. concrete and steel. Timber is a traditional material, having been used in structures for almost ten thousand years [Schweitzer, 2003]. Despite this timber has sparsely been used in the the tallest, longest and largest projects since the industrial revolution. However timber projects are getting bigger, with timber being used for high-rises, with examples as Mjøsa tower and Treet, Norway; measuring respectively 80 and 50 meters tall [Moelven 2018].

The usage of timber is increasing, not only due to its structural and sustainable properties, but also due to its availability. For example is the Swedish forest increasing its net mass with 30% every year [Naturvårdsverket, 2013].

However where usage of timber has been widespread through history is in long span structures, utilizing its high specific stiffness. Many historic buildings have walls of stone or clay and roof trusses of timber. In more recent history this practice is demonstrated with the glulam beams at *Stockholm Central Station* (1927) as an early example and the *Tacoma Dome* with a span of 162 meters as one of the largest.

With the increasing popularity of freeform structures, there are new demands and requirements on materials, design processes and manufacturing methods. Timber is a highly suitable material for these structure due to its workability. A few notable freeform projects of timber is: the *Mannheim Multihalle*, for the Bundesgartenschau 1975, and the *Saville Garden Gridhell*, both *elastic gridshells*. Where *La Seine Musicale* in Paris and *Toskana Therme Bad Sulza* are noteable examples of *rigid gridshells*.

Gridshells are usually divided into these two different types; *elastic gridshells* and *rigid gridshells*. *Elastic gridshells* is a typology of shells created from a planar grid of overlapping laths or thin members, forming the structure through the application of a bending force. This typology was initially studied by Frei Otto [Chilton, Tang, 2017] and has thereafter been thoroughly studied (in recent years by: Poulsen [2015] and Lafuente Hernandez [2015] among others). This typology of shell is considered a structure of high structural efficiency and a simple construction- and manufacturing-process, consisting only of initially straight members. These structures are usually constructed in timber, fibre-reinforced plastics or even aluminium [Lafuente Hernández, 2015].

Rigid gridshells on the other hand can be similar to *elastic gridshells* in form and structural functionality but are assembled from discrete prefabricated members (the different in construction can be seen in illustrated in Figure 1.1). This typology has traditionally been constructed

by steel [Lafuente Hernández, 2015], however other materials can be used. One of the biggest drawbacks in this type of structure has been the complexity of manufacturing of members and connections [Poulsen, 2015]. However with modern production- and design methods this is today a feasible structural typology to design.

The main difference in structural behaviour of the two typologies is that the rigid structure can provide higher out-of-plane resistance, hence its name. This is due to the compromise made when designing elastic gridshells, where members needs to be flexible enough to bend in shape, but stiff enough to provide stiffness for external loads [Lafuente Hernández, 2015], limiting possible cross section size.

The geometric freedom is also a difference between the two. When designing rigid gridshells the shape is highly influential on the performance, however it is possible to compensate for a suboptimal geometry with increased member size or tapering members, due to the discretized system. On the other hand the elastic gridshell is behaving much like a form-active structure, and is thereby somewhat limited in shape.

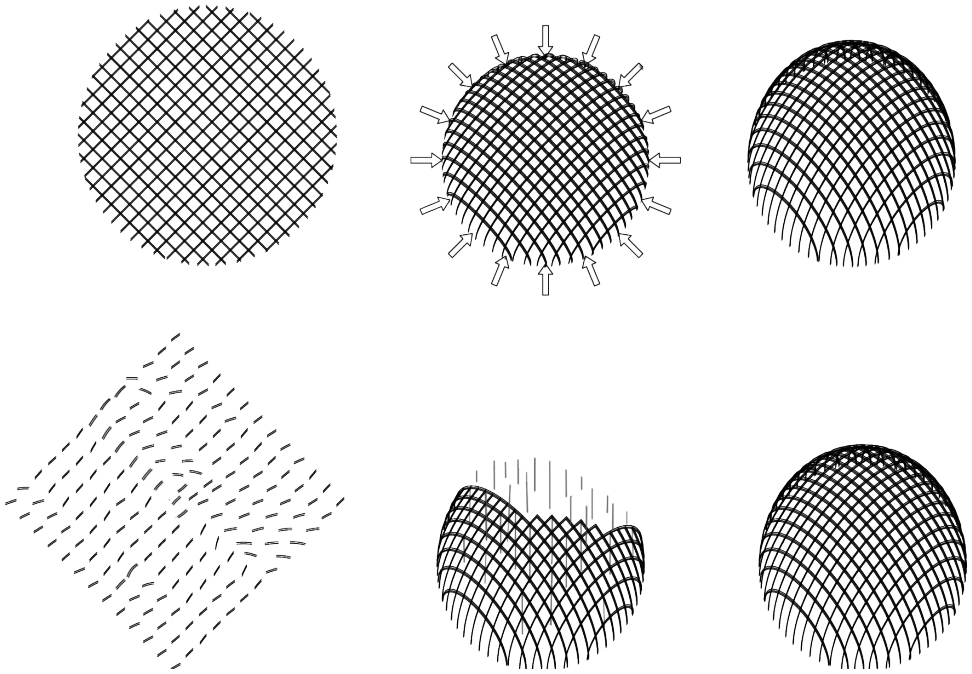

Figure 1.1: *Top: Construction process of elastic gridshell, beginning with a grid of continuous members that takes form by bending. Bottom: Construction process of rigid gridshell, starting with prefabricated members that takes shape through a joinery-process.*

However, the drawbacks in the manufacturing process of rigid shells should be addressed. And while the structural behaviour of the systems are similar, the biggest difference relates to manufacturing and assembly. The progressive construction method means that full structural strength might not be reached until late in the construction process. The long spans will, depending on assembly system, result in a heavy need of scaffolding. Non-bendable members means that geometry needs to be fabricated before assembly, and with large amount of possibly unique members manufacturing must be done in an efficient and customizable way with low to no reduction of strength.

While the grid in an *elastic gridshell* is achieved by overlapping continuous members the joint in *rigid gridshells* are usually more complex. The beam must often either terminate in the joint or be compromised in size to allow for both directions to pass. Joinery in timber can not be performed without strength and stiffness reduction [Aicher. Hezel. Stapf, 2012]. The design of joints must therefore be done in a way that allows easy assembly and sufficient stiffness and strength.

1.2 Purpose

The purpose of the project is to investigate different design parameters and suggest a design-process for freeform, rigid, load carrying timber structures. With emphasis on design parameters with major influence on assembly and manufacturing, since these are the aspects where *rigid gridshells* mainly differs from the *elastic gridshell*. Important parameters are found in geometry, both of the shell itself and of individual members, joinery and assembly systems.

Implications of joinery should be studied. Joints and systems with possibility to assemble for large structures should be found and developed. These joints should be studied in order to evaluate their strength and stiffness. The influence of this semi-rigid behaviour on a full size structure should be analysed.

The purpose could be summarized in the following questions:
• How could one categorize the stiffness of timber joints, and which influence will this have on the performance of a structure?
• How could one design a timber gridshell in order to ensure manufacturability and assembly?
• Which are the most important consideration of geometry in the design process and how will they affect structural performance and economy of the project?

1.3 Method

The first step is to, by a review of current research and various reference projects, create an overview of the limitations of freeform structures in timber. This covers contemporary methods for assembly, manufacturing and geometrical optimisation. As well as a study of material behaviour through norms, calculations and simulations in order to find limitations of the material, and how to evaluate for these criteria.

A method of how to evaluate and implement stiffness in semi-rigid joints will be developed and used in order to analyse the effect of these in global structural calculations. The evaluation of these joints are made with a custom VBA-macro in Microsoft Excel and the simplified model's significance is verified with a FE-model made in MATLAB with toolbox CALFEM.

Geometrical and quantitative analyses, related to the manufacturability, assembly and costs thereof will be performed using Rhinoceros from *Robert McNeel & Associates* extended with custom scripts in plug-in Grasshopper. Through available data and communication with manufacturers and toolmakers the possible methods of manufacture will be evaluated. Rhinoceros

is also the platforms used for work flows aiming for production.

Complex structural analysis is performed with commercial FE-software Sofistik from *Sofistik AG*.

Ideas will be implemented and tested in a case study.

1.4 Limitations

With this study having its main focus on rigid gridshells, this thesis will not focus on structural form-finding of shells.

In the scope of this project engineered timber will be in focus, since the engineered timber is dominant in the production of freeform structures.

This study will not include effects induced by moisture. Timber is a material sensitive for moisture and detailing should also be checked for stresses induced by moisture shrinkage as well as deterioration due to organic effects.

This study should be complemented with physical testing, for verification, this will not be possible to perform within the scope of this study.

While the intention is to keep the discussion general, design will be based mainly on the Eurocodes.

2 References

As an introduction into the subject the following chapter presents a number of selected reference projects. Each of which a *rigid gridshells* representing different approaches to joinery, assembly and manufacturing. In order to present and study some design considerations during the design of this type of structure. And to gain insight in problems and solutions that can occur in the design and manufacturing process.

2.1 Toskana Therme Bad Sulza

Location: Bad Sulza, Germany. Design: Ollertz Architekten. Structure: Trabert und Partner. Year: 1999.
The thermal bath in Bad Sulza is a gridshell with form-found based on a digital hanging-chain model. The structure is based on the Zollinger-system, a reciprocal system which strength is that it can span big distances with short members, by members supporting each other and using relatively simple joinery. With members supporting each other full structural integrity is not reached until late in the construction and there was an extensive need for scaffolding. The Zollinger-system is further described in Section 6.3.1. The principle of this project is illustrated in Figure 2.1.

In this project every member is unique and approximately 3.2 meters long and almost straight. The members are milled to shape, with the exception for the laminated, doubly-curved edge beams [Hofmann, Thompson, 2009]. The connection consists only of a wooden dowel, and relies otherwise on the contact between elements [Chilton, Tang, 2017]. Despite the structure being designed to work in compression, a nailing plate is introduced for tension. The structure is braced with timber boards on top of the beams.

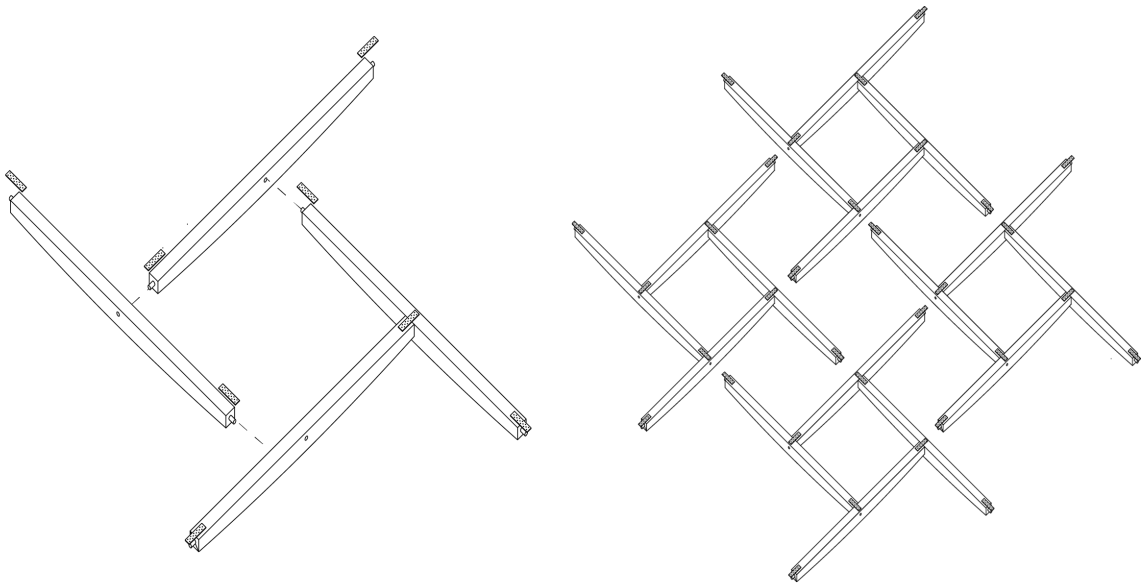

Figure 2.1: *Left: diagram of the assembly of each element. Right: diagram of assembled element.*

2.2 Z-Plus Pavilion

Location: Gossau, Switzerland. Design: Design-to-Production. Structure: SJB Kempter Fitze. Year: 2009.
The *Z-Plus Pavilion* is a small experimental canopy with the aim to further develop the Zollinger-system. The structure consists of two layers of beams shifted to each other, creating an overlap. Where the top layer is continuous, bottom layer is not, and vice versa in the orthogonal direction. Allowing one layer of every grid line to be continuous at every node. This means that the nail-plate from the previous project can be removed, since one member per direction is always continuous, the system also allowing tension and bending. The principle of the system is shown in Figure 2.2.

The members are prefabricated, including holes. Everything is done in an automatic manufacturing-process in a CNC-mill. Since the structure is doubly-symmetric each quarter of the pavilion could be assembled separately. The modularity and its moderate size made it possible to raise the structure without scaffolding.

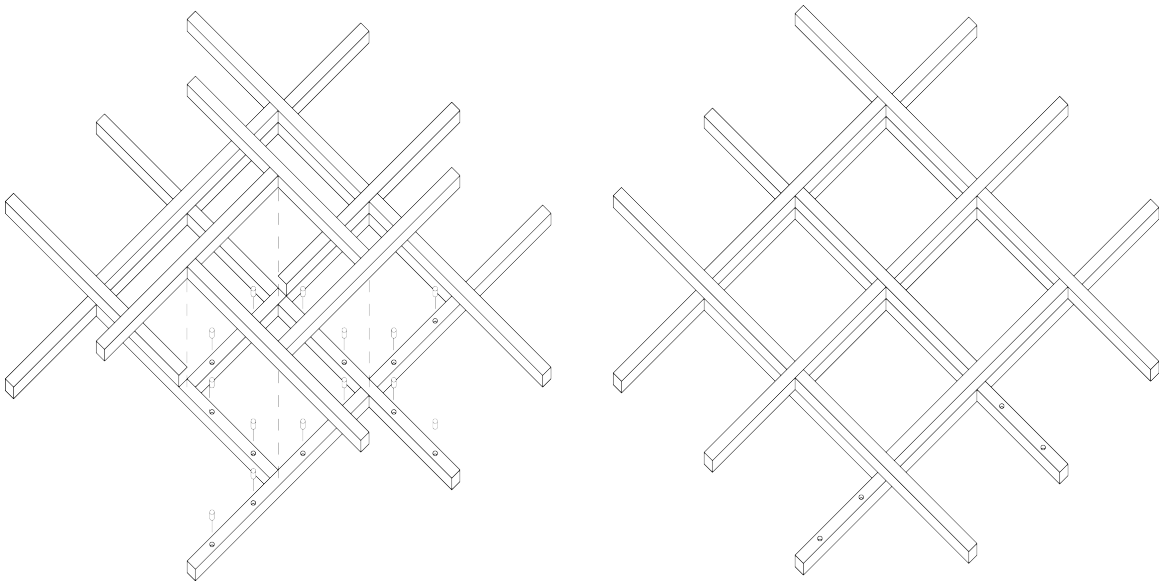

Figure 2.2: *Left: diagram of the assembly of the system. Right: diagram of assembled system.*

2.3 La Seine Musicale

Location: Paris, France. Design: Shigeru Ban Architects. Structure: Design-to-Production, SJB Kempter Fitze. Year: 2016.
La Seine Musicale is a concert-hall in Paris, with a timber and glass façade covering the ellipsoidal auditorium. The joinery in this project was based on traditional half lap joints [Stehling et al. 2017] where corresponding notches are cut in the members, slotting them into each other, creating a smooth crossing. The principle of the system is shown in Figure 2.3.

In this project all members were laminated into form. Due to demands from the architects on "flawless appearance" a criteria was set, that the outermost lamella of the glulam could not be cut through, since this would create a visible glued line on the surface of the beam. This criteria demanded high precision during the bending process, since inaccuracies could not be adjusted afterwards [Stehling et al. 2017].

One finding during the design process is that a tight half lap joint will only have one degree of freedom in which it can be assembled, and with several joints on the same curved members, the assembly is not necessarily guaranteed. The solution in this case was a combination of skewing notches and to plan the order of assembly carefully [Stehling et al. 2017].

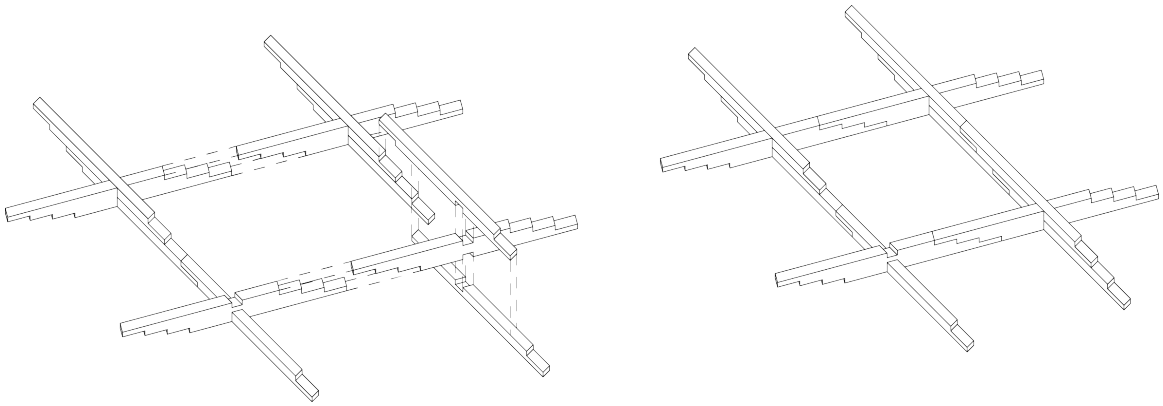

Figure 2.3: *Left: diagram of the assembly of the system. Right: diagram of assembled system.*

2.4 Centre Pompidou Metz

Location: Metz, France. Design: Shigeru Ban Architects. Structure: Arup, Design-to-Production. Year: 2010.
This museum, with a maximum span of 50 meters, is inspired by a Chinese straw hat. Both its form and the idea of a woven structure is taken from the inspiration [Chilton, Tang, 2017]. However since the structure is a rigid gridshell, the structure is made to resemble being a woven structure while not actually being one. Having grid lines in three directions, a hexagonal/triangular grid is created. The cross section is built up by two continuous flanges connected by timber shear blocks, allowing the different grid-lines to be "woven" into each other without reducing cross-section and without significant increase of structural height.

The structure consists of members all milled to shape. Considering that every beam was of very complicated geometry and the sheer amount of members made milling a feasible option, despite the strength-reductions [Chilton, Tang, 2017]. The members are joined longitudinally with slotted-in steel-plates. While the different directions are joined with a really simple joint consisting of a bolt, a spring-washer and a nut. The principle is shown in Figure 2.4.

The structure is covered with an ETFE-membrane to keep the structural weight low, which is highly favourable with respect to the long-term behaviour of the structure.

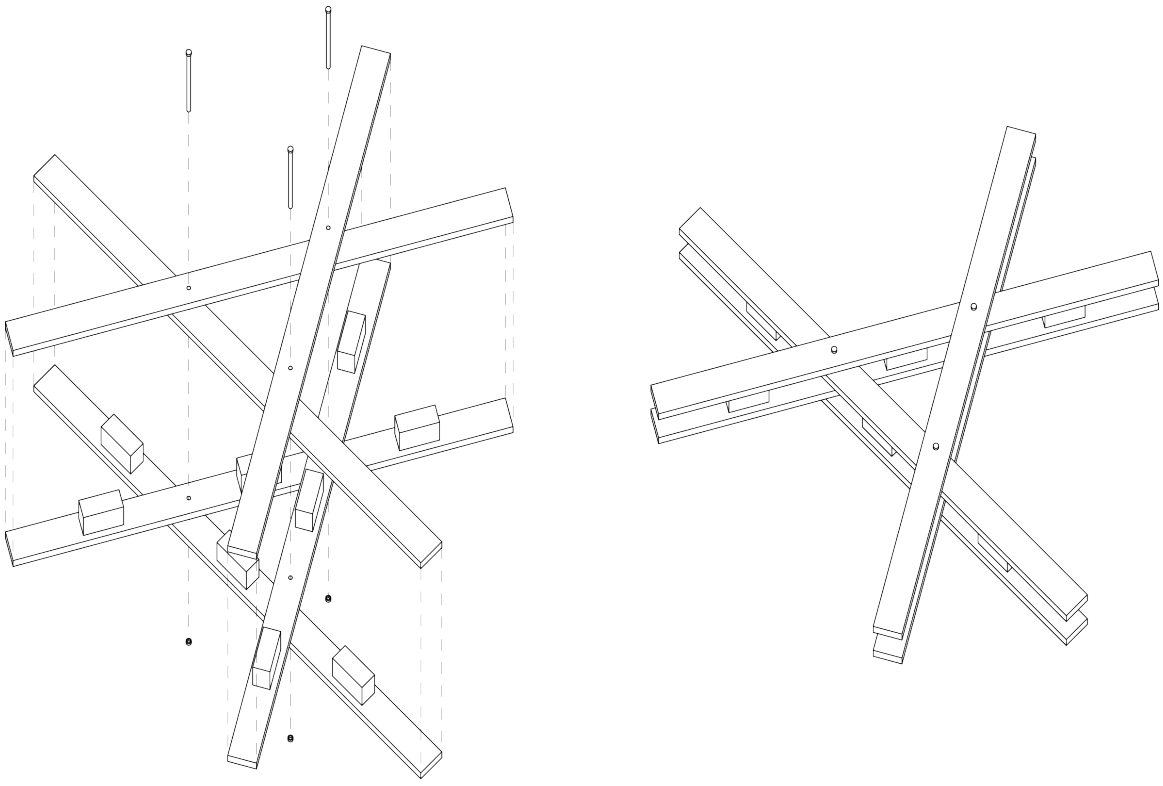

Figure 2.4: *Left: diagram of the assembly of the system. Right: diagram of assembled system.*

2.5 Herbert Art Gallery

Location: Coventry, Great Britain. Design: PRS Architects. Structure: Alan Baxter Ltd. Year: 2009.
Gridshells of steel are usually constructed as beam-node systems. This can also be done in timber structures, often with nodes made from steel and beams of timber.

This roof is constructed of straight timber members, spanning between the nodes. The curvature is created in the nodes, to which the beams are attached at an angle. The visual expression of this structure is a lot different compared to other gridshell systems, due to the visible steel node at each intersection, and the rugged curvature of the system.

The principle of the system is shown in Figure 2.5. The node allows a rather simple attachment of cable bracing. Although no information on this projects, other similar projects, such as the *Canary Wharf Railway Station* by Foster+Partners is built with very sparse scaffolding. Installation performed with a crane and a mobile platform [Rabaglati, Huber, Linke, D. 2014], supported first when the cantilever becomes too long for the bending moment to be resisted by the joint.

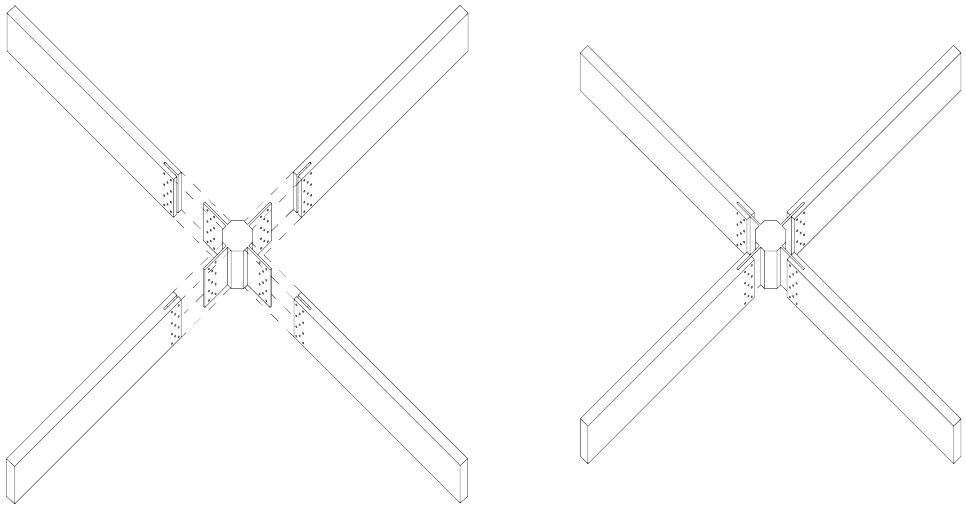

Figure 2.5: *Left: diagram of the assembly of the system (the actual node connects 6 members). Right: diagram of assembled system.*

3 Stiffness of joints

The movements of a body in the three dimensional space can be described by six degrees of freedom; three translations and three rotations. Analogously the stiffness of any point in a three-dimensional structure can be described with the resistance against these six movements. Thus an equivalent spring model for every part of a structure can be defined, with three linear springs and three torsional springs (as seen in Figure 3.1).

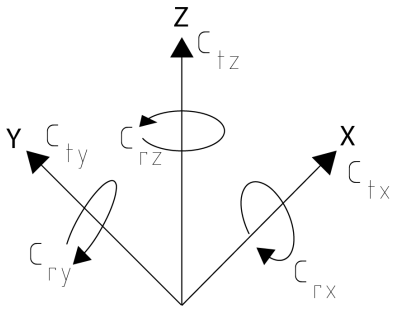

Figure 3.1: *Diagram of the six spring stiffnesses that the system is condensed to*

In engineering practice idealisation is often used. Like either assume pinned connections or fixed connections. In timber however assuming fixed connections would not be a realistic assumption, since timber is so soft that full rigidity is almost impossible to achieve. Assuming pinned connections might lead to oversized members and that the model shows another structural behaviour than will be seen in the built structure. But by replacing these absolute assumptions with a system of six springs a semi-rigid model could be introduced, making the analysis model more realistic.

In timber there might be contributions to the stiffness from different effects. Contribution can come from mechanical fasteners such as dowels, screws and could also come from contact and friction. These might be working together, or separately depending on the layout of the joint.

Working with timber, the orientation of the beams is important, as will further be explained in Chapter 4, due to the orthotropic behaviour of the material. This is accounted for using different Young's modulus and strength values for different directions, where $\boldsymbol{E}_0$ is the Young's modulus parallel to grain and $\boldsymbol{E}_{90}$ is the modulus perpendicular to grain. In glued laminated timber $\boldsymbol{E}_0$ is towards 40 times higher than $\boldsymbol{E}_{90}$, which makes a significant difference.

In the following chapter, a suggested method for evaluation of stiffness for timber joints is presented, to be able to get equivalent spring stiffnesses for joints. This chapter will also derive a beam model where these stiffness can be used to make the boundary conditions more realistic.

3.1 Evaluation

Timber is a relatively soft material, which means that most joint-types can not be considered completely rigid, but also not completely pinned. To account for this, the stiffness of the joints

can be evaluated, giving a more realistic model for the calculations.

The stiffness of mechanical fasteners is accounted for in Eurocode 5 with the *Slip Modulus* $\boldsymbol{K}_{ser}$ [N/m], based on the density and diameter of the fastener according to formulas (see Eurocode 5 [SIS, 2009c (Table 7.1)]). As an example the stiffness for screws, dowels and nails with pre-drilled holes can be calculated as:

$$K_{ser} = \frac{\rho_m^{1.5} d}{23} \tag{3.1}$$

Where:
$\boldsymbol{K}_{ser}$ - *Slip modulus* [N/m]
$\boldsymbol{d}$ - *Diameter*[m]

and for ULS:

$$K_{ULS} = \frac{2}{3} K_{ser} \tag{3.2}$$

The contribution from contact is evaluated with a method suggested by Descamps et. al. [2006]. For components with lengths that is in the same order as the other dimensions of the component (such as spring *k1a* in Figure 3.2) can be calculated with Equation (3.3).

$$k = \frac{EA}{L} \tag{3.3}$$

Where:
k - *Spring stiffness - linear spring* [N/m]
$\boldsymbol{E}$ - *Young's modulus* [N/m^2]
$\boldsymbol{A}$ - *Cross section area* [m^2]
$\boldsymbol{L}$ - *Spring length* [m]

Equation (3.4) is used for components where the length of the component is much bigger than the other dimensions and is an expression for the stiffness of an elastic half space (such as spring *k1b* in Figure 3.2).

$$k = \frac{E\sqrt{A}}{0.85} \tag{3.4}$$

Where:
k - *Spring stiffness - elastic half space* [N/m]
$\boldsymbol{E}$ - *Young's modulus* [N/m^2]
$\boldsymbol{A}$ - *Cross section area* [m^2]

The force-displacement relation for a linear spring is described as:

$$\delta = \frac{F}{k} \tag{3.5}$$

Where:
δ - *Elongation* [m]
$\boldsymbol{F}$ - *Force* [N]
k - *Spring constant* [N/m]

These springs are then combined in series (according to Equation (3.6)) or parallel (according to Equation (3.7)), depending on the layout and how the effects are assumed to interact, to calculate the full stiffness of the system. If the contact stiffness interacts with the stiffness from mechanical fasteners, the *Slip modulus* is also added accordingly.

$$k_{series} = \sum_{i=1} \frac{1}{k_i} \left(+ \sum_{j=1} \frac{1}{K_{ser,j}} \right) \tag{3.6}$$

$$k_{parallell} = \sum_{i=1} k_i \left(+ \sum_{j=1} K_{ser,j} \right) \tag{3.7}$$

Axial Stiffness

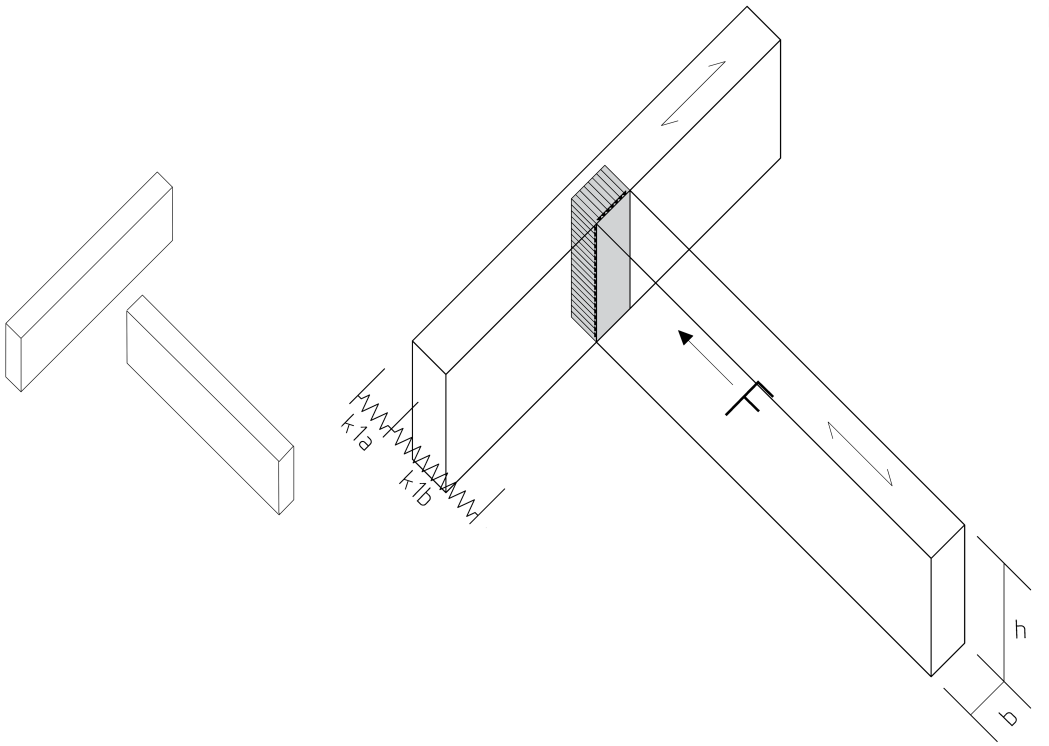

Figure 3.2: *Diagram showing the concept of the stiffness contribution due to contact*

As a demonstration, an example is shown in Figure 3.2, of two equally sized beams with one transferring compression into the other. The stiffness should be calculated for an axial force through the longitudinal beam in contact with a crossing beam. The stiffness is divided into two components: spring k_{1a} and k_{1b}, one for each component in the system.

Spring k_{1a}, representing the crossing member, has a length in the same order as the other dimensions of the beam (thus using Equation (3.3)), with the compression force perpendicular to grain, thus:

$$k_{1a} = \frac{E_{90} b h}{b}$$

Where:
E_{90} - *Young's modulus perpendicular to grain* [N/m^2]
b - *Cross section width* [m]
h - *Cross section heigth* [m]

Spring k_{1b}, on the other hand, has a length much larger than the other dimensions, and the force is parallel to grain, thus, according to Equation (3.4):

$$k_{1b} = \frac{E_0\sqrt{bh}}{0.85}$$

Where:
E_0 - *Young's modulus parallel to grain* [N/m^2]

These are combined to spring k_1 as serial springs according to Equation (3.6):

$$\frac{1}{k_1} = \frac{1}{k_{1a}} + \frac{1}{k_{1b}}$$

Rotational Stiffness

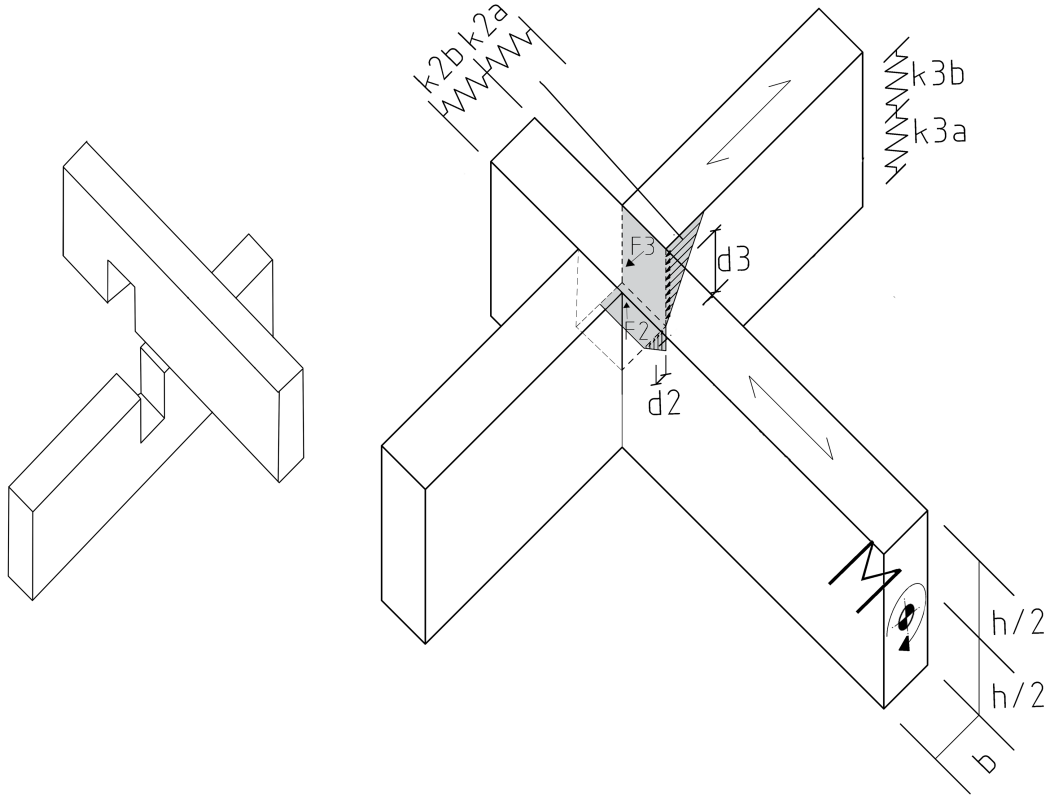

Figure 3.3: *Diagram showing the concept of the rotational stiffness contribution due to contact for a half lap joint*

In the system in Figure 3.3, describing a half lap jont of two beam slid into each other with notches a twisting moment is applied around the centreline of one beam, and the rotational

stiffness is to be calculated.

The stiffness can be calculated starting with the following equation, that is analogous to the force-displacement relation in Equation (3.5), of the relation between rotation and moment in a rotational spring:

$$\theta = \frac{M}{c_r} \tag{3.8}$$

Where:
c_r - *Rotational stiffness* [Nm/rad]
θ - *Rotational angle* [rad]

The moment creates two triangular compression zones (marked in grey in Figure 3.3), with resulting forces of F_2 and F_3, proportional to stiffness of linear springs k_2 and k_3 as:

$$F_2 = k_2 \delta_2$$

$$F_3 = k_3 \delta_3$$

Where:

$$\frac{1}{k_2} = \frac{1}{k_{2a}} + \frac{1}{k_{2b}}$$
$$\frac{1}{k_3} = \frac{1}{k_{3a}} + \frac{1}{k_{3b}}$$

Assuming small rotations the deflection δ can be expressed as:

$$\delta = \sin(\theta) d \approx \theta d$$

Where:
d - *lever arm (2/3 of the full length of compression triangle)* [m]

Resulting in:

$$c_{r2} = \frac{M}{\theta} = \frac{F_2 d_2}{\theta} = \frac{k_2 \delta_2 d_2}{\theta} \approx \frac{k_2 \theta d_2 d_2}{\theta} = k_2 d_2^2$$

and:

$$c_{r3} = k_3 d_3^2 \tag{3.9}$$

The springs are working in parallel, thus:

$$c_{r,tot} = c_{r2} + c_{r3}$$

In case of interaction these stiffnesses are later added to the contribution K_{ser} of mechanical fasteners.

3.2 Implementation

In order to be able to use the spring constants calculated in the previous section a beam model needs to be derived where these stiffness values can be used. A semi-rigid beam model with the simply supported beam and the fixed beam as boundary solution, explaining the behaviour of the beam with supports between fix and hinged. The derivation for a simply supported beam and a fixed beam is therefore shown, as comparison, thereafter the semi-rigid model is derived, with the spring stiffness as a variable.

This beam model will be helpful in order to study the behaviour of a semi-rigid beam and also to classify joint-typologies according to their semi-rigidity. The beam model is also expanded upon in order to be able to use with axial and transversal stiffness values.

The first step is to derive a general equation for the displacement of a beam. From the Euler-Bernoulli beam theory we know:

$$-w''(x) = \frac{M(x)}{EI} \tag{3.10}$$

Where:
w'' - *curvature* [1/m]
$M(x)$ - *Bending moment at* x [Nm]
E - *Young's modulus* [N/m^2]
I - *Area moment of inertia* [m^4]

By substituting the moment in Equation (3.10) with an expression for the moment in a uniformly loaded beam one gets the following equation, from which the curvature (w'') can be accessed:

$$EIw''(x) = Ax + M_A - \frac{qx^2}{2} \tag{3.11}$$

Slope (w') can be accessed from the following expression found by integration:

$$EIw'(x) = \frac{Ax^2}{2} + M_A x - \frac{qx^3}{6} + C_1 \tag{3.12}$$

Deflection (w) can be accessed from the following expression found by integration:

$$EIw(x) = \frac{Ax^3}{6} + \frac{M_A x^2}{2} - \frac{qx^4}{24} + C_1 x + C_2 \tag{3.13}$$

Where:
A - *Reaction force* [N]
M_A - *Support moment* [Nm]
q - *Uniformly distributed load* [N/m]
C_1 - *Integration constant* [Nm^2]
C_2 - *Integration constant* [Nm^3]

3.2.1 Simply supported beam

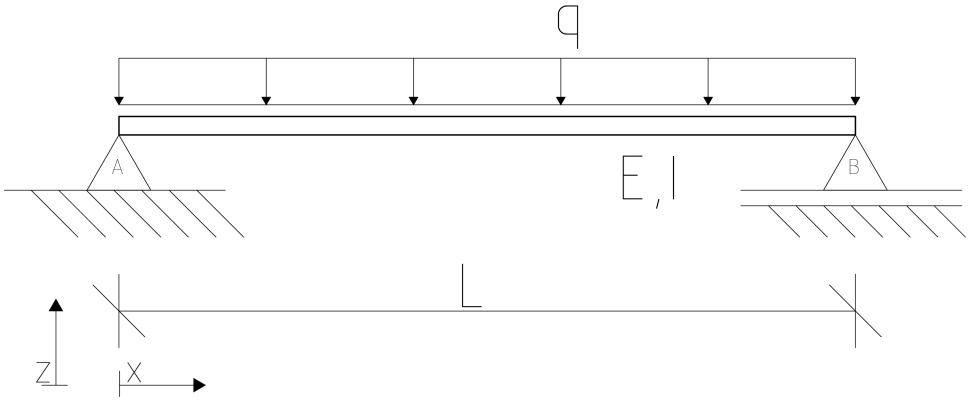

Figure 3.4: *Illustration of the the set-up of a simply supported beam with uniformly distributed loads.*

The equation for the simply supported beam shown in Figure 3.4 is given by starting with Equation (3.13) and using the following boundary conditions and assumptions:

$$w(x = 0) = 0 \Rightarrow C_2 = 0 \tag{3.14}$$

$$w(x = L) = 0 \Rightarrow C_1 = -\frac{AL^2}{6} + \frac{qL^3}{24} \tag{3.15}$$

$$A = \frac{qL}{2}[\text{kN}] \tag{3.16}$$

$$M_A = 0[\text{kN m}] \tag{3.17}$$

Which gives:

$$EIw(x) = \frac{qLx^3}{12} - \frac{qx^4}{24} - \frac{qL^3x}{12} + \frac{qL^3x}{24}$$

Due to symmetry, the maximum deflection would occur in the middle ($x = L/2$). Which gives:

$$EIw(x = L/2) = \frac{qL^4}{96} - \frac{qL^4}{384} - \frac{qL^4}{24} + \frac{qL^4}{48}$$

Which equals:

$$EIw(x = L/2) = \frac{4qL^4}{384} - \frac{qL^4}{384} - \frac{16qL^4}{384} + \frac{8qL^4}{384}$$

Which gives the maximum deflection for a simply supported beam:

$$\delta = -\frac{5qL^4}{384EI} \tag{3.18}$$

Where:
δ - *maximum deflection* [m]

3.2.2 Fixed beam

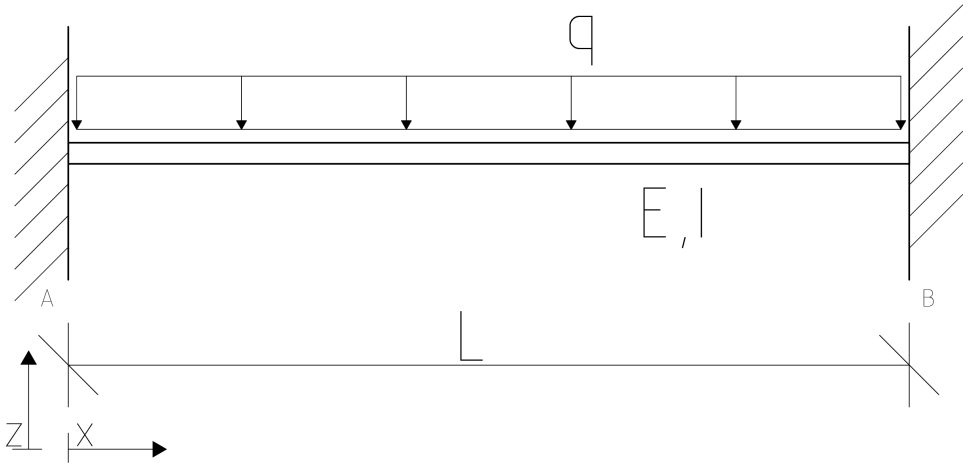

Figure 3.5: *Illustration of the the set-up of a fully fixed beam with uniformly distributed loads.*

The equation for the fixed supported beam shown in Figure 3.5 is given by starting with Equation (3.13) and using the following boundary conditions and assumptions:

$$w(x = 0) = 0 \Rightarrow C_2 = 0 \tag{3.19}$$

$$w'(x = 0) = 0 \Rightarrow C_1 = 0 \tag{3.20}$$

$$A = \frac{qL}{2}[\text{kN}] \tag{3.21}$$

$$M_A = \frac{qL^2}{12}[\text{kN m}] \tag{3.22}$$

Which gives:

$$EIw(x) = \frac{qLx^3}{12} - \frac{qL^2x^2}{24} - \frac{qx^4}{24}$$

And since the beam is symmetric, the maximum deflection would occur in the middle ($x = L/2$). Which gives:

$$EIw(x = L/2) = \frac{qL^4}{96} - \frac{qL^4}{96} - \frac{qL^4}{384}$$

Which equals:

$$EIw(x = L/2) = \frac{4qL^4}{384} - \frac{4qL^4}{384} - \frac{qL^4}{384}$$

Which gives:

$$\delta = -\frac{qL^4}{384EI} \tag{3.23}$$

3.2.3 Semi-rigid beam

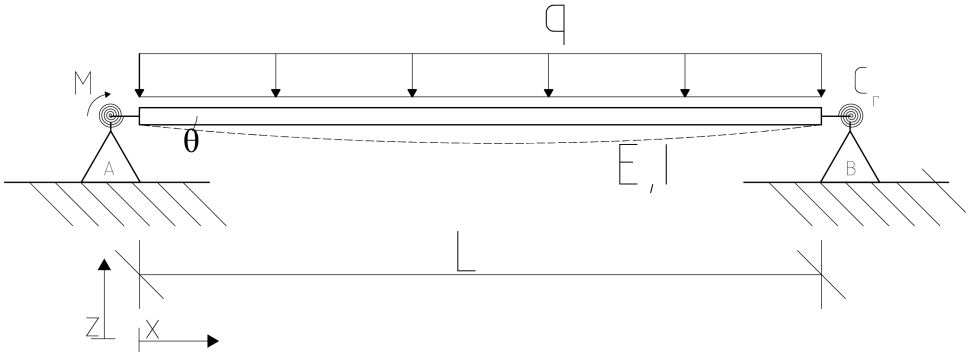

Figure 3.6: *Illustration of the the set-up of a semi-rigid beam with uniformly distributed loads.*

The rigid and the hinged solution will act as boundary solutions. A semi-rigid connection, as shown in Figure 3.6 would place itself in between these two values. The equation for the beam shown in Figure 3.6 is given by starting with Equation (3.13) and redefining the following boundary conditions and assumptions accordingly:

$$w(x=0) = 0 \Rightarrow C_2 = 0 \tag{3.24}$$

$$w(x=L) = 0 \Rightarrow C_1 = -\frac{AL^2}{6} - \frac{M_A L}{2} + \frac{qL^3}{24} \tag{3.25}$$

$$w'(x=0) = \theta = \frac{M_A}{c_r} \Rightarrow \; C_1 = \frac{M_A EI}{c_r} \tag{3.26}$$

Where:
θ - *Rotation at support* [rad]
M_A - *Support moment* [Nm]
c_r - *Rotational stiffness of spring* [Nm/rad]

Combining the boundary conditions defining C_1; Equation (3.25) and Equation (3.26) gives:

$$\frac{M_A EI}{c_r} = -\frac{AL^2}{6} + \frac{M_A L}{2} + \frac{qL^3}{24}$$

Simplifies to:

$$M_A \left(\frac{1}{c_r} + \frac{L}{2EI} \right) = -\frac{qL^3}{24EI}$$

Which can be simplified to:

$$M_A = M_{A,rigid} \frac{1}{\frac{2EI}{c_r L} + 1} \tag{3.27}$$

Where:
$M_{A,rigid} = qL^2/12$ [Nm]

With the substitution:

$$k = \frac{1}{\frac{2EI}{C_r L} + 1}$$

inserted into Equation (3.27) gives:

$$M_A = kM_{A,rigid} = kqL^2/12\text{kN m} \tag{3.28}$$

Here k is the *stiffness factor* defining the relation between the spring stiffness and beam stiffness. The *stiffness factor* will dictate much of the behaviour of the joint as illustrated in Figure 3.7.

(a) The spring is weak in comparison to beam

(b) The spring is strong in comparison to beam

Figure 3.7: *Diagram showing the behaviour of the connection with different ratio of stiffness between spring and beam.*

Equation (3.28) together with the expression for support reaction force

$$A = qL/2\text{kN m} \tag{3.29}$$

inserted into Equation (3.13) gives:

$$EIw(x) = \frac{qLx^3}{12} - k\frac{qL^2x^2}{24} - \frac{qx^4}{24} - \frac{qL^3x}{12} + k\frac{qL^3x}{24} + \frac{qL^3x}{24}$$

Due to symmetry, the maximum deflection would occur in the middle ($x = L/2$). Which gives:

$$EIw(x = L/2) = \frac{qL^4}{96} - k\frac{qL^4}{96} - \frac{qL^4}{384} - \frac{qL^4}{24} + k\frac{qL^4}{48} + \frac{qL^4}{48}$$

Which equals:

$$EIw(x = L/2) = \frac{4qL^4}{384} - k\frac{4qL^4}{384} - \frac{qL^4}{384} - \frac{16qL^4}{384} + k\frac{8qL^4}{384} + \frac{8qL^4}{384}$$

Which gives:

$$\delta = -\frac{5qL^4}{384EI} + k\frac{4qL^4}{384EI} \tag{3.30}$$

where:

$$k = \frac{1}{\frac{2EI}{C_r L} + 1} \tag{3.31}$$

It can be seen that, as the *stiffness factor* k approaches 0, stiffness of the joint being infinitely low, the deflection converges towards the solution of a simply supported beam (Equation (3.18)). As k approaches 1, representing an infinitely stiff joint, the deflection converges to that of a fixed beam (Equation (3.23)). This creates a tunable beam model, where the calculated spring stiffness is a variable and can be used to account for the flexibility of the structure.

To verify the significance of the simplified model, the maximum deflection was calculated for a 10 meter long beam (450x150 mm, GL28c), loaded with 4 kN/m according to the Equation (3.30) and Equation (3.31) above and compared to the results of an FE-model with the same setup. The results from this comparison is shown in Figure 3.8, the correspondence should be considered high, difference being less than 0.1 mm over a span of 10 m, meaning that the ratio of divergence to span is <1:100000, which would be explained by rounding error in the calculations.

As can be seen Figure 3.8, the joint in this set-up could be considered behaving as a hinged joint up to around 10^2 kNm/rad, behaviour being fully dependent on the spring being governed by the behaviour of the beam itself. In between these values the behaviour is influenced by both the stiffness of the joint and the beam.

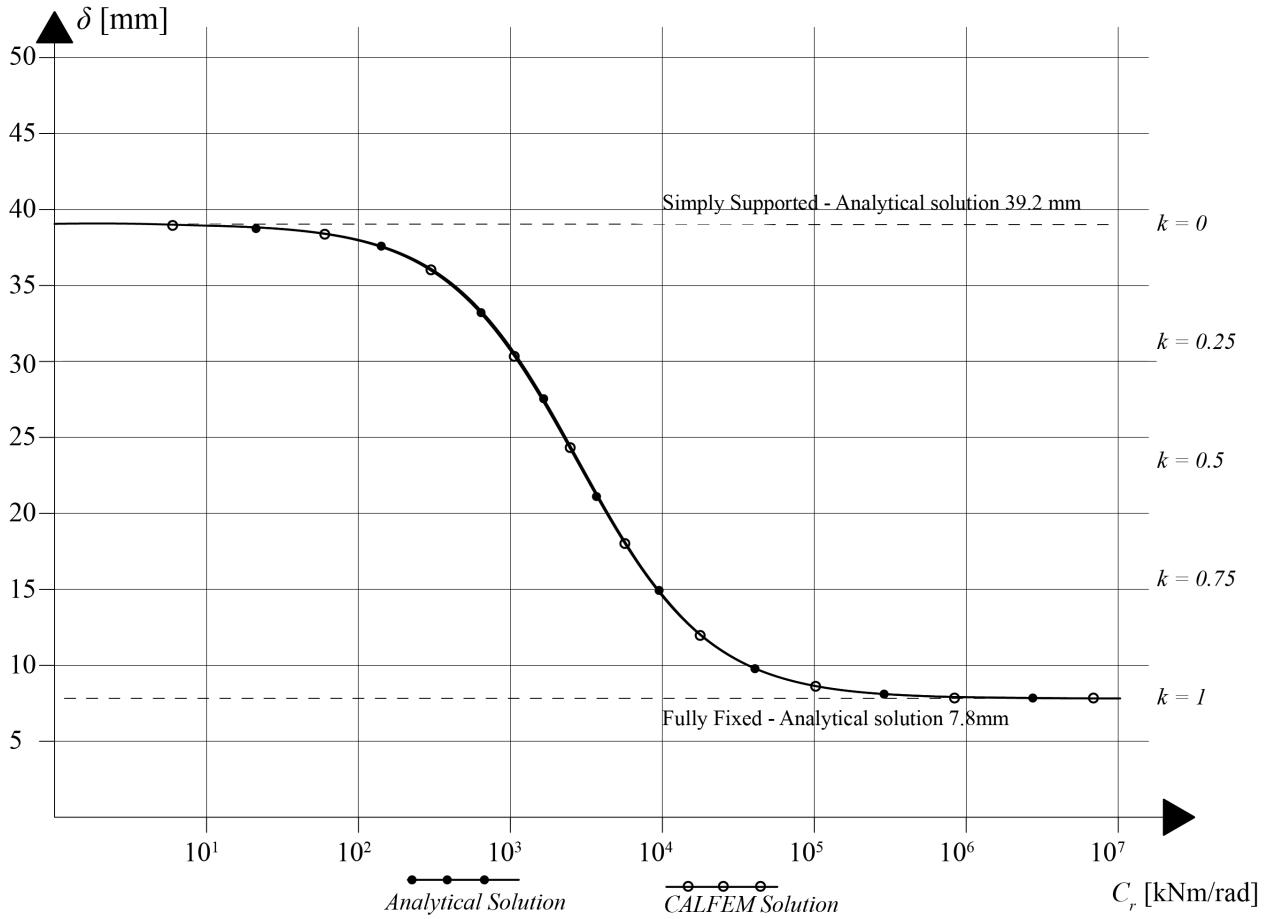

Figure 3.8: *Diagram of the analytical results and FE-results of a semi-rigid beam.*

In order to study the behaviour in a larger system dependent on several joints, in view with final aim of this study, to study gridshells and the accumulated effects. The difference in

behaviour between a rigid, semi-rigid and hinged system is shown in Figure 3.10 - Figure 3.12, by means of a system of 4 beams connected to their supports and each other by a rotational spring with stiffness factor k (as is shown in Figure 3.9), loaded with a uniformly distributed load of 2 kN/m.

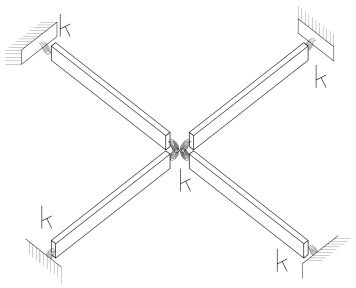

Figure 3.9: *Setup of beam and spring system used in the comparison*

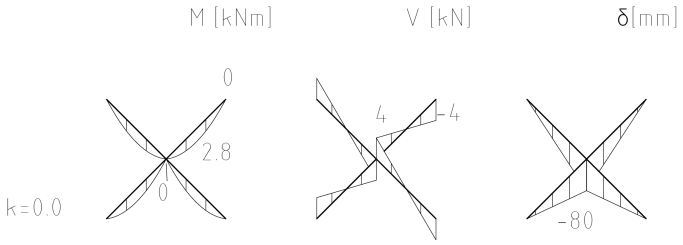

Figure 3.10: *Moment, shear and deflection of the setup shown in Figure 3.9 for a stiffness-factor k=0.0, i.e hinged*

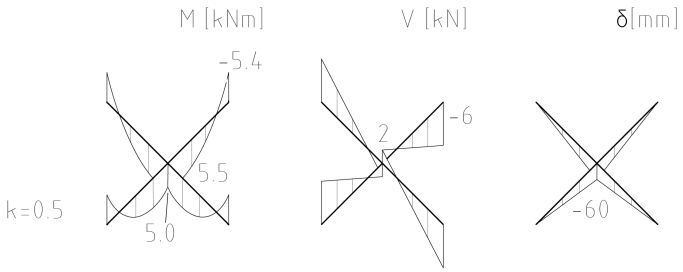

Figure 3.11: *Moment, shear and deflection of the setup shown in Figure 3.9 for a stiffness-factor k=0.5*

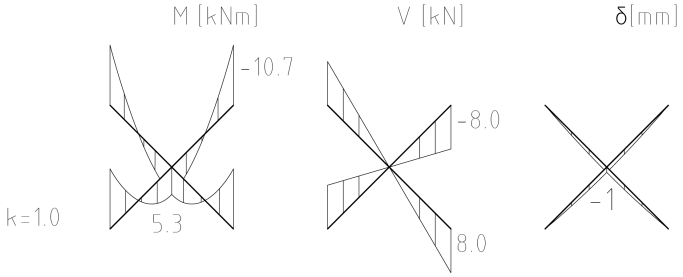

Figure 3.12: *Moment, shear and deflection of the setup shown in Figure 3.9 for a stiffness-factor k=1.0, i.e fixed*

3.2.4 Semi-rigid beam on transverse springs

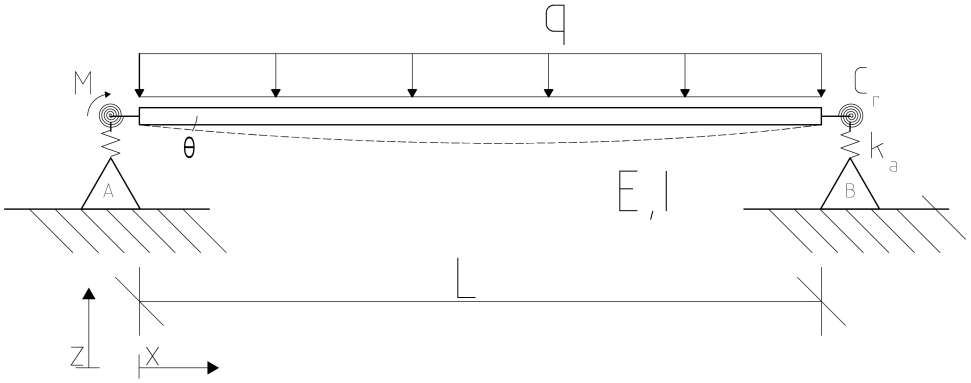

Figure 3.13: *Illustration of the the set-up of a semi-rigid beam on a spring-bedding with uniformly distributed loads.*

The model can be further refined to account for variable stiffness in the vertical translation, giving a system like the one shown in Figure 3.13. This would give the same equation as in Equation (3.30) with the exception of the boundary condition:

$$w(x=0) = -\frac{qL}{2k_a} \Rightarrow C_2 = -\frac{qL}{2k_a}$$

Resulting in:

$$\delta = -\frac{5qL^4}{384EI} + k\frac{4qL^4}{384EI} - \frac{qL}{2k_a} \tag{3.32}$$

where: k_a - *Spring constant translational spring* [N/m]

3.2.5 Axially loaded beam

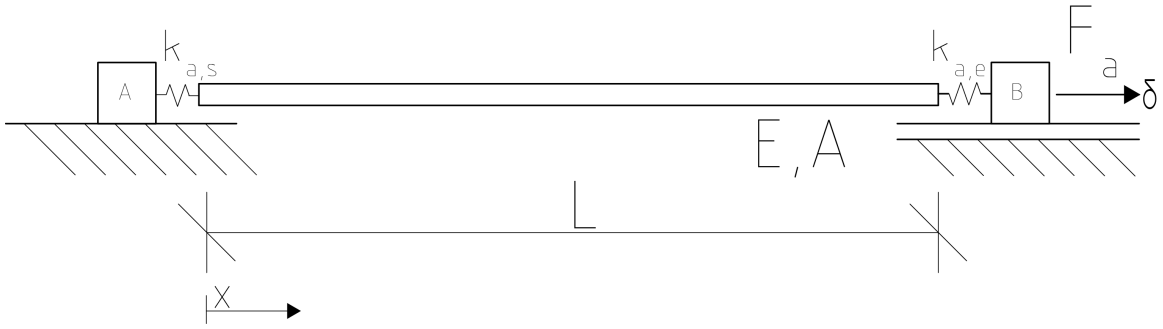

Figure 3.14: *Illustration of the the set-up of a axially loaded loaded beam with longitudinal springs.*

A spring support should be implemented into the axial direction of the beam, as shown in Figure 3.14.

From *Hooke's law* we know:

$$\sigma = E\epsilon$$

Where:

$\sigma = F/A$ - *Normal stress* [N/m^2]
E - *Young's modulus* [N/m^2]
ϵ - strain [-]

Which gives:

$$\frac{F}{A} = E\epsilon \Rightarrow \frac{F}{EA} = \epsilon \Rightarrow \frac{FL}{EA} = L\epsilon = \delta$$

Which, by substitution becomes:

$$\frac{F}{k_{bar}} = \delta$$

Which is analogous to an axial spring as seen in Equation (3.5). Thus since, $k_{a,s}$, $k_{a,e}$ and k_{bar} forms a system of three springs, connected in series, meaning that the axial elongation of the system becomes:

$$\delta = \frac{F}{c_t} \tag{3.33}$$

Where:

$$c_t = \frac{1}{\frac{1}{k_{bar}} + \frac{1}{k_{a,s}} + \frac{1}{k_{a,e}}}$$

Or simplified:

$$\delta = F\left(\frac{1}{k_{a,s}} + \frac{1}{k_{tot}} + \frac{1}{k_{a,e}}\right) \tag{3.34}$$

The maximum axial deflections was calculated for a 10 meter long beam (450x150 mm, GL28c) loaded by 100 kN, according to Equation (3.33) above, and compared to the results of an FE-model of the same setup, to verify the significance of the simplified model. Meaning that the bar stiffness (k_{bar}) is constant while the stiffness of the connections are increased. Results from this comparison can be seen in Figure 3.15, the correspondence should be considered high, with close to no difference between FE-model and analytical results.

As can be seen Figure 3.15, the joint in this set-up is converging towards the behaviour governed by the axial stiffness of the beam at a spring constant of approximately 10^5 kN/m, whereas the behaviour is governed by the spring up until a spring-constant of approximately $7 \cdot 10^3$ kN/m.

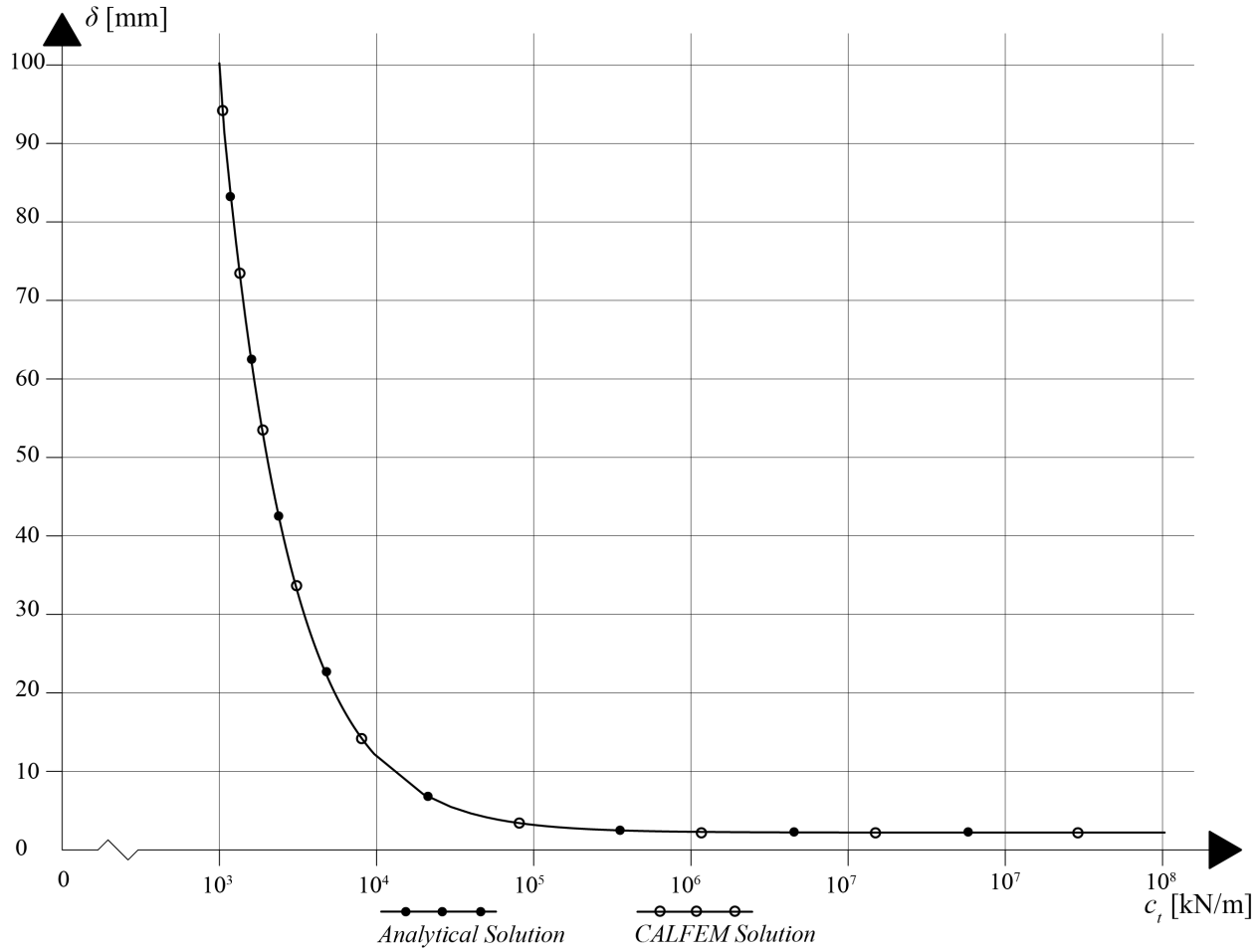

Figure 3.15: *Diagram showing the relation between displacement and axial stiffness for analytical and FE-result of a axially loaded beam on semi-rigid supports.*

3.3 Conclusion

The aim of this chapter was to to introduce a method of evaluating and implement stiffness into calculation models. Now we have a characterized the semi-rigid behaviour, where its clear to see its positioning itself in between the idealised solution of fix and pinned.

Now we also have a model and a method on how to implement this in bigger system, like a gridshell. Something that becomes clear to see is that semi-rigidity is something that can be acceptable in bending, since the cases with low stiffness converges to a solution. While the non-rigid behaviour in axial behaviour seems to converges towards infinity, making a system with non-rigid axial connections a mechanism, thus not functional.

4 Timber

Timber is historically an important construction material, appreciated and used due to its availability and its workability with rather simple tools. Today, apart from the reasons mentioned above, timber is used due to its high specific strength and its low embodied energy.

The first timber structures were built almost ten thousand years ago, and have been used continuously since [Schweitzer, 2003]. With the development of *Engineered wood products* timber overcame two important limitations; the limited dimensions and the imperfections [Gross, 2016] thus being a competitive material for structures in larger scales than before. Engineered wood products are usually sawn timber joined with adhesives. The dimensions of untreated timber are limited to the size of the tree it is cut from, thus by joining, the maximum size can be increased. Untreated timber also contains imperfections such as cracks and knots that will decrease the strength of the material, which is not the case in Engineered timber products, since imperfections can be removed before manufacturing [Johansson, 2015].

Timber is a natural fibre-composite, consisting of longitudinal tracheids, or grains, bound together with lignin, acting as a matrix. Timber thus have a behaviour much like other composites, such as fibre reinforced polymers.

4.1 Structural Behaviour

Timber is, with its composite-behaviour, an orthotropic material, where the material properties are different in each direction. The stronger direction in timber is the *Longitudinal direction*, the direction parallel to grain. The two weaker directions are: the *Circumferential direction* which is the direction following the circumference of the tree and *Radial direction* being the direction towards the center of the tree (shown in Figure 4.1). In most structural applications the two weaker directions are treated as one, *perpendicular to grain* [Johansson, 2015].

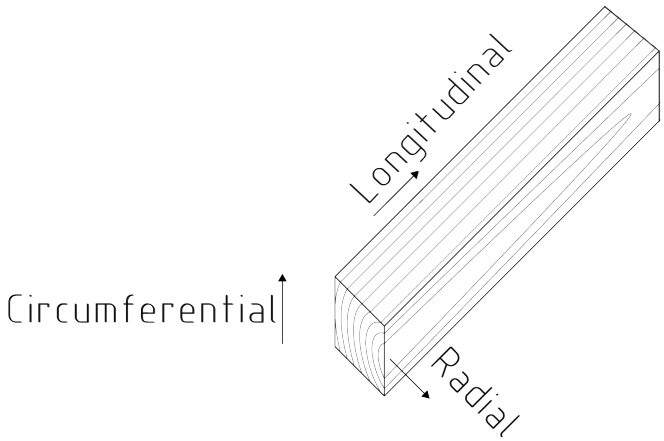

Figure 4.1: *Diagram of the directions in a timber specimen*

Timber structures in Sweden are regulated by Eurocode 5 (SS-EN 1995) [SIS, 2009c]. According to Eurocode the typical design-values of timber, for *Ultimate limit state* checks should be

calculated according to equation Equation (4.1).

$$X_d = X_k \frac{k_{mod}}{\gamma_M} \tag{4.1}$$

Where:
X_d - *Design Strength* [Pa]
X_k - *Characteristic Strength* [Pa]
k_{mod} - *Modification factor that including service class and load-duration* [-]
γ_M - *Partial coefficient* [-]

The interaction between tension and bending for a timber girder shall fulfil the following condition:

$$\frac{\sigma_{t,0,d}}{f_{t,0,d}} + \frac{\sigma_{m,y,d}}{f_{m,y,d}} + k_m \frac{\sigma_{m,z,d}}{f_{m,z,d}} < 1 \tag{4.2}$$

$$\frac{\sigma_{t,0,d}}{f_{t,0,d}} + k_m \frac{\sigma_{m,y,d}}{f_{m,y,d}} + \frac{\sigma_{m,z,d}}{f_{m,z,d}} < 1 \tag{4.3}$$

The interaction between compression force and bending for a timber girder shall fulfil the following condition:

$$\left(\frac{\sigma_{c,0,d}}{f_{c,0,d}}\right)^2 + \frac{\sigma_{m,y,d}}{f_{m,y,d}} + k_m \frac{\sigma_{m,z,d}}{f_{m,z,d}} < 1 \tag{4.4}$$

$$\left(\frac{\sigma_{c,0,d}}{f_{c,0,d}}\right)^2 + k_m \frac{\sigma_{m,y,d}}{f_{m,y,d}} + \frac{\sigma_{m,z,d}}{f_{m,z,d}} < 1 \tag{4.5}$$

Where:
k_m - *Coefficient for redistribution of bending stresses in rectangular cross section, otherwise 1* [-]

Where there is a risk of buckling, the interaction of compression and bending should fulfil:

$$\frac{\sigma_{c,0,d}}{k_{c,y} f_{c,0,d}} + \frac{\sigma_{m,y,d}}{f_{m,y,d}} + k_m \frac{\sigma_{m,z,d}}{f_{m,z,d}} < 1 \tag{4.6}$$

$$\frac{\sigma_{c,0,d}}{k_{c,y} f_{c,0,d}} + k_m \frac{\sigma_{m,y,d}}{f_{m,y,d}} + \frac{\sigma_{m,z,d}}{f_{m,z,d}} < 1 \tag{4.7}$$

Where:
$k_{c,y}$ - *Reduction-coefficient for slender members* [-]

Shear stress should fulfil the following requirement:

$$\tau_d \leq f_{v,d} \tag{4.8}$$

Where:
τ_d - *Shear stress, based on effective width* b_{ef} [Pa]
b_{ef} - *Effective width* $b_{ef} = k_{cr} b$ [m]
k_{cr} - *factor for consideration of cracks.* 0.67 *for glulam* [-]

Compression perpendicular-to-grain should fulfil Equation (4.9) [SIS, 2009c, Eq 6.4]:

$$\sigma_{c,90,d} < k_{c,90} f_{c,90,d} \tag{4.9}$$

Where:
$\sigma_{c,90}$ - *Stress based on* A_{ef} [m^2]
A_{ef} - *Area, where compression zones is increased with 30 mm in the direction along grain.*
$k_{c,90}$ - *Factor considering load configuration, taken as 1* [-]

4.2 Glued Laminated Timber

Glued laminated timber (glulam) is an engineered wood product, a linear structural element (i.e. beams) where lamellas with a thickness of about 10-45 mm are laminated together with uniform grain direction. Similar products are *Cross-laminated timber (CLT)*, a plate material where the lamellas alternate in direction. Further there are *Laminated veneer lumber (LVL)*, consisting of thinner layers, approximately 3 mm and comes as both beams and plates.

Glulam is made by laminating sawn and strength graded pieces of timber together to a bigger section. Strength grading is a process where timber is checked for defects like cracks and knots and are thereafter graded for their expected strength. The use of thinner and sorted elements decreases the risk of hidden defects in glulam compared to structural timber, decreasing the material's partial coefficient as can be seen in Table 4.2.

The lamination also allows for bigger cross-sections than can be achieved from a single tree. It is also possible to increase the length of the beams, usually done with finger-joints. Glulam can also be tailored, by combining materials and strengths, where a common method is to change outer lamellas to a stronger timber-grade, which is then indicated with a *c* at the end of the strength-grade; for example Gl28c (c for combined), to differentiate it from homogeneous, indicated with an *h*, for example Gl28h. The important parts of a glulam beam is shown in Figure 4.2.

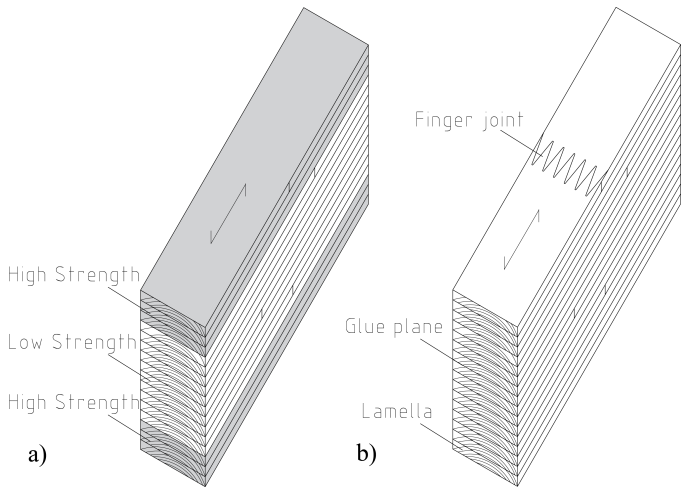

Figure 4.2: *Illustration of Glued laminated timber, and its parts. a) Combined glulam (c-class) b) Homogeneous glulam (h-class)*

Glued laminated timber was introduced in the early 20th century, by Otto Hetzer. One of the most important factors for its breakthrough, apart from the increased length and strength, was its ability to be shaped [Gross, 2016]. If the glueing of the lamellas is done while the lamellas are bent, the beam will be form-stable and the curvature will remain. This method has been common when producing roof-beams for halls, but also bridges. In later years the material has also grown in popularity among architects and designers for use in freeform structures.

Strength values for glued-laminated timber according to Swedish standard SS-EN 14080 can be found in Table 4.1.

Table 4.1: Strength values of Glued Laminated Timber (SS-EN 14080)

Property	**Sign**	**GL28c**	**GL28h**	**GL30h**	**GL30c**
Bending parallel to grain [MPa]	$f_{m,k}$	28.0	28.0	30.0	30.0
Tension parallel to grain [MPa]	$f_{t,0,k}$	19.5	22.4	19.5	24.0
Tension perp. grain [MPa]	$f_{t,90,k}$	0.5	0.5	0.5	0.5
Compression parallel to grain [MPa]	$f_{c,0,k}$	24.0	28.0	24.5	30.0
Compression perp. grain [MPa]	$f_{c,90,k}$	1.2	1.2	1.2	1.2
Shear [MPa]	$f_{v,k}$	3.5	3.5	3.5	3.5
Young's modulus parallel grain [MPa]	$E_{0.05}$	10400	10500	10800	11300
Young's modulus [MPa]	$E_{0,mean}$	12500	13100	13100	13600
Young's modulus perp. grain [MPa]	$E_{90,mean}$	300	300	300	300
Density, characteristic [kg/m^3]	$\rho_{g,k}$	390	430	390	430
Density [kg/m^3]	$\rho_{g,mean}$	430	480	430	480

Table 4.2: Partial coefficient γ_M for different timber products (according to Eurocode 5)

Material	$\gamma_M[-]$
Structural Timber	1.3
Glued laminated Timber	1.25
LVL, Plywood, OSB	1.2
Particle Board	1.3

4.3 Long-term behaviour

There are several properties in timber that are related to time and load duration and that should be considered during design. When loaded for longer periods of time, timber is showing a decrease in strength, related to the creep-rupture effect. The strength loss is of significant order. Well-documented is the strength loss being accelerated with increased moisture content [Hoffmeyer, 2007]. In Eurocode 5, this is considered with the coefficient k_{mod} (values presented in Table 4.3), and the coefficient is chosen based on load duration and service class. Service class is a classification of the environment of the structure, considering temperature and relative humidity, and that will indicate the impact of these effects.

One of the largest studies in this subject was performed in Wisconsin, United States in the 1940's, where beams were tested after a being loaded continuously for 10-years. This study concluded a strength reduction of 40% compared to the initial strength. This study is the

basis of the values in the Eurocodes, presented in Table 4.3 [Sógel, 2010]. Looking at values for one finds that for k_{mod}, service class 1 it is 0.6, meaning a strength reduction of 40 % as was concluded in the experiment in Wisconsin.

Table 4.3: k_{mod} for Structural timber and Glued laminated Timber according to Eurocode 5 [SIS, 2009c]

Service Class	**Load Duration Class**				
	Permanent [-]	Long [-]	Medium [-]	Short [-]	Instant [-]
1	0.6	0.7	0.8	0.9	1.1
2	0.6	0.7	0.8	0.9	1.1
3	0.5	0.55	0.65	0.7	0.9

One consequence of the strength reduction with k_{mod} is that the impact of different load durations will have a very different impact on the structural design, where different load types will be compared to different design-strengths, and should be evaluated separately. Permanent loads e.g. dead-load has the largest reduction, meaning that reducing permanent loads will reduce the utilization of the structure more than reducing other loads.

The design-implication of this is displayed in the following example of a simply supported beam, with input shown in Figure 4.3 and results shown in Table 4.4. The same system is loaded with the same load magnitude, but with different durations assumed. It can clearly be seen that the type of load makes a significant difference in design. If the same load is considered as permanent rather than instantaneous the design utilization is twice as high, which will have huge influence on the design and economy of the project.

Another, related effect is creep deformation, the elastic behaviour of timber is highly time-dependent and increases with time, only a part of the deflections are instantaneous and the deflections increases over time. This means that the final deformation of the material should be checked, as well as the instant. The instant deflections should be checked against the characteristic load combination, whereas the final should be checked against the quasi-permanent combinations [SIS, 2009c].

Material: Gl28c
Length: $l = 4\text{m}$
Width: $b = 0.15\text{m}$
Height: $h = 0.2\text{m}$
Section Modulus: $W_b = \frac{b \times h^2}{6} = 0.001 m^3$
Load: $q_d = 5\text{kN/m}$
Bending Moment: $M_b = \frac{q_d \times l^2}{8} = 10\text{kN m}$
Stress: $\sigma = \frac{M}{W_b} = 10\text{MPa}$

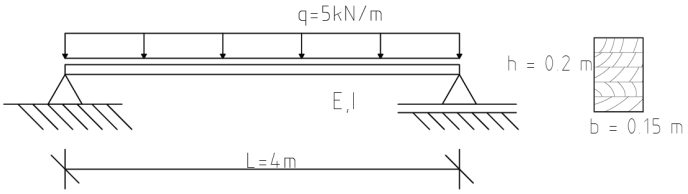

Figure 4.3: *Stress calculations for a simply supported timber beam*

Table 4.4: Comparison between the effect of load duration according to Eurocode 5

	Alternative 1 *Permanent*	**Alternative 2** *Medium term*	**Alternative 3** *Instantaneous*
Service Class	1	1	1
γ_M [-] (Glulam)	1.25	1.25	1.25
k_{mod} [-]	0.6	0.8	1.1
k_{mod}/γ_M [-]	0.48	0.64	0.88
$f_{m,k}$ [Mpa]	28 MPa	28 MPa	28 MPa
$f_{m,d}$ [MPa] (Equation (4.1))	13.4 MPa	17.9 MPa	24.6 MPa
σ [MPa]	10 MPa	10 MPa	10 MPa
Utilization ratio [%]	75 %	56 %	40 %

However, as will be seen in Appendix A, the quasi-permanent load combinations (for roof structures) is mainly influenced by the structural self-weight, as wind can be entirely neglected and effect from snow can be reduced with at least 80 % for these load combinations [Tab A1.1, SIS, 2009a], making the self-weight highly influential in the final deflection. This means that self-weight will be largely influential in the behaviour for both stresses and deflection.

In Eurocode 5, these creep effects are considered through Equation (4.10) - Equation (4.12) [SIS, 2009c] where the Young's modulus $\boldsymbol{E}$, the Shear Modulus $\boldsymbol{G}$ and the Slip Modulus $\boldsymbol{K_{ser}}$ are all decreased.

$$\boldsymbol{E}_{mean,fin} = \frac{\boldsymbol{E}_{mean}}{1 + k_{def}} \tag{4.10}$$

$$\boldsymbol{G}_{mean,fin} = \frac{\boldsymbol{G}_{mean}}{1 + k_{def}} \tag{4.11}$$

$$\boldsymbol{K}_{ser,fin} = \frac{\boldsymbol{K}_{ser}}{1 + k_{def}} \tag{4.12}$$

Where:
$\boldsymbol{E}_{mean}$ - *Young's modulus* [N/m^2]
$\boldsymbol{G}_{mean}$ -*Shear Modulus* [N/m^2]
k_{def} - *Factor for creep, inc. service class* [-], *can be found in Table 4.5*

Table 4.5: k_{def} for *structural timber* and *glued laminated Timber* according to Eurocode 5 [SIS, 2009c]

Material		**Service Class** 1	2	3
Structural timber	k_{def}	0.6	0.8	2.0
Glued laminated timber	k_{def}	0.6	0.8	2.0

Not only the deflections are affected by this, but the reduction of Young's modulus will increase the risk of buckling, making delayed buckling a common failure mode for lattice-domes and gridshells [Holzer, Loferski, Dillard, 1988].

4.4 Manufacture of Curved Members

There are different principles to achieve curvature in timber structures, the most common is presented in the following section. These methods can either be used separately, or combined.

4.4.1 Lamination

Curvature in timber beams can be achieved through lamination, a method only possible to use for glued products, as the process happens during the gluing-process. Where the lamellas during the lamination are clamped to the intended geometry. As the glue dries, the beam will be form-stable. Both single curvature and double curvature can be achieved, with increased complexity [Scheurer et al. 2015].

This process has traditionally been manual, but today there are automatic presses on the market, allowing for high precision in geometry and repeatability. The principle of the method is shown in Figure 4.4.

If the curvature is achieved through lamination, it means that grains will follow the curvature of the beam. Thus cross-grain will be avoided, cross-grain is when grains does not follow the geometry of the beam and is highly unfavourable for the strength of the beam [State Forests of New Wouth Wales, 1995].

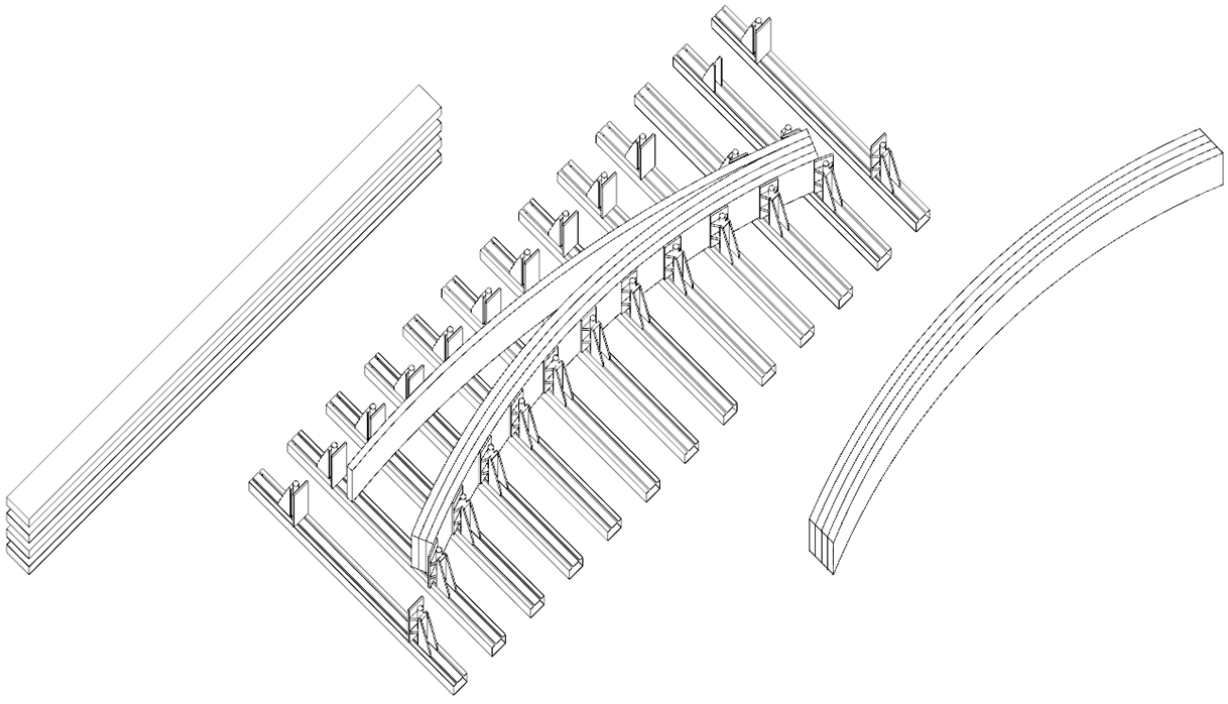

Figure 4.4: *Diagram of the manufacturing process of a curved glulam beam.*

The limitation of this method is the stresses created in the lamellas during bending. The stresses at small radii can be above the limit of structural failure. The immediate, theoretical,

stresses in the outermost grain of the beam can be calculated as [Crocetti, Mårtensson. 2015]:

$$\sigma = \frac{Et}{2r_{in}} \tag{4.13}$$

σ - *Stress* [Pa]
E - *Young's modulus in grain direction* [Pa]
t - *Thickness of lamella* [m]
r_{in} - *Inner radius of beam* [m]

Equation (4.13) shows that the stress is proportional to the thickness of the lamella, meaning that the thicker the lamella, the larger the stresses. The stress is also inversely proportional to the radius, meaning that the smaller the radius the larger the stresses. This means that in beams of very small radii, the thickness of lamellas should be decreased. Beam made of thin lamellas are more labour intensive, thus more expensive.

$$r_{in}/t > 240 \tag{4.14}$$

$$\sigma_{m,d} < k_r f_{m,d} \tag{4.15}$$

where:
$k_r = 0.76 + 0.001\frac{r_{in}}{t}$ - *Coefficient as condition in Equation* (4.14) *is not met*

Stresses during bending needs to be considered to avoid failure during manufacture. But due to the relaxation behaviour of timber, the stresses calculated with Equation (4.13) are not necessarily translatable to tabular bending strength. In Eurocode there is no absolute limit of the minimum radius, but suggests the relation presented in Equation (4.14) [SIS, 2009c] as a limit of when residual stresses should be assumed to remain in the beams and the coefficient k_r, taking this into account should be used [SIS, 2004 - Eq. 6.49].

German and British standards suggest the limit in Equation (4.16) as the minimum possible radius [DIN 1052], in combination with the rules of strength reductions above. Table 4.6 shows the minimum radius for different common lamella thicknesses, including the strength coefficient when applicable.

$$r_{in}/t > 150 \tag{4.16}$$

Table 4.6: Minimum radius for given thicknesses of lamellas for GL28c

Lamella Thickness t [m]	**Radius** R_{in} [m] *Without Reduction*	*With Reduction*
45 mm	10.8 m	6.8 m (k_{cr}=0.91)
40 mm	9.6 m	6.0 m (k_{cr}=0.91)
33 mm	7.9 m	4.9 m (k_{cr}=0.91)
25 mm	6.0 m	3.8 m (k_{cr}=0.91)
20 mm	4.8 m	3.0 m (k_{cr}=0.91)
10 mm	2.4 m	1.5 m (k_{cr}=0.91)
8 mm	1.9 m	1.2 m (k_{cr}=0.91)

If the conditions above are met, the stresses occurring during manufacture does not need to be considered, since the residual stresses are considered to be negligible.

Members with double curvature can be made by lamination, but will be more complex and more expensive, partly because many of the commercial press beds today are not built for more than one bending axis, resulting in either low competition for the contract, or hand-made solutions. Another consequence is that the structure needs to be divided, not only in stronger direction but also in the weaker, as seen in Figure 4.5, resulting in a more labour-intensive solution with more lamellas and more glue-planes.

The technique of laminating glulam can also be used to create blanks for machining. Scheurer et al [2015] suggest five categories of curvature when designing timber structures *Straight, Single curved, Single curved arc, Double curved with no torsion* and *Double curved with torsion*, in rising degree of complexity and price (illustrated in Figure 4.5). While others are using a simpler division, like *Straight*, *Single curved* and *Double curved* [as per correspondence with Blumer-Lehmann, 2018].

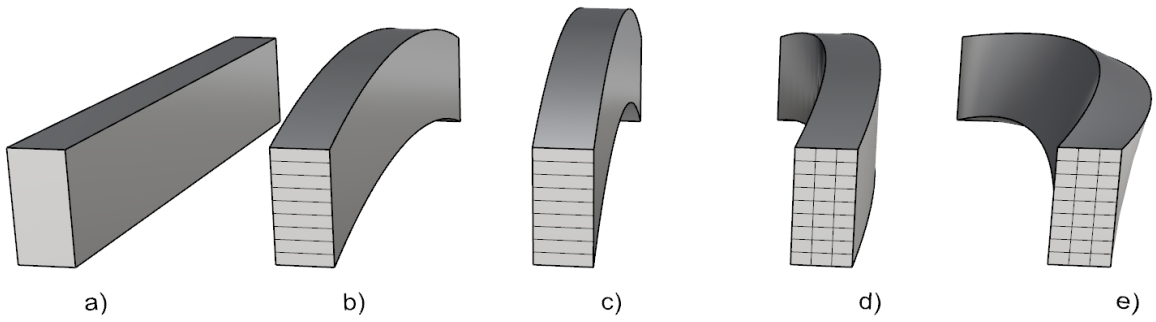

Figure 4.5: *Types of blanks a) Straight b) Single Curved c) Single Curved Arc d) Double Curved without Torsion e) Double Curved with Torsion*

4.4.2 Machining

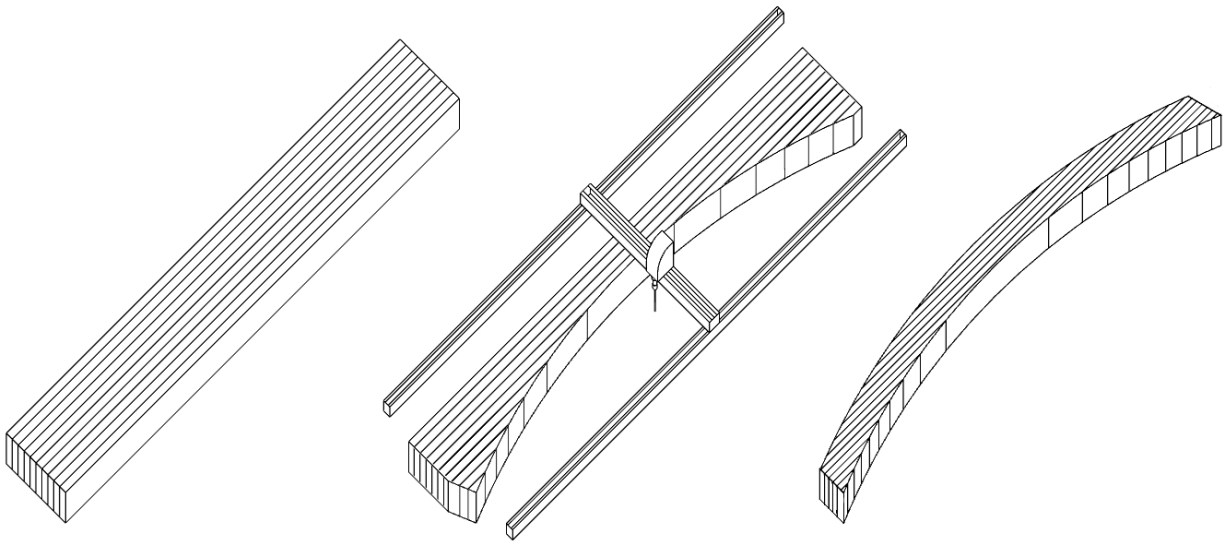

Figure 4.6: *Diagram of the manufacturing process of a milled glulam beam.*

The curved geometry can be cut from a timber blank (an uncut timber piece) which can be any of the basic geometries described in the last section. The principle of the method is shown in Figure 4.6.

Machining allows manufacturing of members with curvature around one or two axes, as well as twisting members, also from straight blanks, making it a time-efficient solution. However, using simple blanks for milling will result in cut fibres, leading to problems with cross-grain and reduction of strength, since the strong direction of the material and the main axis of the beam does not coincide. There will also be material waste, making machining a material-inefficient method, both due to material and strength. The amount of both waste and strength reduction is decreased using bent blanks for machining.

The strength loss coefficient related to beams tapered at angle to grain is given in Equation (4.17), for tapered sides in bending-compression and Equation (4.18), for tapered sides in bending-tension [Eurocode 5. SIS. 2009c. equations 6.39-6.40]. But since a curved beam with uniform cross-section, as would often be the case in a gridshells structure, will be cut on both sides, a simplification can be made, using the higher reduction, which is Equation (4.18) for bending tension.

$$\frac{1}{k_{m,\alpha,c}} = \sqrt{1 + \left(\frac{f_{m,d}}{1.5 f_{v,d}} \tan\alpha\right)^2 + \left(\frac{f_{m,d}}{f_{c,90,d}} \tan^2\alpha\right)^2} \tag{4.17}$$

$$\frac{1}{k_{m,\alpha,t}} = \sqrt{1 + \left(\frac{f_{m,d}}{0.75 f_{v,d}} \tan\alpha\right)^2 + \left(\frac{f_{m,d}}{f_{t,90,d}} \tan^2\alpha\right)^2} \tag{4.18}$$

Using these equations the strength coefficient can be calculated. In Table 4.7 the relation between angle and strength coefficient is presented, with the conservative assumptions of

using the biggest angle on the beam, which for short elements in a gridshell is a reasonable assumption. Presented in this table is also the minimum radius that can be achieved with this angle for two given segment lengths; 1.6 m and 3.2 m, representing one or two grid spacings in the gridshell of the case study, that is presented in Chapter 6.

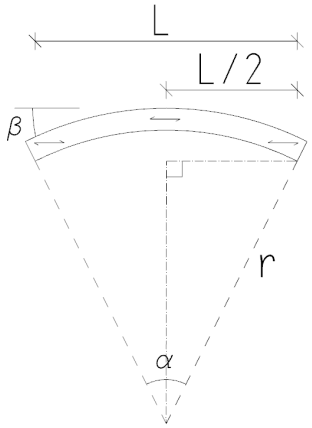

Figure 4.7: *Simplified beam geometry*

The minimum radius is a simplification based on a circular beam element, as shown in Figure 4.7. A longer curved element has a larger central angle and thus larger angles to grain at each ends. If one allows a certain angle for a beam and thus a certain reduction, either the element length or the inner radius of the beam must be changed to make the element fulfil requirements. The relation between the length of the elements and the radius in the example is $L = 2r \sin\beta$ and $\beta = \alpha/2$, which the Table 4.7 is based on.

Already at small angles the reduction of the strength is high, as can be seen in Table 4.7. Interesting is the comparison between Table 4.6 and Table 4.7. To achieve a radius of 4.8 m with lamination, this could be performed without strength reduction, using 20 mm lamella thickness. However if the same beam should fabricated solely by cutting from a straight blank this would demand a strength reduction of 65%, and eliminating the possibility of members longer than 3.2 m

Table 4.7: Strength coefficient factor $k_{m,\alpha,t}$ and $k_{m,\alpha,c}$ and minimum radius for given lengths of lamellas for GL28c/GL28h

Angle	**Strength coefficient [-]**		**Min. Radius [m]**	
β	$k_{m,\alpha,t}$	$k_{m,\alpha,c}$	$L = 1.6$	$L = 3.2$
1°	0.98	1	45.8 m	91.6 m
2°	0.93	0.98	22.9 m	45.8 m
3°	0.85	0.96	15.3 m	30.6 m
4°	0.76	0.92	11.5 m	23 m
5°	0.67	0.88	9.2 m	18.4 m
10°	0.34	0.62	4.6 m	9.2 m
15°	0.19	0.39	3.1 m	6.2 m
20°	0.11	0.25	2.3 m	4.6 m

The somewhat larger manufacturing tolerances of lamination usually means that all members will be milled after lamination, if only to smoothen the surface. This, however, being just a few millimetres at the surface, does not result in any strength reduction. Machining on pre-laminated blanks can also be used to make detailing for joints and pre-drilling for fasteners. Using a pre-shaped beam as blank however has the advantage that problems related to cross-grain will be reduced.

4.4.3 Segmentation

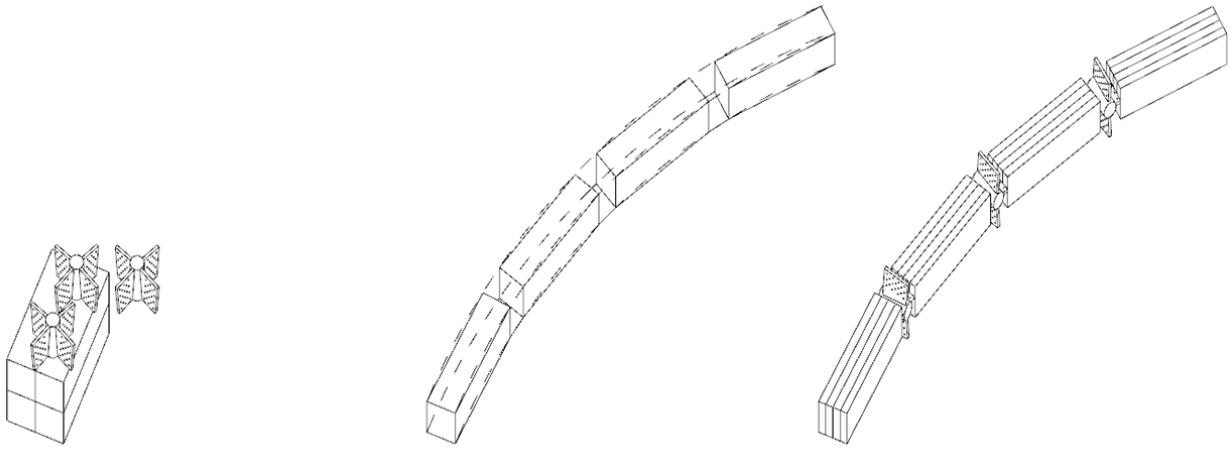

Figure 4.8: *Diagram of the manufacturing process of a segmented glulam beam.*

There are different reasons for segmentation. Segmentation can be used to create pieces possible to transport. The other reason is that segmentation can be a tool to create curvature, as shown in the *Herbert Art Gallery* (Section 2.5).

The grid is divided into non-continuous members, e.g. between every node and beams could potentially be straight in between the nodes creating an impression of curvature. Using straight members to create curvature will however complicate the intersection, since the curvature needs to be built in to the joint. Using straight members, there will be no cross-grain. Using straight members might also affect the smoothness of the surface.

On the other hand, as mentioned, segmentation is usually needed to create members of manageable sizes, e.g. sizes that can fit on a truck. Segmentation can obviously also be done also with curved members. The principle is shown in Figure 4.8.

4.5 Transportation

Glulam beams is a prefabricated product, manufactured off-site and transported on-site. Due to unstable temperature and moisture-conditions the gluing process is not suitable to do in-situ. Transportation governs the size of the members that can be used in the structure, and if the structure contains members exceeding this size, the members have to be assembled

and spliced on-site.

The possible transportation-lengths differs between countries, but the Swedish regulations states that lengths up to 24 meters, including the vehicle can be transported without special measures, while lengths up to 40 meters can be transported with special permission and extra measures taken, i.e. an escorting vehicle and signage [Borgström et al. 2018]. This also applies to the width and height of members, with a maximum height of approximately 3 meters and a maximum width of approximately 2.5 meters [Crocetti, 2016]. The maximum height is something that will affect the transport of curved pieces, where the curvature increases its total height. Thus, the maximum size one can afford or handle should be considered at an early stage since this might have strong impact at design.

5 Geometry

The process of creating the geometry and plan the form of structure and members will be influential on the possibilities and complexity of production and its cost in the later stages of the project. When designing freeform structures it is also important to know what information the drawing or model contains, and what needs to be added, and how well this translates to a real object. This chapter will therefore present a few aspects of digital geometry and how these corresponds to the actual physical objects such as beams and other structural members.

To differentiate between the digital objects and physical objects in the following chapter, the notation *curve* refers to a digital object whereas the physical object is refereed to as *beam* or *bar*, the same applies to the notation *surface*, that is a digital representation of a physical object like a *façade, shell* or *pane*.

5.1 Master Surface

Freeform projects are often based on a master-surface from which the structure is developed, e.g. by mapping a grid onto it. Structures based on a master-surface are often called 2.5-dimensional, since many properties of the geometry are stored and can be extracted from the surface rather than coordinates in space [Nicholas et al. 2016]. A master-surface contains a lot of the information that will be inherited by the beams and façade in the later stage. Among them outer dimensions, curvature and normal directions, something a line-model would not implicitly contain.

Using a master-surface is helpful during the design of geometry. By mapping the grid onto the surface it is easy to evaluate properties such as curvature of the members as well as whatever the façade can be made from planar panes. Using a master-surface, onto which a grid is mapped will also guarantee connectivity between members and, depending on the quality of the surface, continuity in the beams. From a design and geometrical standpoint this is a simplified approach that comes with great benefits for structures like gridshells.

5.2 Grid

The most common types of grids in gridshells are triangular and quadrangular, both coming with advantages and disadvantages. If a grid is to be projected onto a master-surface, as is common-practice in freeform projects, many properties can be decided in the layout of the initial grid. A planar grid consisting of straight members is preferred, since this guarantees a gridshell of curves of single curvature. Since the method is equal to cutting the surface with a plane. This applies to both triangular and quadrangular grids. Projection however might, in areas of surface with severe curvature result in distortion of the grid, with mesh sizes that changes due to the inclination of the surface. In order to get a completely equidistant grid, one can use a grid relaxation or the Chebychev net method [Poulsen, 2015]. An equidistant grid however might create members with double-curvature.

A triangular grid can with very small divergence cover all surfaces [Glymph, 2002] (see

Figure 5.2. The triangle in itself is also stiff for in-plane forces (Figure 5.1), which is a requirement for shell-behaviour, as the forces are transferred in-plane. A triangular pane is also always planar. Disadvantageous for the triangular grid is the node, since more members are connected, and thus increasing complexity. Glazing of a triangular grid is also more complex and expensive, due to increased number of operations during manufacturing [Glymph, 2002].

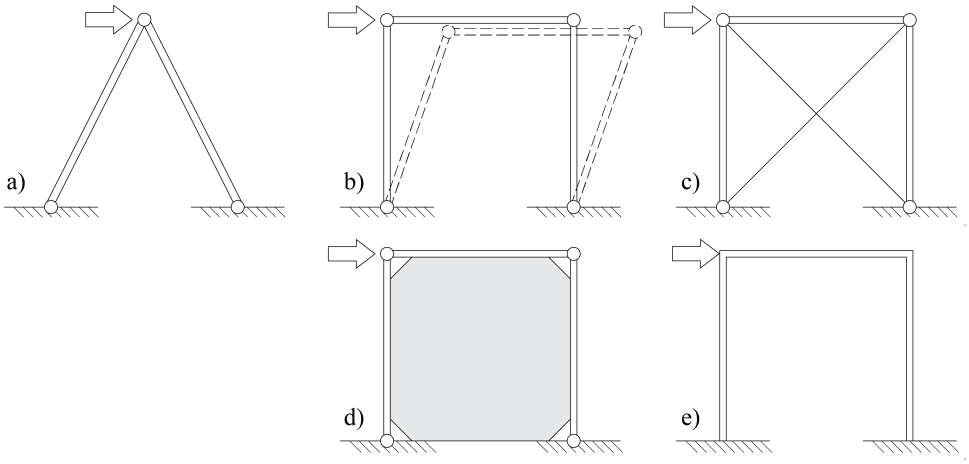

Figure 5.1: *Illustration showing the rigidity of different kinds of grid-elements. a) a triangle is rigid by itself b) A quadrangular element will collapse if not stiffened c)-e) Measures to stiffen a quadrangular element*

A quadrangular grid, not being stiff by itself, needs to be stiffened, to withstand the in-plane shear, either by moment-resisting connections or by bracing (illustrated in Figure 5.1). Bracing can be done by either cross bracing (Figure 5.1*c*) or a stiff pane, such as an timber board (Figure 5.1*d*). As stated earlier is it complicated to achieve full rigidity in timber joints with such thin members as used in gridshells, meaning that option shown in Figure 5.1*e* should not be considered for timber gridshells.

A quadrangular grid can also, in theory, describe any surface but not necessarily with planar quads, the idea of quadrangular meshing of a surface is illustrated in Figure 5.2. However planarity will be needed if using a stiff material, like glass is considered as façade. If planarity is a demand on the structure, the surface might have to be drastically remodelled.

5.2.1 Planarity

Planarity relates to the curvature of each individual sub-surface or pane of the segmented geometry. If the structure is supposed to be clad with a somewhat stiff material like glass or plywood, planarity is an important property in order to keep costs down. While curved panes are possible to manufacture, it is a very complicated and costly process. The concept of discretizing a surface into triangular or quadrangular meshes is shown in Figure 5.2.

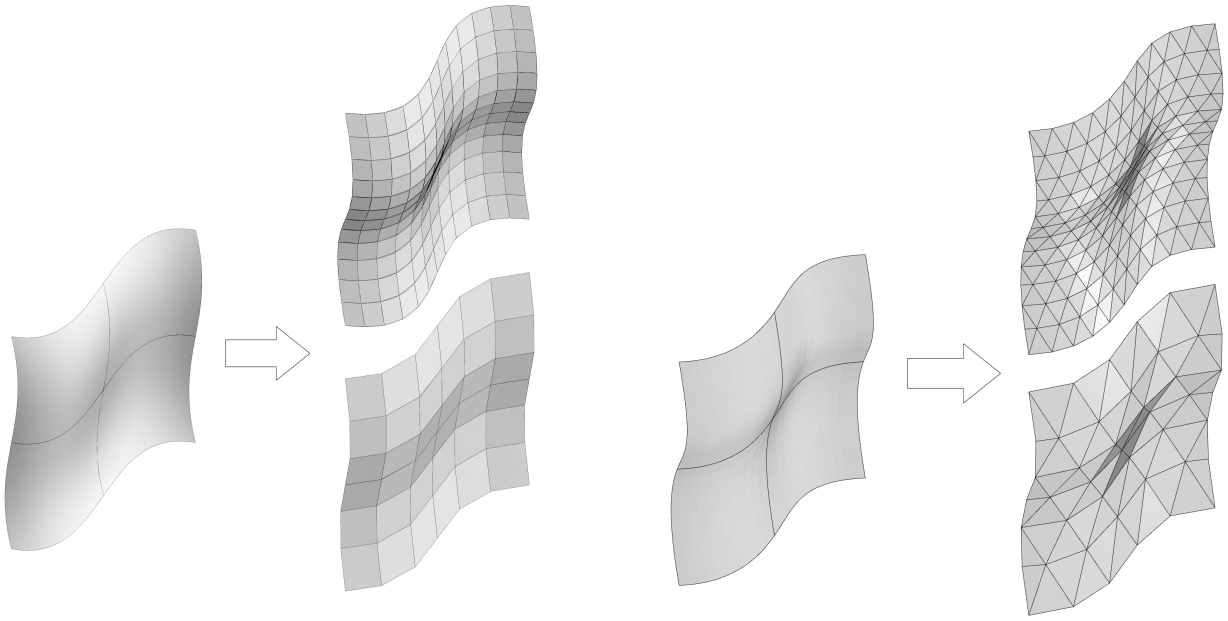

(a) Discretized with planar quadrangular surfaces (b) Discretized with planar triangular surfaces

Figure 5.2: *The concept of discretization of a surface, the discretized surfaces all consists of planar sub-surfaces of different level of coarseness.*

When working with other cladding materials, like timber laths, membranes or open structures, planarity is not a necessity. For example the *Centre Pompidou Metz* being a hexagonal structure covered with a membrane, thus with no need of planarity.

Planarity is strictly a problem when designing a grid based on polygons with more than three corners, since there is always a plane containing all of three arbitrary points. This discussion is thereby mostly applicable to quadrangular and hexagonal grids. Since not every surface can be panellized with planar quads [Schober et al. 2002], the need of planarity is an aspect that should be considered early in the design.

One way to work with planarity, which is the preferable one, is to work with a method that guarantees planarity, such as translational surfaces, but if one want to base the design on a form-found geometry, or a given design-proposal, it is important to be able to evaluate given geometry, to see if it is possible to clad or not.

Planarity can be measured by creating a plane from three points and then measure the distance from the plane to the fourth point, thereby defining the out-of-plane distance. The plane is defined by three points (p_1, p_2, p_3) from the vertices (p_1, p_2, p_3, p_4). The normal to the plane can be calculated from the cross-product of two vectors as:

$$\mathbf{n} = \vec{p_1 p_2} \times \vec{p_1 p_3}$$

From the normal, the plane is being defined, and the distance to the fourth point (p_4) point is measured as:

$$d = \frac{|\mathbf{n} \cdot \mathbf{w}|}{|\mathbf{n}|}$$

where $\boldsymbol{w}$ is a vector between the point p_4 and an arbitrary point on the plane (for example $p_4\vec{p}_2$).

5.3 Curvature

For a two-dimensional curve, the curvature is defined as $\kappa = 1/r$, where r is the radius. Thus the curvature is inversely proportional to the radius. The curvature is positive if the focal-point of the curve is above the curve and vice versa. When talking about curvature of a surface one usually refers to the Gaussian curvature, which is the product of the maximum and minimum principal curvature at the given point ($\kappa = \kappa_1 \cdot \kappa_2 = 1/r_1 \cdot 1/r_2$). A positive Gaussian curvature means that the surface is synclastic, like a sphere while a negative Gaussian curvature means that the surface is anticlastic, like a hyperbolic paraboloid. A zero-Gaussian curvature means that at least one direction is straight, like in a cylinder or a plane (see Figure 5.3).

In gridshells the curvature of the surface itself is not the main interest, but the curvature of the grid. Thus, when evaluating the curvature for a gridshell, it is important to incorporate the grid-lines, with spacing and direction.

The curvature will, besides influencing the structural behaviour, possibly influence available manufacturing-methods. The methods available for forming timber and their corresponding limitations are presented in Section 4.4.

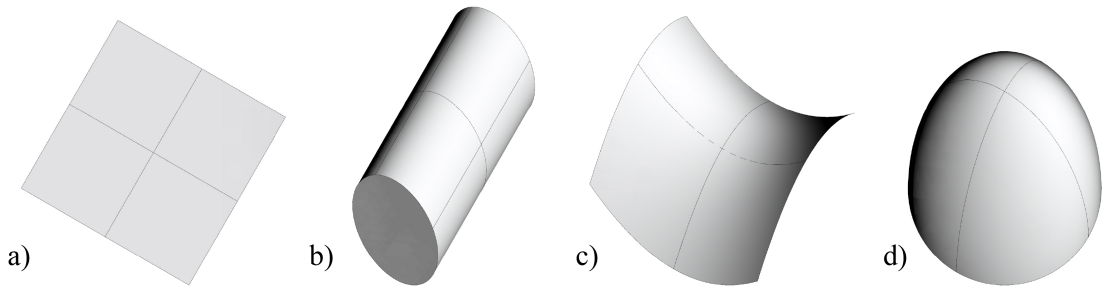

Figure 5.3: *a) Zero Gaussian curvature - $\kappa = 0$ b) Zero Gaussian curvature - $\kappa = 0$. c) Negative Gaussian curvature - $\kappa < 0$. d) Positive Gaussian curvature - $\kappa > 0$.*

Modelling of geometry should be done with the material and the manufacturing method in mind, so that the designed geometry will be possible to manufacture. Each curve in a model represents an object which the material must allow and be able to form, otherwise the drawing and the manufactured outcome will be so different, that assembly can not be ensured.

As a starting point on how to represent freeform timber geometry, the solution can be found in the history of drafting. The *Spline* was a draftman's tool consisting of a thin strip of wood used for drawing curves in the nautical, automotive and aviation industries (illustrated in Figure 5.4). The timber strip was held in place with weights, called ducks. The ducks are creating nodes where translational movements are locked, but free to rotate, the timber strip will then find a shape of minimal strain energy under these boundary conditions [Norton, 2002].

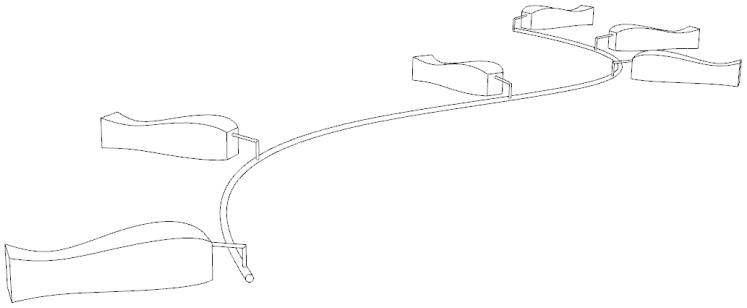

Figure 5.4: *A Draftman's Spline*

As drafting was transferred to computer and CAD-software, this was a functionality that was translated into the digital environment by the development of the *Spline-curve* [Norton 2002] a family of polynomial curves originally created to imitate the behaviour of the spline tool. The spline-curve is defined by a number of control-points, corresponding to the ducks.

Splines are included in many CAD-software, among them *Rhinoceros 3D* where they are included through the extended spline definition *Non-Uniform Rational B-Splines* (NURBS) [Mcneel,2018]. This means that the spline-curve is developed to imitate the behaviour of a thin material with bending stiffness, such as a timber strip. A hypothesis from this analogy would be that a digital geometry defined as a spline-curve, should be transferable to a thin timber strip. And since the lamination process also consists of thin laths held in place at discrete point, it means that this analogy would hold for curved glulam as well.

The analogy for sure holds true if the chosen manufacturing method is machining, since most CAM machinery are based on splines, thus can cut the provided geometry with high precision.

To test this compatibility between curve and beam, and where limitations may occur a FE-simulation of a glulam press was developed by the author. It was created in Grasshopper, to be able to work in a NURBS-environment, and the FE-software Karamba was used to be able to perform material simulations.

The simulations takes an arbitrary curve as input, with the aim of recreating it. From the curve it creates the "workshop data", i.e. the position of clamps and length of the beam. These boundary conditions are then used in order to run a FE-analysis of the lamination process. It creates a beam-element with the thickness of one lamella, and tries to bend it with the given boundary conditions. Thereafter it takes the centreline of the deformed beam which is exported to a geometrical post-processing, described further in Section 6.2.2.

The centreline was also used to evaluate the correspondence between the simulated beam and the curve. Some of the evaluated geometries can be seen in Figure 5.5. In general the correspondence between the NURBS-curves and the beams are high, with small divergences (Figure 5.5 *a*)-Figure 5.5*c*)). Making them suitable as representation, which is also confirmed by Stehling et. al. [2014].

One finding from the simulation is the relation of the spacing of the clamps in the physical press-bed, to the spacing of control-point in the digital curve. Many of the commercial CNC-presses available today has a clamp spacing between 400-600 mm.

Using a NURBS-curve with closer spacing between control points than between the clamps of the press, may result in beams missing nuances or features from the digital geometry (Figure 5.5*e*), creating a resolution problem. This means that features smaller than the spacing will not be represented in the physical object. This is mainly a problem at large differences in the spacing.

Modelling with digital spacing higher than physical spacing makes the correspondence between the geometries high. It is known that an arc on a plane can be defined from three peripheral point. Similar rules applies when planning physical geometry, that curvature takes a certain number of clamps to establish. As in Figure 5.5*f*, where the spacing is not necessarily small, but with several changes of curvature direction, the clamps are not sufficient to catch these changes.

Spacing of control points is also problematic in geometries with few control points, but with low spacing, like with semi-circles (Figure 5.5*d*), since the spacing of control points can not be matched by the clamps. Kinks or other discontinuities are something to avoid, since this is an unnatural behaviour of both splines and of the material, and the correspondence therefore low.

Low correspondence is also found in areas of severe curvature, where the behaviour of the curves are more flexible than the timber, however this is the phenomenon considered with the curvature limitations presented in Section 4.4, thus is the correspondence at small radii already regulated, and the lack of correspondence is therefore not essential.

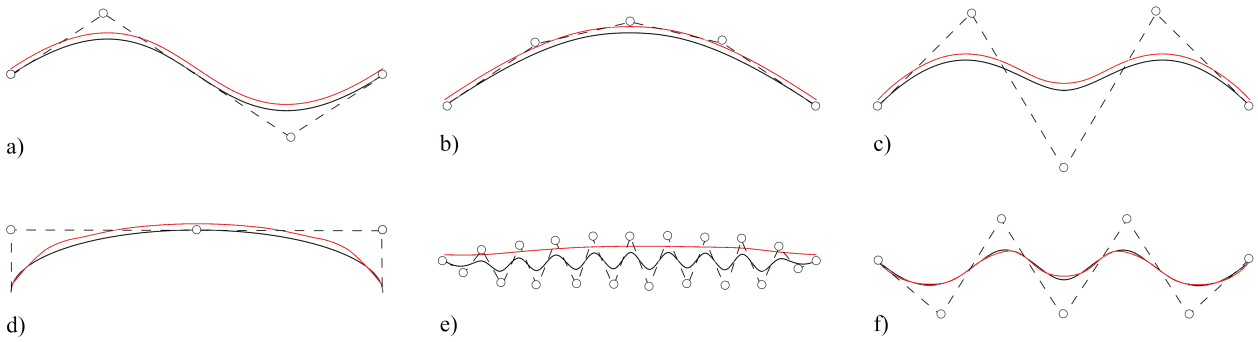

Figure 5.5: *Input geometry with control points (black). Results from FE-model (red). a)-c) correspondence between NURBS and timber d)-f) Some of the problematic modeling behaviour found.*

It can be concluded that NURBS and an elastic material do behave similarly within the limitations above, suggesting that using NURBS as a representation of curved timber beams during a design-process seems suitable, both for bent and cut geometries.

To be able to measure curvature and categorize the structure according to blank types (as

presented in Section 4.4), an algorithm was written in the scope of this project, which analyses the grid in *Rhinoceros* for curvature in one or two directions, geometrical torsion or torsion based on the normal of the master-surface. From these checks it categorizes the curves into a suitable type of blank. The included types of blank are: *straight*, *single curvature*, *single curvature - minor direction*, *double curvature without torsion* and *double curvature with torsion*. The results are then exported into an Excel-interface, where the beams could be analysed separately or as a summary for the entire structure. The interface and functionality of the tool is shown in, for a demo, in Figure 5.6.

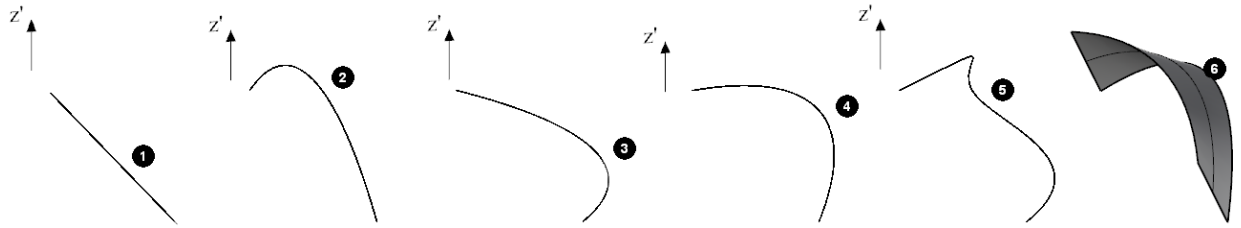

(a) Input geometry, including the numbering added by the tool

Number	Curvature Dir 1	Curvature Dir 2	Torsion	Length [m]	Blank Type
1	0	0	0	20	Straight
2	1	0	0	21,16	Single Curved
3	0	1	0	21,16	Single Curved - Minor
4	1	1	0	21,16	Double Curved Without Torsion
5	1	1	1	22,5	Double Curved With Torsion
6	1	1	1	20,85	Double Curved With Torsion - Surface

(b) Analysis of each element

	Total	Straight	Single Curvature	Single Curvature - Torsion	Double Curvature without Torison	Double Curvature with Torsion		Total Length
Nr of elements	6	1	2	0	1	2		126,83
Ratio	100,0%	16,7%	33,3%	0,0%	16,7%	33,3%		

(c) Summary of analysis

Figure 5.6: *Diagram of the input and output of the Blank-geometry analysis tool for a demo set of curves*

Beam orientation

During the design-process the transition from the digital representation to physical object should be considered. Thinking about what properties are directly translatable and not. For example the transition from *curve* (digital object) to *beam* (physical object). The curve is a uni-axial representation of an object with three dimensions, but a single-curved curve may represent a double-curved beam, depending on the local z-axis of the beam (as can be seen in Figure 5.7).

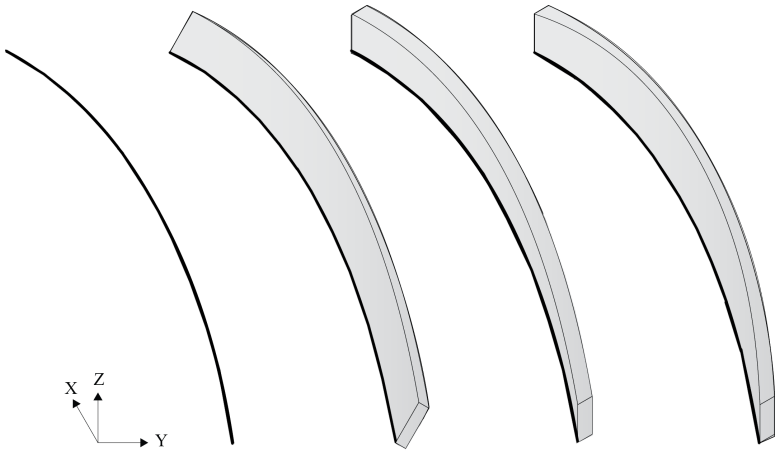

Figure 5.7: *Figure showing the principle that a single-bent curve not necessarily represents a beam in plane bending*

This means that the curvature in three dimensions is not implicit, but something that must be defined, thus a digital grid can be translated into a large number of physical grids, with different degree of feasibility and complexity. In practice there are a few basic rules, such as limited twist, keeping the strong direction of the beam in the direction of the loads and keeping a close to uniform direction of the system throughout the structure. This means that the designer automatically excludes non-important options, but still, considering that nothing is given by the grid itself, a decision needs to be taken on how to arrange orientation of the beams, most importantly defining the local z-direction of the beam.

In roofs, shells and canopies and other covered freeform projects, the façade and the beams are somehow related. Desirable by designers is often that the normal of beam and surface are close to parallel, this might however, if the surface is not made with absolute care result in twisting members. Thus it is not enough to consider the curvature in the digital model during design, but also the orientation.

The matter increases in complexity if one takes several local directions into consideration, each representing different functionalities. A proposal of important directions to consider during timber design is presented in Figure 5.8. The *Beam normal* is the normal of the top face, relating mainly to finish and the connection to the façade. The *Bending axis* (or *Bending axes*) is the axes around which the beam is curved. And the *Assembly direction* is the direction in which the intersecting beam needs to be assembled - in case of directionals joints such as lap joints or brackets. The important point is that these are not necessarily related, and can be changed individually.

Changing these directions have different consequences. Throughout the length of a single member, the *Assembly direction* should be kept constant, since several lap joints, with different directions usually can not be activated simultaneously [Stehling et. al. 2017].

If the *Bending axis* changes, it means that the member is twisting. A non-constant bending axis is possible, but induces a high level of complexity in the manufacturing.

A changing *Beam normal* is mainly a matter of aesthetics and fitness with other members,

to make the visible surface follow a master surface or intersecting beams. The twisting top/bottom surface of the beam needs to, if not bent accordingly, be manufactured, usually through a subtractive process as described in Section 4.4. Although this means that the initial beam needs to be oversized.

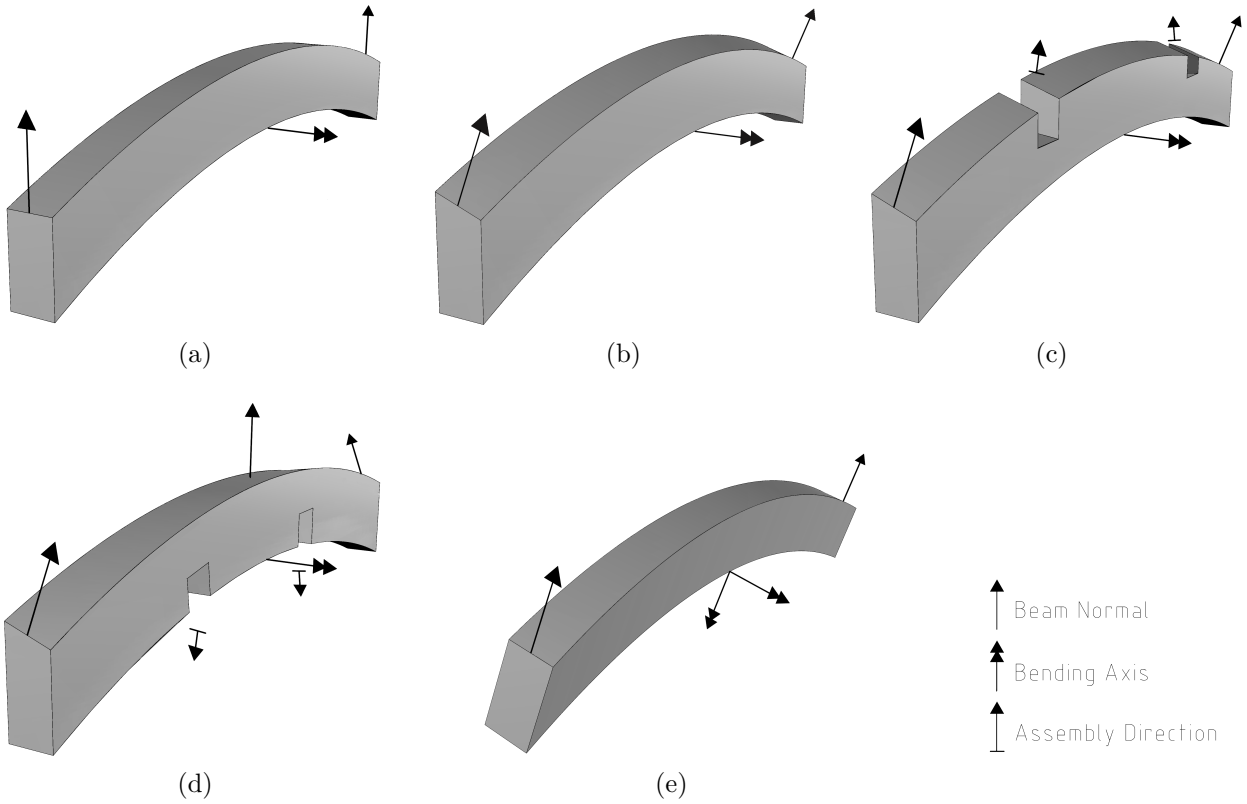

Figure 5.8: *Display of different configurations of the suggested local directions.*

6 Design - Case study

As a case study for a rigid timber gridshell is chosen the project in Figure 6.1. During this chapter, several of the ideas discussed earlier in this report is implemented and tested. The geometry of of the structure is developed and analysed geometrically and structurally. Several joint typologies that can potentially be used for the case study is evaluated for strength and stiffness.

In the end of this chapter is a final proposal, an idea of how to plan and manufacture the case study, taking all aspects from the study into account. There is also a structural analysis performed for the structure, with the actual stiffness of the chosen joint types.

6.1 Conceptual design

In brief the project and the first steps of the structural concepts will be described in the following section.

6.1.1 Context

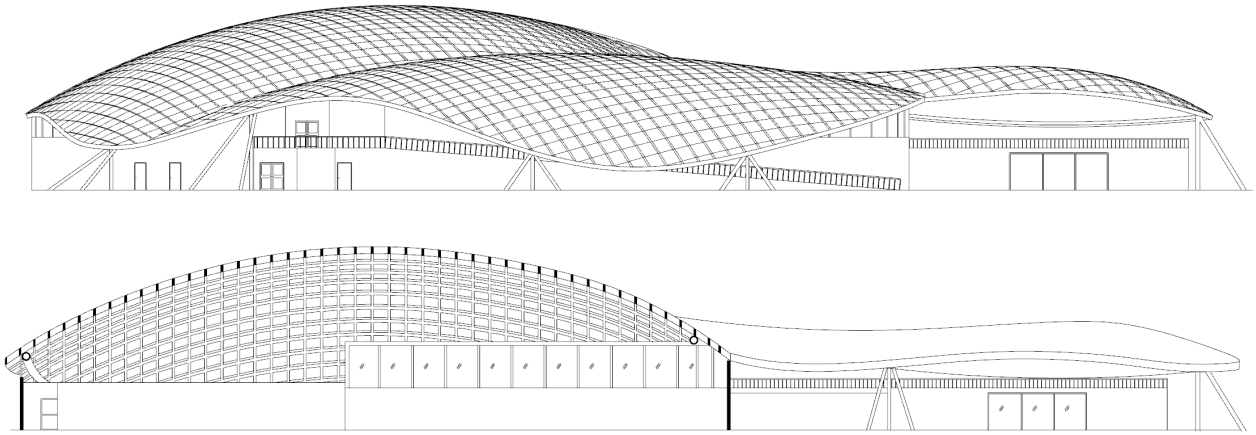

Figure 6.1: *Elevation and section of the case study.*

The building outlines is shown in Figure 6.2. As well as the suggested footprint of the roof structure. The roof covers to building, a large one and a small pavilion to the east and in between the two buildings, the roof is arching over a walkway.

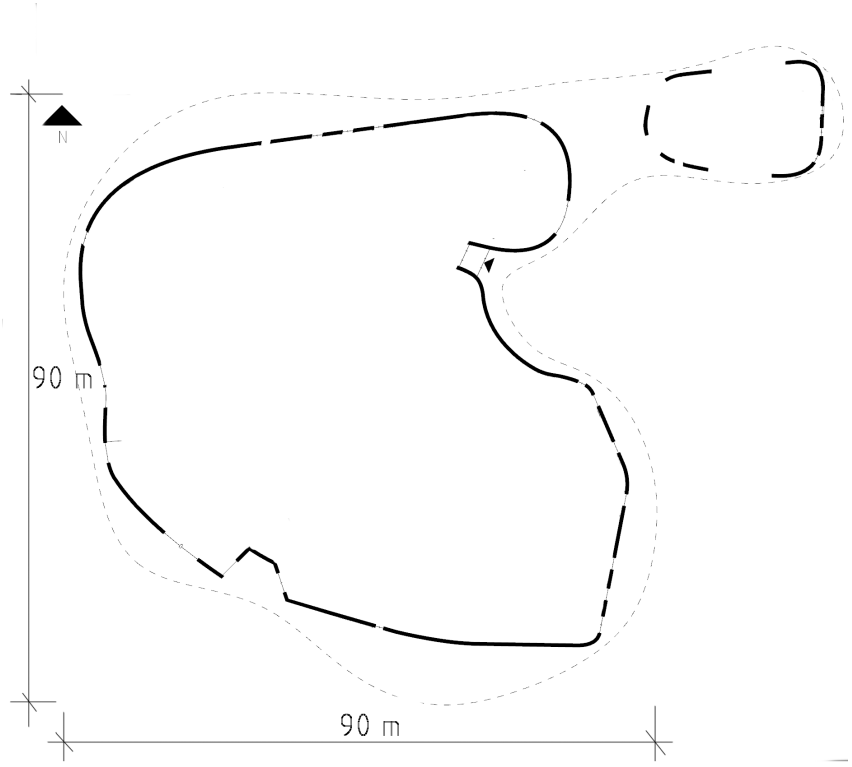

Figure 6.2: *Plan of the case study.*

6.1.2 Structural system

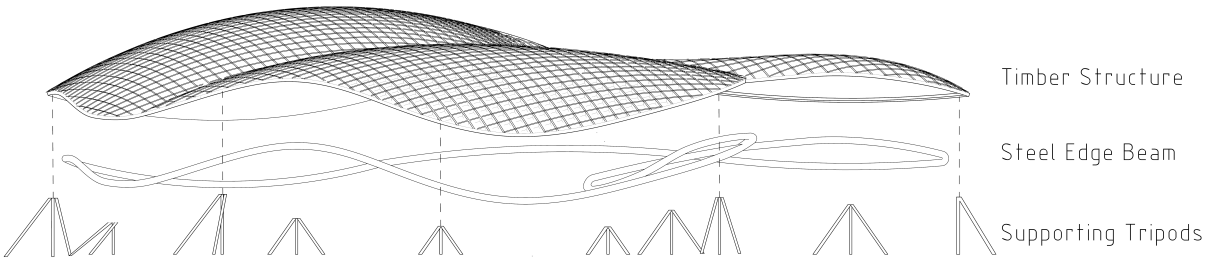

Figure 6.3: *Concept of the structural system of the case study*

The proposed roof-structure (see Figure 6.3) is a timber gridshell, inspired from the dramatic topography of the sourrounding. A quadrangular grid of timber beams was proposed, with a spacing of approximately 1.6 meters. The grid is braced by double layers of timber laths orthogonal to each other, similar to the gridshell in Saville Garden, and with a similar roofing of oak laths on top [Chilton & Tang, 2017]. The roof is intended to be covered, partly by an opaque façade and partly by a translucent. In areas where the structure is glazed or open the structure will be stabilized with cross bracing of equivalent stiffness to the double layered laths.

The roof is supported by a steel edge-beam, which rests on and is stabilized by steel tripods. Apart from these peripheral supports, no further supports are used; that means no internal supports, creating main spans of 90 times 60 meters.

6.1.3 Loads

The building is to be located in Central European-climate. And at the location the snow- and wind conditions are moderate. Since the structure is a roof no live load is applied, since the maintenance will be neglected.

Being a shell structure with relatively low slope, the wind will cause suction on large parts of the structure. The structure is located in a zone of no seismic activity.

Dead load

The dead-load consists partly of the weight of the structural system, mainly timber, which has a relatively low density, keeping the dead-weight low. Self-weight is considered as a permanent load. Full information about the dead loads in the calculations can be found in Appendix A.

In addition to the weight of the structure, the roof-build should be considered as superimposed Dead Load (SDL). A proposal of the roof build in the project is shown in Table 6.1 (also shown in Figure 6.4 with layers to account for different needs, including the bracing of the structure:

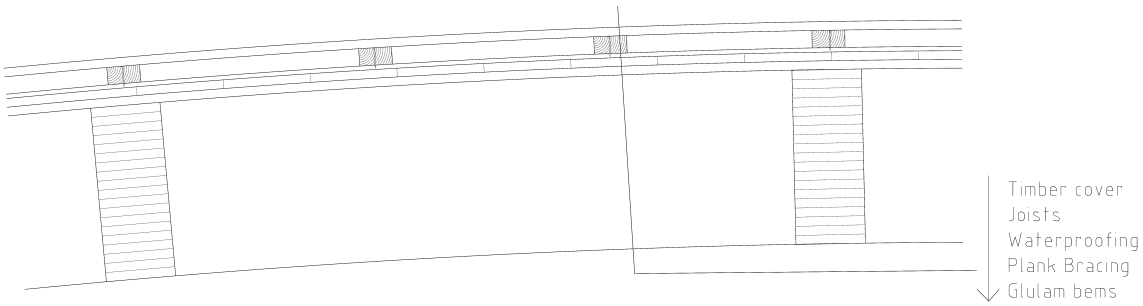

Figure 6.4: *Section of the proposed build of the roof used as a basis for calculations*

Table 6.1: Build of the roof, from inside and out

Material	**Thickness**	**Weigth**	**Purpose**
Light Armatures/Joinery etc.	-	0.5 kN/m^2	-
Glulam beams	-	-	*Structure*
Spruce planks	2 × 25 mm	0.2 kN/m^2	*Bracing*
Tar paper	2 mm	-	*Rain protection*
Joists	60 mm	0.2 kN/m^2	*Assembly*
Cover (Oak)	20 mm	0.1 kN/m^2	*Facade*
Total	162 mm	1.0 kN/m^2	

Snow-load

The characteristic snow load is 0.85 kN/m^2. The load distribution is idealised to that of a distribution on a low sloping roof with slight drift in the valley (see Figure 6.5). The load duration is considered as short-term [SIS, 2009c]. Full information about snow loads considered in the calculations can be found in Appendix A

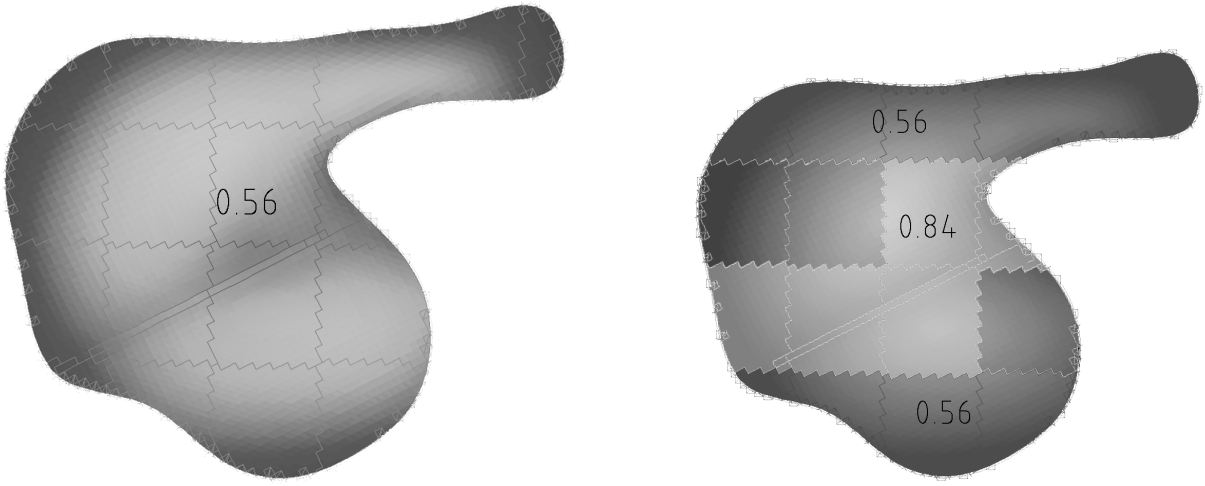

(a) Uniform snow load (b) Drifting snow

Figure 6.5: *Diagram of most important snow loads*

Wind-load

Based on a peak velocity pressure of 0.65 kN/m^2 on a low-sloping dome [SIS,2008, Fig 7.12] which will create suction on large parts of the structure (see Figure 6.6). Considered as short-term load [SIS, 2009c]. Full information about wind loads considered in the calculations can be found in Appendix A

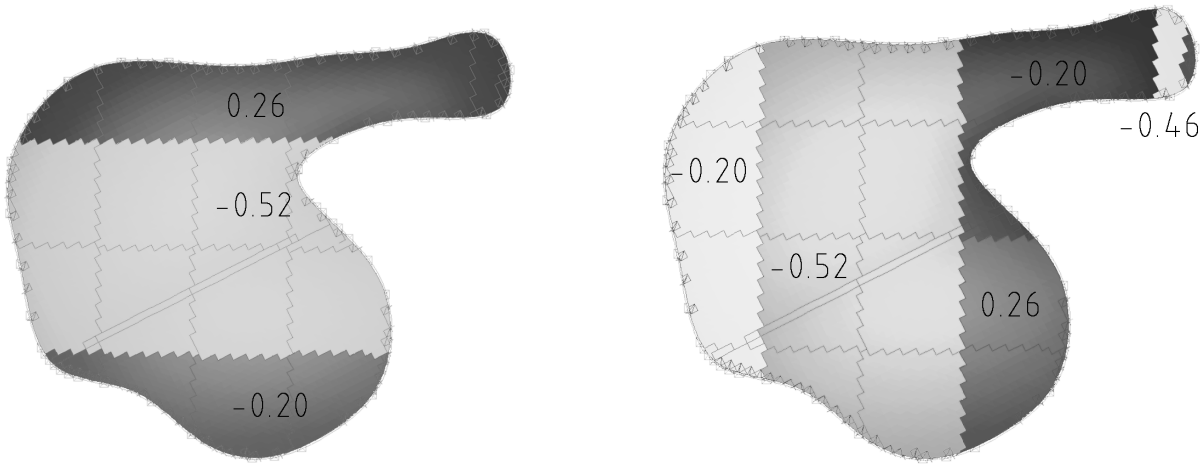

(a) North-south wind loadcase (b) East-west wind loadcase

Figure 6.6: *Diagram of most important wind loads*

Load-combinations

The load combinations for this types of structure are of three different types: *Ultimate limit state* for structural failure. *Serviceability limit state* for deflections and *Quasi-permanent* for long-term deflections. Full information about the load combinations considered in the calculations can be found in Appendix A.

Performance Criteria

The structure should fulfil the design-criteria in Section 4.1 that indicates the allowed stresses in ULS.

A deflection-limit should fulfil the criteria in Equation (6.1) and Equation (6.2) under SLS. Equally important is that ponding is not allowed, regardless the measured the displacement in the area.

$$\delta_{SLS} < l_{span}/200 \tag{6.1}$$

$$\delta_{QP,fin} < l_{span}/200 \tag{6.2}$$

The first natural frequency should be above 1 Hz in order to avoid resonance problems induced by wind.

6.1.4 Geometry

In the process of defining the geometry, starting with the suggested footprint, as shown in Figure 6.2 an early step was to adjust the height of the edge-beam according to the geometric constraints. The edge-beam is higher in areas of first floor entrances and lower in areas with high concentration of supports, to make an arch-like system leading forces to the supports and decrease the height of the supports, the edge-beam is illustrated in Figure 6.7.

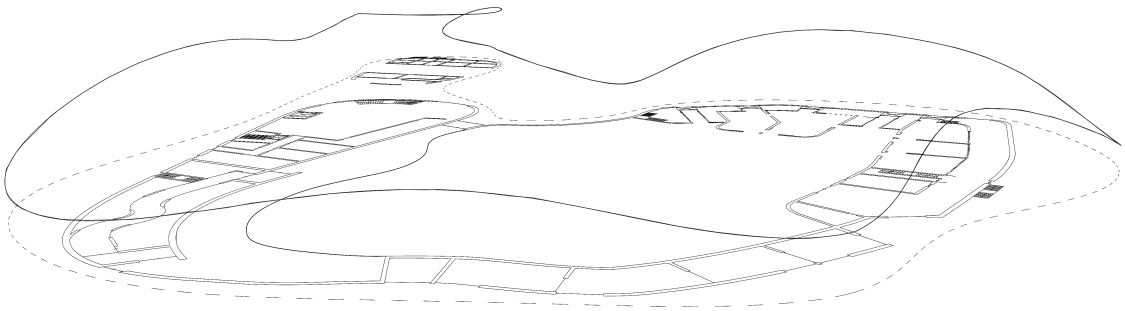

Figure 6.7: *Diagram of the height difference of the edge-beam.*

An initial form-finding was performed in Sofistik, based on a membrane hanging from the edge-beam, with an applied gravitational load and a presstress proportional to the span of the structure, to keep consistency in the height of the different parts. The result after the first iteration is shown in Figure 6.8.

This first proposal was discarded due to aesthetic reasons, not following the concept of the similarity to a dramatic topography. Thus a strip of material with stiffness was introduced, creating a shallower part, much like a valley in the surface. The results can be seen in Figure 6.9. This comes with the consequence of a zone of smaller radius, as well as an area with a concentration of forces.

However, since the building-permit limited the height, by splitting the one peak to two, this allows for a higher curvature which increased shell-behaviour in the structure in general.

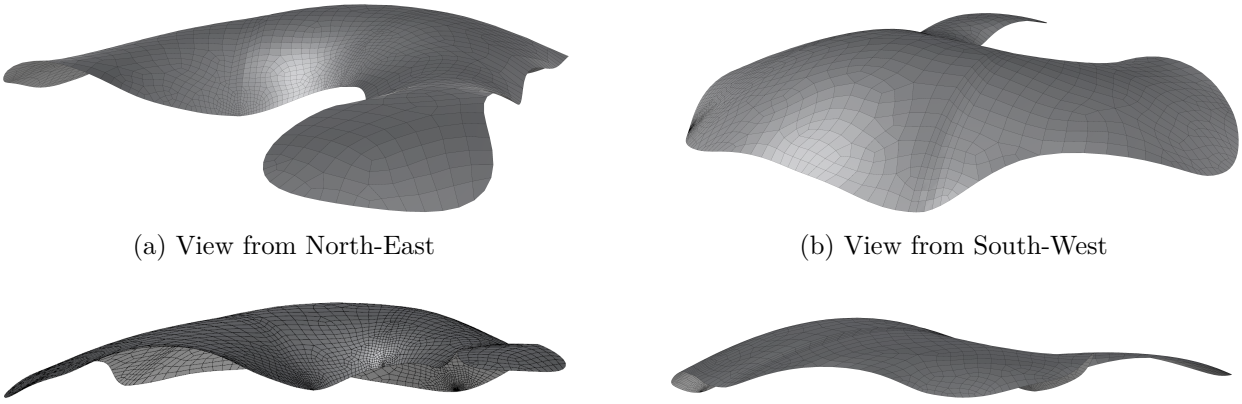

(a) View from North-East

(b) View from South-West

(c) Elevation from East

(d) Elevation from South

Figure 6.8: *Shell after first iteration of form-finding*

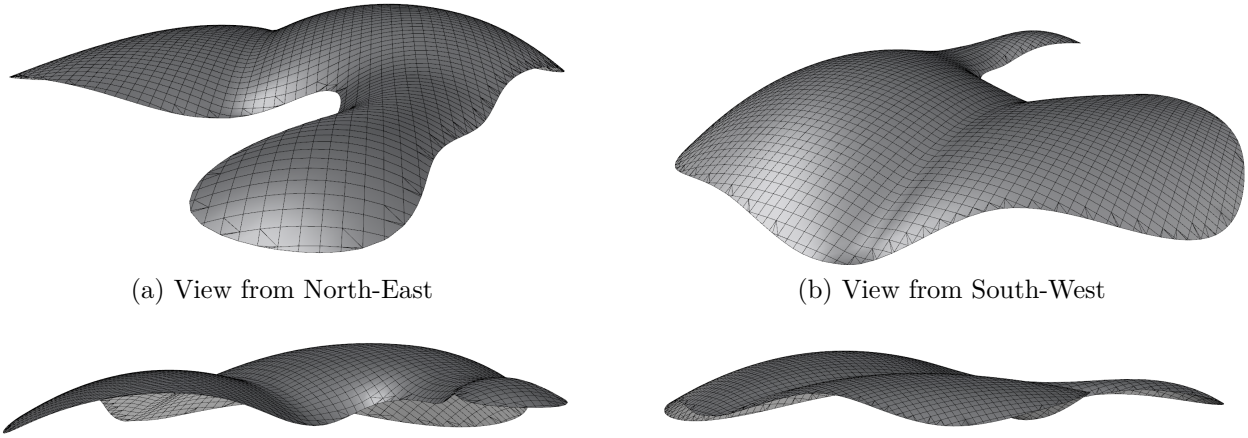

(a) View from North-East

(b) View from South-West

(c) Elevation of shell from East

(d) Elevation of shell from South

Figure 6.9: *Shell after second iteration of form-finding*

A grid, with the proposed 1.6 m spacing in planar state is projected onto the shell-surface, meaning that the grid of the shell is made of single-curved grid-lines. The grid can be seen in Figure 6.9. The orientation was chosen such as to approximately follow the main spans and to match the direction of the valley, to be able to create an arch-like system in this zone.

Curvature Check

Based on this form-found shape, the geometry needs to be evaluated for manufacturing, referring to the methods presented in Section 4.4. The first choice of manufacturing method for these grid beams is lamination, due to the strength reduction related to the other methods. This means that the curvature along the grid lines needs to be evaluated for the possibility of manufacturing.

In the scope of the thesis an evaluation tool is developed in *Grasshopper*, with a direct link to the design-environment in *Rhinoceros*. The tool calculates the radii of the curved beams, and with a given lamella thickness, checks the criteria for strength reduction due to radius (Equation (4.14)). The results are presented in Figure 6.10, it can be seen that the standard lamella thickness of 45 mm is sufficient for a majority of the beams, though the valley needs a maximum lamella thickness of 12 mm. This gives an idea about the feasibility of the geometry.

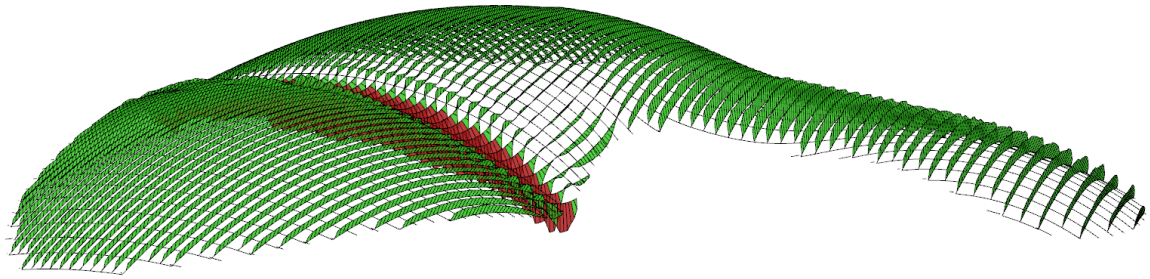

(a) Beams grid line 1 with 45 mm lamella thickness

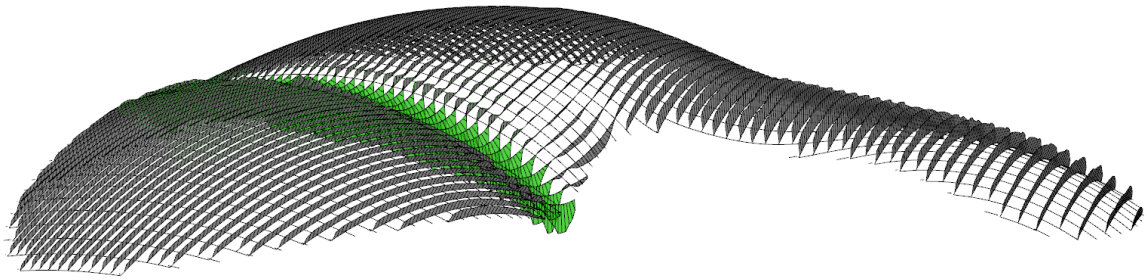

(b) Beams grid line 1 with 12 mm lamella thickness

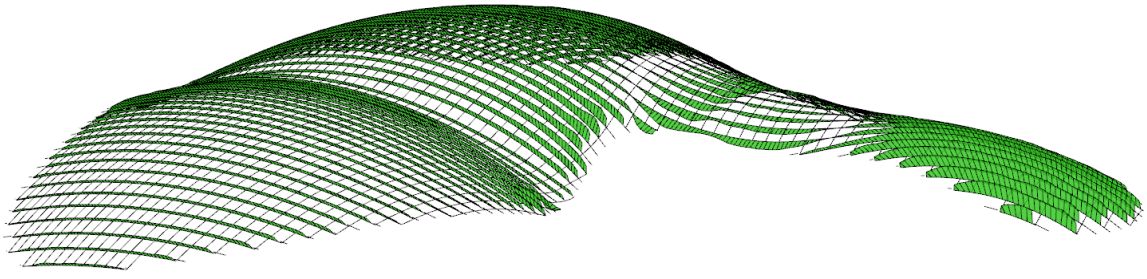

(c) Beams grid line 2 with 45 mm lamella thickness

Figure 6.10: *Evaluation of curvature. Green - the curvature meets the criteria for loss-free lamination (Equation* (4.14)*). Red - the curvature fails to meet the criteria. Grey - already covered by thicker lamella.*

Planarity Check

As described in Section 5.2.1, the planarity of the structure should be considered for covering the structure with a stiff material, for example glass.

The evaluation of the surface, for glazing, is presented in Section 6.1.4 is shown in Figure 6.11. The criteria is set to be that the isolated glass panes can be forced in place if the out-of-plane distance is smaller than $L_{diagonal}/100$. This assumption is common among professionals, while Eekhout and Niderehe [2009] suggest $L_{diagonal}/50$, the smaller value is used as a conservative limit. As can be seen, based on the method in Section 5.2.1 is it not possible to clad the entire structure with glass. According to the architectural program around 30% is supposed to be glazed. This requirements is fulfilled, especially considering that the majority of the non-planar panes is located above the entrance to the park, an area excluded from these 30%. The rest of the structure is intended to be covered with timber laths, a material more flexible and thus not with the same demands on planarity.

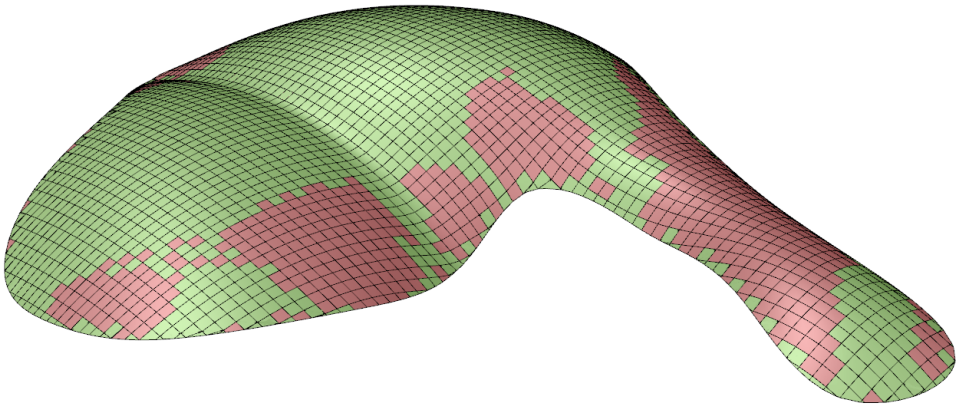

Figure 6.11: *Evaluated surface. Green - possible to clad with glass. Red - not possible to cover with planar panes.*

6.2 Design Development

6.2.1 Geometry

The evaluation of the curvature informed the feasibility of the geometry according to norm and material allowance. To further develop the understanding of the curvature in the structure, as well as developing an understanding manufacturing process and economy in the project, blank type for each element should be evaluated. The blank type, and the curvature of the members is a very influential aspects of the cost and complexity of a timber-structure. There is a large cost-increase related to blank-types, especially when going from from single-curved to double-curved or twisting. The production of single-curvature beam today is often automated, while double-curved beams are mostly made by a manual process, raising the cost. A double-curved beam can be expected to cost 20 times more than a straight one [as per correspondence with Blumer-Lehmann, 2018]. To plan the production line and a budget assumption, the grid should be evaluated according to blank types.

The algorithm presented in Section 5.3 is used to analyse the grid. In order to categorize

acording to blank type. The result is presented in Figure 6.12. As can be seen in the results are the beam length very long, since the check is performed on an unspliced grid. This check should be performed also after the grid system (further described in Section 6.3) is chosen. Although the blank type will remain the same the number and length of beams will change.

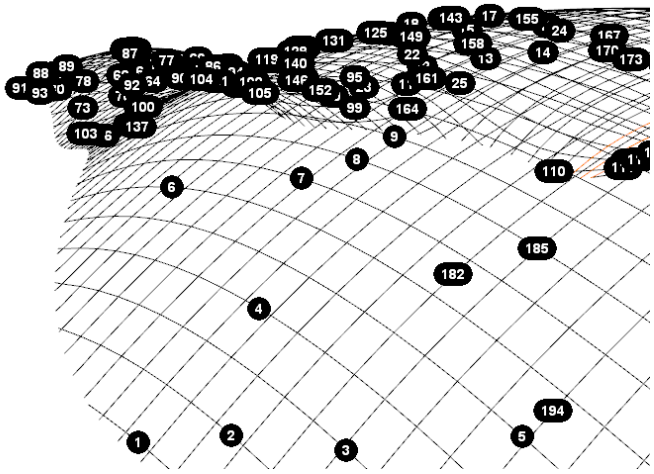

(a) Part of the grid with numbering

Number	Curvature Dir 1	Curvature Dir 2	Torsion	Length [m]	Blank Type
1	1	0	0	8,57	Single Curved
2	1	0	0	20,51	Single Curved
3	1	0	1	28,01	Single Curved With Torsion
4	1	0	1	34,05	Single Curved With Torsion
5	1	0	1	39,29	Single Curved With Torsion
6	1	0	1	44,06	Single Curved With Torsion
7	1	0	1	48,52	Single Curved With Torsion
8	1	0	1	52,79	Single Curved With Torsion
9	1	0	1	56,98	Single Curved With Torsion

(b) Part of the list analysing each element

	Total	Straight	Single Curvature	Single Curvature - Torsion	Double Curvature without Torison	Double Curvature with Torsion		Total Length [m]
Nr of elements	238	1	30	207	0	0		8623
Ratio	100,0%	0,4%	12,6%	87,0%	0,0%	0,0%		

(c) Summary of analysis

Figure 6.12: *Diagram of the input and output of the Blank-geometry analysis tool for the grid of the case study*

Due to the use of a master surface, and having a straight, orthogonal grid to project onto it, a solution with only single-curved beams was guaranteed. Although, when running the grid through the algorithm, with the assumption that all beams should follow the normal of the surface, the result was, expectedly that almost all members were twisting.

Since this structure is covered, the beams act as a direct or indirect support of the façade, and must therefore be connected. In Figure 6.13 a few examples of the interface between beams and façade that can be achieved is presented.

In Figure 6.13(b) torsion of the beams is allowed, and the beam is thus free to follow the surface. The disadvantage is the complexity of manufacturing these members, where the

members needs to be either laminated to torsion or machined to twisting members. This disqualifies this option in the current project. In regions of a very steep surfaces this will result in the strong direction of the beam not being parallel with the direction of the loads.

In Figure 6.13(c), beams are single-curved, without torsion, with the top surface constantly horizontal, possibly leaving a gap between beam and surface. The distance and discrepancy between surface and beams is compensated for by a super-structure, e.g. upstands or frames, that are customized to connect the elements. This creates a simple beam geometry, although the upstands will need customization. It also creates a slightly different aesthetic, where the façade is hovering above the beams. Upstands will also create a system of point loads on the structure, which is a slightly different loading scheme. Another aspect of this solution is that the bottom surface of the different grid-lines will not match, thus the intersection will not be smooth, since members are entering at different angles.

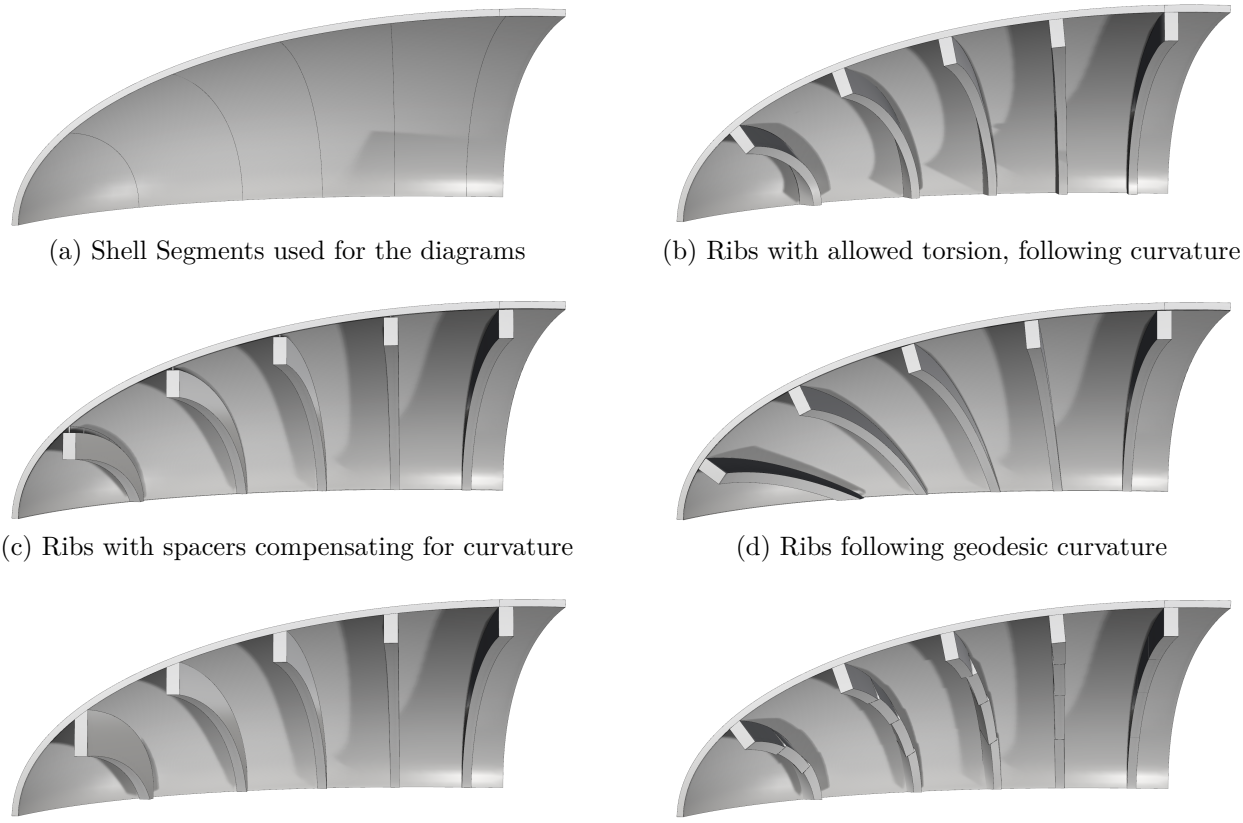

(a) Shell Segments used for the diagrams

(b) Ribs with allowed torsion, following curvature

(c) Ribs with spacers compensating for curvature

(d) Ribs following geodesic curvature

(e) Ribs milled to follow curvature

(f) Ribs segmented to follow curvature

Figure 6.13: *Diagram of different methods of how to relate the surface and the beams*

In Figure 6.13(d), the grid is following the geodesic curvature of the surface, such that naturally no twisting occurs. For most freeform surfaces however the geodesic lines will not form a regular, rectangular grid. This approach can thus not be used without drastic changes to the grid layout in the case study. While a geodesic grid has many desirable properties for beam manufacturing the non-uniformity of these grids in freeform surfaces might prove difficult to cover with a façade.

In Figure 6.13(e), all members are single-curved with the size of each member of the grid

is increased beyond static requirements, and the top surface is machined to match the master-surface thus parallel to the normal of the surface. The high fitness might demand small tolerances in the construction-process and with the machining produces waste-material. However, being based on a laminated solution, it's a strong alternative and due to the post-processed geometry an alternative with high fitness and flexibility.

This is a rather common solution for this kind of projects. According to Scheurer et al. [2013] all members, even if shaped through lamination, need some machining-treatment in order to meet required tolerances. This means that machining of the top-surface could thus be done, without increasing the number of beams that needs to be milled.

In Figure 6.13(f) the structure is segmented, and each segment, while being straight is approximating the direction of the surface along its length and adjusting to this, this will create a close, but not perfect façade-beam fitness. An option might be make a faceted surface and thus create a perfect match. But the visible impression of a continuous element might be ruined due to the members entering nodes with different angles. This will however be a relatively cost efficient solution, where the manufacturing principle of the beam is simple. However this will demand a beam-node system where the node is complicated to manufacture.

6.2.2 Manufacture

The planning of the manufacturing process includes several factors, among them the general curvature, but also dividing beams to certain lengths suitable for both transportation and the structural concept (further discussed in Section 6.4.6). Finally the manufacturing process should be chosen and prepared with geometrical data.

An algorithm and work flow was created in *Grasshopper*, within the scope of this thesis, with the aim of automating this process. The stages are shown briefly in Figure 6.14. Starting with the projection of the grid onto the master-surface (Figure 6.14a and b). Followed by a curvature test, similar to Section 6.1.4, but now an integrated part of the process.

In the next stage the splitting of members. The need of splicing the members is highly dependent of the chosen assembly systems, since some of them, by design have short members (further discussed in Section 6.3). The main criteria for the placement of a splice are:
• $L < L_{max}$ - Where L_{max} is the maximum allowed length and should be defined together with manufacturer and logistic services, further discussed in Section 4.5.
• Since the joint is a weakening the structure, placement should be avoided in zones of high forces.
• Splices in beams right next to each other should not be placed in parallel bays, since this will not allow redistribution of loads. Thus creating a weak line in the structure.
• If the node allows for splicing being integrated in the joint without strength reduction the splicing should be placed at the node (such as in a beam-node system). In systems with long members, the stiffness of the joint is often dependent on the continuous member, thus often not possible to splice it in the node.

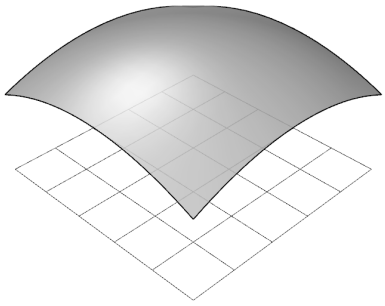

(a) Projection of grid

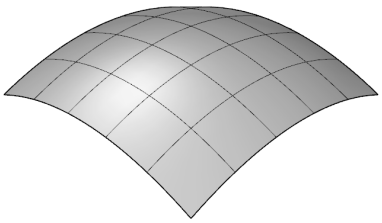

(b) Grid on surface

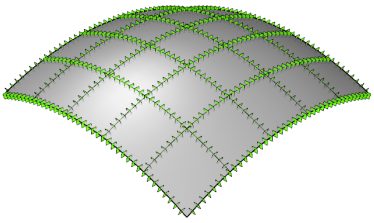

(c) Curvature check of members

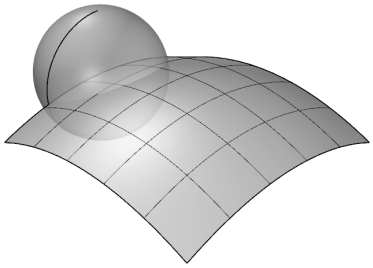

(d) Distance criteria between joints

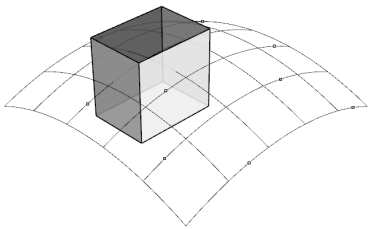

(e) Areas where to avoid splicing

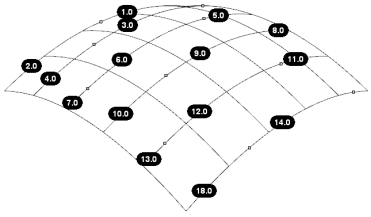

(f) Position cuts and beam numbers

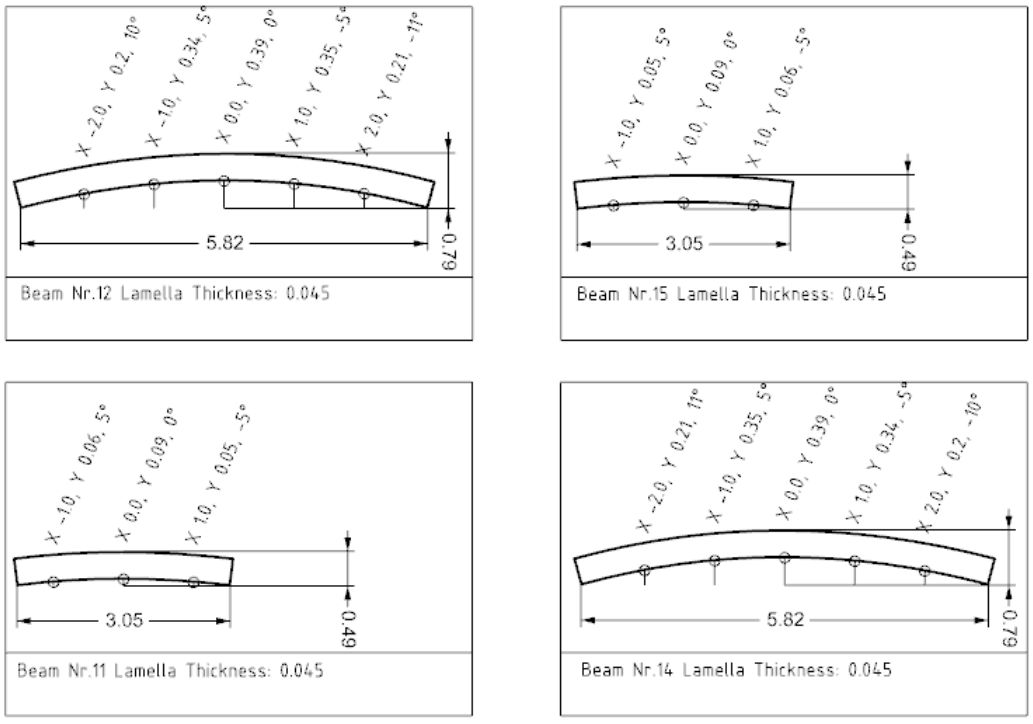

(g) Basis for workshop drawings for curved beams

Figure 6.14: *Stages of the automated process for grid-creation, placement of splices and creation of beam drawings*

The algorithm will propose a number of splicing points based on these criteria (*(f)* in Figure 6.14). It first defines all available splicing points and chooses the corresponding length closest, but smaller than L_{max} thus $L < L_{max}$. This is repeated for the next beam, but another check is performed, if the suggested point is too close to any other splices Figure 6.14*(d)*. The

interface also allows for splice-free zones to be defined by the user Figure 6.14*(e)*, with the intention that one would overlay this with a force-diagram and manually define zones where no splices should be placed.

The algorithm then splits the members. It will take the divided beams and create a basis for the workshop-drawing for each element, based on the clamp-distance in the used press-bed, and the cross-section size. Results include location in the structure (f) and Figure 6.14(g), required lamella thickness and position of clamps, as well as overall dimensions Figure 6.14(g). Data that is helpful for the continued planning-process. This data should be checked to the overall dimensions, and compared to the press-bed of the intended manufacturer, so that the dimensions will not exceed the size of the tool.

A recommendation would be to perform a simulation as the one suggested in Section 5.3, in case of members seeming critical according to the criteria lined out in that chapter. The work-flow presented in that chapter also includes a helpful post-processing-algorithm of the FE-model that will be presented here. It analyses the divergence between the curve, compared simulated beam. Measuring the divergence between physical and digital for a number of criteria.

The first check is the absolute closeness to the given curve, measuring the distance between a number of points on the beams. It also checks for the curvature-criteria presented in Equation (4.14). If divergence between the digital and physical is too big, the algorithm tests to see if it is possible to achieve the form by machining (as described in Section 4.4). This alternative is limited by an angle, to control the strength reduction. Many producers allow for angles up to 5° to be cut. With the same reasoning some curved members can be cut from straight members, if within the angle tolerance (see Figure 6.15 a).

If all these tests fails for a member, the first suggestion is to look into possibilities of redesigning the grid. Otherwise, it is possible to redesign the particular member or consider a another manufacturing method. One alternative is full machining, one could also consider a manual glulam-press, which is more customizable with lower spacing between clamps.

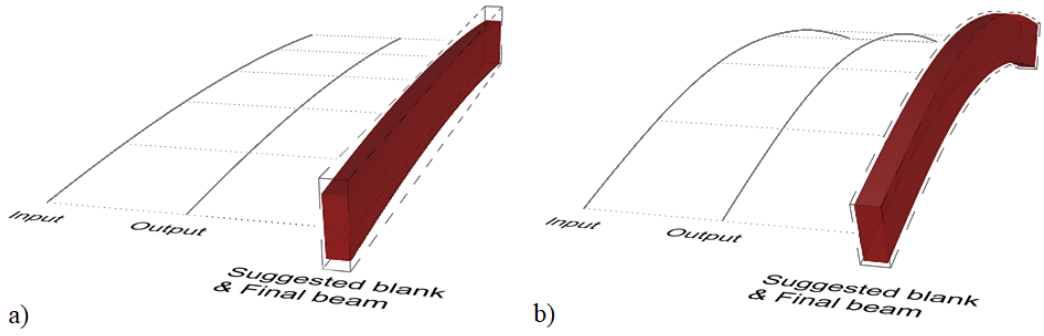

Figure 6.15: *Two examples of the input and output of the press-bed simulation. Beam-geometry in red, suggested blank geometry dashed*

6.2.3 Structure

To get an initial idea of the internal forces in the structure, used for pre-sizing of beams and joints a FE-model of the case-study with rigid connections is used. This model will later be used analysis of the global behaviour of the structure with the reduced stiffness of the joints. The FE-model is shown in Figure 6.16 and the results are presented in Appendix C.

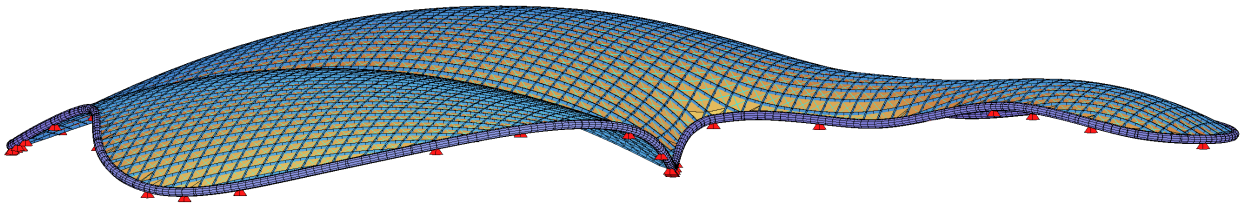

Figure 6.16: *Picture of the FE-Model used in the analysis*

The calculations are performed using the presented FE-model. Some important assumptions made in the analysis are:
- All loads are imposed according to Section 6.1.3.
- All connections between beams in the grid are accounted for as fully rigid.
- All connections between grid and edge-beam are fixated to the edge beam, but allowed to rotate around it.
- The bracing of the structure is modelled by cross-bracing of equal strength to the chosen plate-bracing. The concept explained in Figure 6.17.

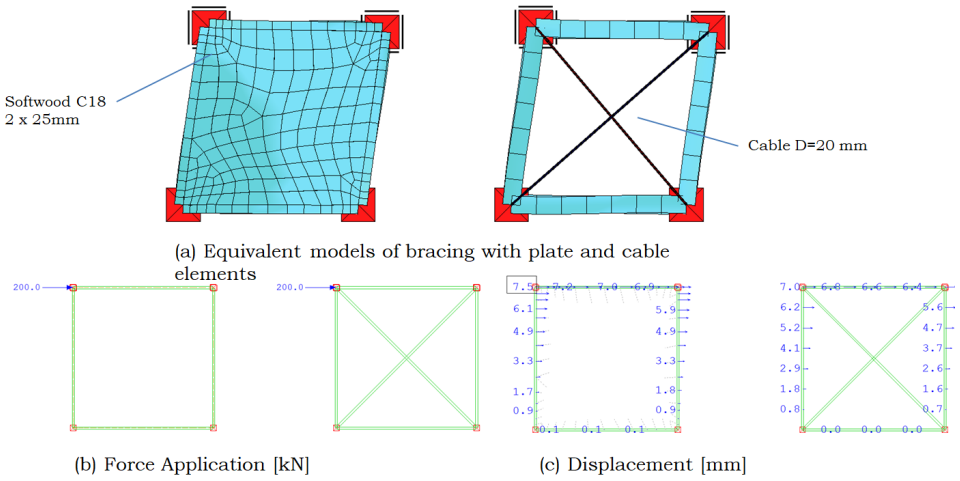

Figure 6.17: *Diagram showing the concept of equivalent bracing.*

- The surface elements do not contribute structurally and are used only to apply loads.
- All supports are pinned and connected to the edge-beam.
- The spacing between the beams are constant at 1.6 meters.
- The beam are modelled with a cross-section of 450x150 mm, using Gl28c.
- Calculation are performed according to third order theory.
- The beams are modelled as curved.

• The beams are meshed also between the nodes.
• When later, the joint stiffness are incorporated in the model they are modelled using *Implicit hinges* in Sofistik (according to Figure 6.18).

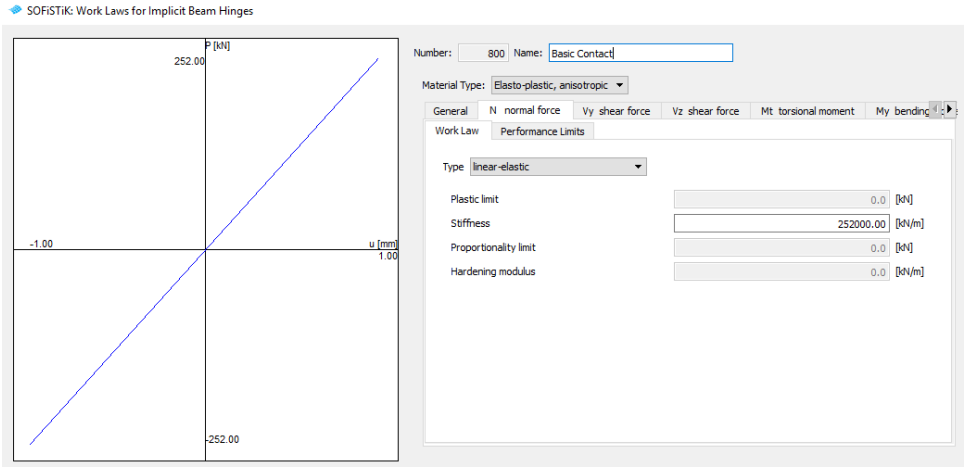

Figure 6.18: *The interface of Implicit Hinges in Sofistik, stiffness for six degrees of freedom can be defined*

All forces from this calculation can be found in Appendix C. A qualitative illustration of the forces is shown in Figure 6.19. The forces are divided into two categories due to their respective load-duration: the permanent, including dead weight and superimposed dead-load, and temporary, including wind and snow which are both considered as short-term loads.

In Figure 6.20, an illustration of the structural behaviour is shown, classified according to the ratio of utilization from bending and from axial forces. High ratio indicates arc- or shell-behaviour since a high degree of the action is seen in axial stress and not in bending.

There is clear shell-behaviour in both spans of the structure. In the valley between the peaks, there is a clear arching behaviour in the longitudinal direction of the valley and a bending-behaviour in its transversal direction.

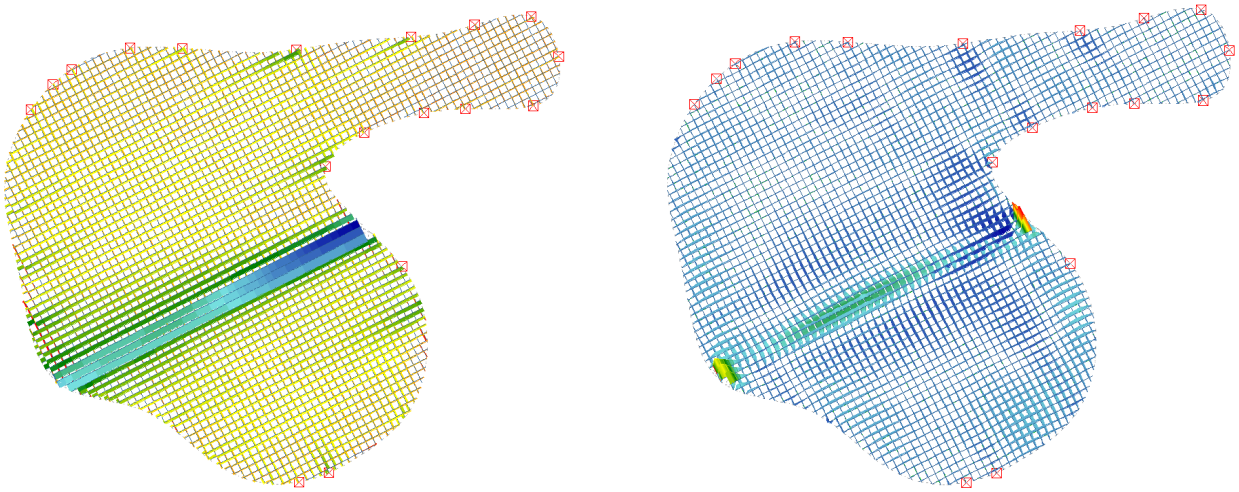

(a) Diagram of normal force - self-weight

(b) Diagram of major axis bending - self-weight

Figure 6.19: *Diagram of force concentration in preliminary models, full results can be found in Appendix C*

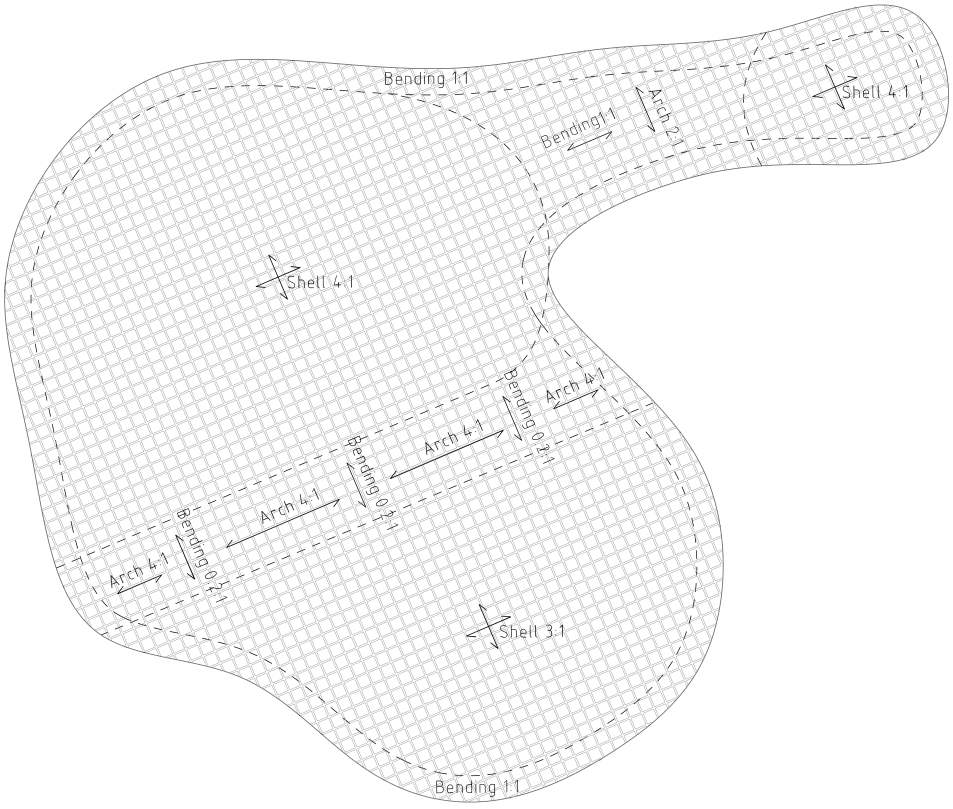

Figure 6.20: *Diagram of areas in the structure, where shell-behaviour is dominant or bending, presented is the ratio of utilization axial:bending*

In order to get the stresses at the outermost fibre of the beam, the stress interaction between moment and axial forces are checked (Equation (6.3)), in order to get an idea if tension might occur anywhere in the joint.

$$\sigma = \frac{N}{A} \pm \frac{M_y}{I} z \tag{6.3}$$

Some typical force situations that can be identified from the initial calculations are:

Shell zones
In areas marked as *shell* in Figure 6.20 the ratio axial:bending is high in both directions, meaning that the normal force is high, while bending is relatively low, indicating a bi-axial vector-active structure (using Engel's notations [1997]).Typical design-forces are:

Table 6.2: Forces in typical *shell* joint

450x150mm	**Permanent**	**Temporary**
Axial force [kN]	- 140	- 110
Major axis bending [kNm]	8	6
Minor axis bending [kNm]	2	1
Major axis shear [kN]	3	2

The utilization is calculated according to Equation (4.6) and Equation (4.7), thus including risk of local buckling. The utilization is calculated both for only the permanent, compared to the design strength for permanent loads. While for the combined loads, they are checked against the design strength of short-term loads. Utilization for the *shell* zones are presented in Table 6.3.

Table 6.3: Utilization for the different load durations in a typical *shell* joint

450x150mm	**Permanent loads** $k_{mod,permanent}$	**All loads** $k_{mod,short}$
Utilization [-]	0.38	0.42

Using Equation (6.3), the net axial force in the joint would typically be:

$$\frac{-140\text{kN}}{0.0675\text{m}^2} \pm \frac{8\text{kN m}}{0.001139\text{m}^4} 0.225\text{m} = -0.49\text{MPa} / -3.65\text{MPa}$$

$$\frac{-250\text{kN}}{0.0675\text{m}^2} \pm \frac{14\text{kN m}}{0.001139\text{m}^4} 0.225\text{m} = -0.94\text{MPa} / -6.5\text{MPa}$$

As can be seen from the stress interaction, no tension occurs in the *shell* joints.

Bending zones
In most of the areas marked as *bending* in Figure 6.20 the ratio axial:bending is low, meaning that the structure is mostly cross-section active. Typical design-forces could be:

Table 6.4: Forces in typical *bending* joint

540x150 mm	**Permanent**	**Temporary**
Axial force [kN]	- 80	- 65
Major axis bending [kNm]	35	18
Minor axis bending [kNm]	5	5
Major axis shear [kN]	- 16	- 9

The utilization is calculated according to Equation (4.6) and Equation (4.7), thus including risk of local buckling. The utilization is calculated both for only the permanent, compared to the design strength for permanent loads. While for the combined loads, they are checked against the design strength of short-term loads. Utilization for the *bending* zones are presented in Table 6.5.

Table 6.5: Utilization for the different load durations in a typical *bending* joint

540x150 mm	**Permanent loads** $k_{mod,permanent}$	**All loads** $k_{mod,short}$
Utilization [-]	0.59	0.65

Using Equation (6.3), the net axial force in the joint would typically be:

$$\frac{-80\text{kN}}{0.0810\text{m}^2} \pm \frac{35\text{kN m}}{0.001968\text{m}^4} 0.27\text{m} = 3.8\text{MPa} / -5.7\text{MPa}$$

$$\frac{-145\text{kN}}{0.0810\text{m}^2} \pm \frac{53\text{kN m}}{0.001968\text{m}^4} 0.27\text{m} = 5.4\text{MPa} / -9.1\text{MPa}$$

As can be seen from the stress interaction, tension will occur in the *bending* joints. This must be considered in the joint design.

Arch zones
Close to the supports of the valley, in areas marked with *arch* in Figure 6.20 the ratio axial:bending is high in one direction indicating a uni-axial vector active structure. Typical design-forces could be:

Table 6.6: Forces in typical *arch* joint

540x200 mm	**Permanent**	**Temporary**
Axial force $[kN]$	-850	-500
Major axis bending $[kNm]$	18	12
Minor axis bending $[kNm]$	5	2
Major axis shear $[kN]$	5	3

The utilization is calculated according to Equation (4.6) and Equation (4.7), thus including risk of local buckling. The utilization is calculated both for only the permanent, compared to the design strength for permanent loads. While for the combined loads, they are checked against the design strength of short-term loads. Utilization for the *arch* zones can be found in Table 6.7.

Table 6.7: Utilization for the different load durations in a typical *arch* joint

540x200 mm	**Permanent loads** $k_{mod,permanent}$	**All loads** $k_{mod,short}$
Utilization [-]	0.77	0.79

Using Equation (6.3), the net axial force in the joint would typically be:

$$\frac{-850\text{kN}}{0.108\text{m}^2} \pm \frac{18\text{kN m}}{0.002624\text{m}^4} 0.27\text{m} = -6.0\text{MPa} / -9.7\text{MPa}$$

$$\frac{-1350\text{kN}}{0.108\text{m}^2} \pm \frac{30\text{kN m}}{0.002624\text{m}^4} 0.27\text{m} = -9.4\text{MPa} / -15.5\text{MPa}$$

As can be seen from the stress interaction, no tension occurs in the *arch* joints.

As can be seen in the choice of cross-sections in the tables above, the 450x150mm cross section was not sufficient and needed to be increased towards the valley and the arched-zone, thus is the utilizations for that zone calculated with a larger cross section. For local areas with higher forces, tapered beams can be used, as shown in Figure 6.21. A combination of cutting and machining allows for smooth tapers.

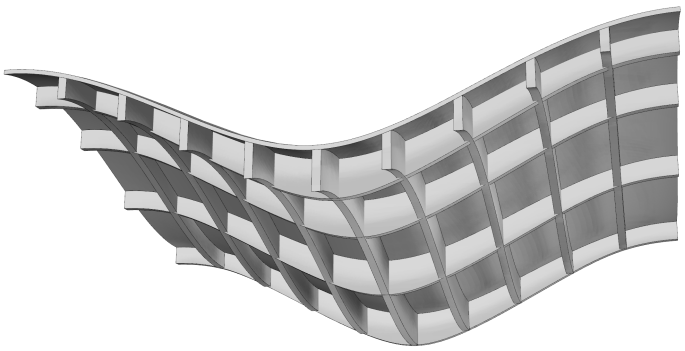

Figure 6.21: *Perspective of concepts of varying beam sizes towards a force-concentration, in this case the valley*

In Figure 6.22 the deflections of the structure with these initial assumptions is presented, this is a benchmark when evaluating the influence of semi-rigid solutions later.

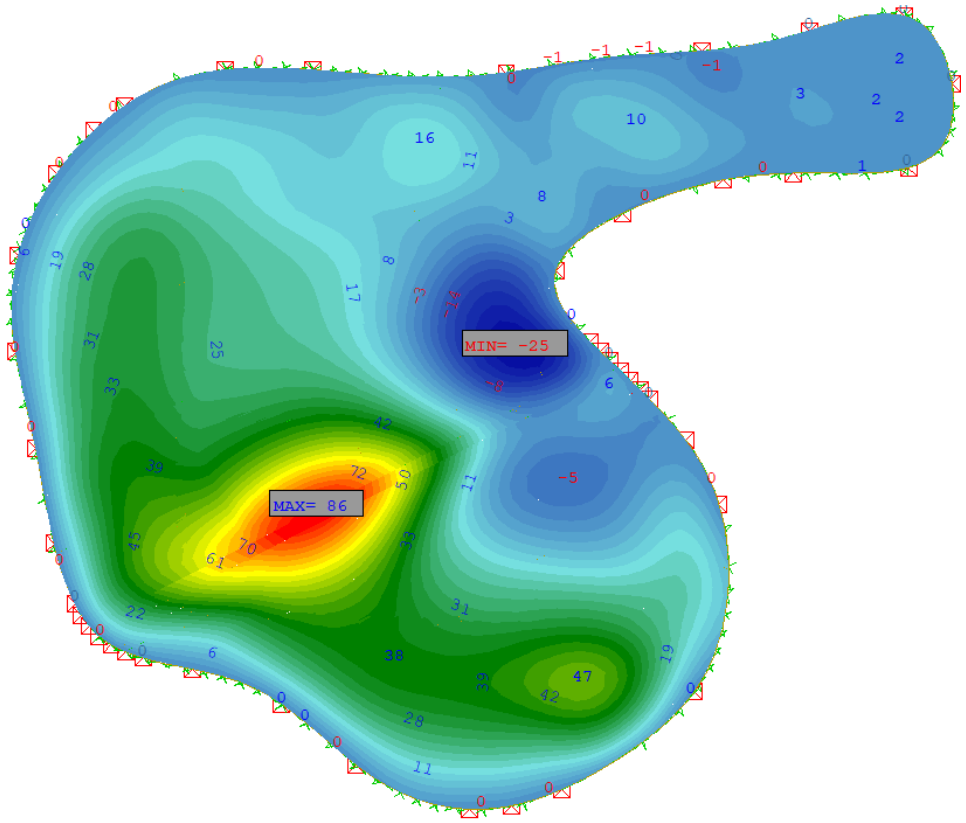

Figure 6.22: *The maximum deflection for the structure with fully fixed connections, under self-weight*[mm]

Global Buckling

To account for global buckling of the shell, a second order linear analysis is executed. The material properties in the analysis was decreased according to Eurocode 5 [SIS, 2009c, 2.2.2(2)]. The primary load case used is the dead weight with the ULS factor of 1.35. To account for the non-linear effects, the buckling factor is divided with a safety factor of 2.

The first buckling mode in the pre-sizing analysis is shown in Figure 6.23. The linear buckling-factor of this structure is 6.64.

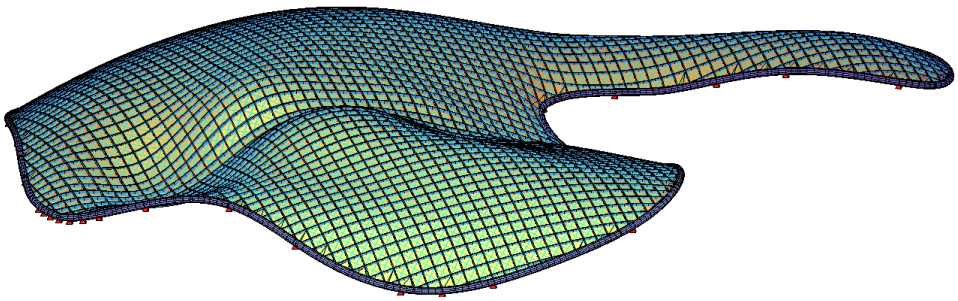

Figure 6.23: *The first Global-buckling mode of the shell with stiff connections*

6.3 Grid Systems

There are different possible layouts of the grid, and it is worth comparing the significant properties of each to the possibilities of the project. The system first of all needs to be possible to assemble to larger grids, preferably with a logic assembly and logical distribution of member sizes.

The assembly system should be planned with a consideration of available transport. If it is known from early on that no large pieces can be transported, one should have a look at system consisting of smaller members.

Another point considering assembly systems is that they should be chosen with regard to the chosen joint type, because as will be shown, not every joint fits with every grid system. Some systems are based on terminating members and some systems based on continuous members, making some system more suitable to be used with certain joints.

This calls for a system where some criteria must be fulfilled:
- The structure should consist of members with similar or uniform sizes
- Beams needs to keep most of their structural integrity
- The system must be geometrically possible to assemble
- Members should be of lengths possible to handle with transport and assembly on site.

A number of systems are presented in the following chapter, and as a demonstration it is shown how every system would assemble the benchmark geometry in Figure 6.24

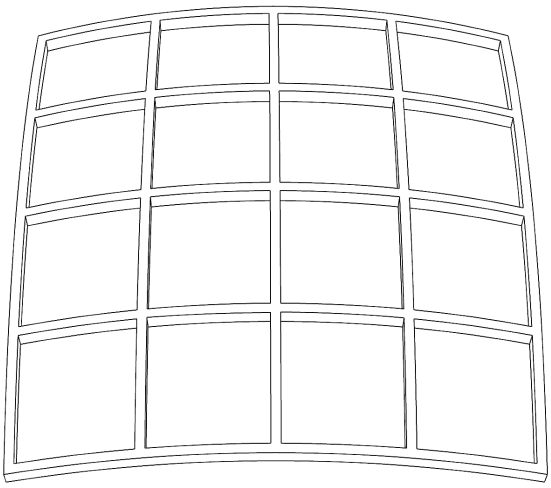

Figure 6.24: *The benchmarked geometry, consisting of five grid-lines in each direction*

6.3.1 Zollinger system

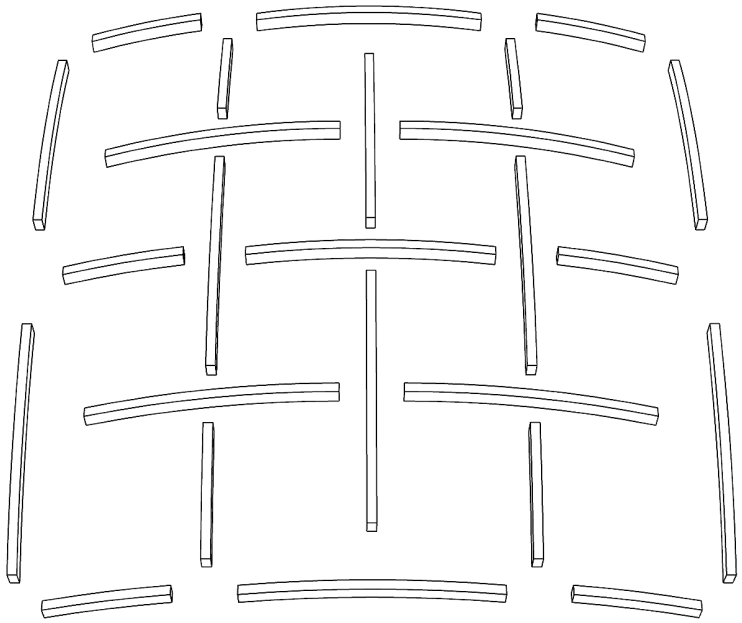

Figure 6.25: *The geometry as constructed by a Zollinger system*

The Zollinger-system, invented in the 1920's by German architect Friedrich Zollinger, is a system that was originally used to construct barrel-vault roofs in single-family houses as well as in long-span halls. The system consists of members crossing two spans, each grid line shifted one step, meaning that in every node, one member is continuous and two members ends. In this system members are identical or with little variations. The principle is shown in Figure 6.25.

This method is also used in more recent projects, among them the *Toskana Therme* in Bad Sulza, Germany, as presented in Section 2.1, where the system is a double-curved surface, and the members thus are unique.

Since the system is using modestly sized members throughout the structure, it is considered practical from the perspective of transportation. Being a reciprocal system, it means that the system is not stable until completed since members are supported by other members. This implies that the structure does require extensive scaffolding. One measure that can be taken to decrease the need of scaffolding is to pre-assemble modules on the ground. With the generally short members modules can be handled easy.

6.3.2 Overlapping system

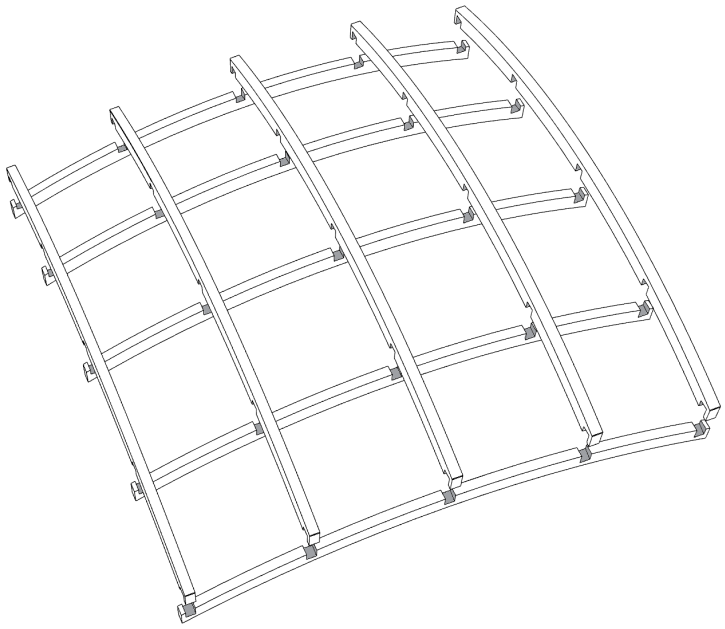

Figure 6.26: *The geometry as constructed of continuous members*

Members crossing nodes is effective considering the number of members needed. Furthermore allows to transfer axial forces through the continuous members. The main disadvantage however is the reduction of cross-section needed if the structural height shall remain the same. A popular alternative is making half lap-joints in both members and slide them into each other, the principle is shown in Figure 6.26. This will however significantly reduce the strength of the beam at the joint.

To overcome the reduced strength at the node, oversized cross-section could be used in the structure. Another option is to reinforce the structure using a steel-plate or lath placed on top of notch and crossing members.

In the *La Seine Musicale*, presented in Section 2.3 this is the principle emplyed. But there used as a façade.

The use of continuous members implies that the need of scaffolding can be reduced, since the continuous arches are self-supporting when mounted. Although, in case of lap joints, the tolerances must be kept to a bare minimum, meaning that scaffolding might be needed to meet tolerances for assembly rather than structural stability.

6.3.3 Woven Joints

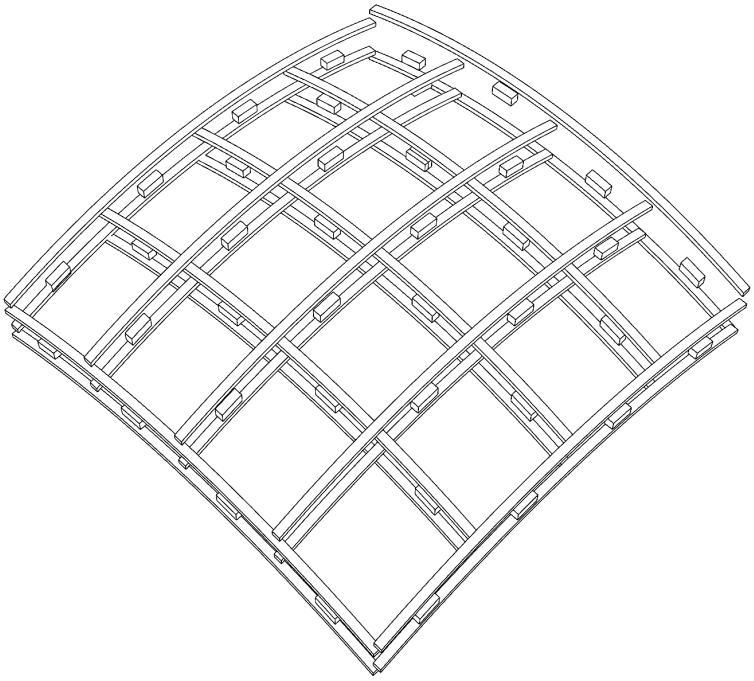

Figure 6.27: *The geometry as constructed with a woven system*

A special case of overlapping joints is the woven joint. With a built up cross section members are intertwined and thus moved out of plane of each other minimizing the increase of structural height while keeping full continuity. This is a common solution in the elastic gridshells like *Mannheim Multihalle* and the *Saville Garden Gridshell*. However this principle has been used in rigid gridshells, such as the *Centre Pompidou Metz*, presented in Section 2.4. It is a double layered structure, in the sense that the flanges of each grid line are passing between the top- and bottom-flange of the other grid lines and the beams are built-up with a discrete web, the principle is shown in Figure 6.27.

This is an interesting solution, with potential of decreasing the amount of prefabricated parts needed, since the flanges could, if thin enough, potentially be bent on-site. A disadvantage with the system in shells is that the removed material will decrease the axial capacity. During the design of these systems it is important to consider the interaction between the local behaviour, i.e. between the shear blocks, and the global behaviour.

With a structure of built-up cross sections, the stability will not be reached until the structure is close to completion, meaning that the need of scaffolding is significant.

6.3.4 Segmented system

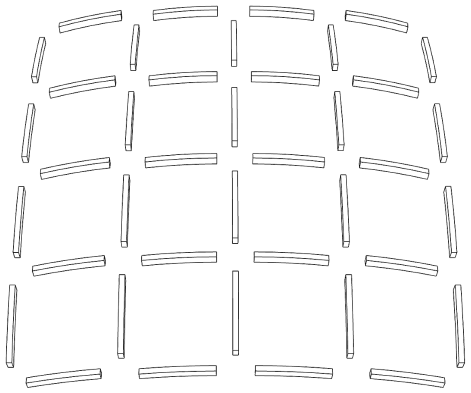

Figure 6.28: *The geometry as constructed with a segmented system*

This is a discrete system with non-continuous beams, where each beam goes between two adjacent nodes, thus never being longer than the grid spacing. The system creates small but many beams and but with the disadvantage of many complicated joints where four members terminate. The beam-node system is typically used in steel gridshells.

The complicated force-situation combined with the limited space is problematic. Some kind of node, steel or timber are commonly used with this system, such as in *Herbert Art Gallery* as presented in Section 2.5 and in the *Canary Wharf Railway Station* by Foster + Partners. The principle is shown in Figure 6.28.

6.3.5 Mixed system

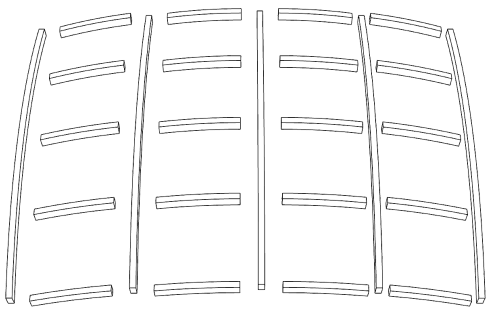

Figure 6.29: *The geometry as constructed with a mixed system*

This mixed system combines the segmented and continuous system, and thus has long continuous members in one direction and members crossing just one span in the other, the principle is shown in Figure 6.29. The system will create one direction that is slightly stronger than the other, meaning that this system is well suited together with geometries with clear strong and weak directions. Since the structure is being stable from the first arch, if the supports are strong enough, it means that the system can be built with a rather simple scaffolding.

6.3.6 Progressive Segmented System

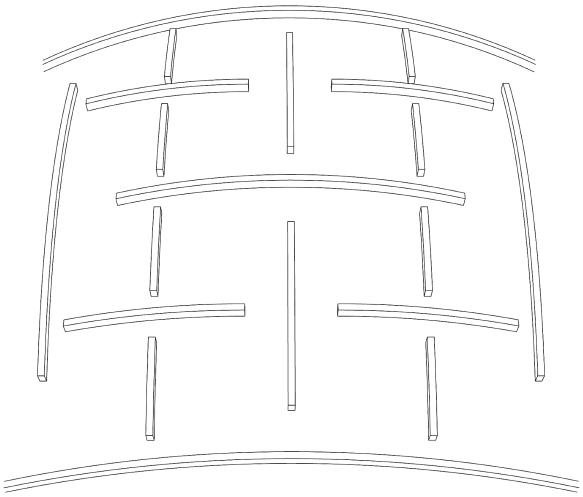

Figure 6.30: *The geometry as constructed with the progressive segmented system*

The progressive segmented system is a special case of the *Mixed System*, refined to having longer members in both directions, as shown in Figure 6.30. It is used in the *French Pavillion* for the 2015 Expo in Milan, by XTU Architects.

One advantage of the system is that, since this system works from the bigger scale to smaller, the need of scaffolding is small. With the large arches installed first and being stable, the smaller arches can supported on them when installed. It also has potential of further prefabrication. Where the smaller members are pre-assembled in a factory.

A rather big disadvantage of the system, is that members should be possible to slide in place, since the circumferential structure it is already assembled, decreasing the available nodes.

6.4 Joint Development

In timber structures, where the joint is usually weaker than the beam itself, the joint often governs member sizes. This differs from the design of steel and concrete where both material have connection-methods with nearly no loss of strength. In timber, a loss of strength in a strong joint of about 30-40% should be expected [Aicher et al, 2012]. This make the development and choice of joint an important task when designing timber structures. In the following section a number of different joints typologies are presented and evaluated, in terms of both structural strength and stiffness.

The main purpose with this chapter is to be able to evaluate and compare different joint typologies according to their strength and stiffness. All joints are therefore based on the same layout. It describes a node in a quadrangular grid, thus connecting 4 beams. All beams are of quality Gl28c and 450x150mm in size.

The calculated stiffness in this chapter is presented according to the coordinates presented in Figure 6.31.

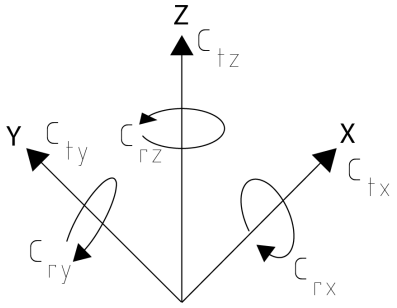

Figure 6.31: *Diagram of the six spring stiffnesses that the system is condensed to*

6.4.1 Basic Contact Joint

The basic joint shown in Figure 6.32 works by beam *1* transferring all forces by contact through beam *2*. Dowel *4* will be considered as only transferring shear. The joint is designed to transfer compression. However plate *3* is mounted to transfer possible tension, mainly in construction stage. With the plate mounted on the top, the joint will not be able to resist bending moment imposed by gravitational loads, and fully relies on the compressive forces to compensate for any bending in the system, much like in a masonry vault.

Enough resistance of beams *1* and *2* is known from earlier steps. The failure mechanism of the joint is then governed by:
1. The compression, perpendicular to grain in zone *a*.
2. The shear capacity of the dowels *4*.

This joint has considerable strength in relation to the low complexity and the low amount of steel. However as seen by comparing Table 6.8 and Table 6.2, the joint would not be able to withstand the forces in the case study, since the axial forces are too big.

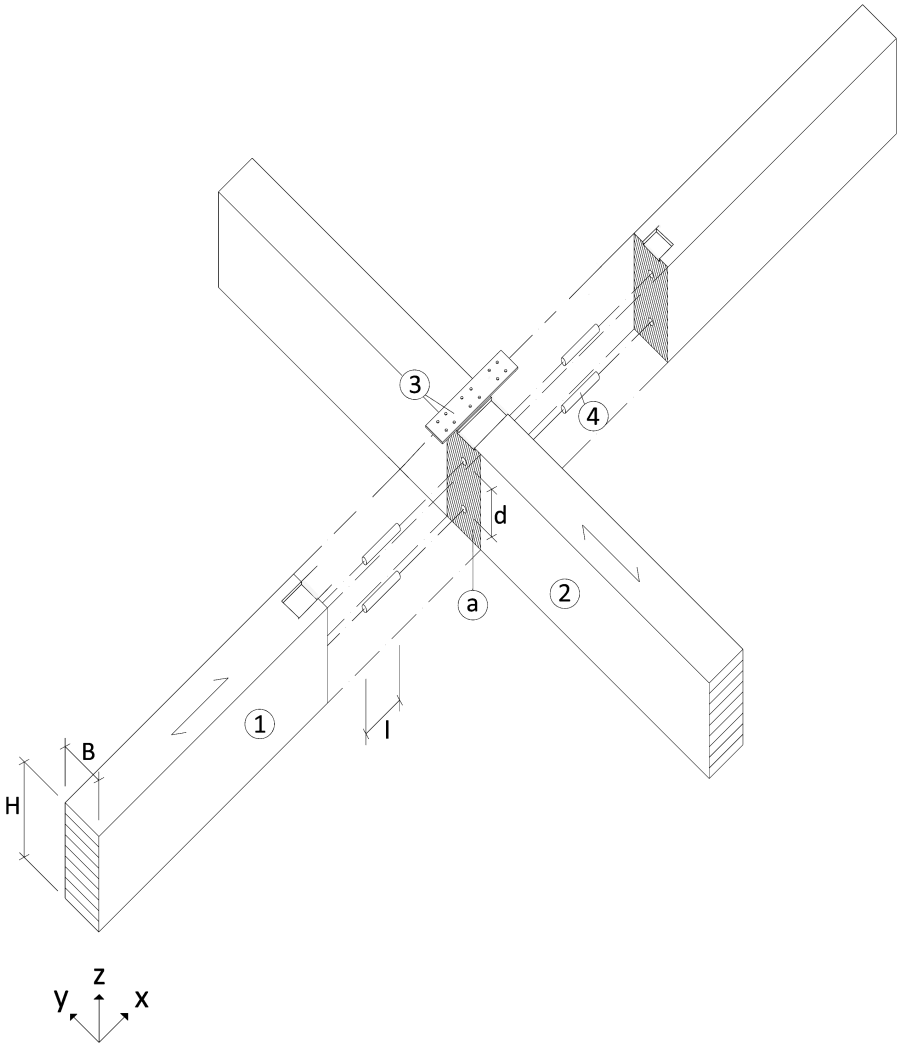

Figure 6.32: *Basic contact joint. Diagram showing the assembly and components of the joint*

The shear failure is rather easy to avoid, by increasing the size of the dowels. However the compression failure, being dependent on nothing but compressive stress induced in the crossing member, can only be avoided by increasing the cross-section size. Changing the timber quality is ineffective since almost no increase in compressive strength perpendicular to grain ($f_{c,90}$) occurs between timber qualities.

This type of joint should be considered for medium sized structures. With mass big enough to ensure that no tension occurs anywhere in the joint. However not too large, in order not to exceed the compression resistance. With the joint being unable to resist large tension forces it follows that if the joint should be used in edge-zones and other areas where the tension might occur, it could be upgraded on site with double threaded screws, marked with *5* in Figure 6.35, which would in a simple way increase the performance.

The strength and stiffness of this joint is given in Table 6.8, the derivation of these values are presented in Appendix B. The effect of the decreased stiffness compared to the initial FE-model (Section 6.2.3) can be observed in Figure 6.34, showing the deflection under dead load if this joint is used for the case study. In Figure 6.33 the first global buckling mode

for the structure is shown, with a linear buckling factor of 2.1, which is too low to be acceptable, but since it is already concluded that the joint is not an option, this will not be a problem. The buckling occurs towards the edge beam, induced by the accumulation of forces there. The natural frequency of the structure is 1.3 Hz, which is acceptable with regard to wind.

During the design and assembly of this joint, the tolerance for the gap between beam *1* and *2* must be kept to a minimum, in order to get the contact needed for functionality. The plate *3* can be assembled with a gap, ensuring contact and being activated only in tension. With the mechanical fasteners being well covered by the timber beams required fire-protection levels for public buildings is achieved with easy measures [Gross, 2016].

The joint is suitable to use together with assembly systems of type *Zollinger* and *Mixed-Systems*. Due to low amount of mechanical fasteners and special operations this should be considered an economic choice.

Table 6.8: Strength and stiffness of the Basic Contact Joint

Basic contact - Strength

	Contact		Fastener		Total	
	Permanent	*Short*	*Permanent*	*Short*	*Permanent*	*Short*
N [kN]	-113	-170	2	3	+18/-80	+18/-120
V_y [kN]	0	0	±19	±28	±19	±28
V_z [kN]	0	0	±15	±22	±15	±22
M_y [kNm]	0	0	0	0	0	0
M_z [kNm]	0	0	0	0	0	0

Basic contact - Stiffness

	Contact		Fastener		Total	
	Initial	*Final*	*Initial*	*Final*	*Initial*	*Final*
c_{tx} [kN/m]	-252000	-158000	+53578	+53578	+53578/-252000	+53578/-158000
c_{ty} [kN/m]	0	0	23260	14539	23260	14539
c_{tz} [kN/m]	0	0	23260	14539	23260	14539
c_{rx} [kNm/rad]	626	391	0	0	626	391
c_{ry} [kNm/rad]	0	0	0	0	0	0
c_{rz} [kNm/rad]	0	0	0	0	0	0

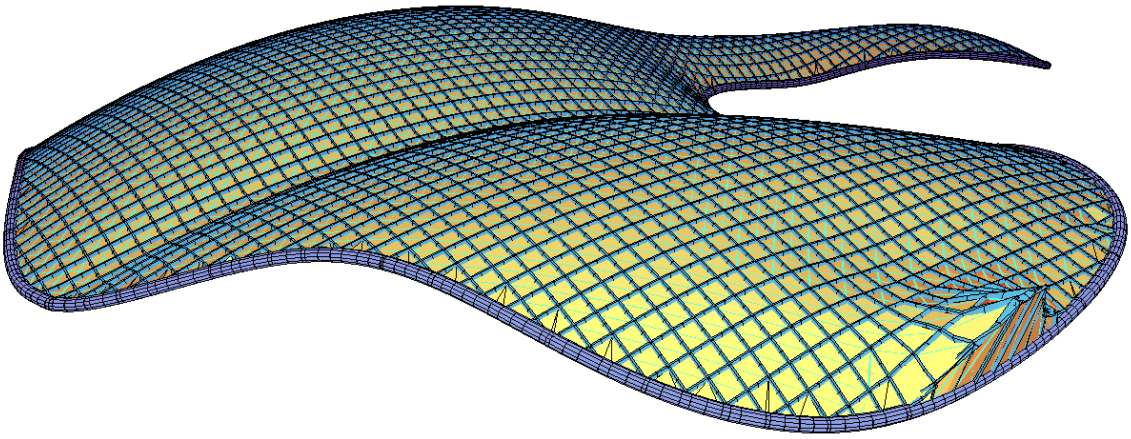

Figure 6.33: *The first global buckling mode using the stiffness of the Basic Contact Joint*

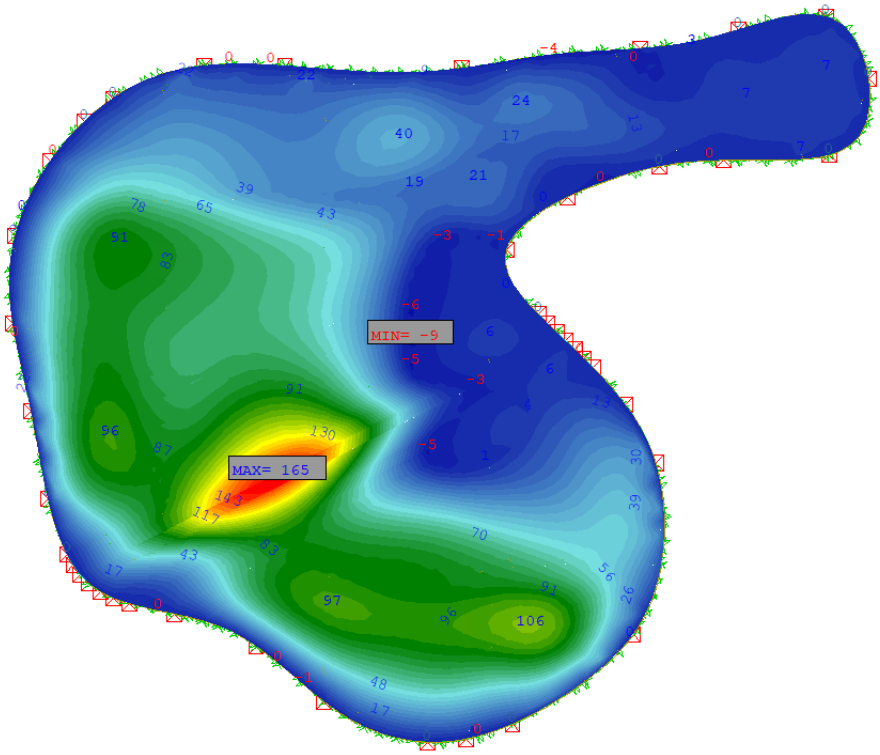

Figure 6.34: *The maximum vertical deflection using the stiffness of the basic contact joint, with the Zollinger system* [mm]

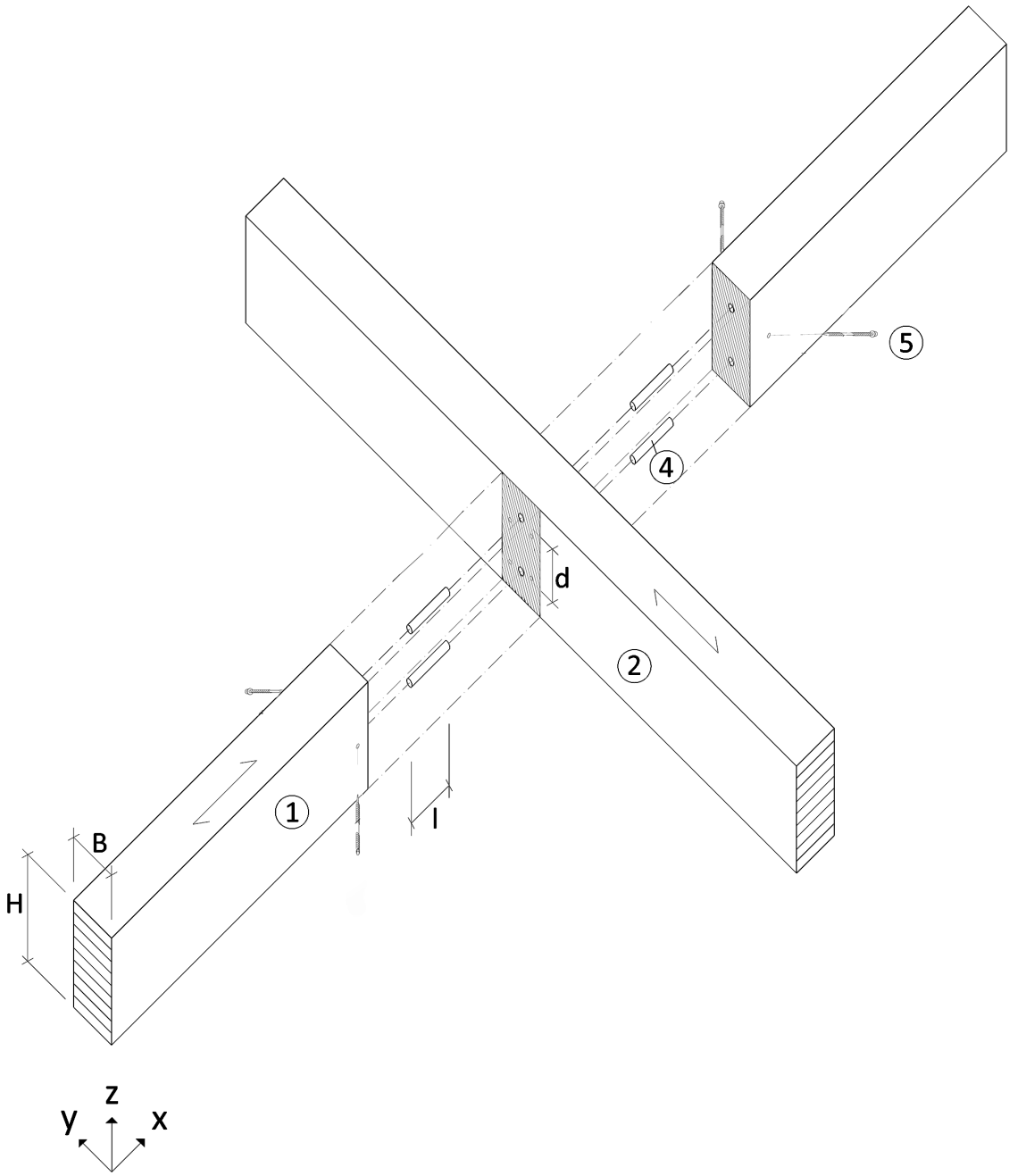

Figure 6.35: *Basic contact joint with tension reinforcement.*

6.4.2 Reinforced Basic Joint

The *Basic Contact Joint* presented in the previous chapter was limited by the compression strength perpendicular to grain. The joint shown in Figure 6.36 imitates the layout of the the previous joint. However the dowels *3* are continuous through beam *2* and anchored in beam *1*. The fasteners can be of different kind, dowels as shown in Figure 6.36 or plates as shown in Figure 6.39.

This layout increases the axial resistance of the joint layout, as well as allows the joint to handle tension and bending. Due to tolerances during installation, the joint is assumed not to be able to have contributions from both contact and mechanical fasteners. So the joint is evaluated such as to have contributions only from the dowels.

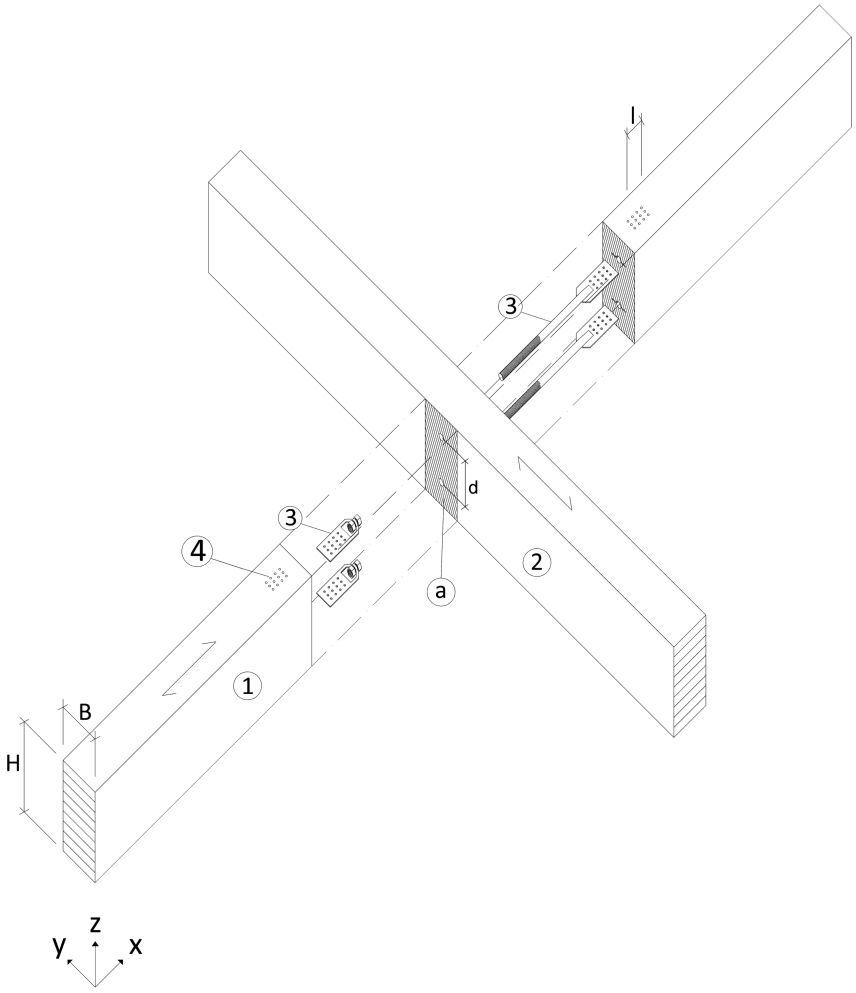

Figure 6.36: *Reinforced basic-type joint. Diagram showing the assembly and components of the joint*

Enough resistance of beams *1* and *2* is known from earlier steps.
1. The strength of steel rod *3* for shear.
2. The strength of steel rod *3* for tension or compression.
3. The strength of the dowel connection *4*.

4. The reduced cross-section of beam *1* at the dowel connection.

Since the stiffness contribution from contact is neglected, strengthening the joint is a matter of increasing the size of the steel rods, until the cross section at *4* or beam *2* fails due to reduced cross-section. The strength and stiffness of this joint can be seen in Table 6.9, the derivation of these values are presented in Appendix B.

The deflection of the case study with this joint applied can be seen in Figure 6.37. In Figure 6.38 the first global buckling mode for the structure is shown, with a linear buckling factor of 5.3, which is sufficient. The buckling occurs at the arch, induced by the high axial forces there. The natural frequency of the structure is 1.3 Hz, which is acceptable with regard to wind.

The joint increases the low axial strength from the *Basic contact joint* with its mechanical fasteners, as well as introducing some bending resistance. As seen when comparing Table 6.9 and the requirements from Section 6.2.3, the joint would well be able to withstand the forces in the case study in the typical *shell zone* (with the notation presented in Section 6.2.3).

In the typical *bending zone*, the resistance of the joint is sufficient in its current layout, although the margins are not big, and the axial force-bending interaction can prove problematic. However the beams in these zones are larger in size to meet the stress requirements. This means that the distance between the dowels (d) can be increased, thus increasing bending resistance considerably. An increased beam size also allows for bigger dowel (*3*). Therefore, this makes this type this joint an alternative also for the *bending zones*.

With Equation (3.28) we can also conclude that the bending moment will be reduced with the decreased stiffness of the joint compared to the forces in the pre-sizing (Section 6.2.3), meaning that the values in Table 6.4 should be considered conservative, thus making the feasibility of this joint in *bending zones* even higher.

The assembly of the joint is rather straightforward. The steel-rods are pushed through beam *2* and assembled, and since the holes at connection are pre-drilled it is possible to find the location and assemble the connection.

The joint is suitable to use together with assembly systems of type *Zollinger* and *Mixed*. The *Reinforced Basic* joint is more complex than the *Basic contact* joint, since more operations need to be performed on the beams and some custom fasteners might be needed, depending on chosen layout.

With the mechanical fasteners being well covered by the timber beams required, fire-protection levels for public buildings is achieved with easy measures [Gross, 2016].

Table 6.9: Strength and stiffness of the Reinforced Basic Joint

Reinforced basic - Strength

	Contact		Fastener		Total	
	Permanent	*Short*	*Permanent*	*Short*	*Permanent*	*Short*
N [kN]	0	0	±268	±402	±268	±402
V_y [kN]	0	0	±19	±28	±19	±28
V_z [kN]	0	0	±15	±22	±15	±22
M_y [kNm]	0	0	±47	±70	±47	±70
M_z [kNm]	0	0	±2	±3	±2	±3

Reinforced basic - Stiffness

	Contact		Fastener		Total	
	Initial	*Final*	*Initial*	*Final*	*Initial*	*Final*
c_{tx} [kN/m]	0	0	183267	114542	183267	114542
c_{ty} [kN/m]	0	0	40182	25114	40182	25114
c_{tz} [kN/m]	0	0	40182	25114	40182	25114
c_{rx} [kNm/rad]	0	0	626	391	626	391
c_{ry} [kNm/rad]	0	0	5612	3507	5612	3507
c_{rz} [kNm/rad]	0	0	0	0	0	0

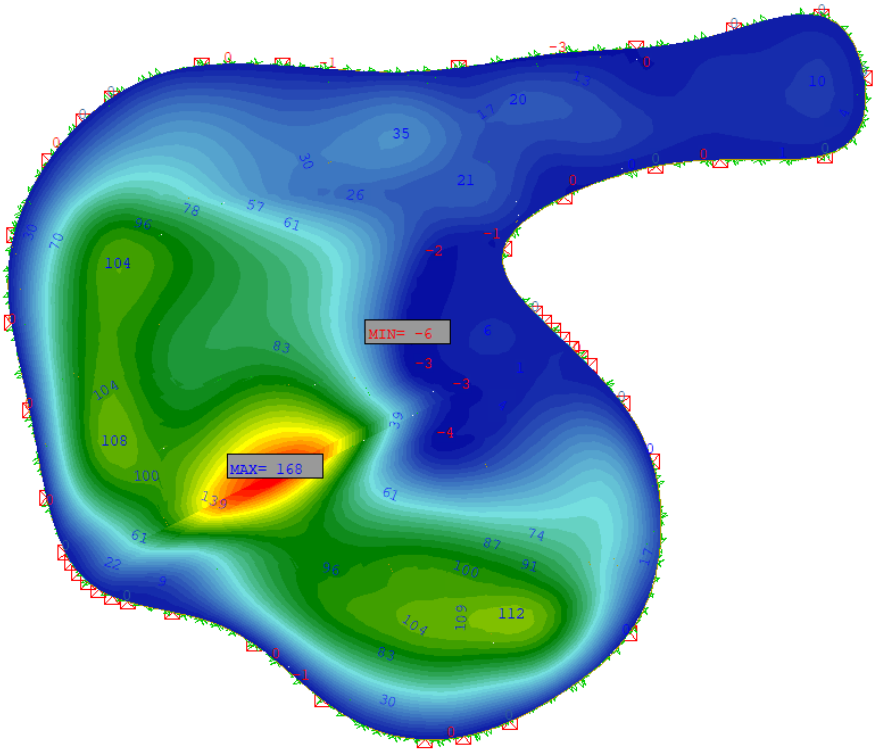

Figure 6.37: *The maximum vertical deflection using the stiffness of reinforced basic joint, with the Zollinger system* [mm]

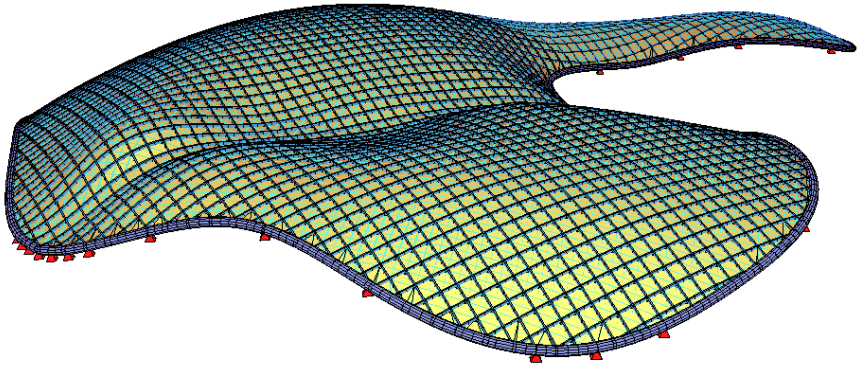

Figure 6.38: *The first global buckling mode using the stiffness of the reinforced basic joint*

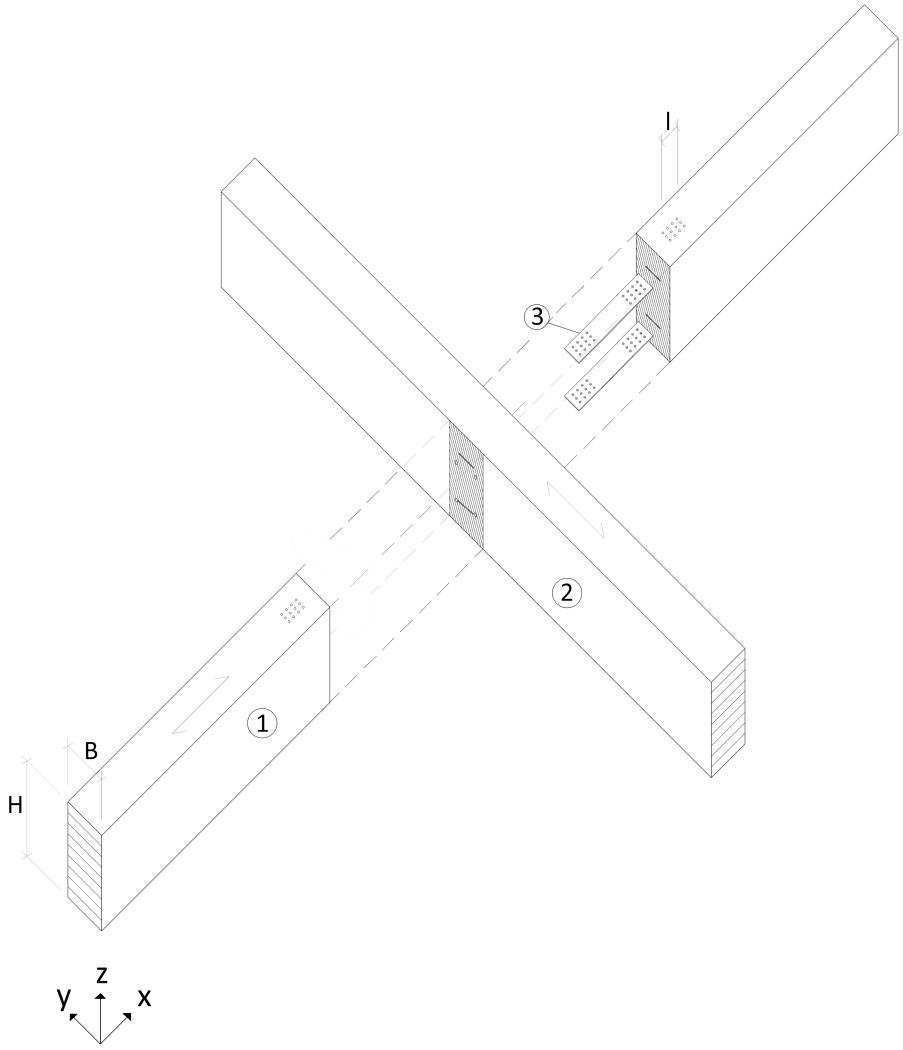

Figure 6.39: *Reinforced basic-type joint - alternative layout. Diagram showing the assembly and components of the joint*

6.4.3 Half Lap Joint

The half lap joint is a common joint in furniture carpentry and medieval structures, mainly in structures exposed to compression, such as vertical trusses or steep roofs. Since the notch in the cross-section drastically decreases the bending and axial resistance of the beam, a timber lamella is mounted above the notch, working as an extra flange, thus maintaining the structural height.

In order to keep the simplicity of the joint, the joint is deigned with such that the extra lamella should be able to bend on site, thus according to Section 6.1.4; 45 mm is an acceptable thickness.

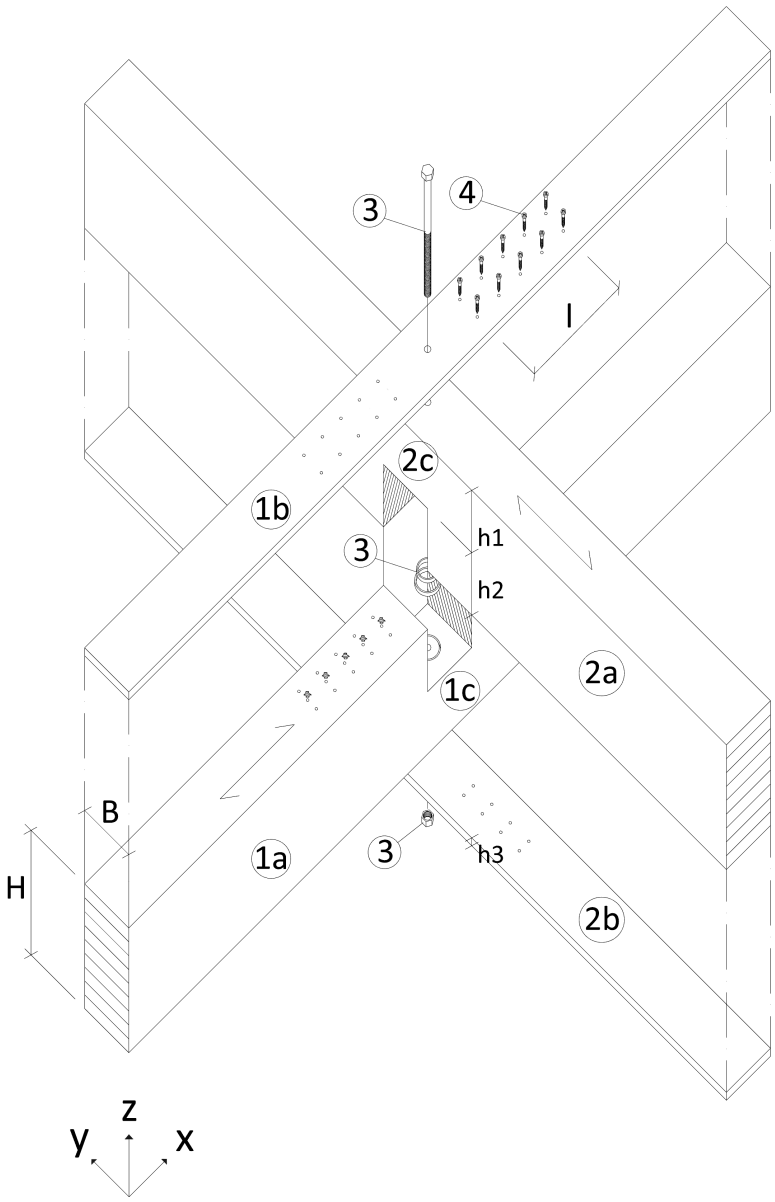

Figure 6.40: *Half lap with extra flange. Diagram showing the assembly and components of the joint*

Enough resistance of beams *1* and *2* is known from earlier steps. The failure mechanism of the joint is then governed by:

1. The reduced cross-sections *1c* and *2c*.
2. The tension strength of extra lath *1b* and *2b*.
3. The screw-connection for the lath *4*.

In Table 6.10 the strength and stiffness of the joint can be seen, the derivation of these values are presented in Appendix B. The deflection of the structure with this joint can be seen in Figure 6.42. In Figure 6.41 the first global buckling mode for the structure is shown, with a linear buckling factor of 6.5, which is sufficient. The buckling occurs at the arch, induced by the high axial forces there. The natural frequency of the structure is 1.4 Hz, which is acceptable with regard to wind.

The screwed connection can easily be increased in size in order not to be the weakest part of the structure. Most of the stiffness in the joints comes from the continuous beams, makes a larger cross-section the absolutely most efficient way to improve the performance. Allowing a pre-shaped lath will be very efficient, since that can increase in size. Since failure of the lamella is one of the weakest links in the joint, a bigger lamella will improve the performance significantly. Although this will heavily increase the cost, since more members needs to be fabricated before brought to site.

The shear ring and bolt *3* is a big contributor to the shear stiffness of the joint, and if the stiffness is lacking, increasing the size of this should improve the performance. If the rotational stiffness of the joint should be increased, one could also exchange bolt *3* to a connection of 4 double threaded wood screws, which could increase the rotational stiffness. This will however reduce the contribution from the mechanical fasteners to the axial stiffness, due to the removal of the shear ring.

Comparing results of Table 6.10 with the demands in chapter Section 6.2.3 it can clearly be used in the *shell zones*. At its current layout, the node is not strong enough for *bending zones*, but if considering the larger cross sections in these zones, the resistance are sufficient.

With high strength, low amount of steel and rather easy, if extensive machining needed this should be considered a economic joint. Since mechanical fasteners are protected by the timber, an adequate fire-protection class is achieved if gaps and drill holes are filled with plugs, mineral wool or fire-protection fillers [Gross, 2016].

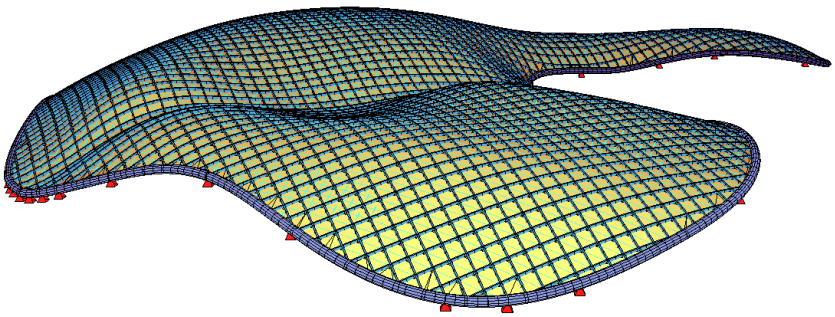

Figure 6.41: *The first global buckling mode using the stiffness of Half lap joint*

Table 6.10: Strength and stiffness of the Half-lap type of joint

Half lap - Strength

	Contact		Fastener		Total	
	Permanent	*Short*	*Permanent*	*Short*	*Permanent*	*Short*
N [kN]	+316/-388	+ 474/-582	±20	±30	+316/-388	+474/-582
V_y [kN]	±50	±75	0	0	±50	±75
V_z [kN]	±8	±12	±35	±52	±42	±64
M_y [kNm]	±32	±48	0	0	±32	±48
M_z [kNm]	±13	±19	0	0	±13	±19

Half lap - Stiffness

	Contact		Fastener		Total	
	Initial	*Final*	*Initial*	*Final*	*Initial*	*Final*
c_{tx} [kN/m]	3798616	2374135	20653	12908	3819269	2387043
c_{ty} [kN/m]	58680	36675	20653	12908	58680	36675
c_{tz} [kN/m]	16460	10287	0	0	16460	10287
c_{rx} [kNm/rad]	4180	2612	693	462	4873	3074
c_{ry} [kNm/rad]	119789	74868	0	0	119789	74868
c_{rz} [kNm/rad]	1636	1022	0	0	1636	1022

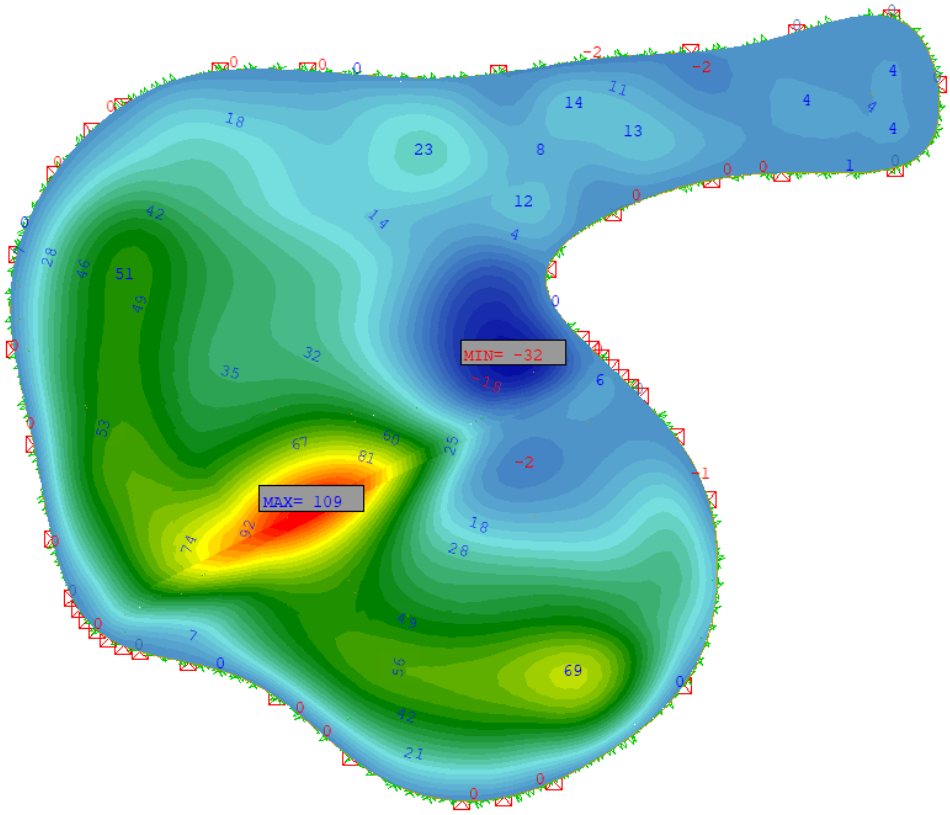

Figure 6.42: *The maximum vertical deflection using the stiffness of the half lap joint, with the overlapping system* [mm]

6.4.4 Steel Node Type 1

Enough resistance of beams *1* and *2* is known from earlier steps. We also assume that the strength of the steel node is high enough to be neglected as failure mechanism. The failure mechanism of the joint is then governed by:
1. The stress in the reduced cross-section in position of the slotted-in steel-plate and screws.
2. The screwed connection *4*.

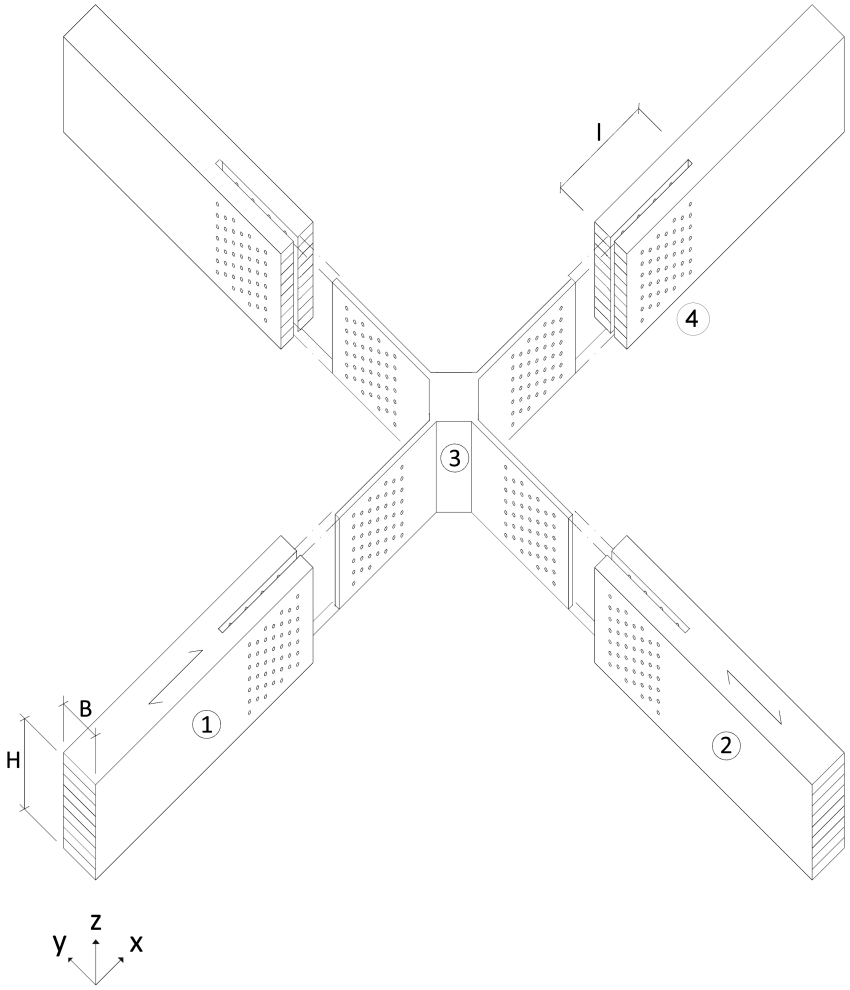

Figure 6.43: *Steel node-type joint. Diagram showing the assembly and components of the joint*

The strength and stiffness of this joint can be seen in Table 6.11, the derivation of these values are presented in Appendix B. The deflection of the case study with this joint applied can be seen in Figure 6.45. In Figure 6.44 the first global buckling mode for the structure is shown, with a linear buckling factor of 5.4, which is sufficient. The buckling occurs at the arch, induced by the high axial forces there. The natural frequency of the structure is 1.3 Hz, which is acceptable with regard to wind.

In the presented version the strength is governed by the screwed connection. Where the length of it (l) became very large, and the length was chosen to be limited to 360 mm. An increased screwed connection would make the node size, as well as the steel weight, very large. This also means that the joint is complicated to strengthen further.

Comparing results of Table 6.11 with the demands in Section 6.2.3 the strength is sufficient for use in both the *shell* zone and *bending zone*.

An alternative, but similar layout, that would increase the capacity of the joint significantly is by using a two bladed solution, having two slotted-in-plates per beam. Doubling the number of shear planes. This solution must be checked to have enough distance between the blades.

A steel node is expensive, since every node needs to be designed and manufactured individually if the grid is not designed with absolute care. In case of exposed steel elements these need to be fire-protected [Just et. al. 2016].

Table 6.11: Strength and stiffness of the Steel node type 1

Steel node type 1 - Strength

	Contact		Fastener		Total	
	Permanent	*Short*	*Permanent*	*Short*	*Permanent*	*Short*
N [kN]	0	0	±352	±528	±352	±528
V_y [kN]	±47	±70	0	0	±47	±70
V_z [kN]	±14	±21	0	0	±14	±21
M_y [kNm]	0	0	±59	±89	±59	±89
M_z [kNm]	±22	±33	0	0	±22	±33

Steel node type 1 - Stiffness

	Contact		Fastener		Total	
	Initial	*Final*	*Initial*	*Final*	*Initial*	*Final*
c_{tx} [kN/m]	0	0	379890	237431	379890	237431
c_{ty} [kN/m]	1155727	722329	0	0	1155727	722329
c_{tz} [kN/m]	0	0	379890	237431	379890	237431
c_{rx} [kNm/rad]	33102	20688	0	0	33102	20688
c_{ry} [kNm/rad]	0	0	17745	11090	17745	11090
c_{rz} [kNm/rad]	20252	12657	0	0	20252	12657

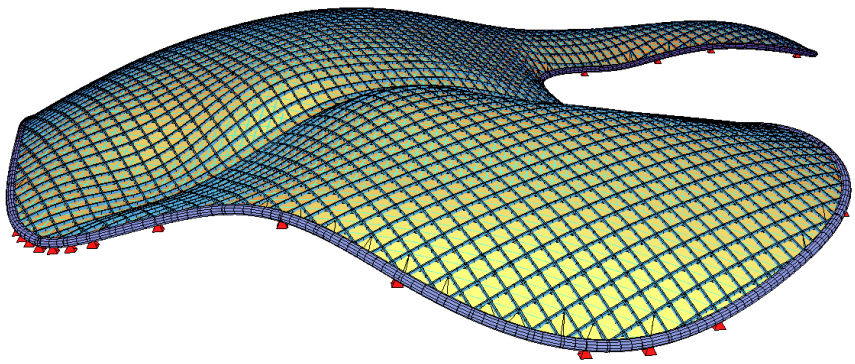

Figure 6.44: *The first global buckling mode using the stiffness of Steel Node Type 1 joint*

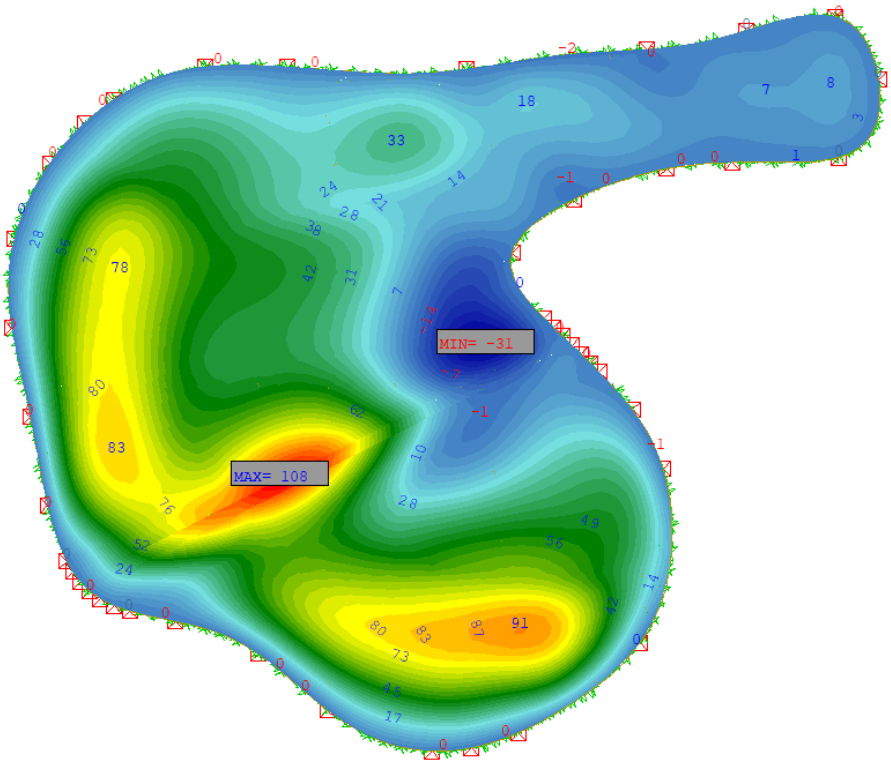

Figure 6.45: *The maximum vertical deflection using the stiffness of Steel Node Type 1 joint* [mm]

6.4.5 Steel Node Type 2

Another type of steel joint is presented in Figure 6.46, but of a different layout. Where the arm on the node is not using a slotted-in-plate, instead using a butt-plate *a* on which the beam *1* and *2* is mounted flush against and then screwed on to.

Enough resistance of beams *1* and *2* is known from earlier steps. The failure mechanism of the joint is then governed by:
1. The withdrawal strength of the screws in connection 4.
2. The strength of the steel node.

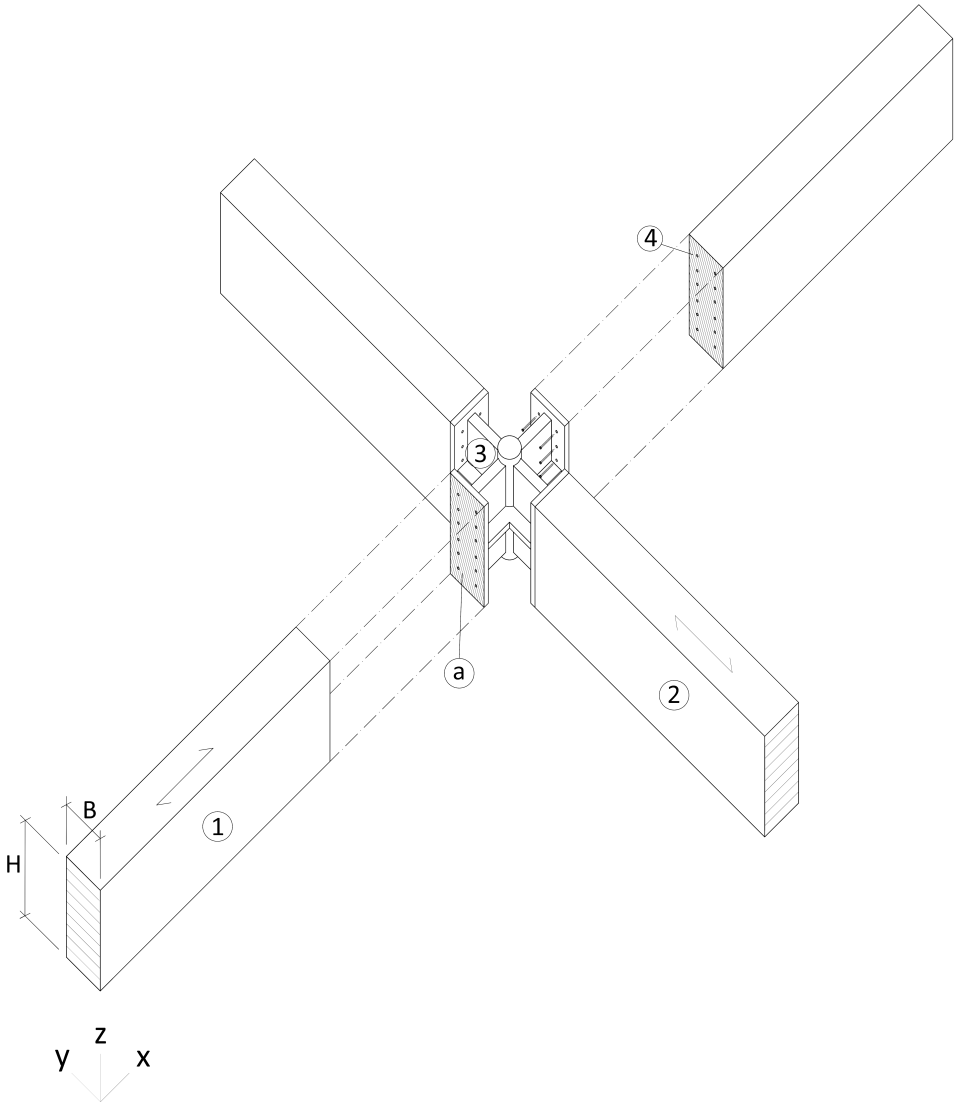

Figure 6.46: *Steel node-type joint*

As with the previous example of steel node, it is relatively strong, but complicated to manufacture, thus expensive. The strengthening of this joint is straightforward, since it is about increasing the capacity of the screw-connection. Although, as with the previous steel node, the size and spacing of fasteners became a limitation and limited the size of the screws to

10 mm, meaning that any major increases in strength needs an increase of the cross section size. The strength and stiffness of this joint layout is presented in Table 6.12, the derivation of these values are presented in Appendix B.

Comparing results of Table 6.12 with demands in chapter Section 6.2.3 the strength is sufficient for use in the *shell* zone. However the moment capacity in the joint is not big enough for use in the *bending* zones, limited by the axial strength of the screws. Looking at the *arch* zones, the bending resistance is not sufficient, but considering the increased cross-section, and that the node is under high compression, the joint will likely work when the forces are interacting.

The deflection of the case study with this joint applied can be seen in Figure 6.48. In Figure 6.41 the first global buckling mode for the structure is shown, with a linear buckling factor of 6.5, which is sufficient. The buckling occurs at the arch, induced by the high axial forces there. The natural frequency of the structure is 1.4 Hz, which is acceptable with regard to wind.

As stated with the last joint of similar type, the nodes needs to be treated with fire-retardant paint.

Table 6.12: Strength and stiffness of the Steel-node type 2

Steel node type 2 - Strength

	Contact		Fastener		Total	
	Permanent	*Short*	*Permanent*	*Short*	*Permanent*	*Short*
N [kN]	+0/-771	+0/-1156	+83	+124	+83/-771	+124/-1156
V_y [kN]	0	0	±42	±42	±42	±42
V_z [kN]	0	0	±42	±42	±42	±42
M_y [kNm]	0	0	±7	±11	±7	±11
M_z [kNm]	0	0	±2	±6	±2	±3

Steel node type 2 - Stiffness

	Contact		Fastener		Total	
	Initial	*Final*	*Initial*	*Final*	*Initial*	*Final*
c_{tx} [kN/m]	-3413608	-2133505	118115	73821	-3413608/118115	-2133505/73821
c_{ty} [kN/m]	0	0	80367	50229	80367	50229
c_{tz} [kN/m]	0	0	80367	50229	80367	50229
c_{rx} [kNm/rad]	0	0	350	218	350	218
c_{ry} [kNm/rad]	0	0	64112	40070	64112	40070
c_{rz} [kNm/rad]	0	0	375	230	375	230

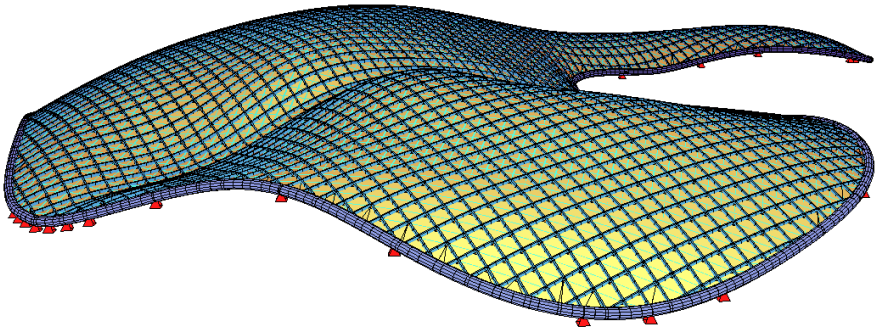

Figure 6.47: *The first global buckling mode using the stiffness of Steel Node Type 2 joint* [mm]

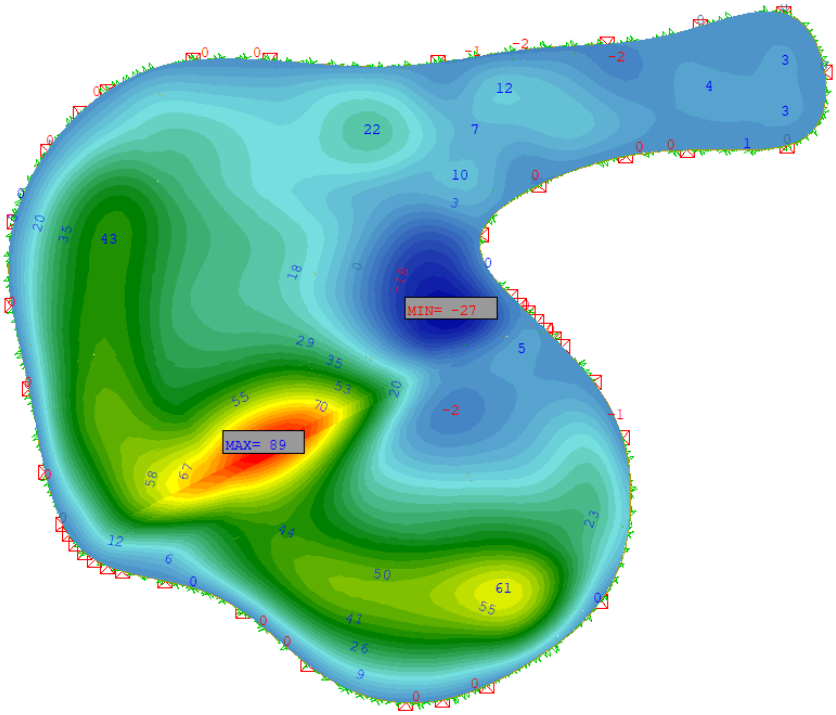

Figure 6.48: *The maximum vertical deflection using the stiffness of Steel Node Type 2 joint*

6.4.6 Splicing Joints

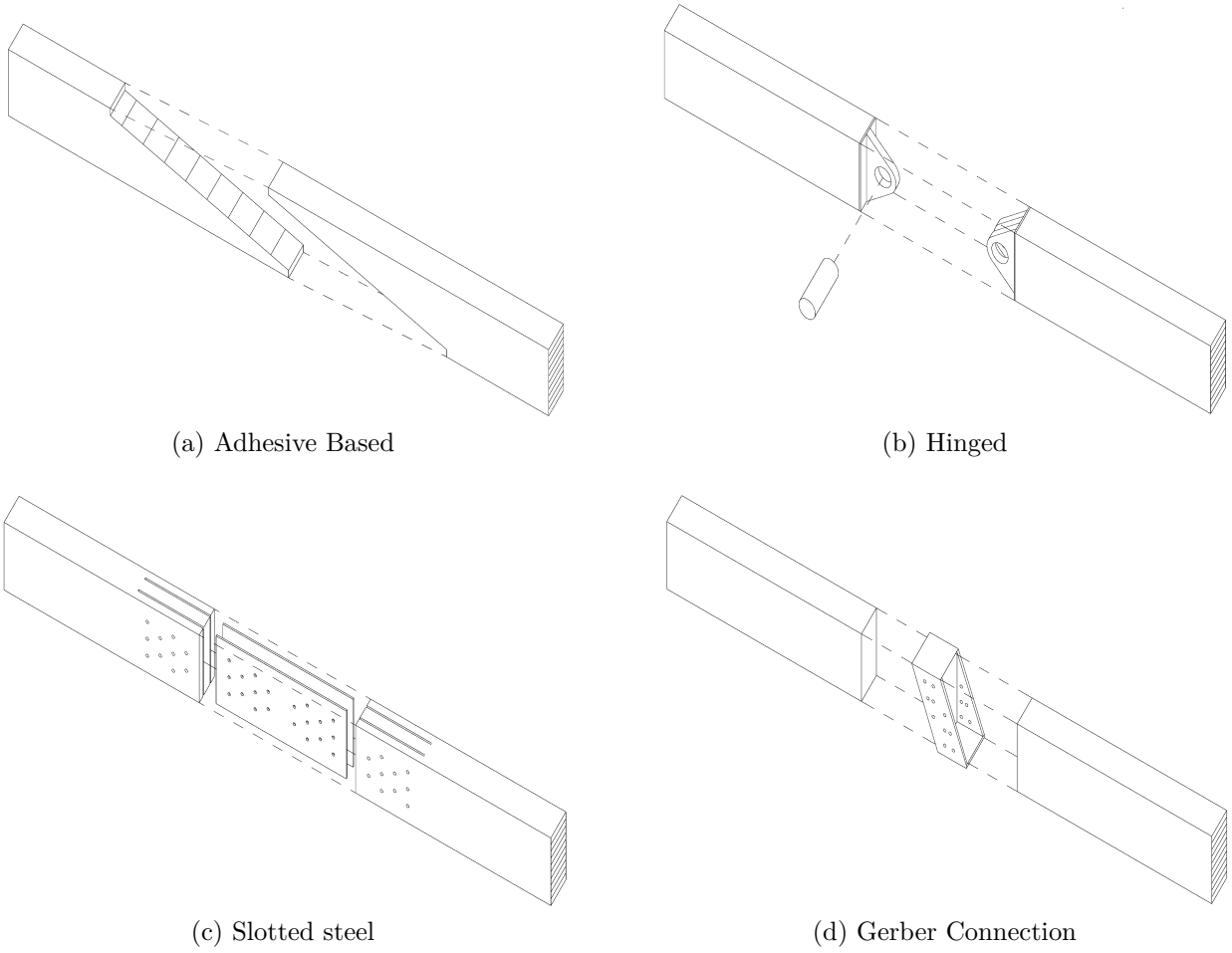

(a) Adhesive Based

(b) Hinged

(c) Slotted steel

(d) Gerber Connection

Figure 6.49: *Diagram of different splicing joints*

The maximum length of beams will change depending on chosen assembly system, where some have a limited size by definition, like the *Zollinger* and the *Segmented*, while others like the *Overlapping* and *Mixed* might have theoretically unlimited lengths. The maximum length of members will then be governed by the available transportation and spliced on site.

A number of options of splice-joints is shown in Figure 6.49. Adhesive joints will have to be performed off-site, meaning that this concept is not useful for this task. Although adhesive based connection have, at an experimental stage, been performed on-site with good results [Aicher et al. 2012].

The other splicing joints proposed should all be placed in areas with low bending moments, and shall be assumed to transfer no bending [Gross, 2016].

6.4.7 Edge Beam Joints

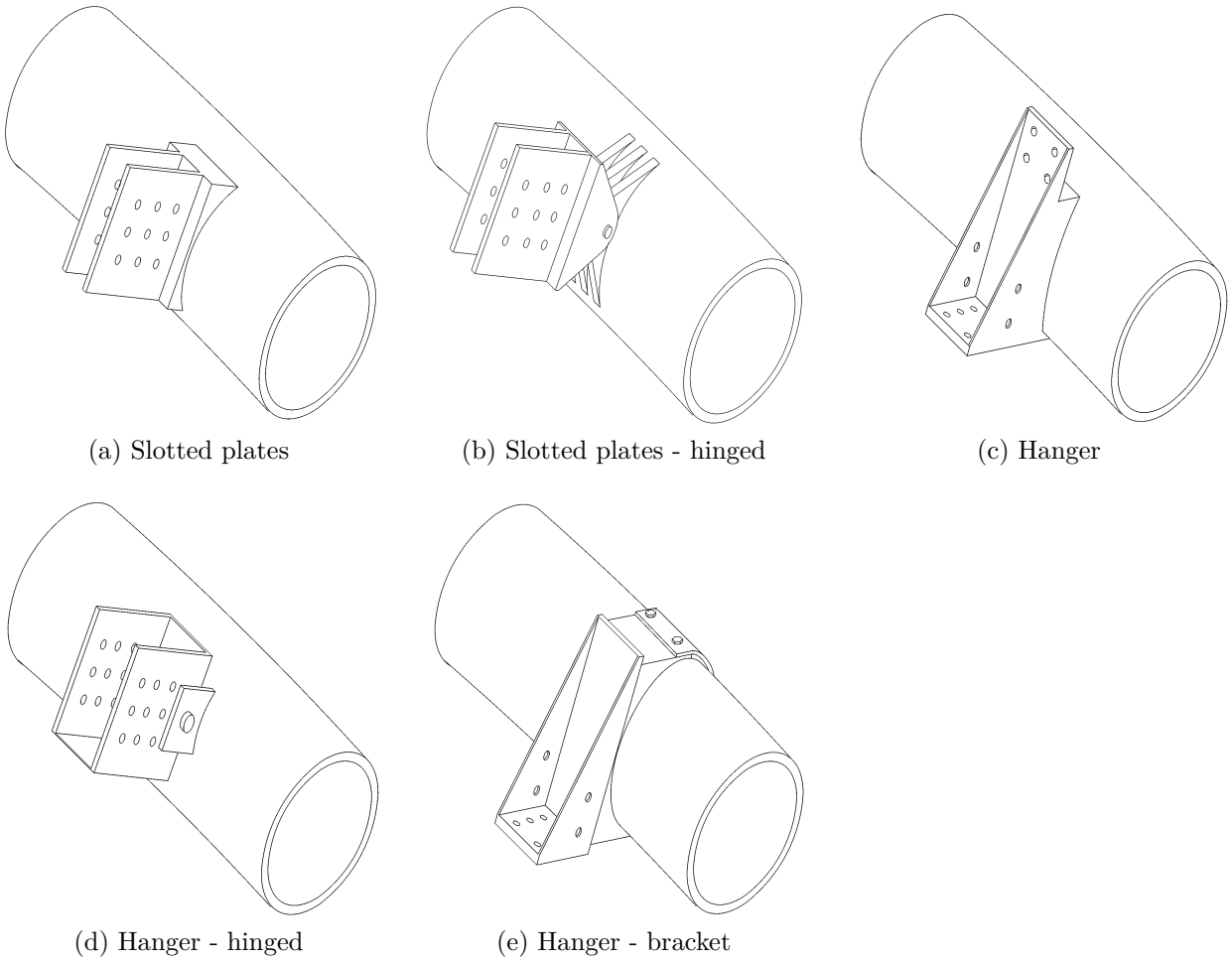

(a) Slotted plates (b) Slotted plates - hinged (c) Hanger

(d) Hanger - hinged (e) Hanger - bracket

Figure 6.50: *Diagram of different joints connecting edge-beam with the grid.*

The structure, as stated in Section 6.1.2 is to be supported by a steel edge beam. The suggestion being that this joint should be performed hinged, or close to hinged to decrease the support-moments for the beams. A number of proposals of this steel-to-timber joint is shown in Figure 6.50. Where some examples, such as b and d as well as e, is articulated, meaning that the moment resistance is zero. While some joints like e and c relies on the low stiffness of timber joints, while the actual connection to the edge-beam is stiff. A rather small screwed connection will not create much bending resistance, thus behaving hinged.

All screws in the connection should either be non-pre-drilled and executed during the actual assembly, or drilled with considerable gap, since all these joint are supposed to have its main force transfer in the contact between timber and steel, and the screws is mainly a matter of holding the beam in place and working in shear. This is crucial, since the screwed connection will not able to withstand the larger forces in the structure. A screwed connection able to withstand these forces will be long and the internal lever arm of such connection, would not make it behave completely hinged.

6.5 Structural Design - Proposal

The suggestion for how to manufacture and assemble the case study is shown in this section. The geometry and structure of the gridshell is shown in Figure 6.51.

The suggested assembly is a combination of methods and joints, in order to simplify the construction process.

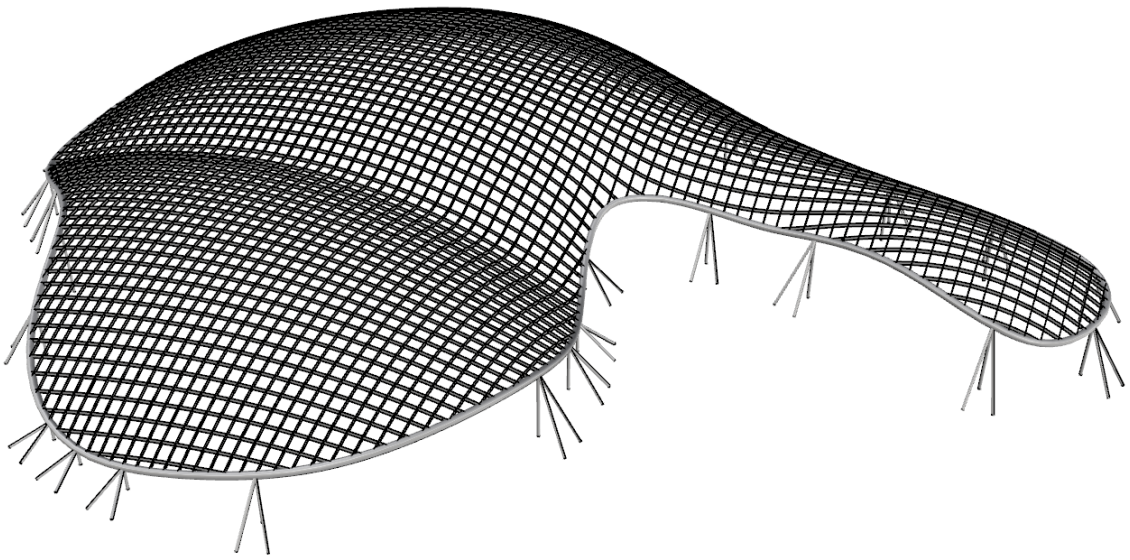

Figure 6.51: *Perspective of the final geometry and structure for the case study*

6.5.1 Assembly system

The proposed assembly system is a combination between the progressive segmentation and an overlapping system. The construction process is based around 5 axes of continuous arches. These are continuous, uninterrupted except for splicing. The beams in the valley is increased in size compared to the rest of the grid, while the other axes uses the same cross-section as the surrounding grid, the suggested layout and manufacturing process is shown in Figure 6.52-Figure 6.53.

With the continuous beams not being crossed by other members they are just spliced, with a double slotted-in-plate according to option *c)* in Figure 6.49. All other grids members should be connected in an overlapping system based on the *Half lap joint*. The overlapping structure is connected to the continuous arches by *Reinforced basic joints*, minimizing the perforation of the continuous axes.

The main reason for the mixed system is that it will allow for a construction-process with low need of scaffolding. The suggested assembly process goes as follows:
1. The tripods and edge-beam is installed (Figure 6.52*a*).
2. All the continuous beams are assembled on the ground and then mounted on the edge beam. The valley has priority, and the members crossing the valley will have to be attached to it. (Figure 6.52*b*)
3. Smaller members are assembled between the arches of the axes, to make the lateral stability

of these higher, these members are installed by *Reinforced basic joints* (Figure 6.52*c*). 4. At positions where needed for deflection and tolerance purposes and also for lateral stability of the arches scaffolding is added. (Figure 6.53*a*)
5. The first layer of beams are installed. Since the arches are already in place, all of these members will be of limited size and since already supported, with limited need of scaffolding. These are attached to the system of arches by *Reinforced basic joints*. Having all its notches for the *Half lap joint* facing upwards. (Figure 6.53*c*)
8. Bracing and roof is constructed. The lath are shaped at site, during the installation.

By adding the continuous members to the structure, stability can be achieved at an earlier stage. With the chosen splicing joints and the uniform cross-section with the rest of the cross section, the main function of the continuous beam is through the assembly, while not affecting the structural behaviour significantly. The splicing joints, with its low rotational stiffness ensures that the beam does not become too stiff, and accumulates moment, ensuring a better distribution of forces in the grid.

6.5.2 Manufacture

Lamination was from early in the process considered the preferable method of manufacture due to the long spans and high forces that introduced high requirements on the structure. And as could be seen in Figure 6.10, every member in the structure can be manufactured using this method, due to the mild curvature of the surface.

All members are single bent, and the *Beam normal* is adjusted to the master surface. This in a machining process that also includes surface treatment of the beams and preparation of notches and pre-drilled holes.

With the half lap joint it is important that every member has its assembly direction in the vertical direction. Uniform direction will allow for construction, since every joint is activated in the same degree of freedom. By using the vertical direction it will allow easy construction with a crane.

With the chosen assembly system, the ambition was to minimize the number of splicing joints in the structure. However, some members have to be spliced, in Figure 6.54, the splicing-algorithm presented in Section 6.2.2 is used on the grid of the case study. The results can be seen in Figure 6.54*a* and *b*, showing the members and the positions where they should be spliced in order to fulling the criteria given earlier. Noted should be that the joints are distributed in a way such that redistribution is allowed. Notable is also that many of the elements are not spliced.

In Figure 6.54*c*, the bounding box for a number of members is shown, and it can be seen that the demands on transportation lined out in Section 4.5 are fulfilled for each one.

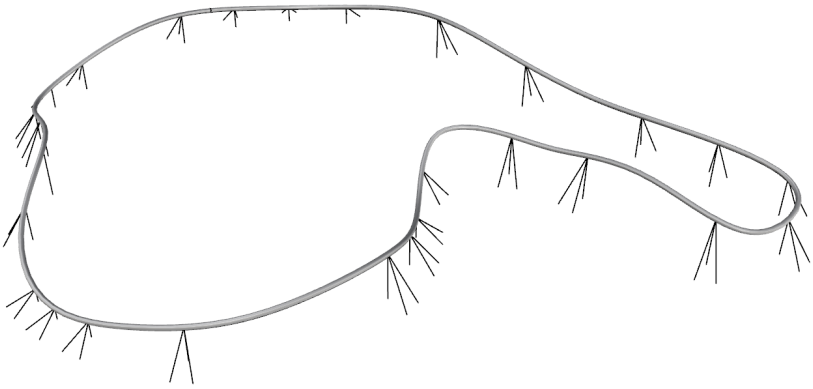

(a) The edge beam is installed

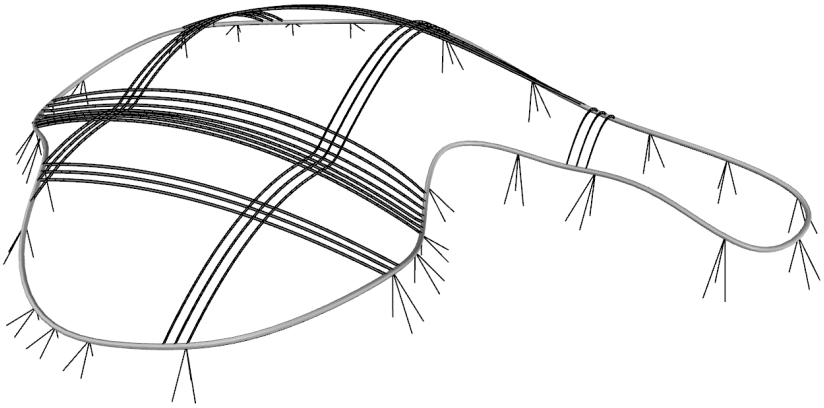

(b) The first spine-arches are installed

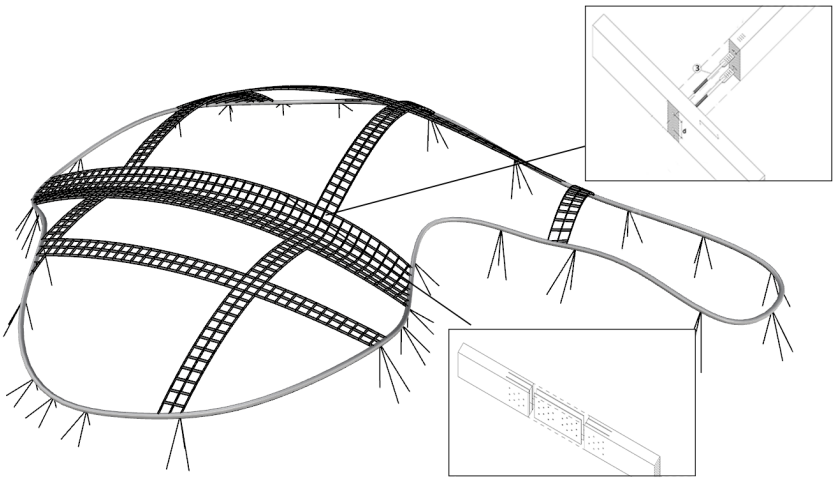

(c) The continuous arches are installed, with short ladder members attached by Reinforced basic joints

Figure 6.52: *Assembly process of the grid - part 1*

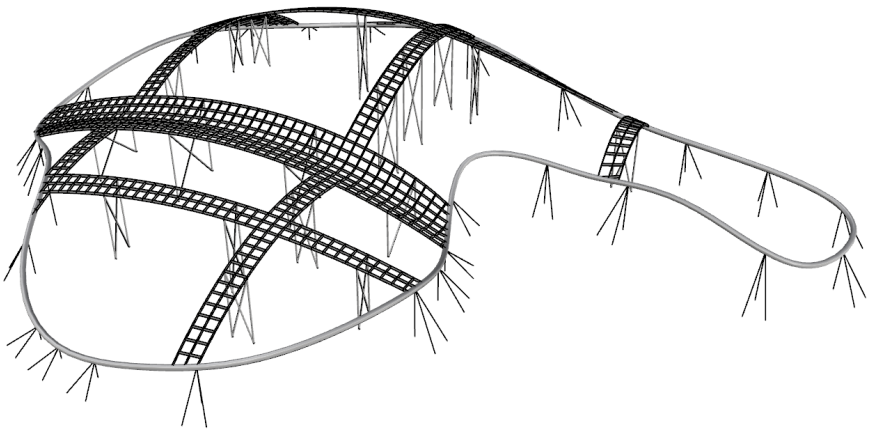

(a) The arches are scaffolded and braced

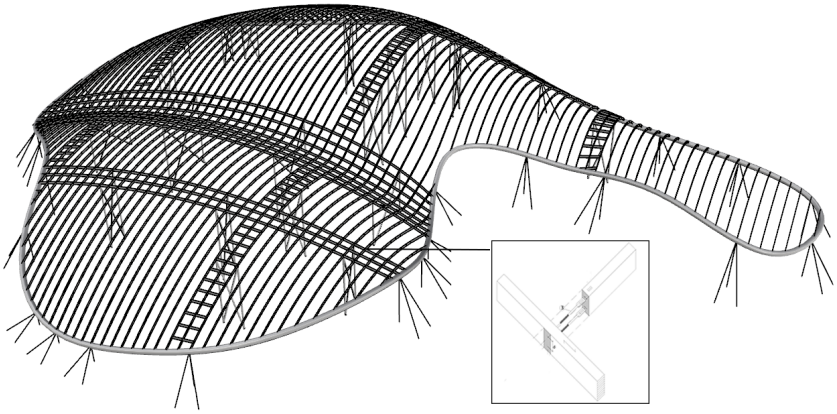

(b) The first layer of beams are installed

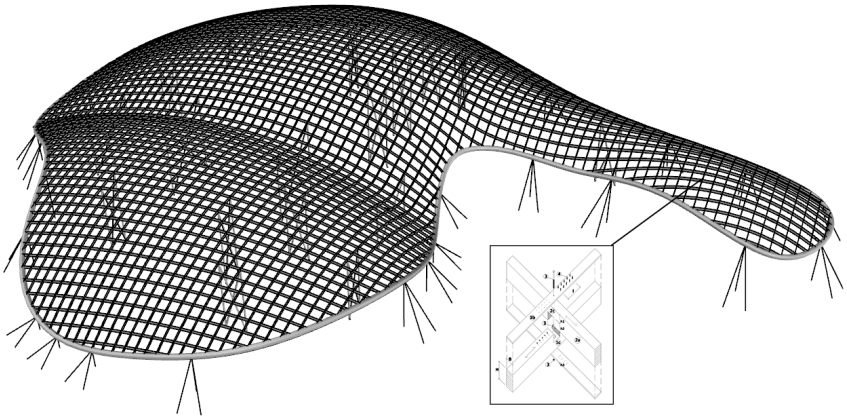

(c) The second layer of beams are installed

Figure 6.53: *Assembly process of the grid - part 2*

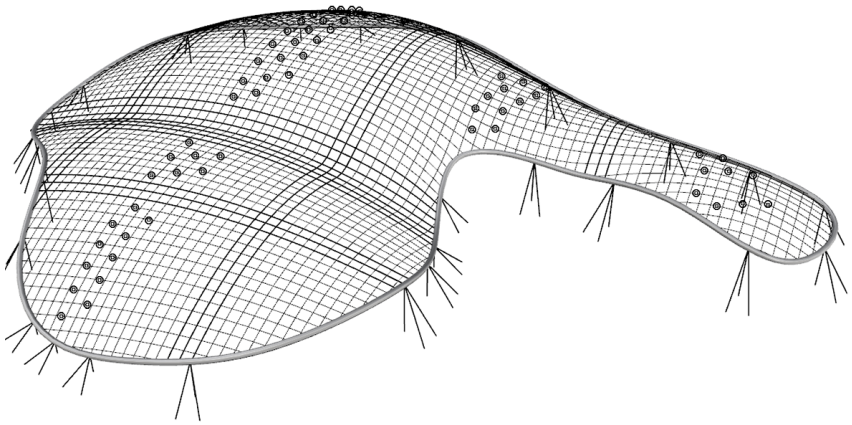

(a) The algorithm is run to find splicing points in first direction

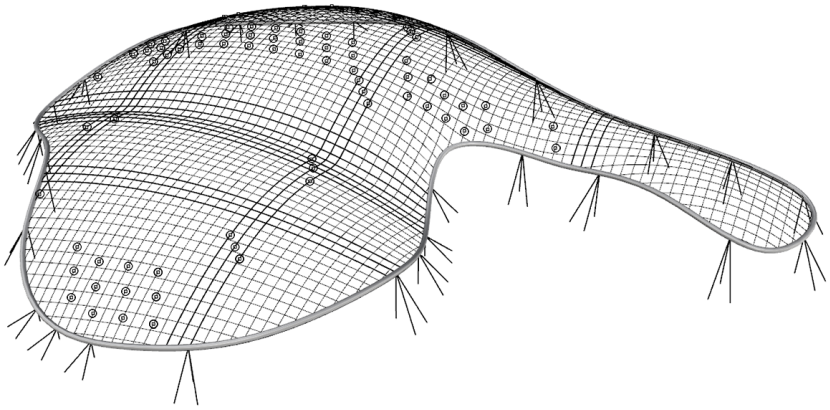

(b) The algorithm is run to find splicing points in second direction

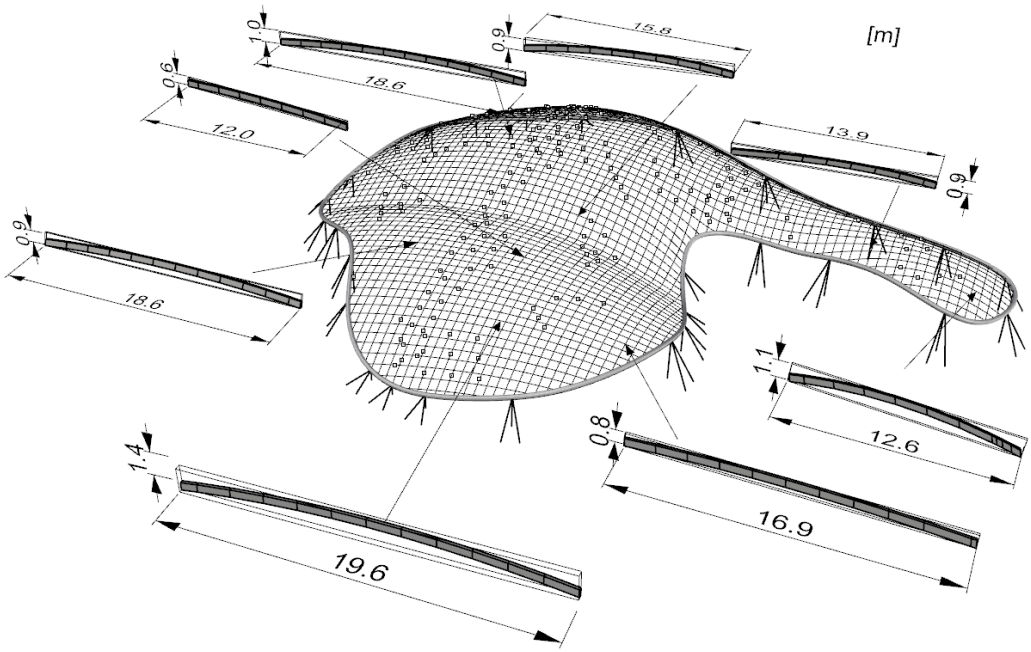

(c) Looking at each of the beams, they have a size that can fit onto a truck

Figure 6.54: *Stages of the automated process for grid-creation, placement of splices and creation of beam drawings*

6.5.3 Performance

An updated calculation of the initial design in Section 6.2.3 is performed. The same model is used, but with the rotational stiffness from Section 6.4 implemented according to the concept lined out in Section 3.2.

With the reduction in stiffness comes, according to Equation (3.30) a reduction of bending moment in the structure. This can clearly be seen in the results of this calculation compared to the pre-sizing, a general decrease of bending moment. This also leads to a redistribution and increase of the axial forces, although in acceptable order. As was expected, with the decreased stiffness, the structure soften and the deflections increased.

In this particular case however this effect was surprisingly small, since the increased deflections in parts of the structure is pushing other parts upwards, almost compensating for the increase in the parts with maximum deflection, deflections can be seen in Figure 6.55. In timber the long-term deflection should be checked as well, and these deflections are shown Figure 6.56. The results are fully shown in Appendix A.

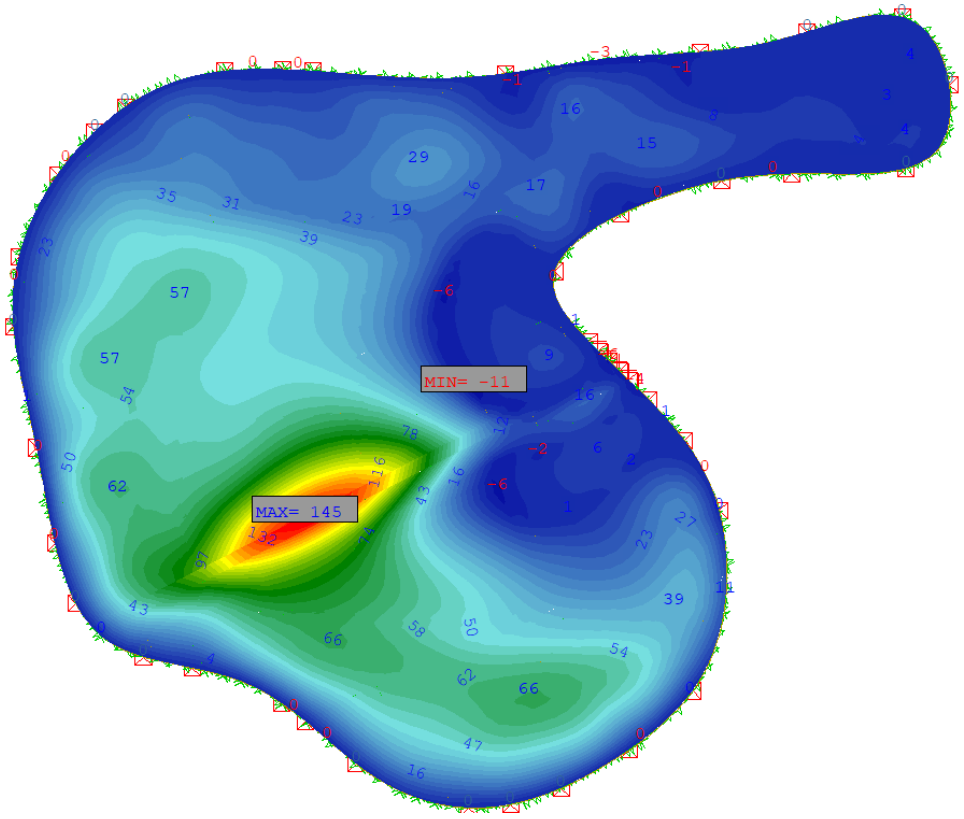

Figure 6.55: *The maximum vertical deflection using the proposed system* [mm]

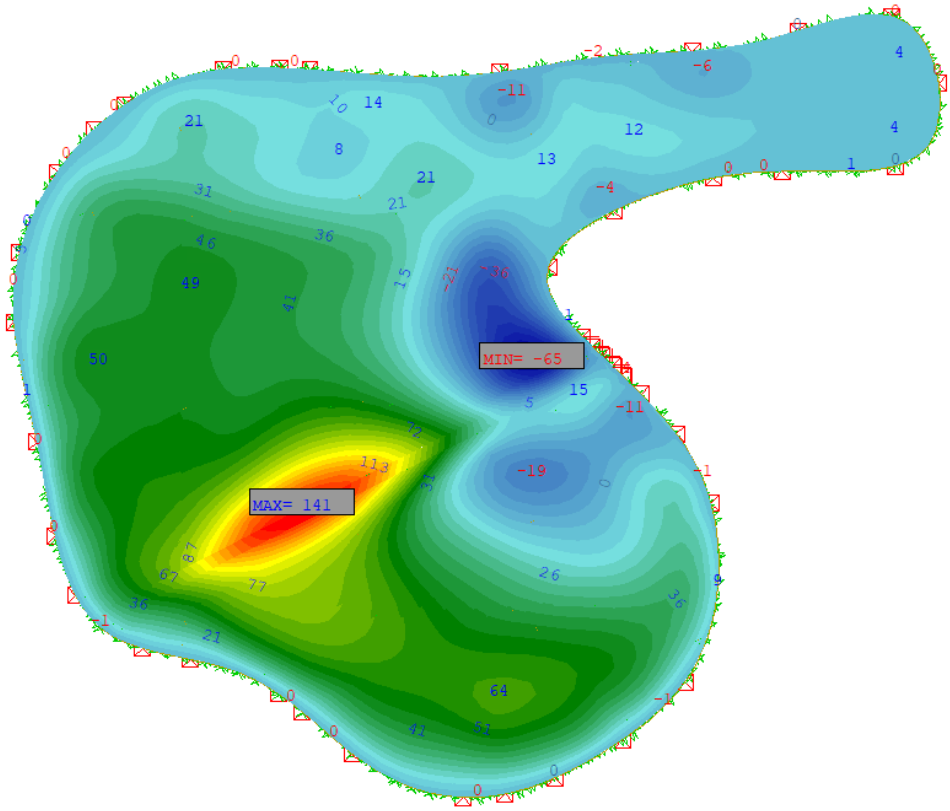

Figure 6.56: *The final, long-term, vertical deflection using the proposed system under the quasi-permanent load case* [mm]

7 Discussion

The results presented in this thesis shows promising results for the manufacturability and design of rigid gridshells over long spans. There also seems to be, as lined out, a great potential of automating some of the most time and cost-intensive steps in the planning process and manufacture of the structure.

Timber as material provide an excellent material to freeform structures, if treated with understanding. The combination of a mean of non-destructive bending and then the possibility of cheap milling with extremely high precision to the final and prepared structural member provides many opportunities.

7.1 Rigidity

The main findings considering the rigidity of joints is separated between the stiffness in bending and axial resistance.

The semi-rigidity in major axis bending of the different joint typologies in Section 6.4 is shown in the comparison that can be seen in Figure 7.1, where the different joint typologies are inserted into Figure 3.8. This provides an overview and a classification of the joints in a behavioural context.

As expected in the hypothesis will the stiffness of the timber joint, when actually approximated, not achieve rigid behaviour. The *Basic contact* will behave as completely hinged, having no bending resistance. The *Steel node type 1* will be the stiffest, which is expected due to the large lever of the screwed connection.

The joints of type *Half lap, Steel node type 2* and *Reinforced basic* behave much like semi-rigid joints. Although, the *Half-lap* has a performance close to rigid, which if drawing the analogy to an I-beam with web-opening, which still behave fairly similarly in bending, could make sense. The full continuity across the intersection in this joint is obviously the key to the high stiffness.

In a continuation of this project, this matter of continuity should be checked. According to Descamps et. al. [2006], the method of stiffness-evaluation used in this projects has proven useful in connection interfaces, thus it could be useful also to check if the assumption is valid also for continuous members.

Reinforced basic is behaving quite a lot less stiff than the others. This obviosuly has to do with a smaller interface between the materials. Both the stiffness for contact and for mechanical fasteners are, through area or diameter of fastener, proportional to the interface-size between components. The conclusion must be that the bigger the interface, the larger the stiffness.

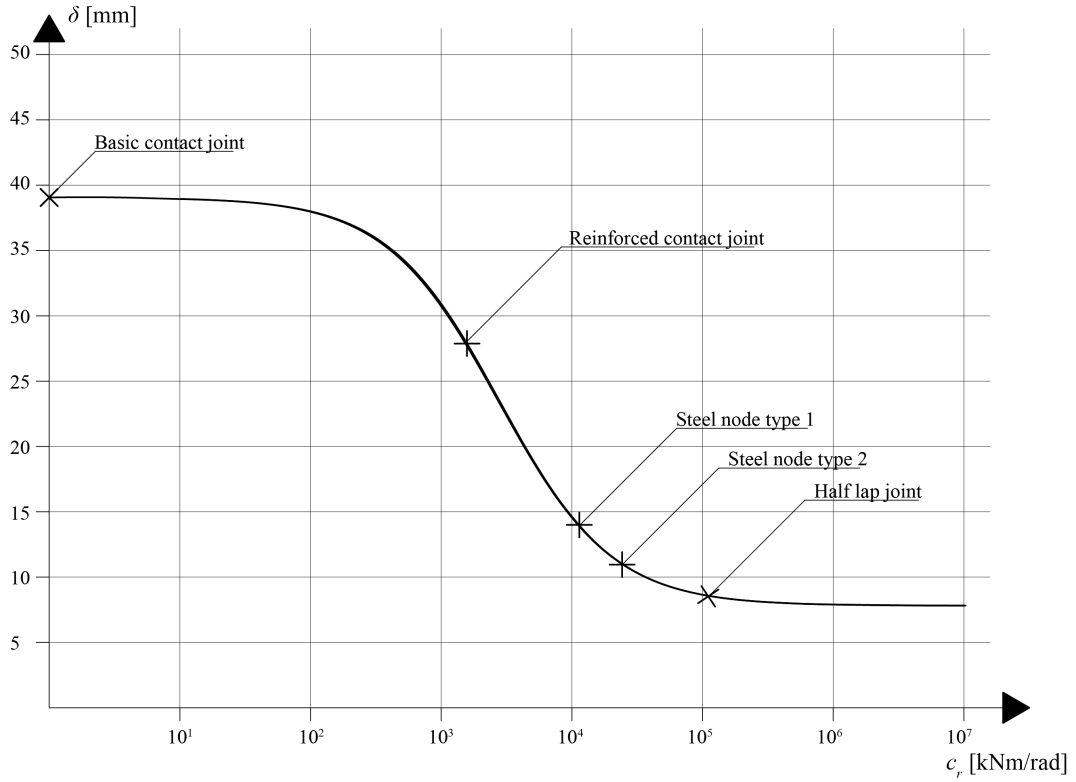

Figure 7.1: *Diagram showing major-axis bending behaviour of the different typologies, based on Figure 3.8*

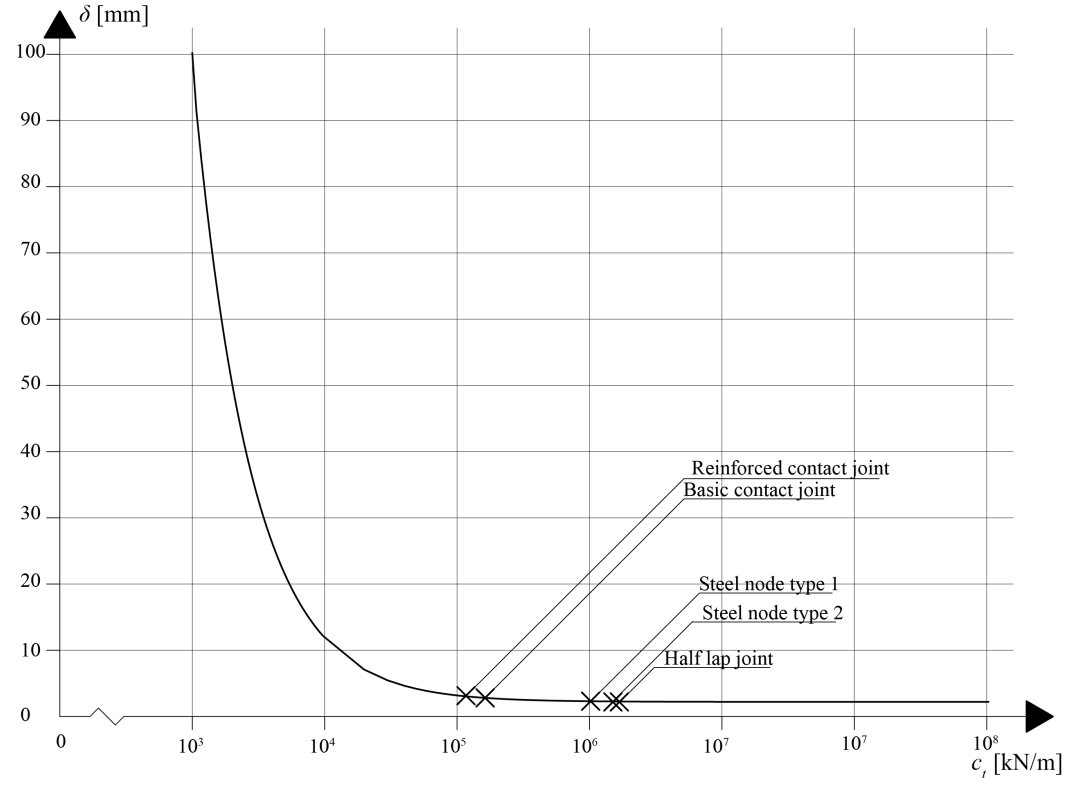

Figure 7.2: *Diagram showing axial deflection behaviour of the different typologies. Based on Figure 3.15*

Another relevant evaluation of the joint-behaviour is the axial behaviour. As the gridshell is a structure intended to work mainly as a *vector active*-structure [Engel, 1997] the axial resistance is of importance and the effect of the possible decrease of stiffness must be neglectable. In Figure 7.2 the relation between the support stiffness and the deflection of the joints is shown. All of the joint typologies have behaviour similar to that of the beam itself. With small to no reduction due to the joint.

Looking at the results, it is interesting to see the relation between joints based on steel, such as *Steel node 1, Steel node 2* and *Reinforced basic* and joints based on timber such as *Basic contact, Half lap*. As can be seen in both comparisons the stiffnesses are in the same range, despite the difference in material (when not designed to behave differently). The *Half lap* has a bending stiffness close to *Steel node 1* and *Steel node 1*. All joints have a similar axial behaviour. This is of course a consequence of governing stiffness being in the interface between the materials, thus is the stiffness of the timber governing also in typologies based on steel.

With the decreased stiffness the structure will not transfer forces through bending to the same extent. And in a structural system based on axial forces, such as gridshells a redistribution of forces will occur. However the closer the structure are to perfect shell behaviour, the smaller the difference will be. Looking at Figure 6.22 and Figure 6.34 comparing the case study in its most and least rigid state, the change in deflection is increased with only a factor 1.7, in a rather a big system.

Looking at the example Figure 3.10 - Figure 3.12 instead, an example based on bending, the difference in deflection is significantly higher, with an increase of factor 80. Since this system relies on bending and if the bending stiffness is 0 the solution will rely on a strongly deformed catenary solution, with the consequence of very high deflections. A conclusion would be that the effect when decreasing bending stiffnes seems of manageable order in gridshells and other structures based mainly on axial forces.

The study performed about the rigidity of joints should be seen as a comparative study and be used as a guide to typologies. It includes a number of the most promising typologies of joints that would be considered in these types of structure, although each of these might have many different layout and builds that might affect the results. The study should be seen as comparative between the typologies and their properties. Failure mechanism and significant behaviour will most likely be similar between the alternatives. However this is not a definitive answer and the stiffness and strength will be dependent on the size of included members. When the typology is chosen, one could perform a parametric study on the joint, in order to increase the certainty of the optimal layout.

7.2 Manufacturability

As shown in Section 6.3 and Section 6.4, there are several possibilities to design and ensure easy assembly. And there exists system for many types of preconditions and constraints one might have. There are systems consisting of short members that ensures easy transportation for tight construction sites and limited handling capacities. On the other hand there are system consisting of longer elements that will reduce the need of scaffolding.

With respect to the manufacturing there are several available methods, with clear strengths and weaknesses. Best practice for cost and structural efficiency seems to be to create the form through lamination when producing each member. Something that earlier has been a cost and labour intensive process. However today there are many automated presses on the market that can produce members with high repeatability and precision, and as shown in Section 6.2.2 also the workshop document and workshop data can be prepared from rather basic information, information already available in the design-team.

Milling is an important tool in the manufacture process, but if the structure is supposed to be load-bearing rather than decorative, the milling should be performed on curved blanks. And milling should primarily be used for finish and detailing.

Something that needs to be expanded upon in further studies is the geometry and build of the façade itself and not only of the structure. In order to ensure avoided ponding as well a useful thermal- and moisture-behaviour. Ponding could especially be a problem in areas with anticlastic curvature, for example in the valley of the case study, since drainage can only occur in one direction, and a slight imperfection can not be compensated in other directions.

7.3 Geometry

There are important choices during the process of geometry planning that will have great impact on the final costs of the project. Where the single most important factor seems to be the increased cost for every new dimension in which the member is curved, this is mainly a matter of what is possible to automate. Today the cost increase between straight and single curved is relatively low, while the step to doubly-curved is a big leap in price. However, while still unusual, there are some automatic presses for doubly-curved beams on the market, and when this becomes common, doubly-curved beams should be cost-feasible as well. However today single curved solutions will in general both perform well, and keep prices down.

Another finding regarding geometry, that was expected, but where the effect exceeded expectations, is the force attraction from that occurs through tapering. In Section 6.2.3, tapering was proposed as a mean of solving the stress concentration in the valley. The increased stiffness however attracted a lot of force to the valley, which is possible to find a solution to in rigid gridshells, since the sizes can be increased. However it is clear to see in a diagram like Figure 6.19 that the *shell zones* with high curvature perform very well. A conclusion would therefore be to keep the curvature as high as possible, while being in a range of curvature when lamination can be performed as a mean of production.

While doubly-curved beams are relatively easy to avoid, with planning of the grid-lines. Geometrical torsion tends to be a more serious problem. Very complex to manufacture and usually present in designs based on a master surface. So as described in Section 6.2.1 there are ways to reconsider the structure in order to avoid manufacturing beams with torsion while maintaining the illusion of beams following the normal direction of the master surface and the façade and having beams with smooth intersections.

To keep cost down in the lamination process it is also important to know limitations booth in terms of curvature and size. Maximum sizes for the press-bed should be checked during the planning stage. To be able to redesign beams for further subdivisions of elements.

Similar findings in the influence of geometry is found in the surface itself, that for quadrangular grid, the grid will not necessarily be possible to cover with planar surfaces. And as with beams, a solution for curved panes will be much costlier than a solution with planar.

On a further notice, something that might keep the costs down is to minimize the permanent loads, e.g. superimposed dead loads, as was shown in Section 4.3 this will have large influence on the design of the structural system and thus the need of material and members.

8 References

Aicher, S. Hezel, J. Stapf, G. (2012). Mechanical and Glued Joints in Glulam of Ultra High Efficiency. *World Conference on Timber Engineering*, 2012, Auckland, Australia.

Borgström, E. Fröbel, J. Gross, H. (2018). *Limträhandbok del 4.* Stockholm: Svenskt Trä.

Chilton, J. Tang, G. (2017). *Timber Gridshells – Architecture, structure and craft.* New York: Routledge.

Crocetti, R. Mårtensson, A. (2015). Design of Structural Timber Elements in ULS. In Bergkvist, P(Eds.), *Design of Timber Structure - Volume 1* (pp. 68-109). Stockholm: Swedish Wood.

Crocetti, R. (2016). Large-Span Timber Structures. *Proceedings of the World Congress on Civil, Structural, and Environmental Engineering*, 2016, Prague, Czech Republic.

Deutsches Institut für Normung (DIN). (2008). *DIN 1052 - Entwurf, Berechnung und Bemessung von Holzbauwerken.* Berlin: Beuth Verlag GmbH.

Descamps, T. Lambion, J. Laplume, D. (2006). Timber Structures: Rotational Stiffness of Carpentry Joints. *9th World Conference of Timber Engineering*, 2006, Portland, Oregon, USA.

Dietsch, P. Brandner, R. (2015). Self-tapping screws and threaded rods as reinforcement for structural timber elements – a state-of-the-art report. *Construction and Building Materials* 97:78-89.

Eekhout, M. Niderehe, S. (2009). The New, Cold Bent Glass Roof of the Victoria & Albert Museum, London. *Glass Performance Days 2009*, 2006, Tampere, Finland

Engel, H. (1997). *Tragsysteme - Structure Systems.* 4th edition. Ostfildern: Hatje Cantz.

Glymph, J. Shelden, D. Ceccato, C. Mussel, J. Schober, H. (2002). A parametric strategy for free-form glass structure using quadrilateral planar facets. *Automation in Construction - Volume 13* (pp. 187-202).

Gross, H. (2016). *Limträhandbok del 1.* Stockholm: Svenskt Trä.

Hoffmeyer, P. (2007). Duration of Load Revisited. *Wood Science Technology*, Volume 41 Issue 8, pp 687-711.

Hofmann, M. Thompson, R. (2009). Innovative DachholzschalenKonstruktion - Toskana Therme. *In 15. Internationals Holzabau-Forum – Aus der praxis – Für die Praxis*, 2009, Garmisch Partenkirchen

Holzer, S M. Loferski, J R. Dillard, D A. (1988). A Review of Creep in Wood: Concepts Relevant to Develop Long-Term Behaviour Predictions For Wood Structures. *Wood and Fiber Science*, Volume 21(4) (pp 376-392)

Johansson, M. (2015). Design of Structural Timber Elements in ULS. In Bergkvist, P(Eds.), *Design of Timber Structure - Volume 1* (pp. 26-68). Stockholm: Swedish Wood.

Just, A. Piazza, M. Östman, B. (2016). Limträ och Brand. In Crocetti, R (Ed.). Fröbel, J (Ed.). *Limträhandbok del 2*. Stockholm: Svenskt Trä.

Lafuente Hernández, E. (2015). *Design and Optimisation of Elastic Gridshells* (PHD-dissertation, Insitut für Konstruktives Entwerfen und Tragwerkslehre der Universität der Künste Berlin, Berlin, Germany). https://opus4.kobv.de/opus4-udk/frontdoor/index/index/docId/994 (accessed 180514).

Lidelöw, H. (2015). Design of timber Joints. In Bergkvist, P(Eds.), *Design of Timber Structure - Volume 1* (pp. 68-109). Stockholm: Swedish Wood.

Moelven. (2018). *Ingenjörskonst: Bygger Världsrekord*. http://www.moelven.com/se/Aktuellt/Mediarum/Reportagearkiv/Ingenjorskonst-Bygger-varldsrekord/ (accessed 180530)

Naturvårdsverket. (2013). *Tilläxt och avverkningar i skogen.* https://www.naturvardsverket.se/Sa-mar-miljon/Statistik-A-O/Klimat-tillvaxt-och-avverkningar-i-skogen/ (accessed 180510).

Norton, R L. (2002) *Cam Design and Manufacturing Handbook*. New York: Industrial Press Inc.

Nicholas, P. Poinet, P. Ramsgaard Thomsen, M. Tamke, M. (2016). Multi-scalar modeling for Free-form Timber Structures. *IASS - Symposium*, 2016, Tokyo, Japan.

Poulsen, E. (2015). *Structural Design and Analysis of Elastically Bent Gridshells* (Master's Thesis, Chalmers University of Technology, Gothenburg, Sweden) http://publications.lib.chalmers.se/records/fulltext/236319/236319.pdf (accessed 180514).

Rabagliate, J. Huber, C. Linke, D. (2014). Balancing Complexity and Simplicity. *Fabricate 2014*, 2014 Zurich, Switzerland.

Robert McNeel & Associates. (2018). *NURBS*. https://www.rhino3d.com/nurbs (accessed 181202).

Scheurer, F. Stehling, H. Tschümerplin, F. Antemann, M. (2013). Design for Assembly - Digital Prefabrication of Complex Timber Structures. *IASS - Symposium*, 2013, Wroclaw, Poland.

Scheurer, F. Simonin, L. Stehling, H. (2015). Energy for Life- the timber structure of the French Pavillion at the EXPO 2015. *IASS - Symposium*, 2015, Amsterdam, Netherlands.

Schober, H. Glymph, J. Ceccato, C. & Mussel, J. (2002). A Parametric Strategy for Freeform

Glass Structures Using Quadrilateral Planar Facets. *ACADIA*, Pomona, USA, pp. 303-321.

Schweitzer, R. (2003). Der Baustoff Holz – von den Anfängen bis zum 19. jahrhundert. In Herzog, T (Ed.). Natterer, O (Ed.). Schweitzer, R. Volz (Ed.), M. Winter, W (Ed.), *Holzbau Atlas* (4th ed.). München: Institut für Internationale Architektur-Dokumentation.

Sógel, K. (2010). Timber Beams Subjected To Long-Term Loading. *Slovak Journal of Civil Engineering*, Volume 3, pp 21-26.

State forests of New South Wales. (1995). The Bending of Timber. *Technical Publication research Division Series*, number 7.

Stehling, H. Scheurer, F. Roulier, J. Geglo, H. Hofman, M. (2017). From Lamination to Assembly – Modelling the Seine Musicale. *Fabricate 2017*, 2017, Stuttgart, Germany.

Stehling, H. Scheurer, F. Roulier, J. (2014). Bridging the Gap from CAD to CAM: Concepts, Caveats and a New Grasshopper Plug-In. *Fabricate 2014*, 2014, Zurich, Switzerland.

SIS (Swedish Standards Institute). (2010). *Eurocode: Basis of Structural Design.* Stockholm: SIS förlag AB.

SIS (Swedish Standards Institute). (2009a). *Eurocode 1: Action on Structures - Part 1-1: General actions - Densities, self-weight. imposed loads for buildings.* Stockholm: SIS förlag AB.

SIS (Swedish Standards Institute). (2009b). *Eurocode 1: Action on Structures - Part 1-3: General actions - Snow loads.* Stockholm: SIS förlag AB.

SIS (Swedish Standards Institute). (2008). *Eurocode 1: Action on Structures - Part 1-4: General actions - Wind actions.* Stockholm: SIS förlag AB.

SIS (Swedish Standards Institute). (2009c). *Eurocode 5: Design of Timber structures - part 1-1: General - Common rules and rules for buildings.* Stockholm: SIS förlag AB.

List of Figures

List of Tables

A Loads and Load Combinations

A.1 Self-Weight

The self-weight of the timber structure is based on GL28c, and calculated through the FE-model. Values are based on Eurocode 1-1 [SIS, 2009a].

$\rho_{Gl28c} = 420\text{kg/m}^3$
$G_{Gl28c} = g\rho_{Gl28c} = 4.1\text{kN/m}^3$

The glass panels are assumed to be $t_{Glass} = 26\text{mm} = (2 \cdot 8\text{mm} + 10\text{mm})$ thick during the calculations, at a density of:

$\rho_{Glass} = 2500\text{kg/m}^3$
$G_{Glass} = g\rho_{glass}t_{glass} = 0.64\text{kN/m}^2$

A.2 Wind

Values are based on Eurocode 1-1-4 [SIS, 2008].

Location:	Stuttgart
Terrain Category:	III
Altitude:	250m
Basic wind velocity:	$v_b = 22.5\text{m/s}$
Density air:	$\rho_{air} = 1.25\text{kg/m}^3$
Basic velocity pressure:	$q_b = 0.5\rho_{Air}v_b = 0.32\text{kN/m}^2$
Exposure factor:	$c_e = III\|15m = 2.0$
Peak velocity pressure:	$q_p = c_e q_b = 0.65\text{kN/m}^2$
Wind pressure external:	$w_e = q_p c_{pi}$
Wind pressure internal:	$w_i = q_p c_{pi}$

A.3 Snow

Values are based on Eurocode 1-1-3 [SIS, 2009b].

Location:	Stuttgart
Snow-Zone:	Germany 2
Altitude:	250m
Characteristic snow load:	$s_k = 0.85\text{kN/m}^2$
Exposure coefficient:	$C_e = 1$
Thermal coefficient:	$C_t = 1$
Shape coefficient:	$\mu = 0.8$ (Dome/Flat roof)
Snow load:	$s = \mu C_e C_t s_k = 0.68\text{kN/m}^2$

A.4 Load Combinations

Loads are combined according to *Equation 6.10* in *Eurocode SS-EN 1990*, with coefficient from *Table A1.1* and *Table A1.2(A)* in said document [SIS,2009a]. The combinations used are as follows:

Ultimate limit state:

$$\sum_{j\geq 1} \gamma_{G,j} G_{k,j} + \gamma_P P + \gamma_{Q,1} Q_{k,1} + \sum_{i>1} \gamma_{Q,i} \psi_{0,i} Q_{k,i}$$

Where:

Partial safety factor permanent-load	$\gamma_{G,j} = 1.35$(1.00 when favourable)
Permanent Load	$G_{k,j}$
Partial safety factor pre-stress	$G\gamma_P = 1.5$(0 when favourable)
Pre-stress	P
Partial safety factor leading variable action	$\gamma_{Q,1} = 1.5$(0 when favourable)
Leading variable action	$Q_{k,1}$
Partial safety factor accompanying variable action	$\gamma_{Q,i}\psi_{0,i}$(According to *Table A1.1*)
Accompanying variable action	$Q_{k,i}$

Serviceability limit state:

$$\sum_{j\geq 1} G_{k,j} + P + Q_{k,1} + \sum_{i>1} \psi_{0,i} Q_{k,i}$$

Where:

Permanent Load	$G_{k,j}$
Pre-stress	P
Partial safety factor leading variable action	$\gamma_{Q,1} = 1.5$(0 when favourable)
Leading variable action	$Q_{k,1}$
Partial safety factor accompanying variable action	$\psi_{0,i}$(According to *Table A1.1*)
Accompanying variable action	$Q_{k,i}$

Quasi permanent loads:

$$\sum_{j\geq 1} G_{k,j} + P + \psi_{2,i} Q_{k,1} + \sum_{i>1} \psi_{2,i} Q_{k,i}$$

Where:

Permanent Load	$G_{k,j}$
Pre-stress	P
Partial safety factor accompanying variable action	$\psi_{2,i}$(According to *Table A1.1*)
Leading variable action	$Q_{k,1}$
Accompanying variable action	$Q_{k,i}$

These equations results in the following load combinations:

Loadcase	Load **combination**
Ultimate limit state	
1	$1.35(G_{timber} + G_{cover}) + 1.5Q_{wind,E} + 0.75Q_{snow,uniform}$
2	$1.35(G_{timber} + G_{cover}) + 1.5Q_{wind,E} + 0.75Q_{snow,drift}$
3	$1.35(G_{timber} + G_{cover}) + 1.5Q_{wind,N} + 0.75Q_{snow,uniform}$
4	$1.35(G_{timber} + G_{cover}) + 1.5Q_{wind,N} + 0.75Q_{snow,drift}$
5	$1.35(G_{timber} + G_{cover}) + 1.5Q_{wind,E}$
6	$1.35(G_{timber} + G_{cover}) + 1.5Q_{wind,N}$
7	$1.35(G_{timber} + G_{cover}) + 1.5Q_{snow,uniform} + 0.9Q_{wind,E}$
8	$1.35(G_{timber} + G_{cover}) + 1.5Q_{snow,uniform} + 0.9Q_{wind,N}$
9	$1.35(G_{timber} + G_{cover}) + 1.5Q_{snow,drift} + 0.9Q_{wind,E}$
10	$1.35(G_{timber} + G_{cover}) + 1.5Q_{snow,drift} + 0.9Q_{wind,N}$
11	$1.35(G_{timber} + G_{cover}) + 1.5Q_{snow,uniform}$
12	$1.35(G_{timber} + G_{cover}) + 1.5Q_{snow,drift}$
13	$1.0(G_{timber} + G_{cover}) + 1.5Q_{wind,E}$
14	$1.0(G_{timber} + G_{cover}) + 1.5Q_{wind,N}$
Serviceability limit state	
101	$1.0(G_{timber} + G_{cover}) + 1.0Q_{wind,E} + 0.5Q_{snow,uniform}$
102	$1.0(G_{timber} + G_{cover}) + 1.0Q_{wind,E} + 0.5Q_{snow,drift}$
103	$1.0(G_{timber} + G_{cover}) + 1.0Q_{wind,N} + 0.5Q_{snow,uniform}$
104	$1.0(G_{timber} + G_{cover}) + 1.0Q_{wind,N} + 0.5Q_{snow,drift}$
105	$1.0(G_{timber} + G_{cover}) + 1.0Q_{wind,E}$
106	$1.0(G_{timber} + G_{cover}) + 1.0Q_{wind,N}$
107	$1.0(G_{timber} + G_{cover}) + 1.0Q_{snow,uniform} + 0.6Q_{wind,E}$
108	$1.0(G_{timber} + G_{cover}) + 1.0Q_{snow,uniform} + 0.6Q_{wind,N}$
109	$1.0(G_{timber} + G_{cover}) + 1.0Q_{snow,drift} + 0.6Q_{wind,E}$
110	$1.0(G_{timber} + G_{cover}) + 1.0Q_{snow,drift} + 0.6Q_{wind,N}$
111	$1.0(G_{timber} + G_{cover}) + 1.0Q_{snow,uniform}$
112	$1.0(G_{timber} + G_{cover}) + 1.0Q_{snow,drift}$
113	$0.0(G_{timber} + G_{cover}) + 1.0Q_{wind,E}$
114	$0.0(G_{timber} + G_{cover}) + 1.0Q_{wind,N}$
Quasi permanent combination	
201	$1.0(G_{timber} + G_{cover})$

B Strength and Stiffness calcualtion of Joints

The following chapter presents calculations for some significant strength and stiffness numbers are presented.

In order to simplify the process two spreadsheets were developed, one, shown in Figure B.1, calculating the strength and stiffness of custom connections of mechanical fasteners loaded in shear, in timber, according to Eurocode 5 [SIS, 2009c, chapter 8.1-8.6 & 8.9].

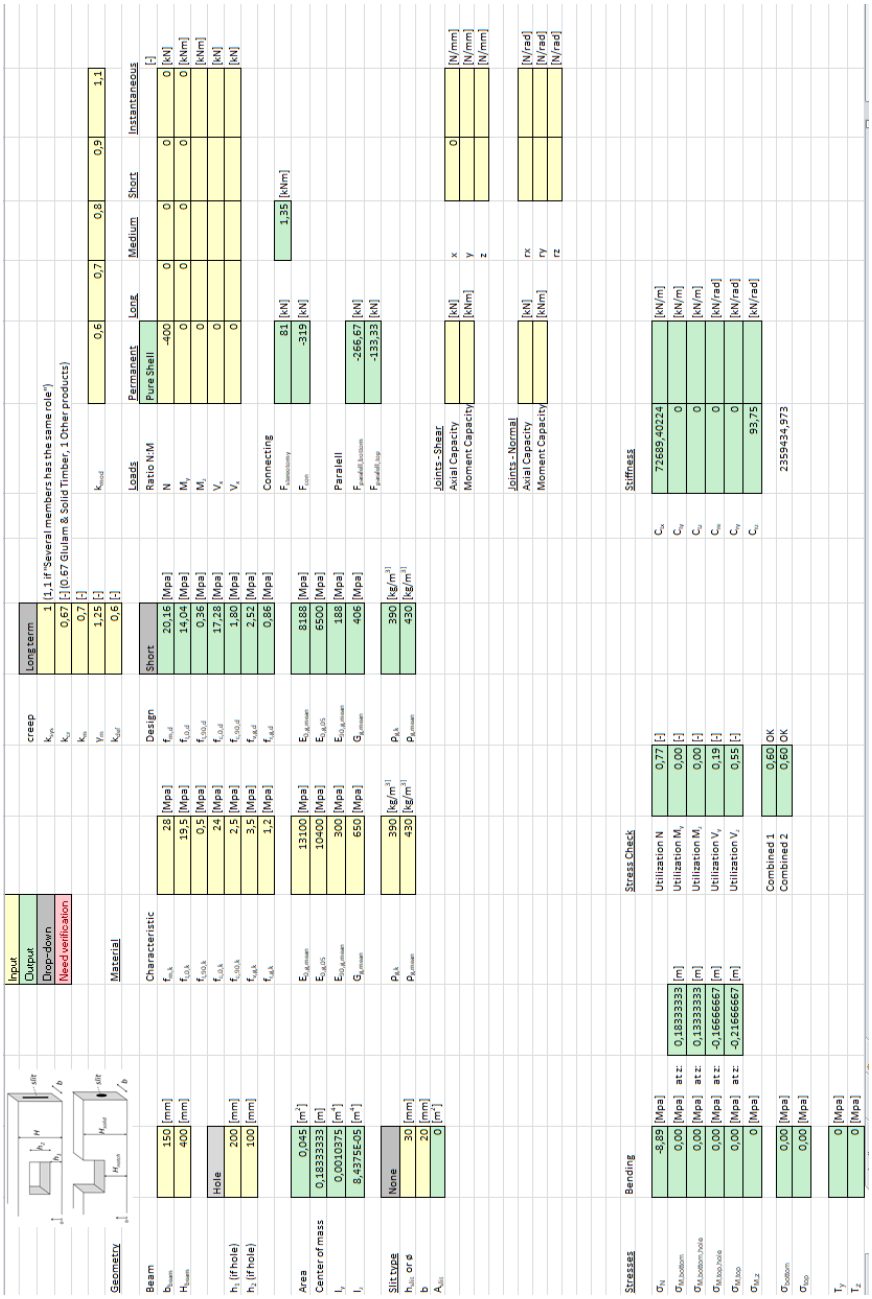

Figure B.1: *Spreadsheet for calculation for mechanical fasteners in timber*

And one spreadsheet (Figure B.2) for timber stress analysis, for rectangular cross section with different kinds of holes and notches for screws and plates included. The spreadsheet also takes into account the strength reduction due to different load durations.

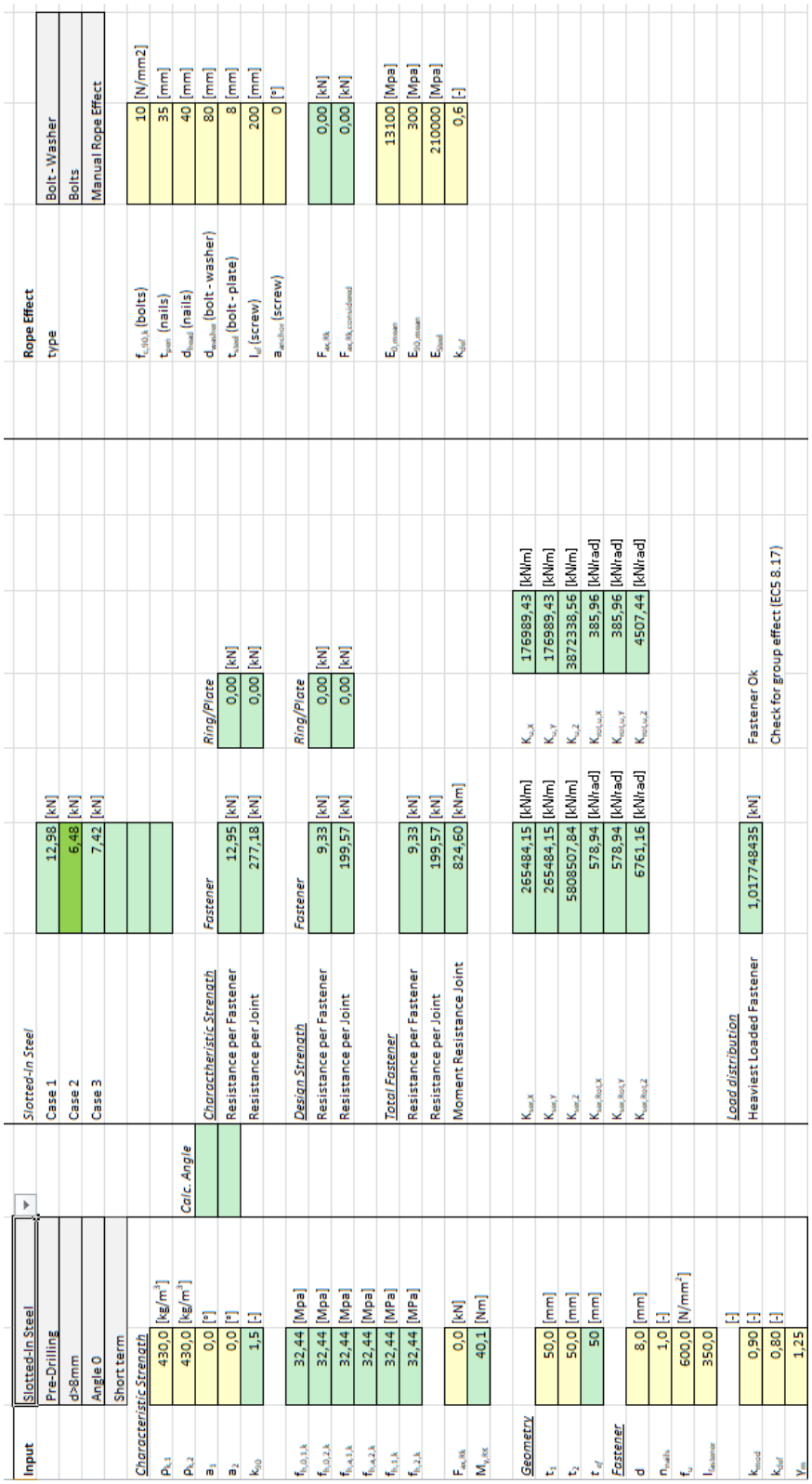

Input	Slotted-In Steel		Slotted-In Steel							Rope Effect	
	Pre-Drilling		Case 1	12,98	[kN]					type	Bolt - Washer
	d>8mm		Case 2	6,48	[kN]						Bolts
	Angle 0		Case 3	7,42	[kN]						Manual Rope Effect
	Short term										
Characteristic Strength										$f_{c,90,k}$ (bolts)	10 [N/mm2]
$\rho_{k,1}$	430,0	[kg/m^3]								t_{pen} (nails)	35 [mm]
$\rho_{k,2}$	430,0	[kg/m^3]	*Calc. Angle*							d_{head} (nails)	40 [mm]
a_1	0,0	[°]		*Characteristic Strength*		*Fastener*		*Ring/Plate*		d_{washer} (bolt - washer)	80 [mm]
a_2	0,0	[°]		Resistance per Fastener		12,95	[kN]	0,00	[kN]	t_{steel} (bolt - plate)	8 [mm]
k_{90}	1,5	[-]		Resistance per Joint		277,18	[kN]	0,00	[kN]	l_{ef} (screw)	200 [mm]
										a_{anchor} (screw)	0 [°]
$f_{c,0,1,k}$	32,44	[Mpa]		*Design Strength*		*Fastener*		*Ring/Plate*			
$f_{c,0,2,k}$	32,44	[Mpa]		Resistance per Fastener		9,33	[kN]	0,00	[kN]	$F_{ax,Rk}$	0,00 [kN]
$f_{c,\alpha 1,k}$	32,44	[Mpa]		Resistance per Joint		199,57	[kN]	0,00	[kN]	$F_{ax,Rk,considered}$	0,00 [kN]
$f_{c,\alpha 2,k}$	32,44	[Mpa]									
$f_{t,1,k}$	32,44	[MPa]		*Total Fastener*						$E_{0,mean}$	13100 [Mpa]
$f_{t,2,k}$	32,44	[MPa]		Resistance per Fastener		9,33	[kN]			$E_{90,mean}$	300 [Mpa]
				Resistance per Joint		199,57	[kN]			E_{steel}	210000 [Mpa]
$F_{ax,Rk}$	0,0	[kN]		Moment Resistance Joint		824,60	[kNm]			k_{def}	0,6 [-]
$M_{y,Rk}$	40,1	[Nm]									
Geometry				$K_{ser,X}$		265484,15	[kN/m]	$K_{u,X}$	176989,43 [kN/m]		
t_1	50,0	[mm]		$K_{ser,Y}$		265484,15	[kN/m]	$K_{u,Y}$	176989,43 [kN/m]		
t_2	50,0	[mm]		$K_{ser,2}$		5808507,84	[kN/m]	$K_{u,2}$	3872338,56 [kN/m]		
t_{ef}	50	[mm]		$K_{ser,Rot,X}$		578,94	[kNrad]	$K_{Rot,u,X}$	385,96 [kNrad]		
Fastener				$K_{ser,Rot,Y}$		578,94	[kNrad]	$K_{Rot,u,Y}$	385,96 [kNrad]		
d	8,0	[mm]		$K_{ser,Rot,2}$		6761,16	[kNrad]	$K_{Rot,u,2}$	4507,44 [kNrad]		
n_{nails}	1,0	[-]									
f_u	600,0	[N/mm^2]									
$l_{fastener}$	350,0										
		[-]		*Load distribution*							
k_{mod}	0,90	[-]		Heaviest Loaded Fastener		1,017748435	[kN]	Fastener Ok			
k_{def}	0,80	[-]						Check for group effect [EC5 8.17)			
γ_m	1,25										

Figure B.2: *Spreadsheet for calculation for cross-sections.*

B.1 Basic Contact Joint

The parts included in the joint are:

Table B.1: Size and material of members included in the Basic Contact Joint

Member	Material	Size
Beams *1* and *2*	GL28c	450x150 mm
Dowels *4*	f_u=600MPa	ø-30 mm l-175 mm
Screw plate *3*	s355	t=14mm w = 100mm
Screws for plate *3*	f_u=600MPa	2x1 8x60 screws (spacing 64mm lengthwise)

The strength values comes from Table 4.1 and Equation (4.1):

B.1.1 Axial direction

Compression

The strength and stiffness in axial direction will be limited by the compression perpendicular to grain according to Equation (4.9) gives and:

$A_{ef} = HB_{ef} = 0.45\text{m} \cdot (0.15 + 2 \cdot 0.03)\text{m} = 0.0945\text{m}^2$
$k_{c,90} = 1$ [-]

$$f_{c,90,d} = \frac{2.5\text{MPa} \cdot 0.6}{1.25} = 1.2\text{MPa}$$

$$\sigma_{c,90,d} < k_{c,90} f_{c,90,d,permanent} \Rightarrow N < k_{c,90} f_{c,90,d,permanent} \cdot A_e f = 113\text{kN}$$

$$\sigma_{c,90,d} < k_{c,90} f_{c,90,d,short} \Rightarrow N < k_{c,90} f_{c,90,d,short} \cdot A_e f = 170\text{kN}$$

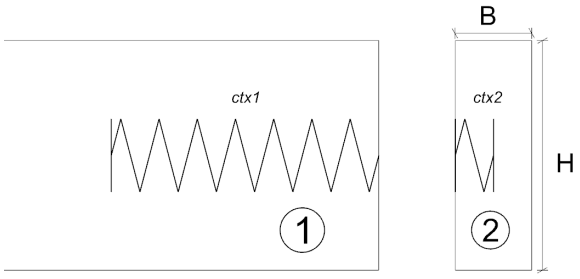

Figure B.3: *Section though the joint showing the spring model*

The stiffness in the axial direction comes from the contact of the two surfaces (system in Figure B.3). Thus is there one spring in beam *1* and one spring in beam *2*. The spring is calculated for half the joint, in order to be able to define the support for each member. This gives, according to Equation (3.3) and Equation (3.4):

$$c_{tx,1} = \frac{E_{0,mean}\sqrt{A}}{0.85} = \frac{13.1\text{GPa} \cdot \sqrt{0.45\text{m} \cdot 0.15\text{m}}}{0.85} = 4004000\text{kN m}^{-1}$$

$$c_{tx,2} = \frac{E_{90,mean}A}{0.5B} = \frac{0.3\text{GPa} \cdot 0.45\text{m} \cdot 0.15\text{m}}{0.075} = 270000\text{kN m}^{-1}$$

With the springs working in series, the stiffness can be added by Equation (3.6):

$$\frac{1}{c_{tx}} = \frac{1}{c_{tx,1}} + \frac{1}{c_{tx,2}} = \frac{1}{4004\text{kN m}^{-1}} + \frac{1}{130\text{kN m}^{-1}} \Rightarrow c_{tx} = 252000\text{kN m}^{-1}$$

Tension

The tensile capacity of the joint will be limited by either the stress in the screw plate or the strength of the connection. The shear capacity of joint is calculated according to Johansen's theory method (shown in the next section, *Shear*). This gives that the strength of the 2-by-1 screwed connection of 8x60mm screws can be concluded as:

$$F_{v,R,k} = 5.25\text{kN}$$

Which gives a total design strength of the joint as:

$$F_{v,R,d,tot} = n_{screws}\frac{F_{v,R,k}k_{mod}}{\gamma_m} = 2\frac{5.25\text{kN} \cdot 0.6}{1.25} = 5\text{kN}$$

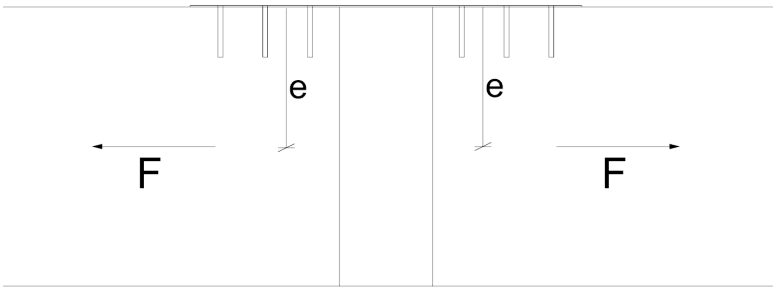

Figure B.4: *Section through the joint, showing the eccentricity for stress in screw plate*

The other limiting factor can be stress in the nail plate from the eccentric force (Figure B.4). According too:

$$\frac{N}{A_{net}} + \frac{M_y}{I_{y,net}}z < \frac{f_y}{\gamma_{M,2}}$$

Where:
$A_{net} = t_{plate}(w_{plate} - 2d_{screw}) = 0.012\text{m}(0.1\text{m} - 2 \cdot 0.008\text{m}) = 0.001\text{m}^2$

$F_{assumed} = 2\text{kN}$

$$M_y = Fe = F_{assumed} H/2 = 2\text{kN} \cdot 0.225\text{m} = 0.45\text{kN m}$$

$$I_{y,net} = \frac{b_{net} h^3}{12} = \frac{0.084 \cdot 0.012^3}{12} = 1.2 \cdot 10^{-8}\text{m}^4$$

$$z = t_{plate}/2 = 0.006\text{m}$$

$$\gamma_{M,2} = 1.25$$

$$f_y = 355\text{MPa}$$

Gives:

$$\frac{f_y}{\gamma_{M,2}} = 284\text{MPa} > \frac{N}{A_{net}} + \frac{M_y}{I_{y,net}} z = \frac{2\text{kN}}{0.001\text{m}^2} + \frac{0.45\text{kN m}}{1.2 \cdot 10^{-8}\text{m}^4} 0.006\text{m} = 225\text{MPa}$$

The tension capacity of the joint is thus limited, by the stress in the nail plate, to:

$$N_{tension} = F_{assumed} = 2\text{kN}$$

B.1.2 Shear - strong axis

The shear strength, with its contribution from Dowels *4* will be calculated with the Johansen's Theory for a mechanical fastener, in a timber-timber interface with one shear plane [SIS, 2009c, Eq. 8.6]. The direction of the force in both members will be perpendicular to grain. Thus (according to Eurocode 5 [SIS, 2009c, Eq. 8.30-8.33]:

$$f_{h,0,k} = 0.082(1 - 0.01d)\rho_k = 0.082(1 - 0.01 \cdot 30\text{mm}) \cdot 430\text{kg m}^{-3} = 24.7\text{MPa}$$

$$k_{90} = 1.35 + 0.015d = 1.35 + 0.015 \cdot 30\text{mm} = 1.8\ [\text{-}]$$

$$f_{h,\alpha,k} = \frac{f_{h,0,k}}{k_{90} \sin^2(\alpha) + \cos^2(\alpha)} = \frac{24.7}{1.8 \sin^2(90) + \cos^2(90)} = 13.7\text{MPa}$$

$$M_{y,Rk} = 0.3 f_u d^{2.6} = 0.3 \cdot 600 \cdot 30^{2.6} = 1246774\text{N m}$$

With these input, the governing case from the Johansen's theory [SIS, 2009c, Eq. 8.6] gives a characteristic dowel strength of:

$$F_{v,Rk} = 15.2\text{kN}$$

which gives the total, design strength of:

$$V_z = F_{v,Rd,tot,permanent} = n \frac{F_{v,Rk} k_{mod,permanent}}{\gamma_m} = 2 \frac{15.2\text{kN} \cdot 0.6}{1.25} = 15\text{kN}$$

$$V_z = F_{v,Rd,tot,short} = n \frac{F_{v,Rk} k_{mod,short}}{\gamma_m} = 2 \frac{15.2\text{kN} \cdot 0.9}{1.25} = 22\text{kN}$$

The stiffness is calculated with Equation (3.1) as:

$$K_{ser} = \frac{\rho_m^{1.5} d}{23} = \frac{430\text{kg m}^{-3\,1.5}30\text{mm}}{23} = 11630\text{kN m}^{-1}$$

Since the dowels work in parallel, the stiffness can be added according to Equation (3.7):

$$c_{tz} = nK_{ser} = 2 \cdot 11630 = 23260\text{kN m}^{-1}$$

B.2 Reinforced Basic Joint

The parts included in the joint are:

Table B.2: Size and material of members included in the Basic Contact Joint

Member	Material	Size
Beams *1* and *2*	GL28c	450x150 mm
Dowels *3*	f_y=355MPa	⌀-30 mm l-250 mm (spacing 350mm)
Dowels *4*	f_u=600MPa	32 per connection d-8mm l-80 mm

B.2.1 Normal Force

The strength in normal direction will be governed either by the strength of dowel *3* or the strength of the dowel connection at *4*. The resistance per dowel should fulfil the requirement:

$$N_{dowel} < A_{dowel} \cdot f_y = \pi r^2 f_y = \pi \cdot 0.015^2\text{mm} \cdot 355\text{MPa} = 250\text{kN}$$

The dowels *4* connecting the dowels *3* to the beams will be calculated according to Johansen's theory, for a slotted-in steel plates. For the basic of input values for Johansen's theory, the equations are presented in the calculations for the *Basic contact joint*.

The minimum distance for dowel connections are specified in Eurocode 5, table 8.5 [SIS, 2009c]. Since the connections will be loaded parallel to grain, the minimum distances will be:

Table B.3: Size and material of members included in the Reinforced Contact Joint

Type	Distance
Longitudinal spacing	$5d$
Transversal spacing	$3d$
Transversal spacing to edge	$3d$

Thus a connection of 4 dowels crosswise (spacing 24mm) and 8 dowels lengthwise (spacing 48mm) of d=8 mm can be fitted. The characteristic strength per dowel is $F_{v,R,k} = 6.48\text{kN}$, should for a slotted-in steel plate be doubled due to double shear planes [SIS, 2009c, 8.2.2(1)] meaning that the design strength of the fastener is:

$$F_{v,R,d} = n_{shearplanes}\frac{F_{v,R,k}k_{mod}}{\gamma_m} = 2\frac{6.48\text{kN} \cdot 0.6}{1.25} = 6.22\text{kN}$$

To account for the group effect for dowels along grain, an effective number of bolts should be used, according to [SIS, 2009c, Eq. 8.34]:

$$n_{ef} = min\left(n; n^{0.9}\sqrt[4]{\frac{a_1}{13d}}\right) = 8^{0.9}\sqrt[4]{\frac{48}{104}} = 5.4$$

Thus, the total normal strength of screwed connection thus becomes:

$$n_{big,dowels}n_{ef}n_{crosswise}F_{v,R,d} = 2 \cdot 5.4 \cdot 4 \cdot 6.22\text{kN} = 2 \cdot 134\text{kN} = 268\text{kN}$$

The axial stiffness of the the system will have contributions from the dowel connection *4* and from the dowels *3*. For the stiffness of the dowels *3* according to Equation (3.3):

$$c_{t,x,dowel4} = \frac{E_{steel} A_{dowel}}{L} = \frac{210\text{GPa} \cdot 0.00071\text{m}^2}{0.125\text{m}} = 1187522\text{kN m}^{-1}$$

And for Dowel connection *3* the stiffness (according to Equation (3.1)) becomes:

$$K_{ser} = \frac{\rho_m^{1.5} d}{23} = \frac{430^{1.5} \cdot 8}{23} = 3103\text{kN m}^{-1}$$

$$c_{t,x,dowel3} = n \cdot K_{ser} = 32 \cdot 3103 = 99296\text{kN m}^{-1}$$

These are combined in series:

$$c_{t,x} = n_{dowel3} \left(\frac{1}{c_{t,x,dowel3}} + \frac{1}{c_{t,x,dowel4}} \right) = 2 \cdot 91633\text{kN m}^{-1} = 183267\text{kN m}^{-1}$$

B.2.2 Major bending

According to Lidelöw [2015] the moment capacity of a a dowel connection can be calculted as:

$$F_{v,R,d,i} = \frac{M r_i}{I_p} \Rightarrow M = \frac{F_{v,R,d,i} I_p}{r_i}$$

Where:
r_i - *Distance from the center point of connection to fastener* [m]
I_p - $\Sigma r_i^2 \Rightarrow I_p = 2 \cdot 0.175\text{m}^2 = 0.06125$ [m^2] - *Polar Moment of Inertia*

Which gives:

$$M = \frac{F_{v,R,d,i} I_p}{r_i} = \frac{134\text{kN} \cdot 0.06125\text{m}^2}{0.175\text{m}} = 46.9\text{kN m}$$

The rotational stiffness is calculated with Equation (3.9), which gives:

$$c_{ry} = \Sigma c_{t,x,i} r_i^2 = 91633 \cdot 0.175^2 + 91633 \cdot 0.175^2 = 5612\text{kN m}^{-1}$$

B.2.3 Shear strong axis

This calculation is done in the same way, with the same dimensions as for the *Basic contact* joint:

B.3 Half lap joint

The parts included in the joint are:

Table B.4: Size and material of members included in the Half lap Joint

Member	Material	Size
Beams *1* and *2*	GL28c	450x150 mm
Bolt + Shear ring *3*	f_u=600MPa	d_{bolt}=20 mm d_{ring}=60 mm
Dowels *4*	f_u=600MPa	dowels 8x90 continuously s=104 mm

B.3.1 Normal Force

The resistance against normal forces is calculated by combining the resistance of the reduced cross section *2c* (cross section shown in Figure B.5) and the shear capacity of bolt and shear ring *3*.

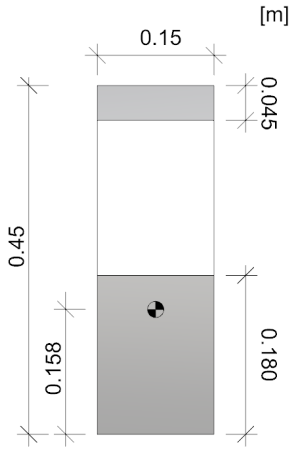

Figure B.5: *Section though the beam showing dimensions and the center of mass in the beam*

The capacity of the bolt and shear ring is calculated with Johansen's theory (see the calculations for the *Basic Contact Joint*) with the addition of the capacity of shear rings as described in Eurocode 5 [SIS, 2009c, 8.4]. The resistance of the beam for axial forces is calculated according to:

$$N < f_{c,0,d} A_{red} = \frac{f_{c,0,d} k_{mod}}{\gamma_m} \cdot A_{red} = \frac{24\text{MPa} \cdot 0.6}{1.25} \cdot 0.15\text{m}(0.180 + 0.045) = -388\text{kN}$$

$$N < f_{t,0,d} A_{red} = \frac{f_{t,0,d} k_{mod}}{\gamma_m} \cdot A_{red} = \frac{19.5\text{MPa} \cdot 0.6}{1.25} \cdot 0.15\text{m}(0.180 + 0.045) = 316\text{kN}$$

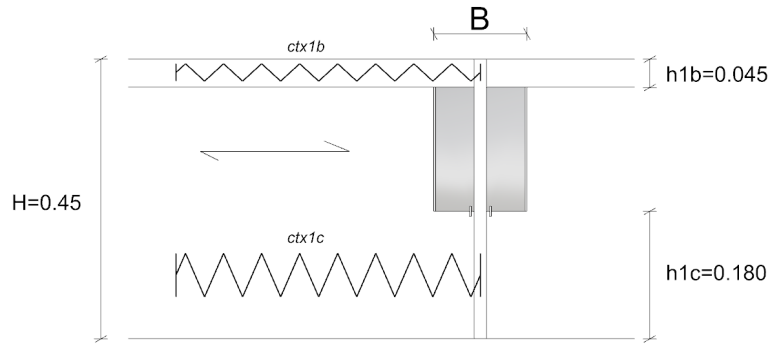

Figure B.6: *Section though the joint showing the spring model*

The axial stiffness in the joint can be calculated as the combined effect of 3 springs (according to Figure B.6), one elastic half-space for the lath *1b*, one elastic half space for the continuous part of the beam *1c* (according to Equation (3.4)), combined with he stiffness contribution from the bolt and ring *3*. Thus:

$$c_{t,x,1b} = \frac{E_{0,mean}\sqrt{BH_{1b}}}{0.85} = \frac{13.1\text{GPa}\sqrt{0.15 \cdot 0.045}}{0.85} = 1266205\text{kN m}^{-1}$$

$$c_{t,x,1c} = \frac{E_{0,mean}\sqrt{BH_{1c}}}{0.85} = \frac{13.1\text{GPa}\sqrt{0.15 \cdot 0.180}}{0.85} = 2532411\text{kN m}^{-1}$$

The contributions from the dowels and ring is calculated according to Eurocode 5 [SIS, 2009c, Table 7.1]:

$$K_{ser,bolt} = \frac{\rho_m^{1.5} d}{23} = \frac{430^{1.5} \cdot 20}{23} = 7753\text{kN m}^{-1}$$

$$K_{ser,ring} = \frac{\rho_m d}{2} = \frac{430 \cdot 60}{2} = 12900\text{kN m}^{-1}$$

These springs work in parallel, the stiffness can be added according to Equation (3.7):

$$c_{tx,contact} = c_{t,x,1c} + c_{t,x,1b} = 1266205\text{kN m}^{-1} + 2532411\text{kN m}^{-1} = 3798616\text{kN m}^{-1}$$

$$c_{tx,fastener} = K_{ser,bolt} + K_{ser,ring} + c_{t,x,1c} + c_{t,x,1b} = 7753\text{kN m}^{-1} + 12900\text{kN m}^{-1} = 20653\text{kN m}^{-1}$$

B.3.2 Major bending

The reduced cross section, including its centre of mass, can be seen in Figure B.5. The area moment of inertia is calculated to:

$$I_y = \Sigma I_{y,i} + \Sigma A a^2 = \frac{0.15\text{m} \cdot 0.180^3\text{m}}{12} \frac{0.15\text{m} \cdot 0.045^3\text{m}}{12} +$$

$$+0.15\text{m} \cdot 0.205\text{m} \cdot 0.068^2\text{m} + 0.15\text{m} \cdot 0.045\text{m} \cdot 0.27^2\text{m} = 6.89 \cdot 10^{-4}\text{m}^4$$

Where:
$I_{y,i}$ - *Area moment of inertia for each part* [m^4]

A - *Area* [m^2]
a_i - *Distance local and global centre of mass* [m]

The asymmetric cross section will create larger bending stresses in the uppermost fibre than in the lower (for gravitational loads), and the maximum bending can be calculated as:

$$M_y < \frac{f_{m,d} z}{I_y} = \frac{13.44\text{MPa} \cdot 0.289\text{m}}{6.93 \cdot 10^{-4}\text{m}^4} = 32\text{kN m}$$

To get the joint to work, the connection between the lath and the beam is designed according to Eurocode's rules for composite beams with mechanical fasteners [SIS, 2009, Appendix B].

With:
$d = 8\text{mm}$ - *diameter screw*
$s = 104\text{mm}$ - *spacing lengthwise*

$K_{ser,tot} = 2K_{ser} = 2 \cdot \frac{(430\text{kg/m}^3)^{1.5} \cdot 8\text{mm}}{23} = 6202\text{kN mm}^{-1}$ - *Slip modulus, 3 screws/row*
$l = 1.6\text{m}$

Gives:
$\gamma_1 = 0.15$
$a_1 = 221\text{mm}$
$a_2 = 3.7\text{mm}$
$(EI)_{ef} = 1.15 \cdot 10^{13}\text{Nm}^2$

The maximum shear force occurs in the *Bending zones* and is:
$V_{Permanent} = 16\text{kN}$
$V_{Short} = 9\text{kN}$
$V_{Tot} = 25\text{kN}$

This gives that every row of two screws shall be designed for the force:

$$F_{v,R,d,Tot} = 4.64\text{kN} > \frac{\gamma_1 E_1 A_1 a_1 s_1}{(EI)_{ef}} V_{Tot} = \frac{0.14 \cdot 13100\text{N mm}^{-1} \cdot 6750\text{mm} \cdot 221\text{mm} \cdot 104\text{mm}}{1.15 \cdot 10^{13}\text{Nm}^2} 25000\text{N} =$$

$$= 0.653\text{kN}$$

Which the prescribed connection fulfils.

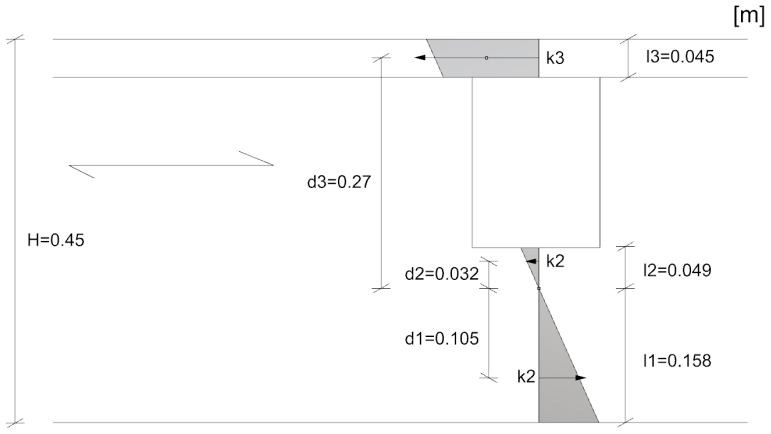

Figure B.7: *Section though the joint showing the spring model*

The stiffness is calculated with contribution from the continuous parts as well, according to the Figure B.7. Three linear springs can be defined, these are translated to rotational stiffness through Equation (3.9). Thus:

$$k_1 = \frac{E_{0,mean}\sqrt{Bl_1}}{0.85} = \frac{13.1\text{GPa} \cdot \sqrt{0.15 \cdot 0.158}}{0.85} = 2372611\text{kN m}^{-1}$$

$$k_2 = \frac{E_{0,mean}\sqrt{Bl_2}}{0.85} = \frac{13.1\text{GPa} \cdot \sqrt{0.15 \cdot 0.047}}{0.85} = 1294037\text{kN m}^{-1}$$

$$k_3 = \frac{E_{0,mean}\sqrt{Bl_3}}{0.85} = \frac{13.1\text{GPa} \cdot \sqrt{0.15 \cdot 0.045}}{0.85} = 1266205\text{kN m}^{-1}$$

This gives the rotational stiffness:

$$c_{r,y,1} = k_1 d_1^2 = 2372611\text{kN m}^{-1} \cdot 0.105^2\text{m} = 26158\text{kN m rad}^{-1}$$

$$c_{r,y,2} = k_2 d_2^2 = 1294037\text{kN m}^{-1} \cdot 0.032^2\text{m} = 1325\text{kN m rad}^{-1}$$

$$c_{r,y,3} = k_3 d_3^2 = 1266205\text{kN m}^{-1} \cdot 0.27^2\text{m} = 92306\text{kN m rad}^{-1}$$

Combined this becomes:

$$cr, y = c_{r,y,1}+c_{r,y,2}+c_{r,y,3} = 26158\text{kN m rad}^{-1}+1325\text{kN m rad}^{-1}+92306\text{kN m rad}^{-1} = 119789\text{kN m rad}^{-1}$$

B.4 Steel Node 1

The parts included in the joint are:

Table B.5: Size and material of members included in the Steel Node 1 Joint

Member	Material	Size
Beams *1* and *2*	GL28c	450x150 mm
Steel plate *3*	f_y=355MPa	t-10mm
Dowels *4*	f_u=600MPa	5x7 dowels spacing:70x42mm

B.4.1 Normal Force

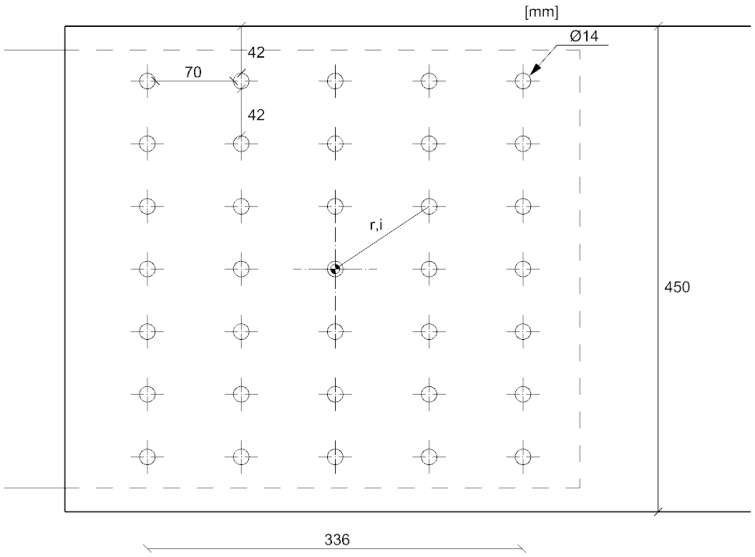

Figure B.8: *Layout of the screwed connection*

The strength of this joint lies entirely in the screwed connection, the layout of which is shown in Figure B.8. The connection is designed according to the minimum distance in Table B.3. Through Johansen's theory, the characteristic strength per dowel is $F_{v,R,k} = 31.3\text{kN}$ design strength of the fastener becomes:

$$F_{v,R,d} = \frac{F_{v,R,k} k_{mod}}{\gamma_m} = \frac{31.3\text{kN} \cdot 0.6}{1.25} = 15.02\text{kN}$$

To account for the group effect for dowels along grain, an effective number of bolts should be used, according to [SIS, 2009c, Eq. 8.34]:

$$n_{ef} = min\left(n; n^{0.9}\sqrt[4]{\frac{a_1}{13d}}\right) = 5^{0.9}\sqrt[4]{\frac{70}{182}} = 3.35$$

Thus, the total normal strength of screwed connection thus becomes:

$$N = n_{ef} n_{crosswise} F_{v,R,d} = 3.35 \cdot 7 \cdot 15.02\text{kN} = 352\text{kN}$$

The maximal forces that can be taken by the steel node exceeds this, since the strength of the steel node becomes:

$$N_{node,compression} < A_{node} f_y = t_{plate}(h_{plate} - n_{width} d) f_y = 0.01\text{m} \cdot (0.44 - 7 \cdot 0.014)\text{m} \cdot 355\text{MPa} = 1214\text{kN}$$

$$N_{node,tension} < A_{node} \frac{f_y}{\gamma_{M,2}} = t_{plate}(h_{plate} - n_{width} d) f_y = 0.01\text{m} \cdot (0.44 - 7 \cdot 0.014)\text{m} \cdot \frac{355\text{MPa}}{1.25} = 971\text{kN}$$

The axial stiffness of the the system will have its only contribution from the dowel connection *4*. According to Eurocode 5 you are allowed to double the stiffness for connections timber-steel [SIS, 2009c, 7.1(3)] and double it again for the two shear planes. The stiffness (according to Equation (3.1)) becomes:

$$K_{ser} = 2 \cdot 2 \frac{\rho_m^{1.5} d}{23} = 2 \cdot 2 \frac{430^{1.5} 14}{23} = 21708\text{kN m}^{-1}$$

$$c_{t,x,dowel3} = n \cdot K_{ser} = 35 \cdot 5427 = 379890\text{kN m}^{-1}$$

B.4.2 Major bending

According to Lidelöw [2015] the moment capacity of a dowel connection can be calculated as:

$$F_{v,R,d,i} = \frac{M r_i}{I_p} \Rightarrow M = \frac{F_{v,R,d,i} I_p}{r_i}$$

Where:
r_i - *Distance from the center point of connection to fastener* [m]
I_p - $\Sigma r_i^2 \Rightarrow I_p = 0.93$ - *Polar Moment of Inertia* [m^2]

Which gives:

$$M = min\left(\frac{F_{v,R,d,i} I_p}{r_i}\right) = \frac{15\text{kN} \cdot 0.93\text{m}^2}{0.23\text{m}} = 59\text{kN m}$$

Until the first fasteners fails.

And as for the rotational stiffness, according to Equation (3.9) and since all the dowels works in parallel, the rotational stiffness becomes:

$$c_{r,y} = \Sigma K_{Ser,i} {r_i}^2 = 20252\text{kN m rad}^{-1}$$

B.5 Steel Node 2

The parts included in the joint are:

Table B.6: Size and material of members included in the Steel Node 1 Joint

Member	Material	Size
Beams *1* and *2*	GL28c	450x150 mm
Steel Node *3*	f_y=355MPa	t-10mm arm length - 150 mm
Self-tapping screws *4*	f_u=600MPa	6x2 dowels 8x200mm

The screw layout of the joint is shown in Figure B.9.

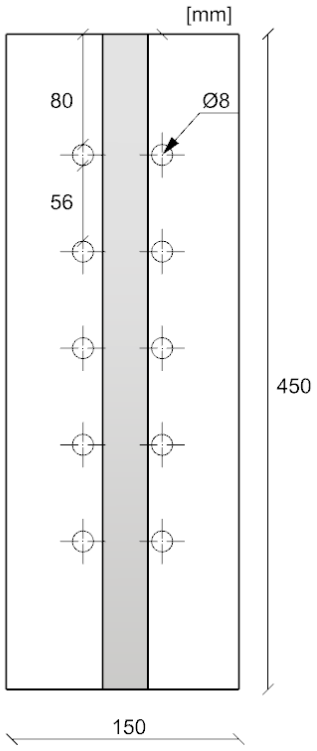

Figure B.9: *Layout of the screwed connection*

B.5.1 Normal Force

The joint is limited in compression by the compression parallel to grain for the beam, when it pushes against the steel plate, thus:

$$N_{compression,permanent} < \frac{f_{c,0,k} k_{mod}}{\gamma_M} A_{net} = \frac{24\text{MPa} \cdot 0.6}{1.25}(0.15 \cdot 0.45 - 10 \cdot 5 \cdot 10^{-5}\text{m}^2) = 771\text{kN}$$

$$N_{compression,short} < \frac{24\text{MPa} \cdot 0.9}{1.25}(0.15 \cdot 0.45 - 10 \cdot 0.00005\text{m}^2 = 1156\text{kN}$$

The tensile capacity of the joint is dependent on the withdrawal strength ($F_{ax,k,Rk}$) of the screws, defined in Eurocode 5 as [SIS, 2009c, Eq.8.38]:

$$F_{ax,k,Rk} = \frac{n_{ef} f_{ax,k} d l_{ef} k_d}{1.2\cos(\alpha)^2 + \sin(\alpha)^2}$$

Where:
$n_{ef} = n^{0.9} = 12^{0.9} = 9.35$ - *Effective number of screws, considering group effects*
$f_{ax,k} = 0.52 d^{-0.5} l_{ef}^{-0.1} \rho_k^{0.8} = 13.8\text{N/mm}^2$ - *Characteristic withdrawal strength perpendicular grain*
$l_{ef} = 200\text{mm}$ - *Threaded length of screw*
$d = 8\text{mm}$ - *Screw diameter*
$k_d = min(d/8; 1) = 1$
$\alpha = 0$ - *Angle to grain*[°]

This gives:

$$F_{ax,k,Rk} = \frac{9.36 \cdot 13.8\text{N/mm}^2 \cdot 8\text{mm} \cdot 200\text{mm} \cdot 1}{1.2\cos(0)^2 + \sin(0)^2} = 173\text{kN}$$

$$F_{ax,d,Rk,permanent} = \frac{F_{ax,k,Rk} k_{mod}}{\gamma_M} = \frac{173\text{kN} \cdot 0.6}{1.25} = 83\text{kN}$$

The axial stiffness for compression is calculated with an equivalent spring corresponding to the beam and one for the steel node:

$$k_{timber} = \frac{E_{0,mean}\sqrt{A_{net}}}{0.85} = 4166058\text{kN m}$$

$$k_{steel} = \frac{E_{steel} A_{net}}{L} = \frac{210\text{GPa} \cdot 0.03\text{m} \cdot 0.45\text{m}}{0.15\text{m}} = 18900000\text{kN m}$$

$$c_{t,x} = \left(\frac{1}{k_{timber}} + \frac{1}{k_{timber}}\right)^{-1} = 3413608\text{kN m}$$

The axial stiffness for self-tapping screws can be calculated as [Dietsch, Brandner, 2015]:

$$K_{ser,ax} = 780 d^{0.2} L_{ef}^{0.4} = 9842\text{kN m}$$

Gives a total axial stiffness of:

$$c_{t,x,tension} = 780 d^{0.2} L_{ef}^{0.4} n = 118115\text{kN m}$$

B.5.2 Major bending

According to Lidelöw [2015] the moment capacity of a a dowel connection can be calculated as:

$$F_{v,R,d,i} = \frac{M r_i}{I_p} \Rightarrow M = \frac{F_{ax,d,Rk} I_p}{r_i}$$

In order to account for the group effect the ration betwene effective and actual number of screws is used:

$$F_{ax,d,Rk} = \frac{n_e f}{n} \frac{F_{ax,k,Rk} k_{mod}}{\gamma_M} = \frac{9.35}{12} \frac{18.5\text{MPa} \cdot 0.6}{1.25} = 6.9\text{kN m}$$

r_i - *vertical distance from point of connection to fastener* [m]
I_p - $\Sigma r_i^2 \Rightarrow I_p = 0.14$ [m^2] - *Polar Moment of Inertia*

Which gives:

$$M = min\left(\frac{F_{v,R,d,i} I_p}{r_i}\right) = 6\text{kN m}$$

Until the first fasteners fails.

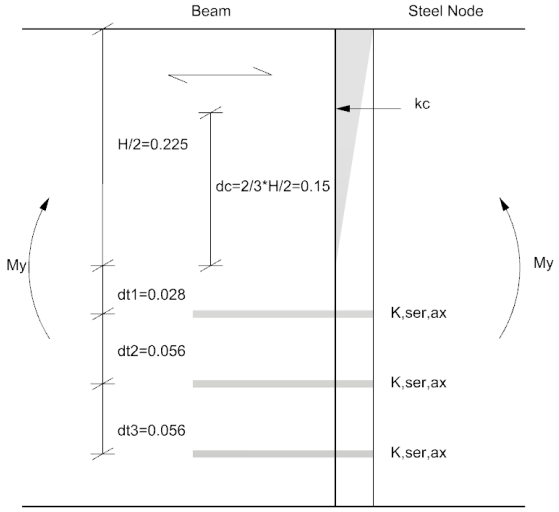

Figure B.10: *Section though the joint showing the spring model*

And as for the rotational stiffness, as can be seen in Figure B.10, there is a contribution from the compression zone in the interface between materials, defined as the spring k_c and from the screws that acts in tensions:

$$k_{steel} = \frac{EA}{L} = \frac{E_{steel} BH/2}{t} = \frac{210\text{GPa} \cdot 0.15\text{m} \cdot 0.225\text{m}}{0.01\text{m}} = 708750000\text{kN m}^{-1}$$

$$k_{timber} = \frac{E\sqrt{A}}{0.85} = \frac{E_{timber}\sqrt{BH/2}}{0.85} = \frac{13.1\text{GPa}\sqrt{0.15\text{m}} \cdot 0.225\text{m}}{0.85} = 2831321\text{kN m}^{-1}$$

$$k_c = \left(\frac{1}{k_{steel}} + \frac{1}{k_{timber}}\right)^{-1} = 2820055\text{kN m}^{-1}$$

According to Equation (3.9) and since all the springs works in parallel, the rotational stiffness becomes:

$$c_{r,y} = \cdot\Sigma K_{Ser,ax,i} {z_1}^2 + k_c d_c^2 = 2 \cdot 9842\text{kN m} \cdot 0.028^2\text{m2} \cdot 9842\text{kN m} \cdot 0.092^2\text{m2} \cdot 9842\text{kN m} \cdot 0.156^2\text{m} +$$
$$+2820055\text{kN m} \cdot 0.15^2 = 64112\text{kN m rad}^{-1}$$

C Initial Internal Forces

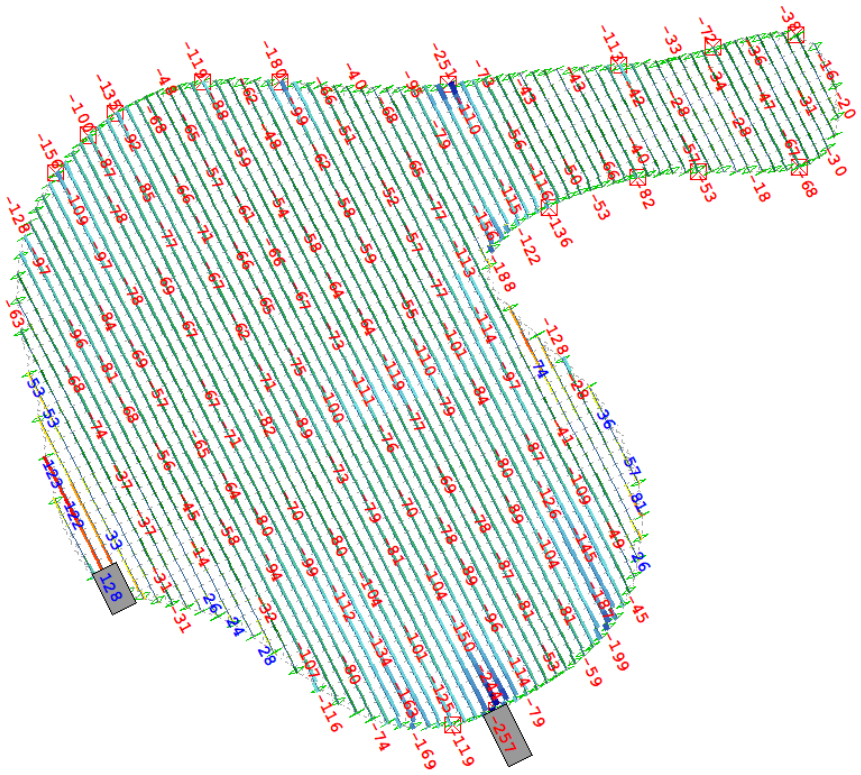

Figure C.1: *Axial forces due to permanent loads [kN]*

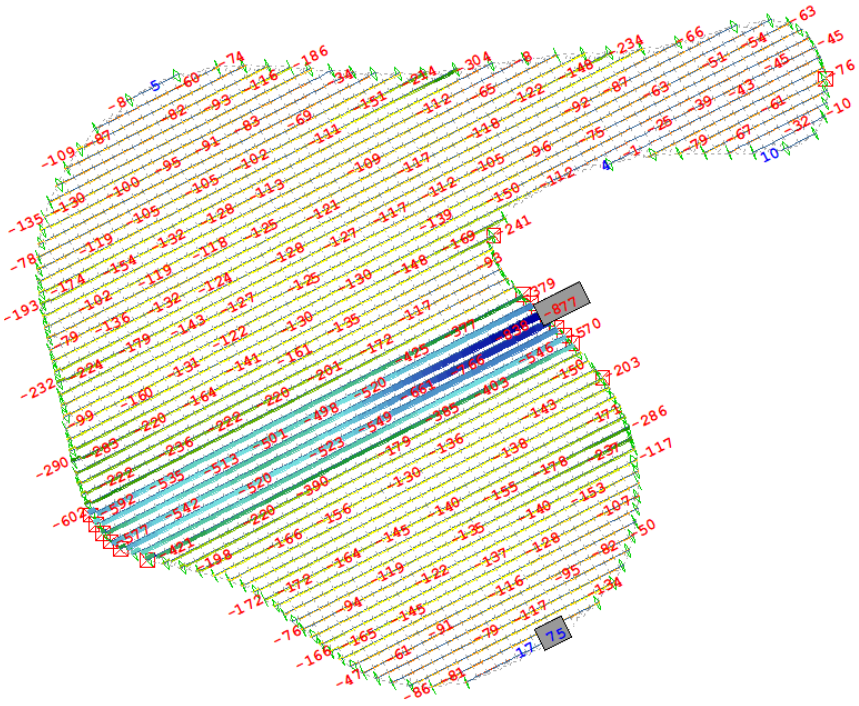

Figure C.2: *Axial forces due to permanent loads [kN]*

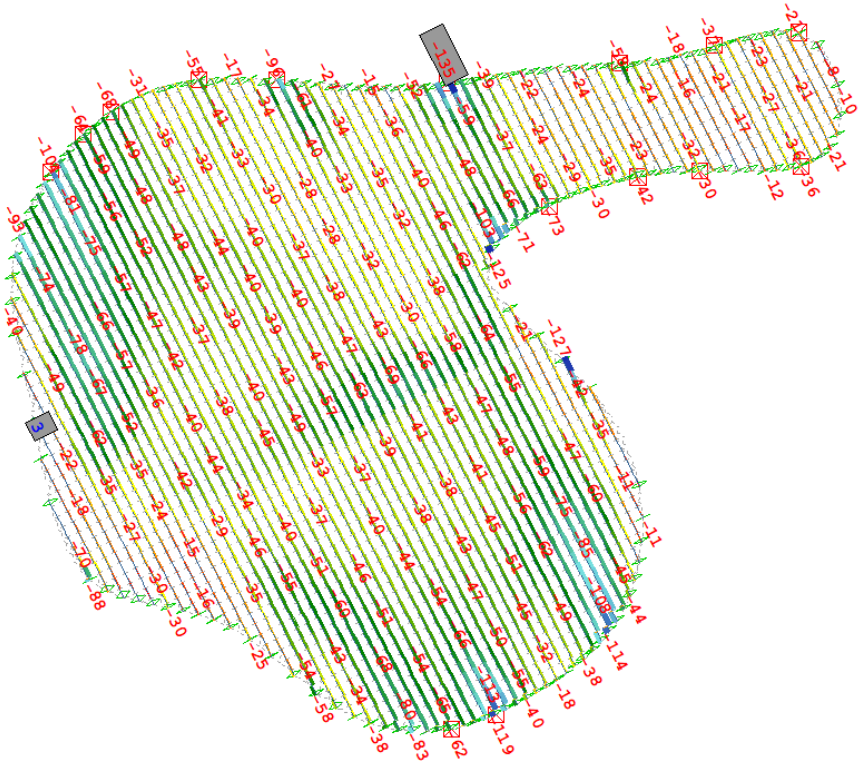

Figure C.3: *Axial forces due to short duration loads [kN]*

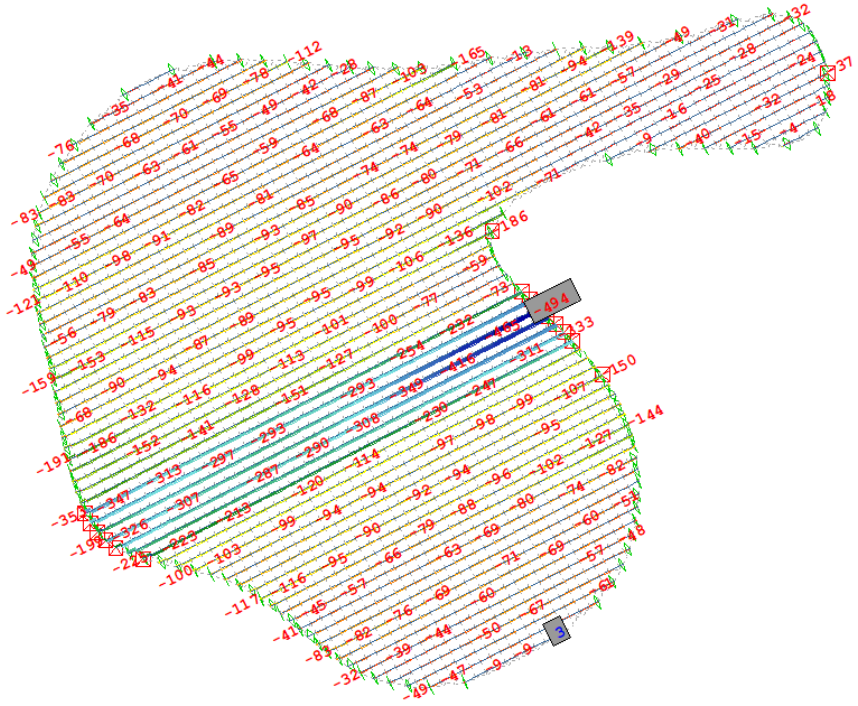

Figure C.4: *Axial forces due to short duration loads [kN]*

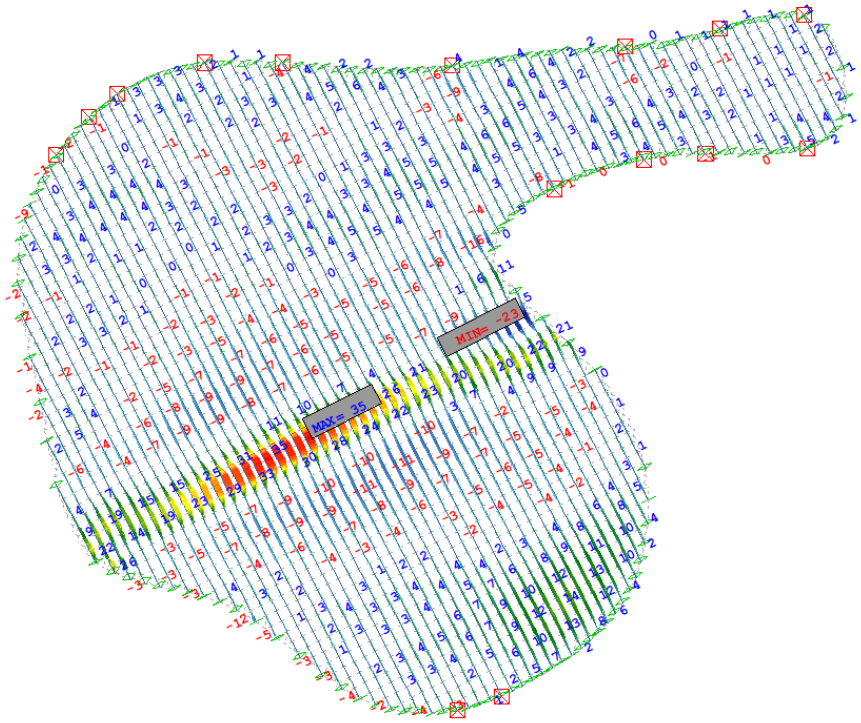

Figure C.5: *Major axis bending due to permanent loads [kNm]*

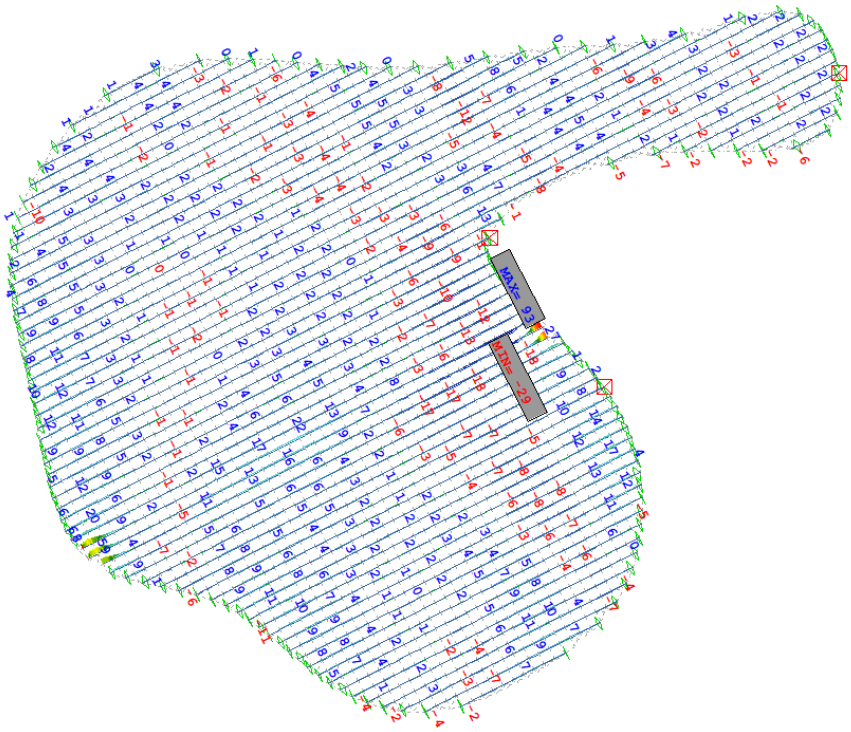

Figure C.6: *Major axis bending due to permanent loads [kNm]*

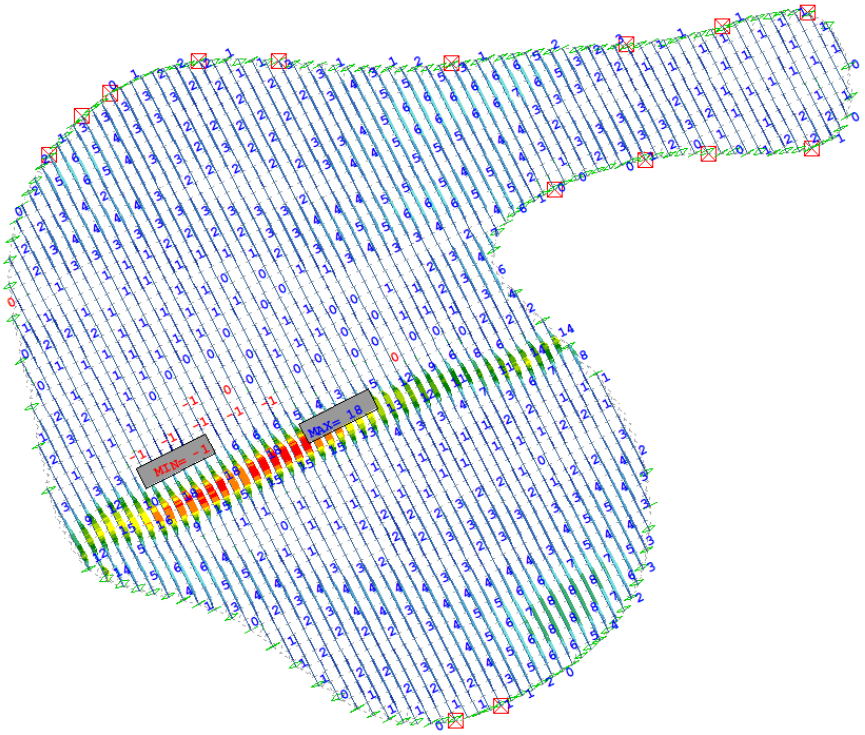

Figure C.7: *Major axis bending forces due to short duration loads [kNm]*

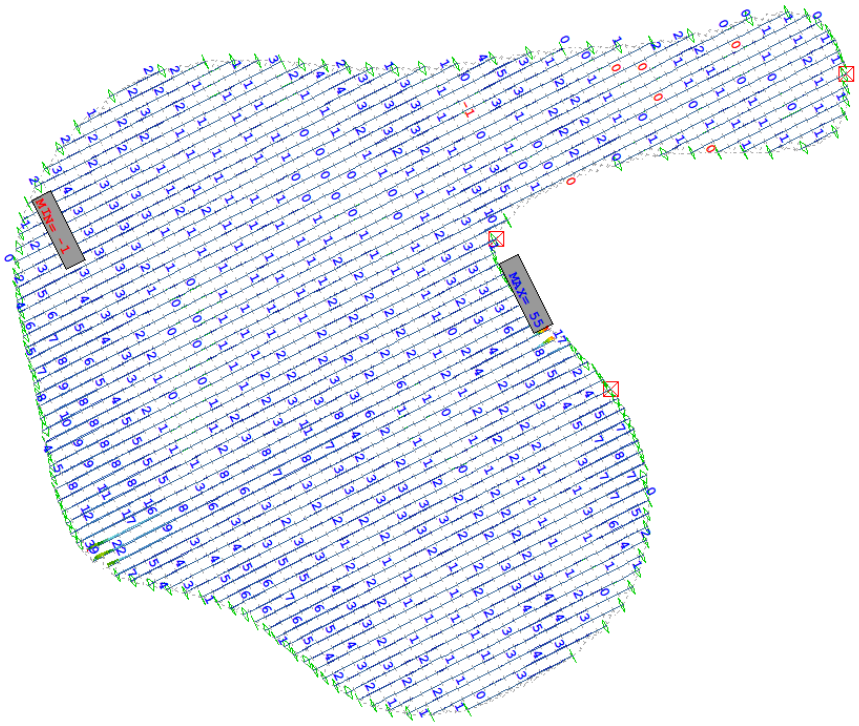

Figure C.8: *Major axis bending forces due to short duration loads [kNm]*

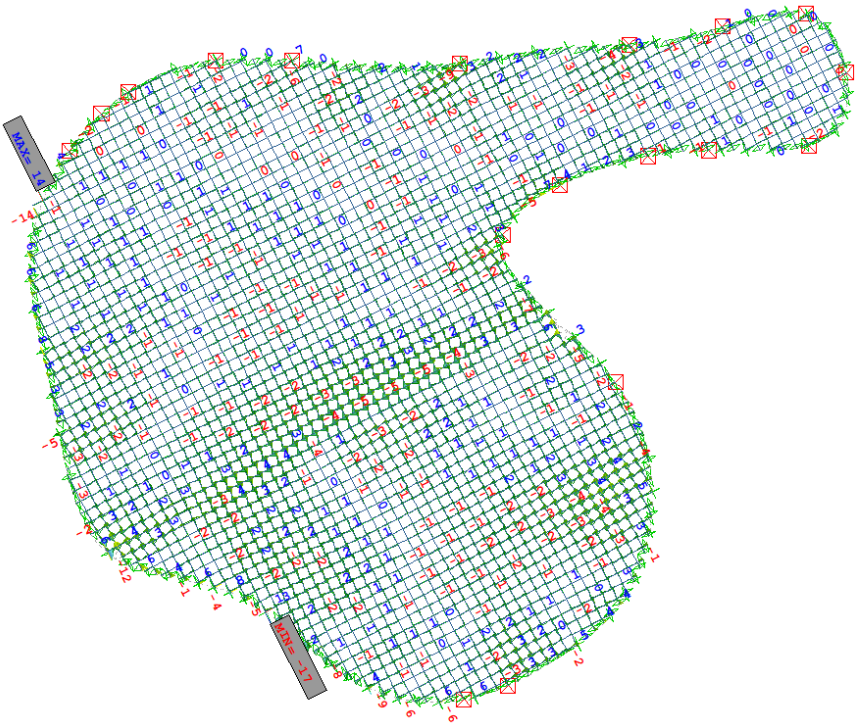

Figure C.9: *Minor axis bending due to permanent loads [kNm]*

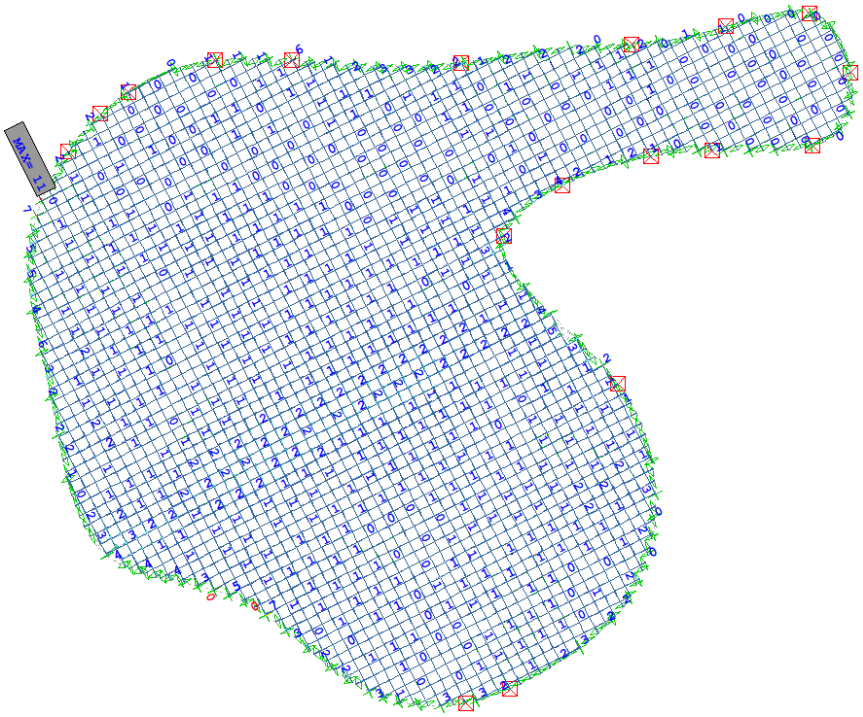

Figure C.10: *Minor axis bending forces due to short duration loads [kNm]*

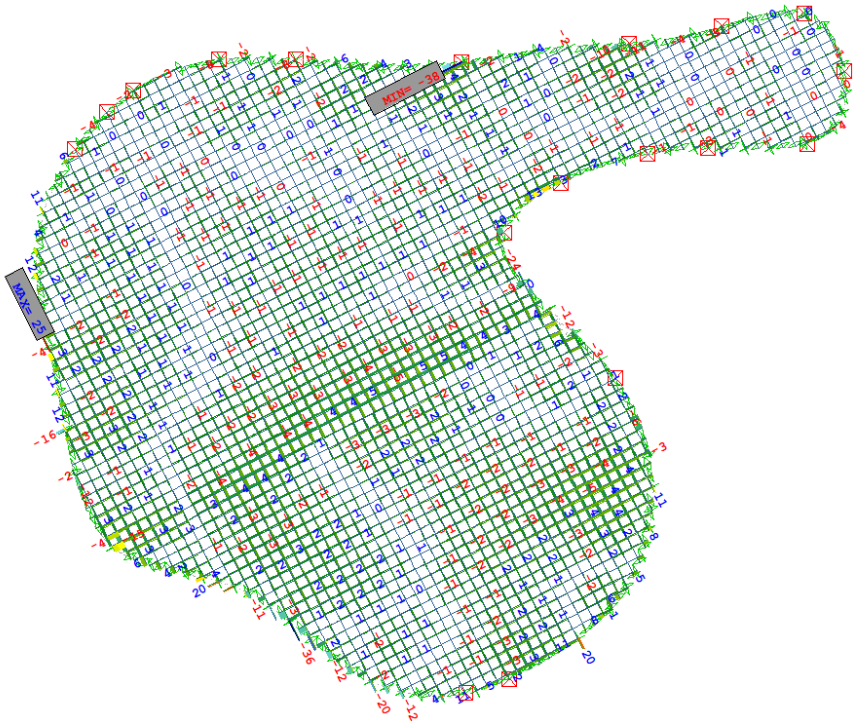

Figure C.11: *Major axis shear due to permanent loads [kN]*

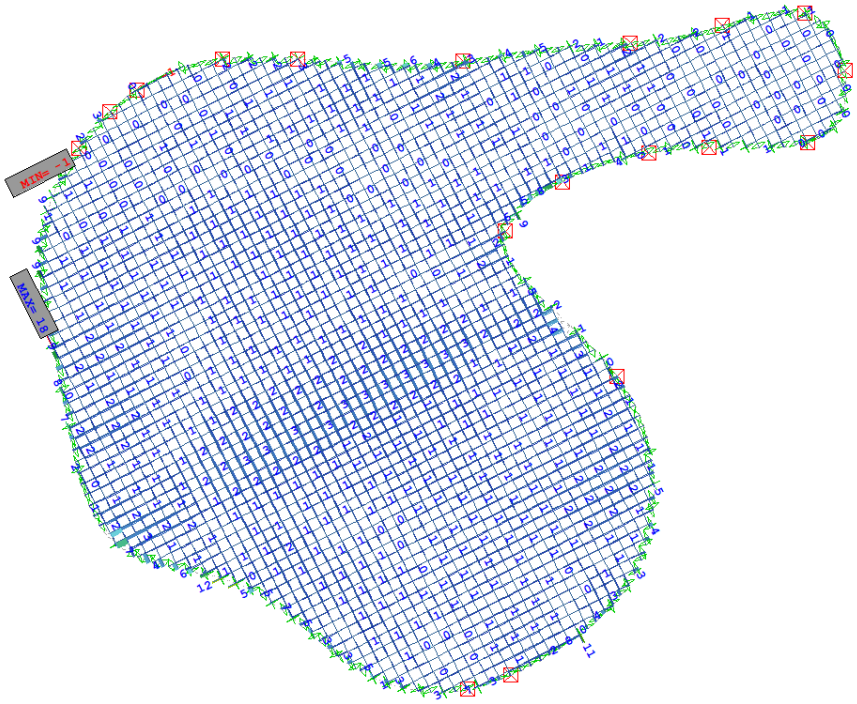

Figure C.12: *Major axis shear due to short duration loads [kN]*

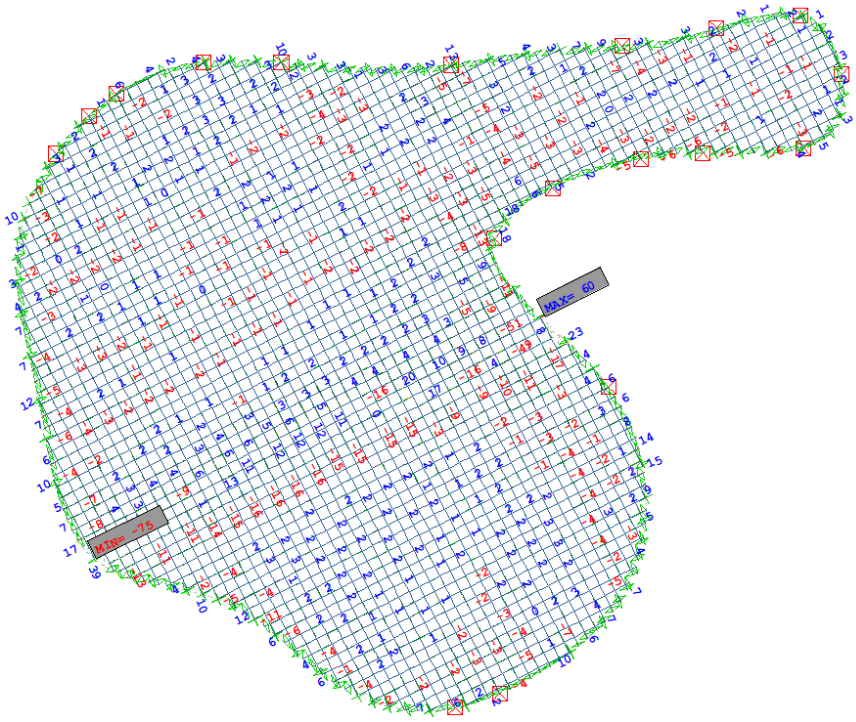

Figure C.13: *Minor axis shear due to permanent loads [kN]*

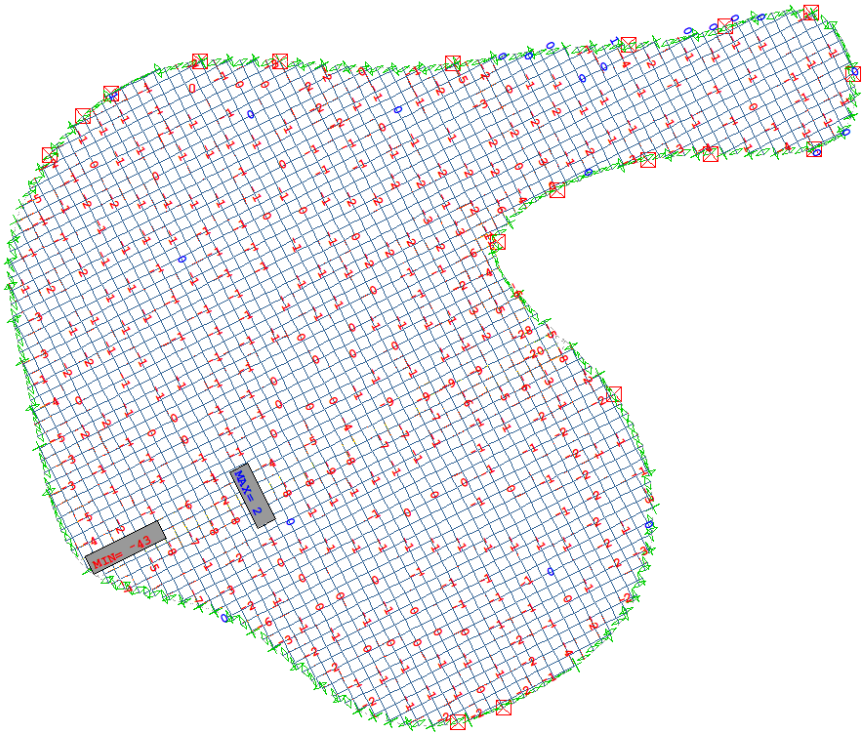

Figure C.14: *Minor axis shear due to short duration loads [kN]*

D Final Internal Forces

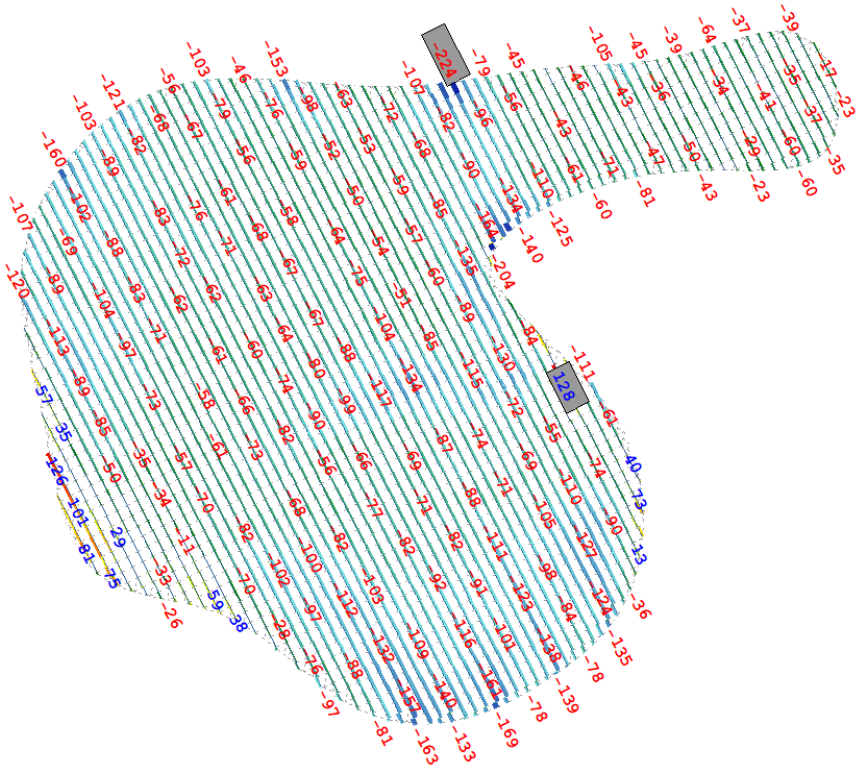

Figure D.1: *Axial forces due to permanent loads [kN]*

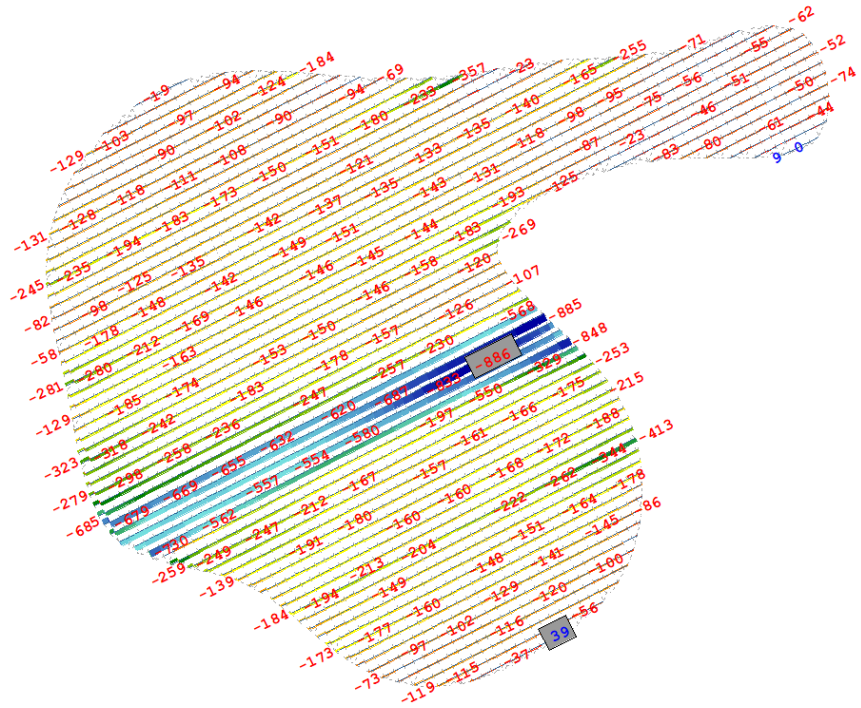

Figure D.2: *Axial forces due to permanent loads [kN]*

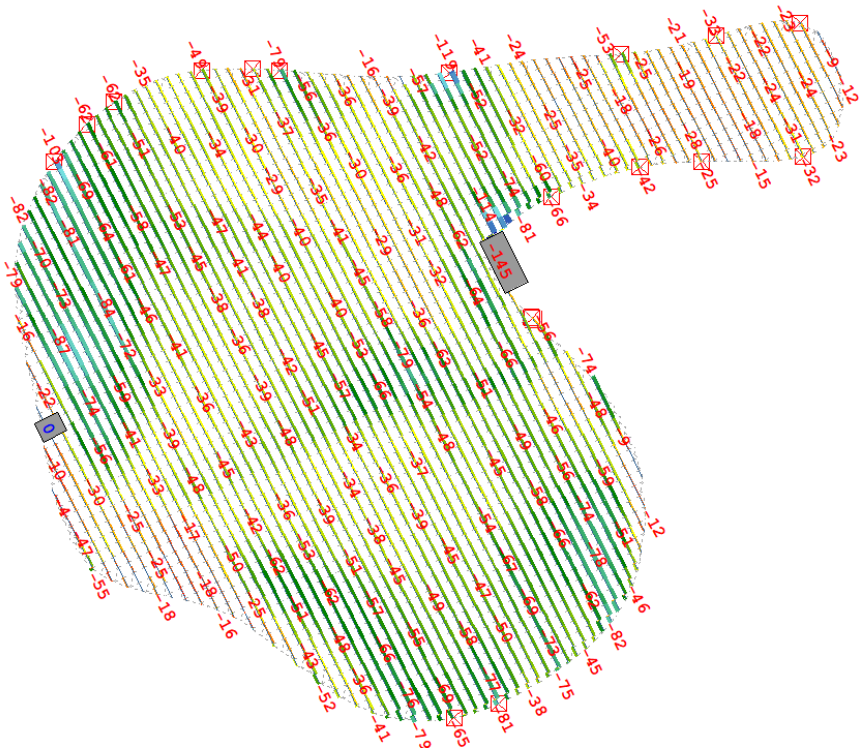

Figure D.3: *Axial forces due to short duration loads [kN]*

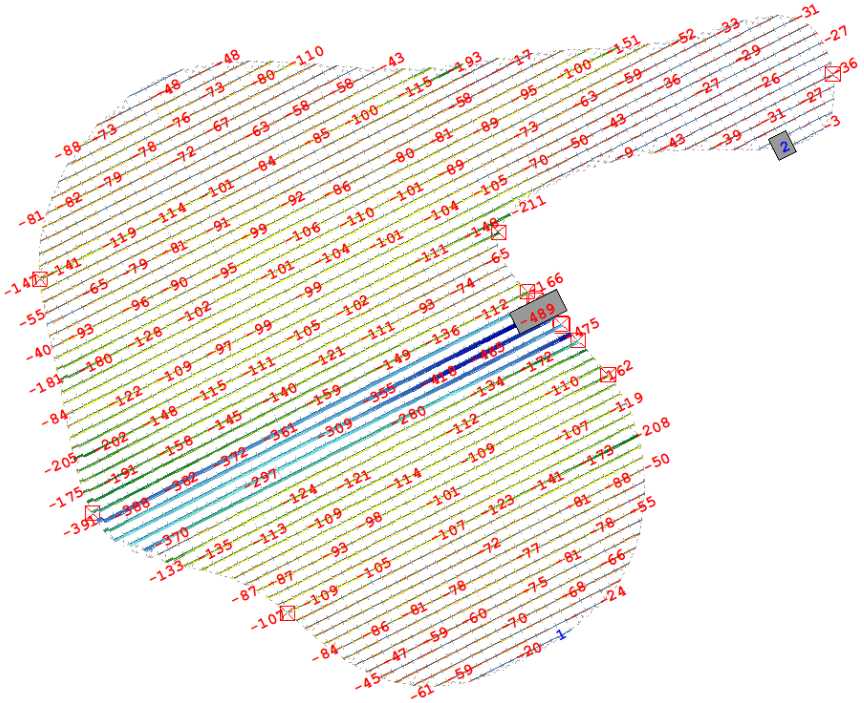

Figure D.4: *Axial forces due to short duration loads [kN]*

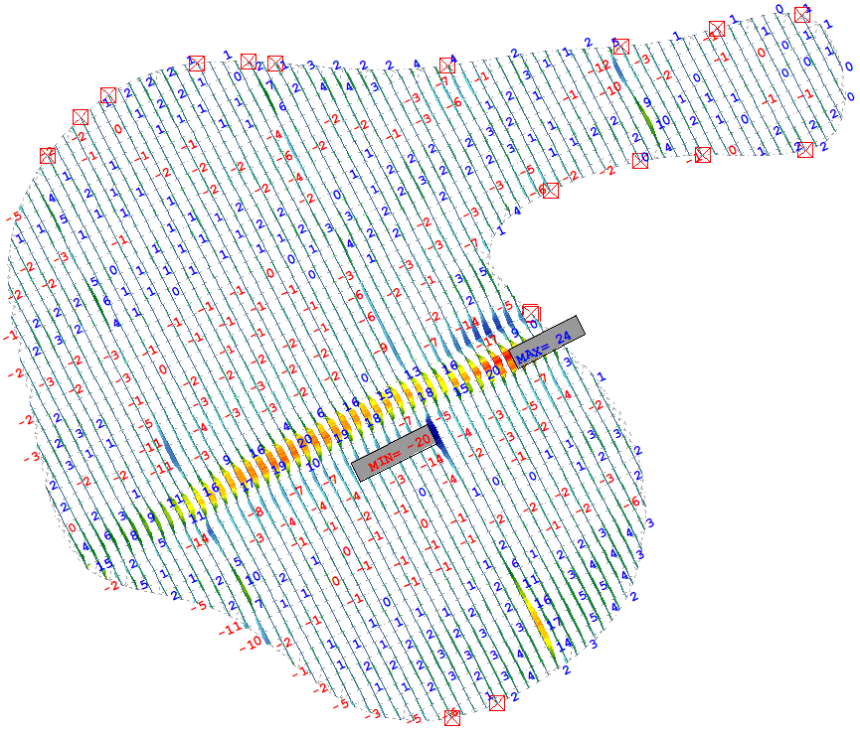

Figure D.5: *Major axis bending due to permanent loads [kNm]*

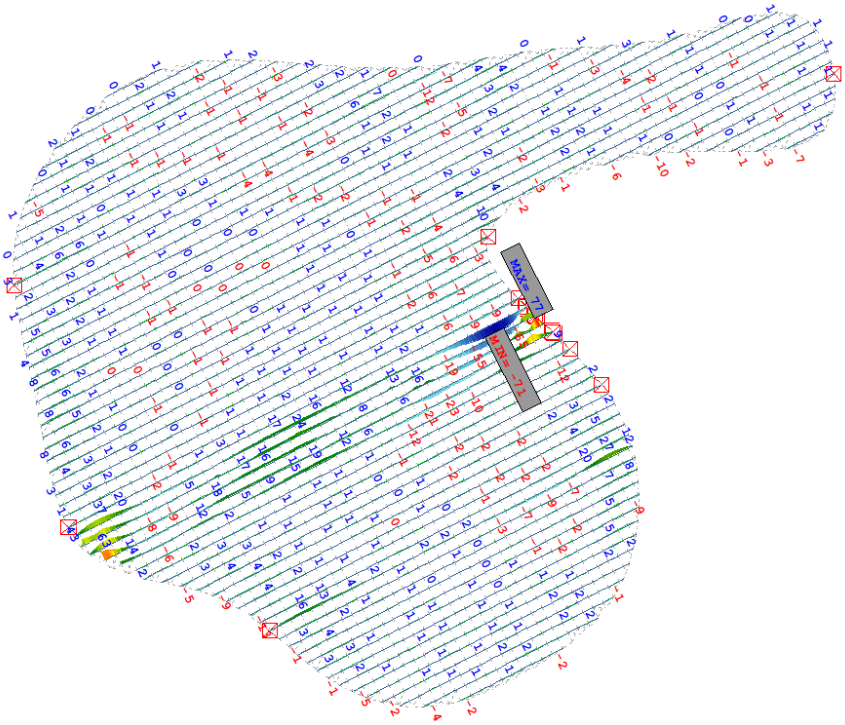

Figure D.6: *Major axis bending due to permanent loads [kNm]*

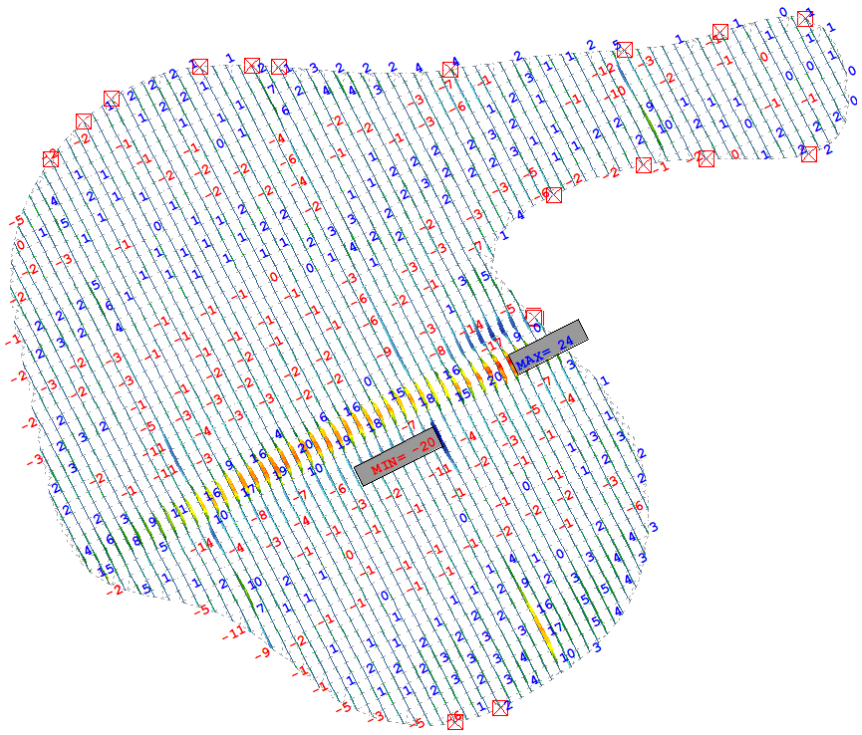

Figure D.7: *Major axis bending forces due to short duration loads [kNm]*

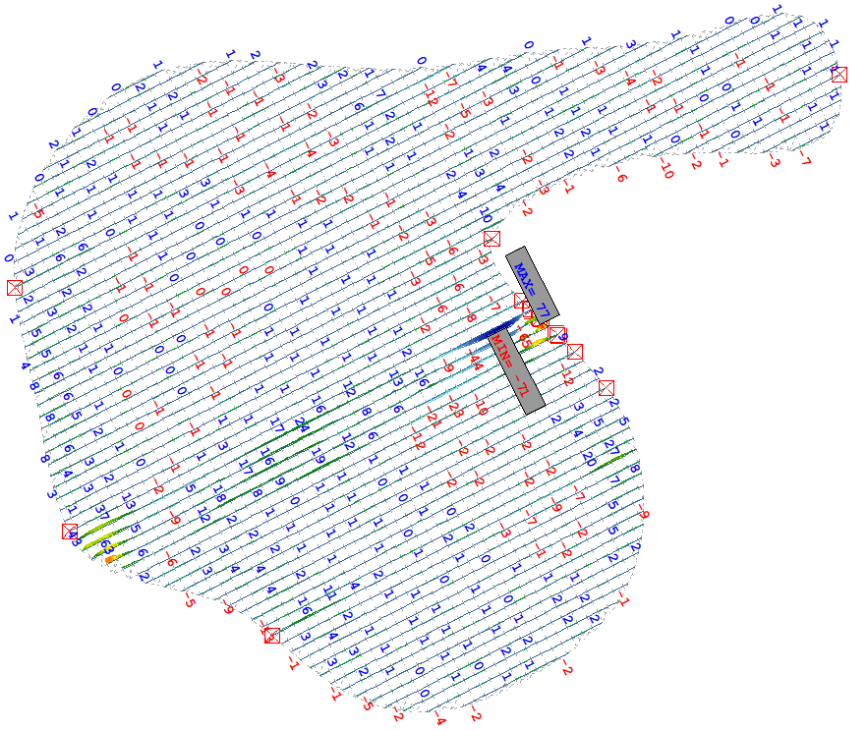

Figure D.8: *Major axis bending forces due to short duration loads [kNm]*

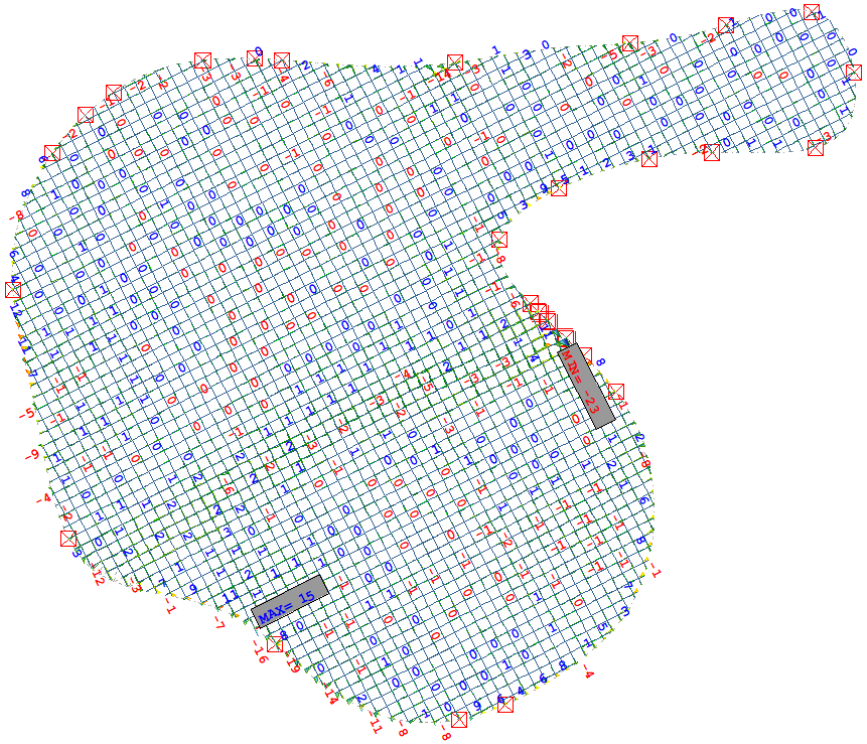

Figure D.9: *Minor axis bending due to permanent loads [kNm]*

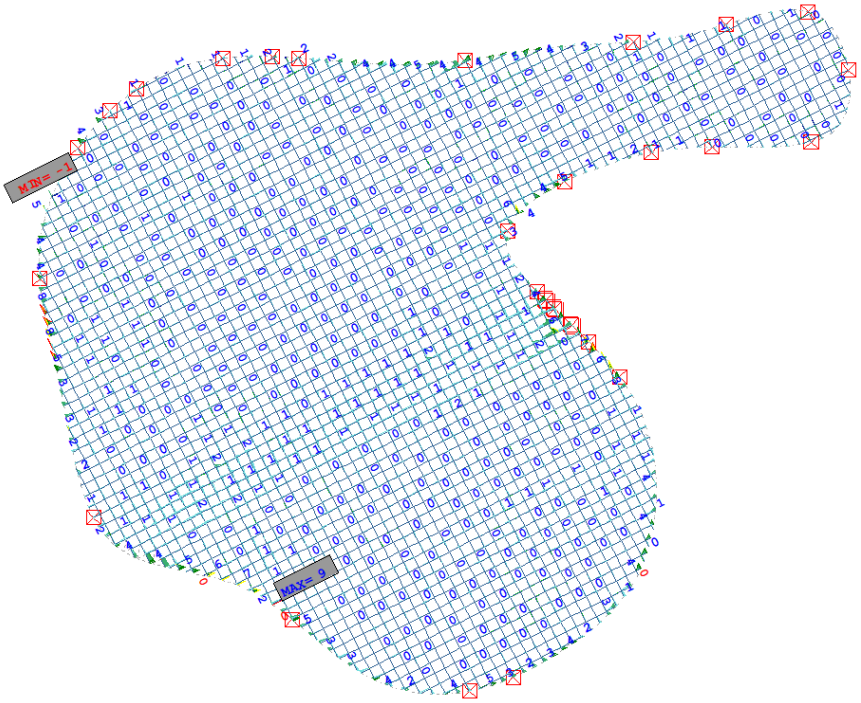

Figure D.10: *Minor axis bending forces due to short duration loads [kNm]*

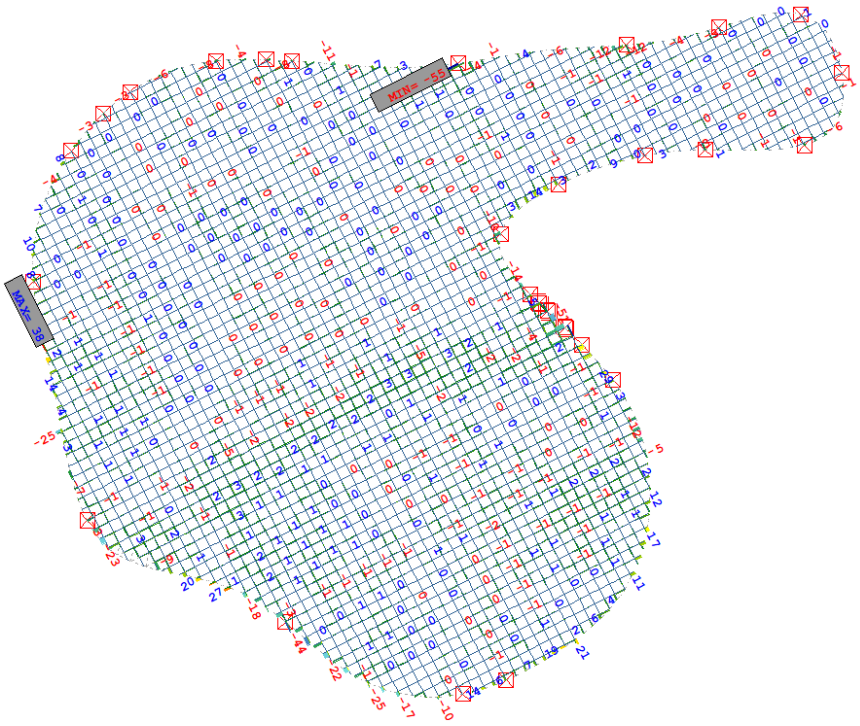

Figure D.11: *Major axis shear due to permanent loads [kN]*

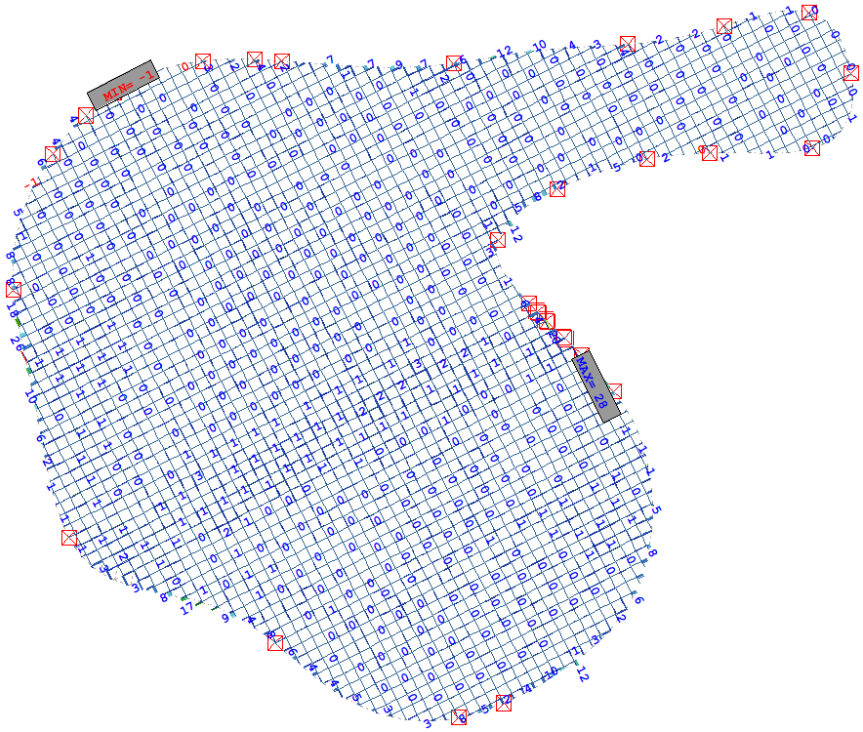

Figure D.12: *Major axis shear due to short duration loads [kN]*

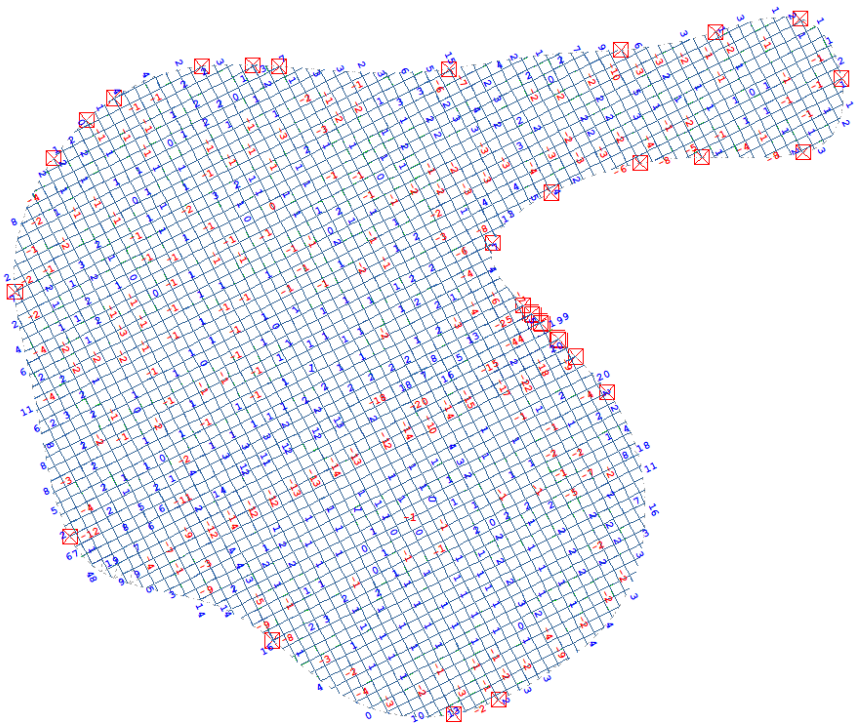

Figure D.13: *Minor axis shear due to permanent loads [kN]*

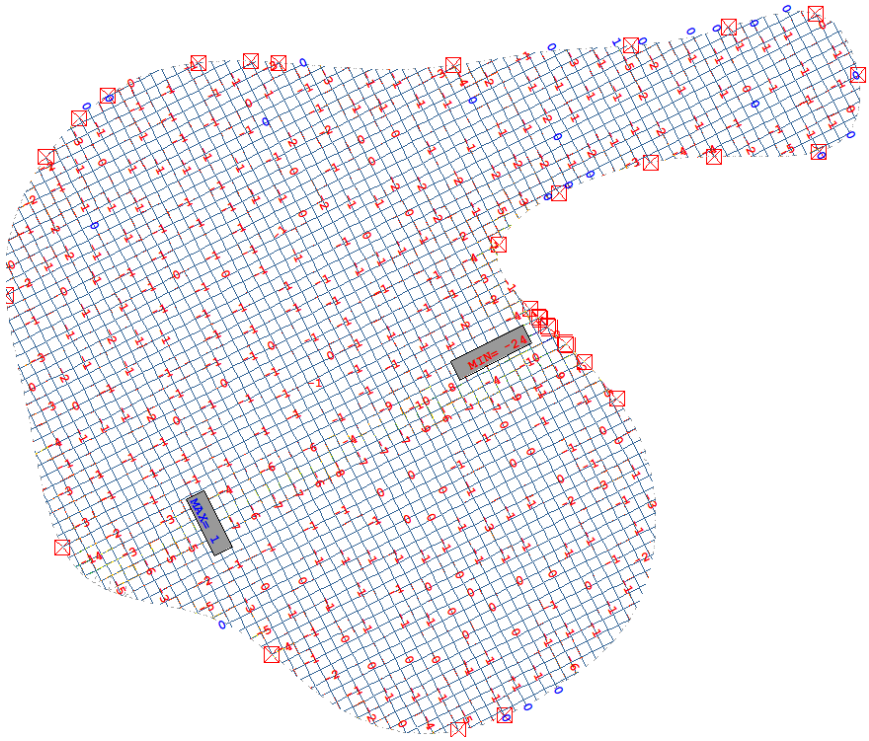

Figure D.14: *Minor axis shear due to short duration loads [kN]*